Application of Structural Geology to Mineral and Energy Resources of the Central and Western United States

U.S. GEOLOGICAL SURVEY BULLETIN 2012

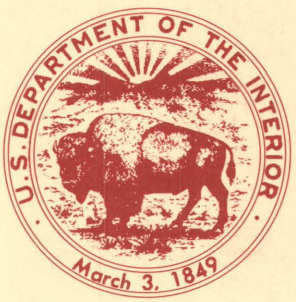

Application of Structural Geology to Mineral and Energy Resources of the Central and Western United States

Edited by CHARLES H. THORMAN

Papers presented at a workshop sponsored by the U.S. Geological Survey,
October 9–10, 1990, Colorado School of Mines, Golden, Colorado

U.S. GEOLOGICAL SURVEY BULLETIN 2012

U.S. DEPARTMENT OF THE INTERIOR
MANUEL LUJAN, JR., Secretary

U.S. GEOLOGICAL SURVEY
Dallas L. Peck, Director

UNITED STATES GOVERNMENT PRINTING OFFICE: 1992

For sale by
Book and Open-File Report Sales
U.S. Geological Survey
Federal Center, Box 25286
Denver, CO 80225

Library of Congress Cataloging-in-Publication Data

Application of structural geology to mineral and energy resources of the central and western United States : papers presented at a workshop sponsored by the U.S. Geological Survey, October 9–10, 1990, Colorado School of Mines, Golden, Colorado / edited by Charles H. Thorman
p. cm. — (U.S. Geological Survey bulletin ; 2012)
Includes bibliographical references.
Supt. of Docs. no.: I 19.3:2012
1. Geology, Structural—Southwestern States—Congresses. 2. Geology, Structural—West (U.S.)—Congresses. 3. Ore deposits—Southwestern States—Congresses. 4. Ore deposits—West (U.S.)—Congresses. I. Thorman, Charles H. II. Geological Survey (U.S.) III. Series.
QE75.B9 no. 2012
[QE627.5.S85]
557.3 s—dc20 92–10747
[553'.0978] CIP

CONTENTS

[Letters designate chapters]

PREFACE

This volume includes some of the papers presented at a workshop sponsored by the U.S. Geological Survey and held October 9–10, 1990, at the Green Center, Colorado School of Mines, Golden, Colorado. The workshop presented current research by U.S. Geological Survey scientists who are using structural geology in their investigations into the mineral and energy resources of the United States. The figure below shows the areal distribution of the 12 chapters included herein; the papers are lettered on the figure according to their position in the text of this report.

One of the most important aspects of this workshop was a demonstration of the integrating of many disciplines in unraveling the structural evolution of an area, regardless of scale. The application of structural geology by itself provides only a limited amount of information and leaves many aspects of the evolution of an area unresolved.

Integration of geophysical techniques (gravity, seismic, and audio-magneto-telluric) with detailed and regional geology in sedimentary and volcanic terranes establishes the basis for new approaches to exploration for hydrocarbons in Arizona, Colorado, Utah, Wyoming, and Montana (chapters D, E, J, K). Field studies at detailed to regional scales (chapters A, C, F, G, H, I, L) present data that call for moderate to major revision of thinking in areas often thought to be well understood. These studies emphasize the continuing need to remap so-called well-understood areas, as well as the need to map those areas for which only limited data are available. Detailed petrologic studies in Missouri and Arizona (chapters A, L) of both carbonate and volcanic rocks cause us to reconsider our concepts of the origin of well-established rocks units and thus their implications regarding the structural evolution of those areas. Depositional patterns can be key indicators of the tectonic control of paleotopographic highs, a major factor in basin evolution, as suggested for the Anadarko Basin (chapter B). The application of isotopic dating in structurally complex areas has greatly increased our knowledge of the relative timing and duration of events that influenced the migration of mineralizing and hydrocarbon fluids and gases (chapters G, H). With a better grasp of the time involved, we can better correlate the various deformational and migrational events in Utah and eastern Nevada.

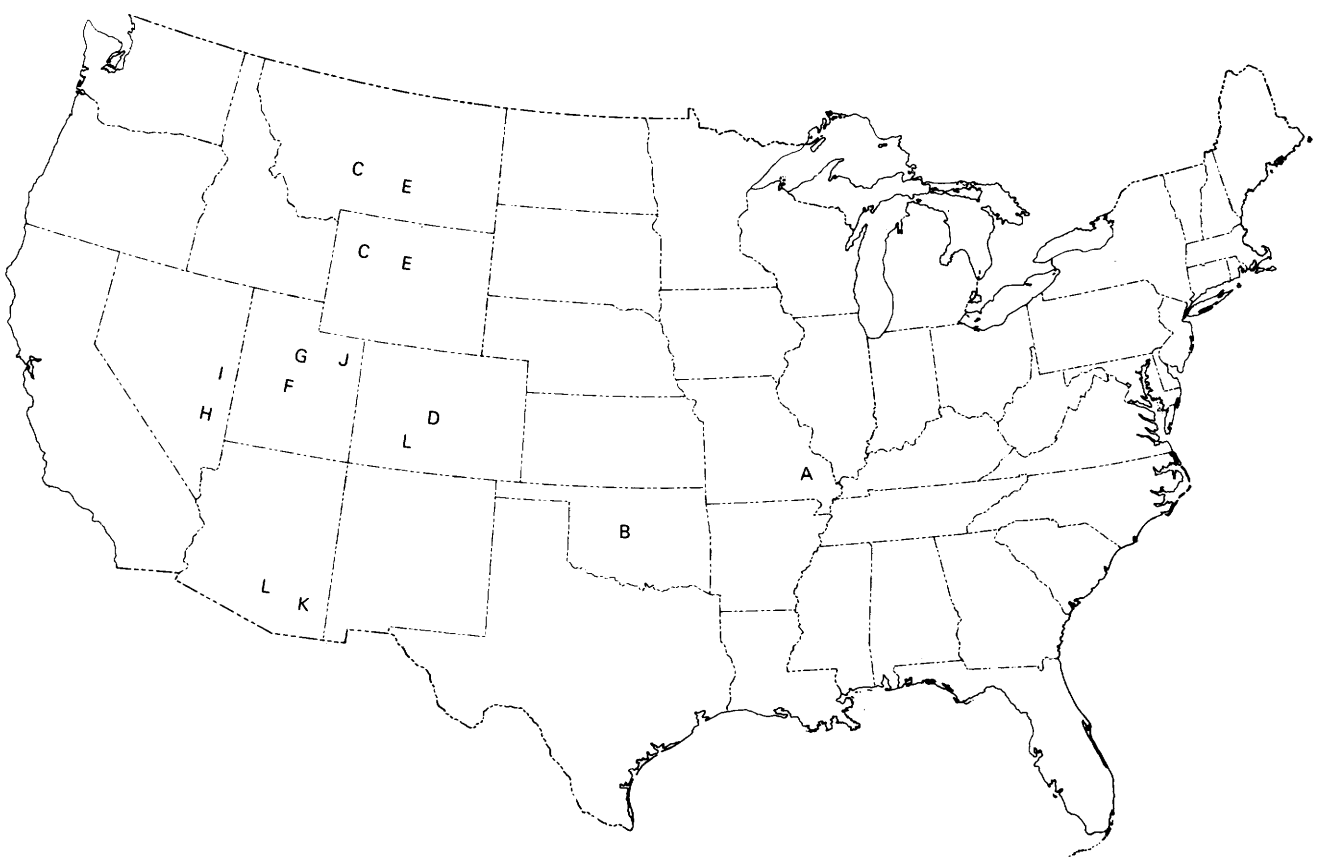

Chapter A

Microstructures in the Cambrian Bonneterre Formation, Lamotte Sandstone, and Basal Clastic Rocks of Southeast Missouri and Northeast Arkansas—Implications of Regional Sulfide Occurrence in Stylolites and Extensional Veinlets for Ore Genesis

By S.F. DIEHL, M.B. GOLDHABER,
C.D. TAYLOR, H.S. SWOLFS, and C.A. GENT

U.S. GEOLOGICAL SURVEY BULLETIN 2012

APPLICATION OF STRUCTURAL GEOLOGY TO MINERAL AND ENERGY
RESOURCES OF THE CENTRAL AND WESTERN UNITED STATES

CONTENTS

FIGURES

TABLES

Microstructures in the Cambrian Bonneterre Formation, Lamotte Sandstone, and Basal Clastic Rocks of Southeast Missouri and Northeast Arkansas—Implications of Regional Sulfide Occurrence in Stylolites and Extensional Veinlets for Ore Genesis

By S.F. Diehl[1], M.B. Goldhaber[2], C.D. Taylor[2], H.S. Swolfs[1], *and* C.A. Gent[2]

Abstract

Petrologic and structural observations of stylolites and veinlets in the Cambrian Bonneterre Formation, Lamotte Sandstone, and basal siliciclastic rocks in the Reelfoot Rift indicate that episodes of tectonic activity and fluid-flow events related to ore deposits in southeast Missouri may be genetically related. From the Reelfoot Rift to the Ozark Uplift, these microstructures, including stylolites parallel with stratification and small-scale extensional veinlets normal to both bedding and stylolites, contain authigenic phases of ore affinities. Sulfide-mineral deposition in both horizontal stylolites and vertical microfractures is evidence for mineralizing fluid migration along microstructures and indicates that the Lamotte Sandstone was not solely a homogeneous conduit as envisioned in many models of metals transport.

Detailed petrologic studies of drill-hole samples from the Reelfoot Rift, from the carbonate platform partially buried beneath the Mississippi Embayment northwest of the rift, and from the Ozark Uplift show that stylolite development began early in the diagenetic history of the Cambrian carbonate and siliciclastic sequence and probably continued through Paleozoic time. Extensional veinlets sealed by incremental mineral growth are commonly associated with the stylolites. Petrographic examination indicates that the microstructures have several generations of epigenetic mineral fillings. Multiple deformational events are inferred to have induced the flow of mineralizing fluids in the microstructures.

Manuscript approved for publication October 31, 1991.

[1] U.S. Geological Survey, Box 25046, MS 966, Denver, Colorado 80225.

[2] U.S. Geological Survey, Box 25046, MS 973, Denver, Colorado 80225.

INTRODUCTION

The Reelfoot Rift (fig. 1) has only recently been recognized as a major crustal structure of the southern Midcontinent (Ervin and McGinnis, 1975; Kane and others, 1981; Hildenbrand, 1985). The existence of the Reelfoot Rift was first interpreted from potential-field data as part of studies of the New Madrid Seismic Zone (McKeown and Pakiser, 1982). Recognition that the rift represented a very deep basin prompted the oil industry to conduct an exploration program that included seismic reflection surveys and drilling of deep holes in the upper Mississippi Embayment (Howe and Thompson, 1984).

The Reelfoot Rift adjoins the southeast Missouri lead belts, which are centered around the Middle Proterozoic St. Francois Mountains (fig. 1). Ores in the lead belts are hosted in the Cambrian Bonneterre Formation and, to a lesser extent, the underlying Lamotte Sandstone. Together the lead belts, which consist of the Old Lead Belt and New Lead Belt or Viburnum Trend, represent the largest known concentration of lead in the crust of the Earth (Kisvarsanyi and others, 1983) and contain significant amounts of zinc, copper, and cobalt. The dominance of lead over zinc and the abundance of copper and cobalt are atypical for Mississippi Valley–type (MVT) deposits worldwide (Sangster, 1983). Yet this suite of metals, particularly copper and cobalt, is commonly associated with rift/red-bed sequences (Mitchell and Garson, 1981), and the source for these elements in southeast Missouri may possibly be in the adjacent red and gray feldspathic siliciclastic rocks such as those penetrated by drill holes in the Reelfoot Rift (Hayes, 1985; Kissin, 1988).

A second major ore district, the Illinois-Kentucky fluorspar district, is also spatially, and perhaps genetically,

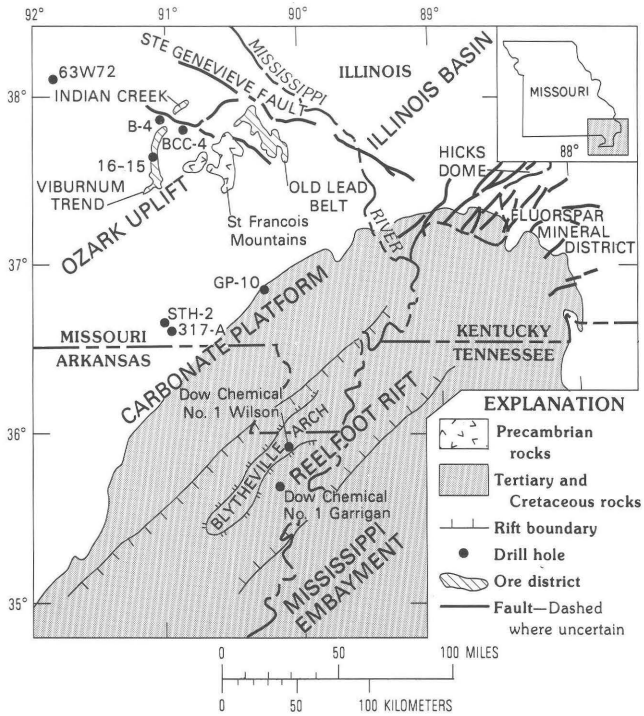

Figure 1. Map showing location of drill holes, structural regions, and ore districts.

related to the Reelfoot Rift. Ore deposits in this district are structurally controlled and hosted by Mississippian-age sedimentary rocks that overlie rocks in the rift to the northeast of the study area (fig. 1). The district is spatially related to the Hicks Dome "cryptovolcano," which contains an underlying breccia enriched in Th, Nb, Y, Be, rare-earth elements, P, Ti, and F. Both alkalic igneous activity responsible for enrichment in this elemental suite and fluorine deposits commonly are rift related (Mitchell and Garson, 1981).

Analyses of cuttings and core from two of the deepest drill holes penetrating into rift-fill sedimentary rocks of the upper Mississippi Embayment provide new information on processes of rock alteration and potentially on the movement of mineralizing fluids. Samples from drill holes in the subsurface carbonate platform northwest of and contiguous with the Reelfoot Rift and samples from drill holes within the lead belt in the Ozark Uplift were analyzed petrographically and geochemically to identify possible flow paths between the rift and the southeast Missouri ore districts. The analyses provide a regional perspective of changes or similarities in the petrologic characteristics of rocks from a basinal-fill environment, onto a carbonate platform, and then to depositional pinchouts against structurally high Precambrian crystalline rocks.

Acknowledgments.—We wish to thank the Missouri Division of Geology and Land Survey, the Arkansas Geological Commission, and Magmont Mines for providing core samples. Allison Palmer (Geological Society of America) and Michael Taylor (U.S. Geological Survey) identified fossils and provided biostratigraphic correlations. Critical reviews by George Breit, Paula Hansley, and Frank McKeown (U.S. Geological Survey) were very helpful. Sulfur isotope analyses were done in the laboratory of R.O. Rye (U.S. Geological Survey).

METHODS

Drill cuttings, core, and junk basket samples used for this study were selected from the Bonneterre Formation, Lamotte Sandstone, and older stratigraphic units in the Reelfoot Rift.

Standard-size thin sections were prepared from the sample suite and stained with potassium ferricyanide, Alizarin Red-S, and sodium cobaltinitrate to identify ferroan carbonate, nonferroan carbonate, and potassium feldspar, respectively. Authigenic minerals, structural fabric, and the paragenetic sequence of minerals were determined by using a petrographic microscope and a Cambridge 250 Mark 2' scanning electron microscope (SEM) equipped with an energy-dispersive X-ray spectrometer.

Samples from the Dow Chemical No. 1 Wilson and No. 1 Garrigan drill holes (fig. 2) were analyzed to determine their elemental and isotopic composition. Elemental analyses were made by using inductively coupled plasma spectroscopy and a LECO sulfur analyzer; sulfur isotope analyses were made by using gas-source mass spectrometry. Results are reported relative to Cañon Diablo troilite (CDT).

STRUCTURAL SETTING OF DRILL HOLES AND DESCRIPTION OF SAMPLES

Reelfoot Rift

The Wilson drill hole is off the shoulder of the Reelfoot Rift, where modern seismicity is relatively low. In contrast, the Garrigan drill hole is in the central part of the rift in the seismically active Blytheville Arch. Samples from both drill holes record episodic extensional deformation which repeatedly reopened fractures that were then sealed by epigenetic mineral cements (Diehl and McKeown, 1989; Diehl and Goldhaber, 1990).

Wilson Drill Hole

The Wilson drill hole (total depth 14,613 ft, 4,454 m) is the deepest drill hole in the Reelfoot Rift that penetrates the Precambrian basement. The basal clastic rocks in this hole are divided into a basal red feldspathic arenite overlain by a gray feldspathic to quartz arenite. From limited

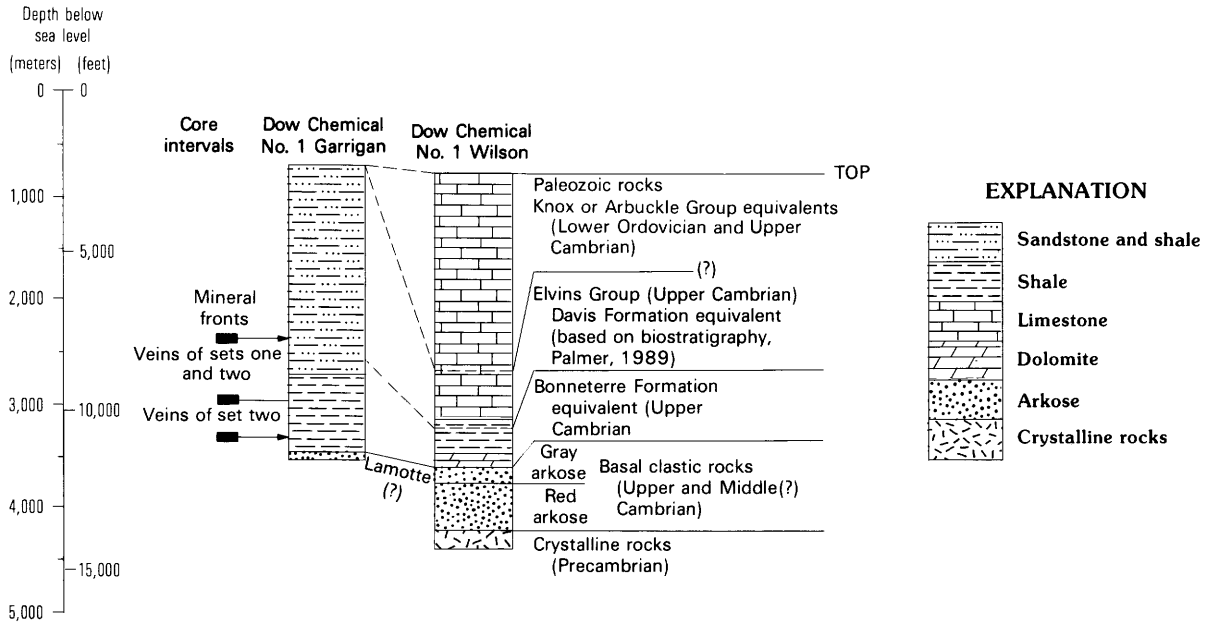

Figure 2. Lithologic logs and stratigraphic correlation of the Dow Chemical No. 1 Wilson and No. 1 Garrigan drill holes in the Reelfoot Rift. Location of drill holes shown in figure 1. Modified from McKeown and others (1990) and Collins and others (1992).

biostratigraphic data, A.R. Palmer (written commun., 1989) interpreted the Bonneterre-Davis Formations equivalent contact to be between 10,800 and 10,920 ft (3,292–3,328 m) (Collins and others, 1992). We believe that the underlying gray feldspathic to quartz arenite may be the equivalent of the Lamotte Sandstone (fig. 2).

In these arenites, siderite and trace amounts of anhydrite, barite, pyrite, and galena are intergranular cements; most of these authigenic minerals are also vein fillings. From 12,600 to 13,900 ft (3,841–4,237 m), an overlapping sequence within veins of early fluid inclusion trails is followed by quartz-sealed veins, then a succession of siderite, dolomite, and ferroan dolomite (table 1). Most of the mineral fillings in the fractures are well laminated and have distinct boundaries between carbonate phases.

Stylolites in this part of the section are parallel with bedding, nonsutured, and wavy and show slickensided clay and offset fractures that are normal to the plane of the stylolite. The stylolites host trace amounts of barite, pyrite, and euhedral epigenetic monazite. Authigenic monazite is also present at Hicks Dome to the northeast in rocks of the fluorspar mineral district of southern Illinois and northwestern Kentucky (fig. 1), but a genetic connection has not been established.

Sulfur isotope data on sulfide minerals (dominantly FeS_2) from the gray arenite are listed in table 2 and plotted as a histogram in figure 3. The data in part overlap with values for main-stage ore minerals in the Viburnum Trend of the southeast Missouri district.

Several inferences may be made based on the crystal habits of the epigenetic minerals. The drusy habit of quartz and siderite in the veinlets suggests precipitation in a fluid-filled fracture (Beach, 1977), and the euhedral monazite suggests hydrothermal fluid flow along the stylolites.

Garrigan Drill Hole

The Garrigan drill hole (total depth 12,038 ft, 3,669 m) bottoms in a quartz and feldspathic arenite that may be equivalent to the Lamotte Sandstone. It should be noted, however, that the entire siliciclastic section above the basement rock in the rift has been informally divided into the "St. Francois formation" and "Reelfoot arkose" by other researchers and is considered older than the Lamotte Sandstone (Weaverling, 1987; Houseknecht, 1989). From biostratigraphic data (Taylor and others, 1991; Collins and others, 1992) (fig. 2), we infer that an overlying sequence of interbedded black shale and siltstone may be equivalent to the Bonneterre Formation or, possibly, to the Elvins Group. This drill hole presents a problem of stratigraphic correlation because the rock types do not correspond to the stratigraphy in the Wilson drill hole or other adjacent drill holes within the rift (McKeown and others, 1990).

A variety of authigenic phases are in horizontal stylolites, vertical carbonate-filled fractures, and gray epigenetic mineral fronts in the Garrigan drill hole (fig. 4). Stylolites occur in swarms, are parallel with bedding, and are commonly deformed (fig. 5). Early diagenetic framboidal pyrite, organic matter, clay minerals, and cerium phosphate minerals (monazite?) are concentrated along these stylolites.

Table 1. Descriptions of some thin sections of microfractures and stylolites in core samples from the Reelfoot Rift, carbonate platform, and Ozark Uplift structural regimes

[Drill-hole locations shown on figure 1. na indicates not applicable. Fractures are normal to bedding; stylolites are parallel with bedding. Minerals are listed in paragenetic sequence]

Drill hole and sample depth (ft)	Structural regime and rock unit	Host rock	Mineral assemblage in fracture	Number of fracture generations	Stylolite amplitude or thickness	Mineral assemblage in stylolite	Remarks
Wilson 12,633	Reelfoot Rift; basal clastic rocks (Lamotte Sandstone?)	Feldspathic arenite	Quartz, siderite, dolomite, ferroan dolomite; clay, hematite	5–7?	na	na	Incremental cracking and resealing of fractures.
Wilson 12,782	Reelfoot Rift; basal clastic rocks	Quartzarenite	Quartz, dolomite, chlorite, minor pyrite	3–4?	0.1–0.4-mm-thick seam	Minor pyrite, barite, monazite, organic matter	Tension gashes associated with stylolites are offset.
Wilson 13,649	Reelfoot Rift; basal clastic rocks	Feldspathic arenite	Dolomite, illitic clay, quartz, hematite	3	0.4–0.6-mm-thick seam	Minor pyrite, monazite, organic matter	Incremental cracking and resealing of fractures.
Garrigan 8,000	Reelfoot Rift; Bonneterre(?) Formation	Siltstone, black shale	Quartz, siderite, ferroan dolomite, ferroan calcite	4	0.9-mm-thick seam	Siderite, illitic clay, thorite, sphalerite, pyrite	Stylolite is layered, deformed.
Garrigan 11,420	Reelfoot Rift; Bonneterre(?) Formation	Black shale, siltstone	Quartz, chlorite, dolomite, ferroan dolomite, ferroan calcite	5	2.6–3.0-mm-thick seam	Calcium phosphate, illitic clay, minor pyrite	Incremental cracking and resealing of fractures; thrust zone.
GP–10 1,817.2	Carbonate platform; Bonneterre Formation	Silty dolostone	Marcasite, brecciated marcasite, pyrite, marcasite	3–4?	0.6–2.0-mm-thick seam	Marcasite, brecciated marcasite, pyrite, marcasite	Tension gashes associated with stylolites; brecciation between periods of sulfide deposition.
GP–10 2,654.4	Carbonate platform; Lamotte Sandstone	Litharenite	Dolomite	1	0.2–1.0-mm-thick seam	Illitic clay, pyrite, minor stannite	Illitic clay has horizontal slickensides showing thrust movement.
GP–10 2,671.1	Carbonate platform; Lamotte Sandstone	Silty limestone, litharenite	na	na	0.6-mm-thick seam	Illitic clay, pyrite, monazite, barite, iron-manganese oxides, calcium phosphate	None.
STH–2 2,700	Carbonate platform; Lamotte Sandstone	Quartzarenite	Dolomite, pyrite	2?	na	na	Quartz grains have undulatory extinction.

Table 1. Descriptions of some thin sections of microfractures and stylolites in core samples from the Reelfoot Rift, carbonate platform, and Ozark Uplift structural regimes—Continued

Drill hole and sample depth (ft)	Structural regime and rock unit	Host rock	Mineral assemblage in fracture	Number of fracture generations	Stylolite amplitude or thickness	Mineral assemblage in stylolite	Remarks
317–A 2,474	Carbonate platform; Lamotte Sandstone	Quartzarenite	na	na	1.0–2.4-mm-thick seam	Illitic clay, pyrite, carbonate, organic matter	Stylolites are layered, deformed.
B–4 1,349	Ozark Uplift; Lamotte Sandstone	Quartzarenite	na	na	0.9–3.7-mm-thick seam	Major pyrite	Colloform texture of sulfides in stylolites.
BCC–4 1,284	Ozark Uplift; Lamotte Sandstone	Quartzarenite	na	na	0.4–1.0-mm-thick seam	Major pyrite	Colloform texture of sulfides in stylolites.
BCC–4 1,482.5	Ozark Uplift; Lamotte Sandstone	Quartzarenite	na	na	2.4–4.8-mm-thick seam	Major pyrite	Pyrite brecciated along stylolite.
BCC–4 1,509.5	Ozark Uplift; Lamotte Sandstone	Quartzarenite	na	na	<0.1-mm-thick seam; 0.2 mm amplitude	Pyrite	Poikilitic carbonate enclosing detrital clay on surfaces of quartz grains indicates fluctuation in static water level.
16–15 917.9	Ozark Uplift; Bonneterre Formation	Silty limestone	na	na	0.5–1.0 mm amplitude	Pyrite, chalcopyrite, galena	Galena deformed along stylolites; clay has horizontal slickensides.

Table 2. Compilation of sulfur isotope data from the Garrigan and Wilson drill holes

[Drill-hole locations shown in figure 1. $\delta^{34}S$ in per mil]

Depth (ft)	$\delta^{34}S$	Description
Dow Chemical No. 1 Garrigan		
7,975	26.6	Pyrite in mineral front.
7,977	25.9	Pyrite in laminated shale associated with mineral front.
7,980.25	30.9	Pyrite in mineral front.
7,986	12.4	Pyrite in black shale.
7,992.5	23.8	Pyrite in mineral front.
7,993.1	27.6	Pyrite in stylolite crosscut by carbonate-filled fracture.
7,998	28.6	Shale with visible pyrite.
10,210.6	18.4	Total sulfur from ground core.
10,225.3	16.2	Total sulfur from ground core.
11,405.8	0	Total sulfur from ground core.
11,420	1.2	Total sulfur from ground core.
11,420.8	6.7	Total sulfur from ground core.
Dow Chemical No. 1 Wilson		
12,300–12,600	27.6	Pyrite-rich gray arenite; bulk rock sample
12,300–12,600	17.1	Heavy liquid concentrate containing pyrite from gray arenite; bulk rock sample

Sphalerite is present both as a residual mineral in these deformed stylolites and as an epigenetic mineral associated with late-stage carbonate precipitation. Trace amounts of thorite are within the layers of clay minerals and organic matter in the deformed stylolites; however, it has not been determined if the thorite is residual or epigenetic.

Carbonate-filled veins are essentially vertical, commonly doubly terminated, or bounded against horizontal stylolites or shaley interbeds, or dispersed into the mineral fronts (fig. 4). The lateral extent of these veins is not known, but they extend the full 10-cm diameter of the core. Azimuths of the veins measured by Swolfs and others (1990) in a section of oriented core, from 7,973 to 8,002 ft (2,430–2,439 m) depth, form two sets (fig. 6). Set one is oriented N. 41° E., subparallel with the rift axis. Set two is oriented N. 35° W., subperpendicular with the rift axis.

Crosscutting relationships indicate that veins of set two are older than those of set one. Set one veins, which are only in the siltstone beds, may have formed during a prolonged period of extension (Swolfs, 1991). Set two veins, present in the siltstone beds and underlying shale sequence, extend over a greater vertical interval (3,000 ft, 914 m) and may have formed during deformation of regional extent (Swolfs and others, 1990).

From the edges of the set one veins toward their centers, the mineral coatings consist successively of drusy quartz, siderite, ferroan dolomite, then ferroan calcite (fig. 7). The ferroan dolomite and ferroan calcite are optically continuous, in contrast to laminated mineral crusts having distinct phase boundaries in fractures in the Wilson and other drill holes outside of the seismically active zone. The only sulfide mineral recognized in fractures of the Garrigan drill hole is trace amounts of cubic pyrite.

Both set one and set two veins are crosscut by epigenetic mineral fronts (fig. 4) that represent reduced zones superimposed on more oxidized host rock as evidenced by elevated sulfur content; total sulfur ranges from less than 0.01 weight percent sulfur in "barren" host rock to as much as 1.05 weight percent sulfur in the mineral fronts (figs. 4, 8). The pyrite in the mineral fronts is euhedral and coarse grained and is unlike early diagenetic framboidal pyrite.

In addition, the isotopic systematics of epigenetic pyrite are unlike those of diagenetic pyrite (table 2, fig. 3). The epigenetic pyrite is isotopically heavy. Several of the values are even heavier than main-stage sulfide in the Viburnum Trend; however, at isotopic equilibrium, FeS_2 is 2–5 percent heavier than ZnS/PbS forming from the same H_2S source. In addition to the sulfur enrichment, metals are also enriched. A positive correlation exists between the epigenetic sulfide sulfur and the concentration of lead and cobalt in the mineral fronts (fig. 9). Furthermore, several elements of affinity to ore-forming processes have been identified in mineral fronts

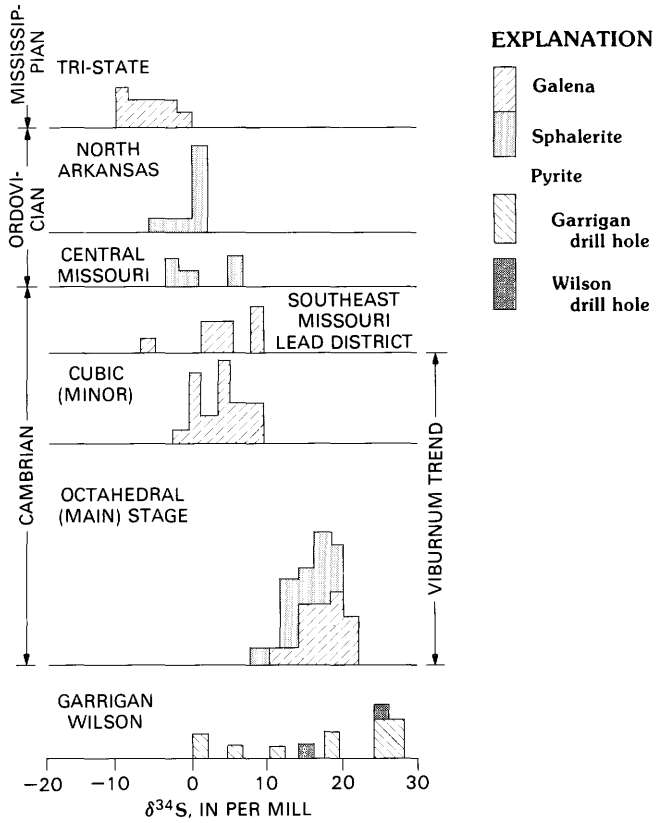

Figure 3. Sulfur isotope values for samples from the Dow Chemical No. 1 Garrigan and No. 1 Wilson drill holes in the Reelfoot Rift are heavy, similar to those for octahedral main-stage sulfide minerals in various ore districts. Location of drill holes shown in figure 1.

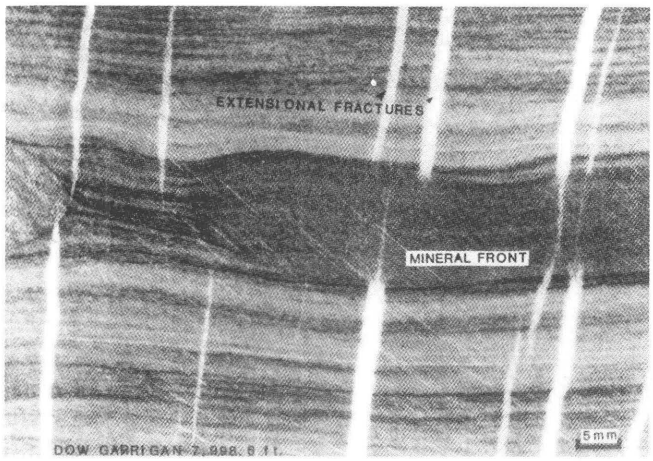

Figure 4. Carbonate-filled veinlets are vertical, commonly double terminating or bounded against stylolites, shaly interbeds, or epigenetic mineral fronts. Dow Chemical No. 1 Garrigan drill hole, depth 7,998.6 ft (2,438.0 m) (location shown in figure 1).

by using SEM—Au, Ag, Cr, Cu, Ni, Pb, Zn, and rare-earth elements. Chromium and nickel are associated with authigenic iron-rich clays, gold and silver with authigenic albite, and sphalerite and galena as mineral coatings on ferroan calcite. The enrichment of sulfur and metals in the mineral fronts suggests a relationship between mineral-front genesis and at least local migration of metalliferous fluids in the rift.

Several generations of diagenetic cement fillings in the fractures predate the mineral fronts; however, the introduction of mineralizing solutions may have caused reopening of earlier quartz- and siderite-filled fractures because ferroan calcite is present in the mineral fronts and as the last diagenetic cement in the fractures (Diehl and Goldhaber, 1990; Diehl and others, 1990). The incremental growth of minerals in the fractures matches the succession of authigenic minerals that form pore-filling cements. Bulk-rock X-ray diffraction of a mineral front versus a barren zone shows that siderite and ferroan dolomite pore-filling cements are prevalent in the unaltered barren zones, whereas calcite is more abundant in the mineral fronts.

Carbonate Platform

Drill-holes GP–10, STH–2, and 317–A are in the regional carbonate platform that borders the Reelfoot Rift to the northwest (Palmer, 1989; Diehl and Goldhaber, 1990) (fig. 1). This platform is partially buried beneath Cretaceous sedimentary rocks that fill a southwest-plunging syncline known as the Mississippi Embayment (Stearns and Marcher, 1962). Stylolites and associated fractures form lateral and vertical permeable channels in the deeply buried Cambrian Bonneterre Formation and underlying Lamotte Sandstone (table 1).

GP–10 Drill Hole

Drill-hole GP–10 penetrates through the Cretaceous overburden at the edge of the embayment and into Cambrian-age sedimentary rocks. Stylolites in the Bonneterre Formation in this drill hole are layered by successive events of mineral precipitation, with intervening periods of dissolution and tectonic movement (table 1). For example, at 1,817.2 ft (554 m), the genetic sequence can be interpreted as follows: (1) early marcasite fills the sockets in a stylolite, (2) marcasite is brecciated by a tectonic event, (3) because of deformation the stylolite is opened to fluid flow, (4) pyrite precipitates from the fluid, and (5) marcasite is again deposited (fig. 10).

In the underlying Lamotte Sandstone, copper and tin sulfide minerals, probably stannite, precipitated along the

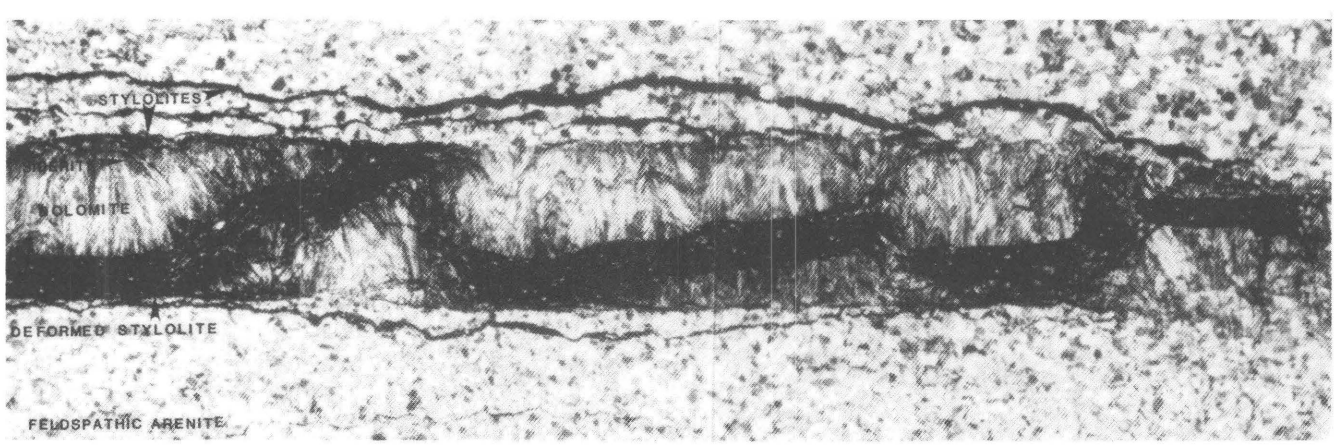

Figure 5. A reversal of stress orientation has caused the normally ductile stylolite-filling material to break in a brittle manner. This deformation, which may be due to overpressure conditions or a paleoearthquake, opened permeable channels for mineralizing solutions. Dow Chemical No. 1 Garrigan drill hole, depth 7,999.9 ft (2,438.5 m) (location shown in figure 1).

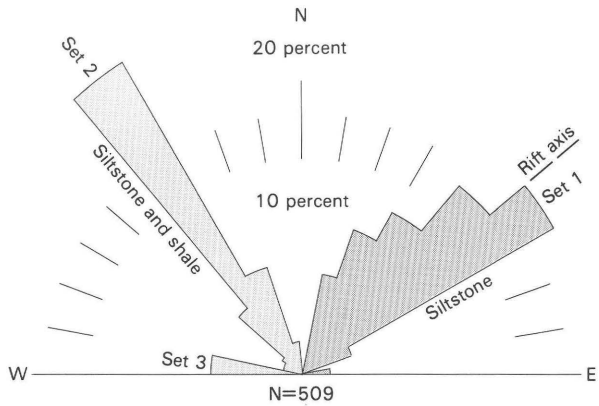

Figure 6. Two sets of fracture attitudes are in core from the Dow Chemical No. 1 Garrigan drill hole. Set one is parallel with the rift axis, and set two is perpendicular to the rift axis. These fracture attitudes match fracture orientations in the fluorspar mineral district (T.S. Hayes and L.W. Snee, oral commun., 1991).

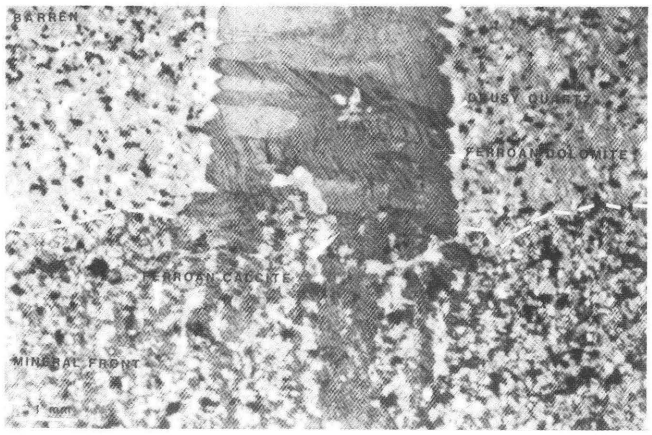

Figure 7. Closeup view of fracture shown in figure 4. The fracture disperses in the mineral front. Ferroan calcite is the last mineral to precipitate in both the mineral front and the fracture.

stylolites. Copper mineralization in this drill hole seems to be confined to stylolites in the Lamotte Sandstone.

STH–2 Drill Hole

Drill-hole STH–2 is also on the carbonate platform. Healed vertical fractures contain pyrite and dolomite but do not demonstrate multiple episodes of extensional movement (table 1). In general, cores from Cambrian strata away from the Reelfoot Rift show less evidence of the tectonic episodes that produced multiple sets of vertical fractures within the rift.

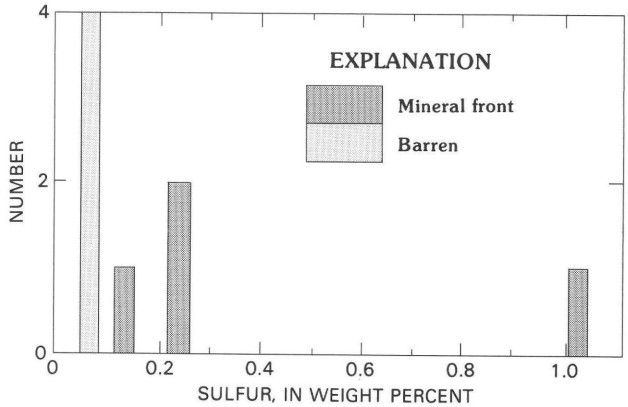

Figure 8. Total sulfur contents are elevated in the diagenetic mineral fronts, from ≤0.01 weight percent sulfur in barren host rock to as much as 1.05 weight percent sulfur in the mineral fronts.

317–A Drill Hole

Although the number of extensional microfracture reactivations decreases northwest from the rift, stylolites continue to record multiple precipitation and deformation events in the Lamotte Sandstone and in carbonate rocks on the platform (fig. 11). In drill-hole 317–A, stylolites are zoned with layers of clay, organic matter, and carbonate minerals (table 1). Right-angle shearing of normally ductile residual material concentrated in stylolites is common. Each deformation feature observed in a stylolite may not be due to the same tectonic event, but each can be related to the introduction of a mineralizing fluid.

Ozark Uplift

Structurally controlled lead-zinc ore deposits surround Precambrian granite knobs of the St. Francois Mountains (Ohle and Brown, 1954) (fig. 1). Ore deposits of this type are present in both the Old and New Lead Belts. Ore minerals, particularly in the Old Lead Belt, are concentrated along stylolitic zones, especially in compactional breccias (Tarr, 1936; Ohle, 1985; Hayes and others, 1989).

16–15 Drill Hole

Drill-hole 16–15 is within the Viburnum Trend in the Ozark Uplift (fig. 1). Ore mineralization is common along clay-filled stylolites throughout the dolomitized Bonneterre Formation in this drill hole. Slickensides are abundant in the residual clay that fills the stylolites. As clay-lined stylolites underwent slippage, galena deformed ductilely along

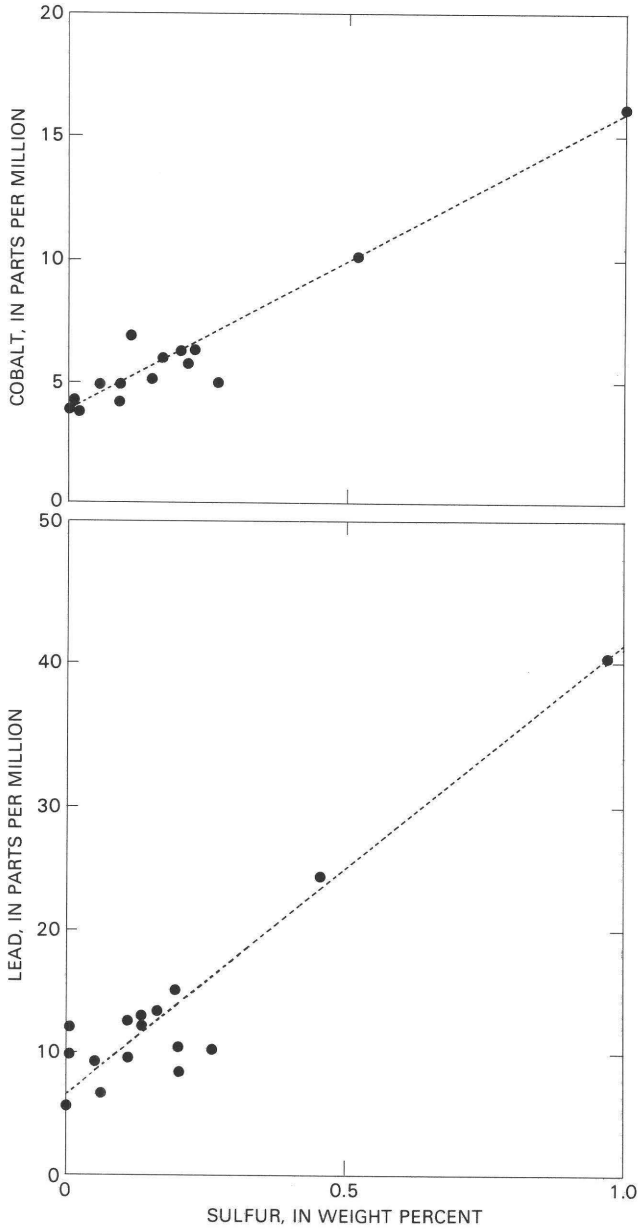

Figure 9. Several trace elements, including lead and cobalt, positively correlate with sulfide sulfur in mineral fronts in the Dow Chemical No. 1 Garrigan drill hole. This correlation may imply that these elements were introduced during the sulfidization event.

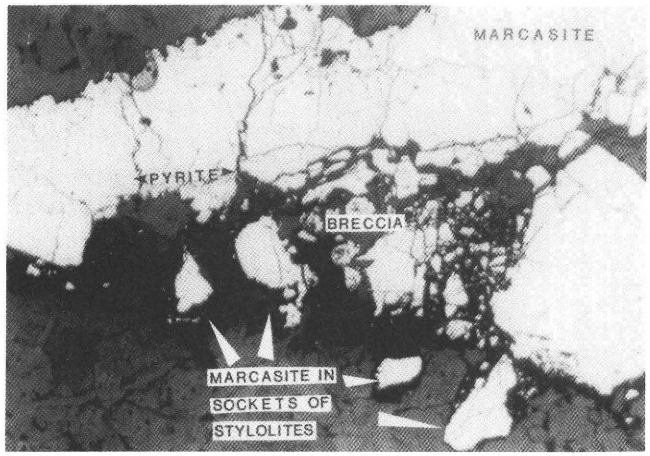

Figure 10. Sequential precipitation and brecciation of marcasite and pyrite along a stylolite indicates that stylolites were active sites for both the deposition and dissolution of minerals. Drill-hole GP–10, depth 1,817.2 ft (553.9 m) (location shown in figure 1).

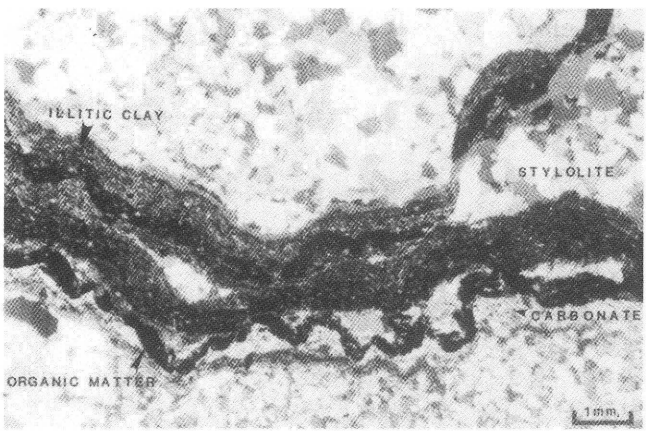

Figure 11. Layering of mineralization in a deformed stylolite. Note the right-angle shearing. Drill-hole 317–A, depth 474 ft (144.5 m) (location shown in figure 1).

cleavage planes rather than undergoing brittle failure because it is a softer mineral than pyrite or marcasite. The deformed galena encloses and partly replaces pyrite and chalcopyrite (fig. 12, table 1).

B–4 and BCC–4 Drill Holes

In drill-holes B–4 and BCC–4, north of the St. Francois Mountains (fig. 1), sulfide minerals along stylolites show similar alternating mineral precipitation and deformation fabric similar to that observed in other cores (table 1). For example, sulfides in stylolites in drill-hole B–4 are brecciated, similar to those in drill-hole GP–10. The breccia fragments are very angular and internally fractured.

Stylolites or pressure solution seams in drill-hole BCC–4 are lined with pyrite. Quartz grains along the stylolite boundaries are partly dissolved, whereas remnant intergranular pyrite is not (fig. 13). Parallel sets of pyrite-filled stylolitic seams are present repetitively throughout the drill hole. Well-developed geopetal structures that suggest development in a vadose environment (Walker and others, 1978) are detrital clay minerals on the upper surfaces of quartz grains

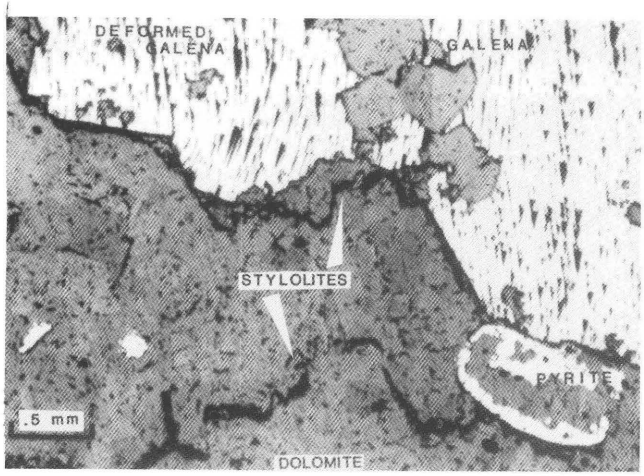

Figure 12. Black triangular pits are curved cleavage planes in galena, possibly due to ductile deformation along a stylolite. Slickensided clay in stylolites show thrust movement. Drill-hole 16–15, depth 915 ft (278.9 m) (location shown in figure

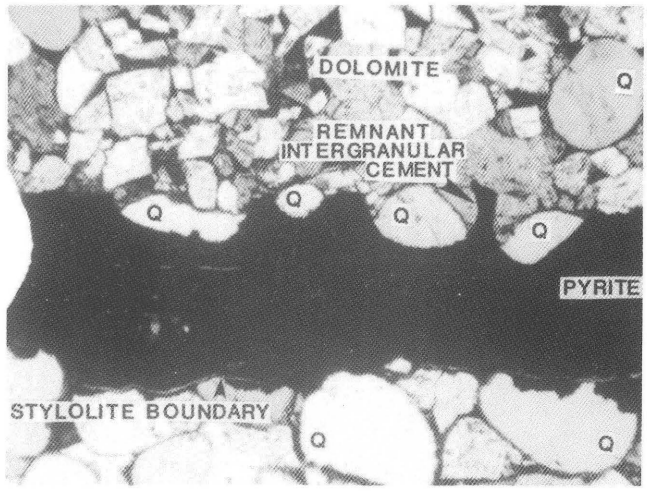

Figure 13. Quartz grains have been partially dissolved along a stylolitic boundary either by pressure solution or introduction of an acidic fluid; however, pyrite has been unaffected. Remnant "arms" of intergranular pore-filling pyrite remain above the partially dissolved quartz grains. Drill-hole BCC–4, depth 1,284 ft (391.4 m) (location shown in figure 1).

and pendant quartz cement. Later cementation of these geopetal structures by sparry calcite indicates precipitation in a phreatic environment.

The development of the pyrite-filled stylolitic seams probably was related to a fluctuation of static water level. The change in relative position of the static water level could have occurred through a change in recharge rates that was climatically controlled or through tectonic movement such as the rotation of fault blocks.

DISCUSSION

Microstructures and Mineralization

Nonsutured low-amplitude stylolites are commonly layered with a variety of minerals. The mineral layers consist of (1) residual clay minerals and organic matter, (2) authigenic carbonate minerals and quartz, and (3) both residual and epigenetic iron sulfide minerals. These stylolites are weak surfaces, susceptible to deformation during tectonic movement. The presence of slickensided clay in stylolite seams and brecciated layers is evidence for bedding-parallel slip that indicates changes in stress orientation during or subsequent to the formation of the stylolite. The breccia is interpreted to be tectonic in origin and not a result of simultaneous precipitation and dissolution along the stylolite. Tectonically deformed stylolites commonly contain barite, monazite, pyrite, marcasite, thorite, and sphalerite. The probable epigenetic origin of these minerals suggests that the stylolites are not just pressure solution features but are also active sites for fluid flow and precipitation of minerals.

Vertical, intergranular, mineral-healed veinlets are associated with stylolites and are commonly offset along the stylolite surfaces. The veinlets or fractures probably are extensional in origin, possibly due to tectonic stretching of the layered sedimentary rocks. Structurally controlled fluid flow through these veinlets is indicated by repeated opening and resealing of fractures by successive generations of quartz, barite, siderite, dolomite, clay, calcite, and pyrite. Both the number of vein generations and the number of epigenetic minerals filling those veins are greatest in the Reelfoot Rift and decrease in frequency to the northwest across the carbonate platform and into the Ozark Uplift. This trend may indicate an association between the formation of fractures, fluid movement in the rift, and local seismic activity.

Sulfide mineralization in the stylolites and microfractures demonstrates that these microstructures existed as metal-bearing fluid-flow paths in the Lamotte Sandstone and Bonneterre Formation. Although we are not necessarily observing the same deformational event along stylolites in the Reelfoot Rift and the Ozark Uplift, each deformation event recorded in the stylolites and associated fractures can be related to an introduction of mineralizing fluids.

Epigenetic mineral fronts in rift sedimentary rocks demonstrate at least local migration of ore-bearing fluids. That fluid migration, combined with similarities in heavy sulfur isotopes in sulfide minerals in the rift and Ozark Uplift, suggests that ore-bearing fluids may have passed through the rift sedimentary rocks onto the carbonate platform and into the Ozark Uplift. This supports the general concept of the rift as a flow path for ore-bearing fluids.

Other lines of evidence also suggest that ore-bearing fluids that formed the ore districts originated in or passed through the Reelfoot Rift.

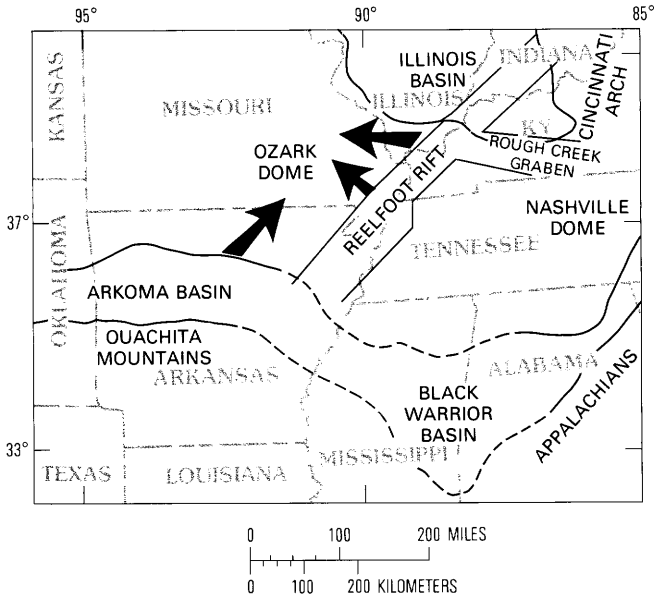

Figure 14. The Appalachian and Ouachita foldbelts may have created a hydraulic head through topographic relief in the Late Pennsylvanian to Early Permian that influenced the flow of hot brines north and northwest (bold arrows) to form the Mississippi Valley–type deposits (Leach and Rowan, 1986). Dates for mineralization in the lead-zinc districts overlap with timing of the Ouachita tectonism. Heavy lines are province boundaries; dashed lines indicate projections of boundaries beneath sediments of Mississippi Embayment.

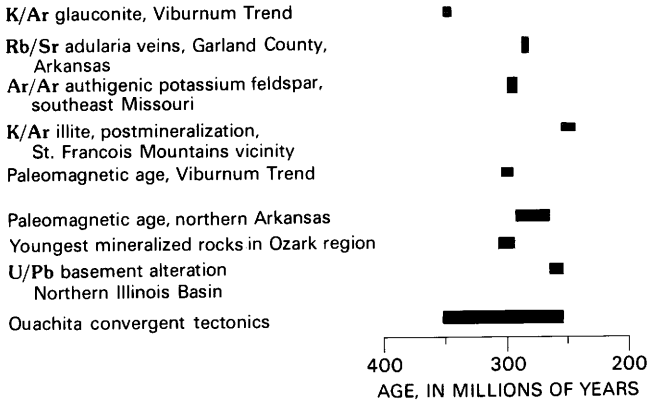

Figure 15. Authigenic minerals and their ages in relation to the timing of Mississippi Valley–type ore deposition (Posey and others, 1983; Rothbard, 1983).

1. Lead, zinc, and copper are enriched in acid-insoluble residues derived from Cambrian platform carbonate rocks in the area between the ore districts and Reelfoot Rift (Erickson and others, 1988; M.B. Goldhaber, unpub. data).

2. Authigenic potassium feldspar is widespread in the Lamotte Sandstone. A broad zone of dissolution of these overgrowths in the Lamotte Sandstone adjacent to the northwest boundary of the rift suggests that an acidic fluid, spatially related to the rift, was responsible for the dissolution. An acidic pore fluid would have also been capable of carrying metals and H_2S in solution (Diehl and others, 1989).

3. Sulfur isotope data for epigenetic sulfide minerals in Cambrian arenites in the rift are similar to data for mainstage-mineralized rocks in the Viburnum Trend (fig. 3).

Mechanisms for Fluid Migration

Models proposed to induce flow of metal-bearing brine fluids include gravity-driven, compaction-driven, and seismic-pumping mechanisms (Bethke, 1985; Leach and Rowan, 1986; Clendenin and Duane, 1990). Leach and Rowan (1986) postulated that the Ouachita orogeny may have created a hydraulic gradient through topographic relief that influenced the flow of hot brines from the Arkoma Basin northward to the Ozark region to form the Mississippi Valley–type deposits (fig. 14). Their interpretation is supported by dates for mineralization in the lead-zinc districts that overlap with the timing of Ouachita tectonism (fig. 15). Arguments for the hydraulic gradient theory are based primarily on a regional study of fluid inclusions and inferred homogenization temperatures as a function of distance from the Ouachita front. We do not yet have data on fluid inclusions in samples from the Reelfoot Rift and carbonate platform, but our geochemical, isotopic, petrographic, and microstructural data support the concept that ore fluids may have originated or migrated through the deep basins associated with the Reelfoot Rift (McKeown and others, 1990).

Numerical models of compaction-driven flow by Bethke (1985) indicate that compaction may induce the migration of ore-bearing brines but that velocities were too low to have a causal effect on the formation of the Mississippi Valley–type ores. Gravity-driven flow is the most likely mechanism but requires topographically high areas around the Ozarks. Both the Ouachita and Appalachian foldbelts, which were initiated in the Late Mississippian and Early Pennsylvanian and reached their greatest development during the Late Pennsylvanian to Permian, have been suggested as topographically high areas during the late Paleozoic. Other structurally high areas in the late Paleozoic were the Pascola Arch and probably the contiguous Blytheville Arch (McKeown and others, 1990). On the basis of restoration of the stratigraphic section in the Pascola area, Stearns and Marcher (1962) estimated that at least 2.5 km and as much as 4.5 km of rocks were eroded from the arch before Late Cretaceous subsidence. The actual relief of any postulated topographic high area during the late Paleozoic cannot be estimated, however, with any reasonable validity. The postulated topographic high areas are reasonable, but any one or all may have caused separate gravity-driven hydrologic-flow systems.

The Reelfoot Rift is today a seismically active area and was also active at times in the geologic past. Some researchers have advocated seismic pumping (or suction pumping) as

an alternative fluid-drive mechanism (Clendenin and Duane, 1990; Sibson, 1990). Seismic pumping probably had very local effects confined to the rift interior as indicated by the decrease away from the rift axis of the complexity of fractures and the number of generations of minerals filling fractures in Cambrian deposits (table 1). Events such as earthquakes and nuclear explosions produce compressional waves that cause fluid- pressure disturbances in aquifers.

Regional Fracture Patterns

A key in any argument attempting to relate ore-forming processes in southeast Missouri and the structural fabric of rift sediments presented here concerns the relative timing of mineral precipitation in the two areas. At present, we cannot establish a direct timing link, but indirect evidence implies a relationship. Fracture azimuths measured in the Garrigan drill hole in the Reelfoot Rift (fig. 6) are subparallel with those observed in the Illinois-Kentucky fluorspar district, northeast of the rift (fig. 1). Mica from peridotite dikes filling fractures whose directions are close to set two of figure 6 has been dated at 275 Ma (Zartman, 1977). Mineralization filling fractures whose orientations are subparallel with set one (fig. 6) has recently been dated at 200–240 Ma (T.S. Hayes and L.W. Snee, oral commun., 1991). If the similarity in fracture direction in the two parts of the rift indicates a similarity in time of formation, then inspection of figure 15 indicates that the epigenetic phases described here could have formed at the time of Mississippi Valley–type ore genesis.

SUMMARY

Based on our observations in southeast Missouri and northeast Arkansas, stylolites and fractures acted as fluid-flow conduits throughout the subsurface, and mineralization accompanied deformation events recorded in these microstructures. Another implication of our work is that the Lamotte Sandstone and the underlying siliciclastic units, informally referred to as the Reelfoot arkose in the rift (Houseknecht, 1989), may not have acted as homogeneous aquifers for migrating fluids. Evidence in these rocks suggests microstructural control of fluid flow, as well as intergranular flow through pore space.

REFERENCES CITED

Beach, A., 1977, Vein arrays, hydraulic fractures and pressure-solution structures in a deformed flysch sequence, S.W. England: Tectonophysics, v. 40, p. 201–225.

Bethke, C.M., 1985, A numerical model of compaction-driven groundwater flow and heat transfer and its application to the paleohydrology of intracratonic sedimentary basins: Journal of Geophysical Research, v. 90, no. B8, p. 6817–6828.

Clendenin, C.W., and Duane, M.J., 1990, Focused fluid flow and Ozark Mississippi Valley–type deposits: Geology, v. 18, p. 116–119.

Collins, D.S., Taylor, M.E., Repetski, J.E., and Palmer, A.R., 1992, New sedimentologic and paleontologic data for the Dow Chemical #1 B.L. Garrigan drill hole, Mississippi County, Arkansas: U.S. Geological Survey Open-File Report 92–6.

Diehl, S.F., and Goldhaber, M.B., 1990, Microstructures in the Cambrian Bonneterre Formation and Lamotte Sandstone of southeast Missouri—Sulfide occurrence in stylolites and extensional microfractures [abs.], *in* Thorman, C.H., ed., Workshop on Application of Structural Geology to Mineral and Energy Resources of the Central Region: U.S. Geological Survey Open-File Report 90–0508, p. 2–5.

Diehl, S.F., Goldhaber, M.B., and Mosier, E.L., 1989, Regions of feldspar precipitation and dissolution in the Lamotte Sandstone, Missouri—Implications for MVT ore genesis [abs.], *in* U.S. Geological Survey–Missouri Geological Survey Symposium; Mineral-Resource Potential of the Midcontinent, program and abstracts: U.S. Geological Survey Open-File Report 89–169, p. 5–7.

Diehl, S.F., Goldhaber, M.B., and Taylor, C.D., 1990, Trace mineralization in Late Cambrian Reelfoot rift sediments—Dow Chemical #1 Garrigan drill hole, Mississippi County, Arkansas: Geological Society of America, Abstracts with Programs, p. A137.

Diehl, S.F., and McKeown, F.A., 1989, Diagenesis and structural fabric of Cambrian basal clastics—The Dow Chemical #1 Wilson drill hole, Mississippi County, Arkansas: Geological Society of America, Abstracts with Programs, p. A349.

Erickson, R.L., Chazin, B., Erickson, M.S., Mosier, E.L., and Whitney, H., 1988, Tectonic and stratigraphic control of regional subsurface geochemical patterns, Midcontinent, U.S.A.: North American Conference on Tectonic Control of Ore Deposits and the Vertical and Horizontal Extent of Ore Systems, University of Missouri-Rolla, Proceedings, p. 435–446.

Ervin, C.P., and McGinnis, L.D., 1975, Reelfoot rift—Reactivated precursor to the Mississippi Embayment: Geological Society of America Bulletin, v. 86, p. 1287–1295.

Hayes, T.S., 1985, A model for genesis of red-bed-evaporite-associated stratabound copper deposits and potential within the Springfield 1°×2° Quadrangle and surrounding areas, *in* Martin, J.A., and Pratt, W.P., eds., Geology and mineral resource potential of the Springfield 1°×2° Quadrangle, Missouri, as appraised in September, 1985: U.S. Geological Survey Bulletin 1942, p. 95–101.

Hayes, T.S., Palmer, J.R., and Rowan, E.L., 1989, Correlation of hydrothermal dolomite generations across the Mississippi Valley–type mineralizing system of the Ozark region: U.S. Geological Survey Open-File Report 89–169, p.12–13.

Hildenbrand, T.G., 1985, Rift structure of the northern Mississippi Embayment from the analysis of gravity and magnetic data: Journal of Geophysical Research, v. 90, p. 12607-12622.

Houseknecht, D.W., 1989, Earliest Paleozoic stratigraphy and facies, Reelfoot Basin and adjacent craton, *in* Gregg, J.M., Palmer, J.R., and Kurtz, V.E., eds., Field guide to the Upper Cambrian of southeastern Missouri—Stratigraphy, sedimentology, and economic geology: University of Missouri-Rolla, p. 25–42.

Howe, J.R., and Thompson, T.L., 1984, Tectonics, sedimentation, and hydrocarbon potential of the Reelfoot rift: Oil and Gas Journal, Nov. 12, p. 179–190.

Kane, M.F., Hildenbrand, T.G., and Hendricks, J.D., 1981, Rift structure of the northern Mississippi Embayment from the analysis of gravity and magnetic data: Journal of Geophysical Research, v. 90, no. B14, p. 12607–12622.

Kissin, S.A., 1988, Nickel-cobalt-native silver (five-element) veins—A rift-related ore type: North American Conference on Tectonic Control of Ore Deposits and the Vertical and Horizontal Extent of Ore Systems, University of Missouri-Rolla, Proceedings, p. 268–279.

Kisvarsanyi, G., Grant, S.K., Pratt, W.P., and Koenig, J.W., 1983, International Conference on Mississippi Valley–type Lead-Zinc Deposits: University of Missouri-Rolla, Proceedings, 596 p.

Leach, D.L., and Rowan, E.L., 1986, Genetic link between Ouachita foldbelt tectonism and the Mississippi Valley–type lead-zinc deposits of the Ozarks: Geology, v. 14, p. 931–935.

McKeown, F.A., Hamilton, R.M., Diehl, S.F., and Glick, E.E., 1990, Diapiric origin of the Blytheville and Pascola arches in the Reelfoot rift, east-central United States—Relation to New Madrid seismicity: Geology, v. 18, p. 1158–1162.

McKeown, F.A., and Pakiser, L.C., 1982, Investigations of the New Madrid, Missouri, earthquake region: U.S. Geological Survey Professional Paper 1236, 201 p.

Mitchell, A.H.G., and Garson, M.S., 1981, Mineral deposits in global tectonic settings: London, Academic Press, 405 p.

Ohle, E.L., 1985, Breccias in Mississippi Valley–type deposits: Economic Geology, v. 80, p. 1736–752.

Ohle, E.L., and Brown, J.S., 1954, Geologic problems in the southeast Missouri lead district: Geological Society of America Bulletin, v. 65, p. 201–222.

Palmer, J.R., 1989, Late Upper Cambrian shelf depositional facies and history, southern Missouri, *in* Gregg, J.M., Palmer, J.R., and Kurtz, V.E., eds., Field guide to the Upper Cambrian of southeastern Missouri—Stratigraphy, sedimentology, and economic geology: University of Missouri-Rolla, p. 1–24.

Posey, H.H., Stein, H.J., Fullagar, P.D., and Kish, S.A., 1983, Rb-Sr isotope analyses of Upper Cambrian glauconites, southern Missouri—Implications for movement of Mississippi Valley–type ore fluids in the Ozark region, *in* Kisvarsanyi, G., and others, eds., International Conference on Mississippi Valley–type Lead-Zinc Deposits, Proceedings: University of Missouri-Rolla, p. 166-172.

Rothbard, D.R., 1983, Diagenetic history of the Lamotte Sandstone, southeast Missouri, *in* Kisvarsanyi, G., and others, eds., International Conference on Mississippi Valley–type Lead-Zinc Deposits, Proceedings: University of Missouri-Rolla, p. 385–395.

Sangster, D.F., 1983, Mississippi Valley–type deposits—A geologic melange, *in* Kisvarsanyi, G., and others, eds., International Conference on Mississippi Valley–type Lead-Zinc Deposits, Proceedings: University of Missouri-Rolla, p. 7–19.

Sibson, R.H., 1990, Faulting and fluid flow, *in* Short course on fluids in tectonically active regimes of the continental crust: Mineralogical Association of Canada, chap. 4, p. 93–132.

Stearns, R.G., and Marcher, M.V., 1962, Late Cretaceous and subsequent structural development of the northern Mississippi Embayment area: Geological Society of America Bulletin, v. 73, p. 1387–1394.

Swolfs, H.S., 1991, Structural characteristics in the Dow Chemical B.L. Garrigan #1, Mississippi County, Arkansas [abs.], *in* Lowell, G.R., and Clendenin, C.W., eds., Louis Unfer, Jr., Conference on Geology of the Mid-Mississippi Valley Region: Southeast Missouri State University, June 13–14, 1991, Cape Girardeau, Missouri, Missouri Department of Natural Resources Special Report, Proceedings, p. 39–43.

Swolfs, H.S., McKeown, F.A., and Glick, E.E., 1990, Episodes of extension recorded in Cambrian rocks in the Reelfoot Rift, Mississippi Embayment: Eos, v. 71, no. 17, p. 638.

Tarr, W.A., 1936, Origin of the southeastern Missouri lead deposits, part I: Economic Geology, v. 31, p. 712–754.

Taylor, M.E., Collins, D.S., Repetski, J.E., and Palmer, A.R., 1991, Upper Cambrian biostratigraphic correlations in the Reelfoot basin, northeastern Arkansas [abs.], *in* Lowell, G.R., and Clendenin, C.W., eds., Louis Unfer, Jr., Conference on Geology of the Mid-Mississippi Valley Region: Southeast Missouri State University, June 13–14, 1991, Cape Girardeau, Missouri, Missouri Department of Natural Resources Special Report, Proceedings, p. 51–55.

Walker, T.R., Waugh, B., and Crone, A.J., 1978, Diagenesis in first-cycle desert alluvium of Cenozoic Age, southwestern United States and northwestern Mexico: Geological Society of America Bulletin, v. 89, p. 19–32.

Weaverling, P.H., 1987, Early Paleozoic tectonic and sedimentary evolution of the Reelfoot–Rough Creek rift system, midcontinent, U.S.: Columbia, University of Missouri, M.S. thesis, 116 p.

Zartman, R.E., 1977, Geochronology of some alkalic rock provinces in eastern and central United States: Annual Review of Earth and Planetary Sciences, v. 5, p. 257–286.

Chapter B

Tectonic Controls on Deposition and Source-Rock Properties of the Woodford Shale, Anadarko Basin, Oklahoma—Loading, Subsidence, and Forebulge Development

By TIMOTHY C. HESTER, JAMES W. SCHMOKER, and HOWARD L. SAHL

U.S. GEOLOGICAL SURVEY BULLETIN 2012

APPLICATION OF STRUCTURAL GEOLOGY TO MINERAL AND ENERGY RESOURCES OF THE CENTRAL AND WESTERN UNITED STATES

CONTENTS

FIGURES

Tectonic Controls on Deposition and Source-Rock Properties of the Woodford Shale, Anadarko Basin, Oklahoma—Loading, Subsidence, and Forebulge Development

By Timothy C. Hester[1], James W. Schmoker[2], *and* Howard L. Sahl[3]

Abstract

The Woodford Shale (Late Devonian–Early Mississippian) is an organic-rich, highly compacted black shale that is a significant hydrocarbon source rock in the Anadarko Basin of Oklahoma. The Woodford can be subdivided into lower, middle, and upper informal members based on geophysical-log character. Depositional patterns of these three members were shaped by the tectonic evolution of the Southern Oklahoma Aulacogen.

Depositional patterns of the Woodford Shale reveal a positive paleotopographic feature, parallel with and about 75 mi (120 km) north of the Amarillo-Wichita Uplift, that divided the Woodford into northeast and southwest depocenters and was a hinge line separating areas of differential basement movement during Woodford time. Three lines of evidence suggest that the paleotopographic high was tectonically rising before and during a Late Devonian (pre-Woodford) episode of regional erosion and throughout Woodford time: (1) erosional channels on the pre-Woodford unconformity do not cross the axis of the paleotopographic high; (2) the Late Devonian Misener Sandstone, which was deposited on the pre-Woodford unconformity in topographic lows, is not present along the axis of the paleotopographic high; and (3) Woodford sediments thicken from the paleotopographic high toward both the southwest and northeast.

The paleotopographic high can be explained as a forebulge that developed on the basin margin as the direct result of loading and subsidence along the central trough of the Southern Oklahoma Aulacogen. The ratio of basin subsidence to uplift of the paleotopographic high is in reasonable agreement with a theoretical forebulge model. The distance between the paleotopographic high and the load axis of the Southern Oklahoma Aulacogen is comparable to that between the Goodman Swell (a forebulge of the Midcontinent Rift System) and its nearest load axis.

INTRODUCTION

The Woodford Shale is one of several organic-rich black shales of Late Devonian and Early Mississippian age in basins of the North American Craton. If thermally mature, these black shales are economically important as hydrocarbon source rocks. The Woodford Shale is widely regarded as a major source of oil and gas in the Anadarko Basin of Oklahoma (Cardott and Lambert, 1985).

Source-rock properties of the Woodford Shale are dependent on original depositional patterns and subsequent thermal-maturation history. This report describes effects of the tectonic evolution of the Anadarko Basin on depositional and thermal-maturity patterns of the Woodford Shale in the Oklahoma part of the Anadarko Basin (fig. 1). The geologic and structural setting and the depositional and thermal-maturity patterns of the Woodford are reviewed, and then the significance of these patterns and their tectonic implications are discussed.

The data on which conclusions of this report are based are mostly from Hester and others (1990). The present report focuses on relations between tectonic evolution and Woodford sedimentation, rather than on the physical character of the formation, as is emphasized by Hester and others (1990).

GEOLOGIC AND STRUCTURAL SETTING

The Woodford Shale is a highly radioactive, carbonaceous and siliceous, dark-gray to black shale. In terms of geophysical-log character, the Woodford can be generally

[1]U.S. Geological Survey, Box 25046, MS 971, Denver, Colorado 80225.

[2]U.S. Geological Survey, Box 25046, MS 960, Denver, Colorado 80225.

[3]Advantage Resource, Inc., 1775 Sherman Street, Suite 1375, Denver, Colorado 80203.

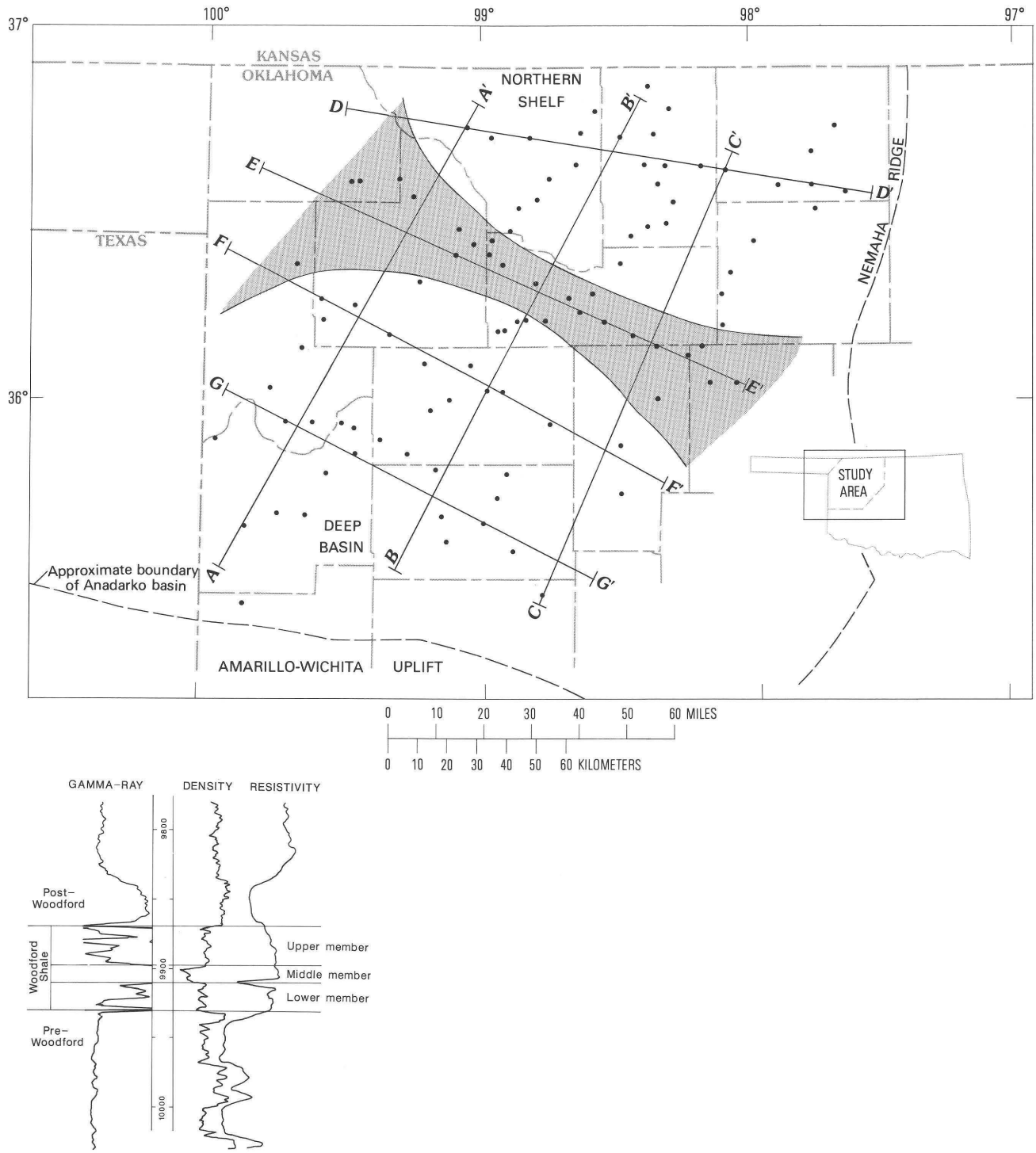

Figure 1. Map showing study area, lines of cross sections, locations of wells (solid circles) used in this study, and major structural features, Anadarko Basin. Log suite shows characteristic signatures of lower, middle, and upper members of Woodford Shale. Modified from Hester and others (1990).

described as two similar shales separated by a less dense, more radioactive, and commonly more resistive middle shale member. For this reason, and to better document variations and regional trends within the Woodford, the formation is considered here in terms of three informal members (Hester and others, 1988)—the lower, middle, and upper members of the Woodford Shale (fig. 1). The primary physical basis for this subdivision is the higher kerogen content of the middle member. Total organic carbon (TOC) calculated from log-derived formation density (Hester and others,

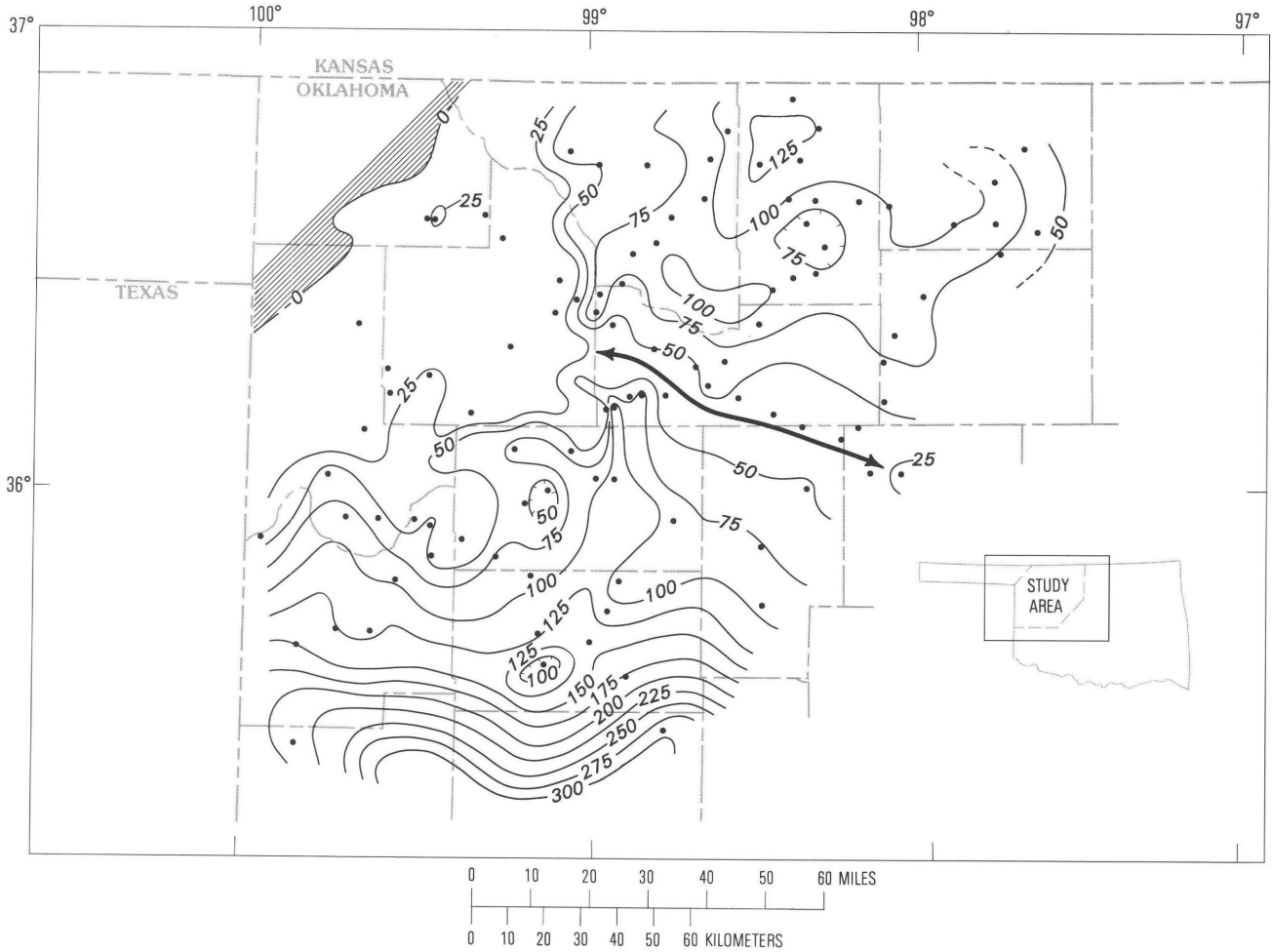

Figure 2. Thickness of Woodford Shale. Heavy line with arrows marks axis of paleotopographic high that separates Woodford into northeast and southwest depocenters. Area where Woodford Shale is absent is hachured. Contour interval 25 ft (7.6 m). Solid circles show locations of wells used in this study. Modified from Hester and others (1990).

1990) averages 3.2, 5.5, and 2.7 weight percent within the study area (fig. 1) for the lower, middle, and upper members of the Woodford Shale, respectively.

The Woodford Shale was deposited on a major regional unconformity developed in Late Devonian time (Amsden, 1975) and is conformably overlain by shale and limestone of Mississippian age. Total thickness of the Woodford ranges from near zero to about 125 ft (40 m) on the northern shelf areas and increases to more than 700 ft (210 m) in limited parts of the deep Anadarko Basin (Amsden, 1975). Maximum thickness in the area of this study is about 300 ft (90 m) (fig. 2).

The Anadarko Basin is a two-stage Paleozoic basin (Perry, 1989). The Woodford was deposited on the predominantly carbonate sediments of the first-stage Southern Oklahoma Aulacogen (Feinstein, 1981). The present-day configuration of the basin, reflected by structure on top of the Woodford (fig. 3), developed primarily during a post-Woodford second-stage episode of foreland-style downwarping.

DEPOSITIONAL PATTERNS

The axis of a positive paleotopographic feature that influenced deposition throughout Woodford time is shown in figure 2. This positive feature, parallel with and about 75 mi (120 km) north of the (post-Woodford) Amarillo-Wichita Uplift, divided the Woodford into southwest and northeast depocenters and was a hinge line separating areas of differential basement movements.

Northeast of the hinge line, the maximum thickness of the lower member of the Woodford is only about 25 ft (8 m). Southwest of the hinge line, toward the deep axis of the southern Oklahoma aulacogen, the lower member thickens to more than 150 ft (46 m). Local thickness variations of the lower member (fig. 4) result from the filling of topographic depressions on the eroded surface of the pre-Woodford unconformity. During deposition of the lower member, the northeastern part of the study area was quite stable as compared to the central trough of the Southern Oklahoma Aulacogen, which was actively subsiding.

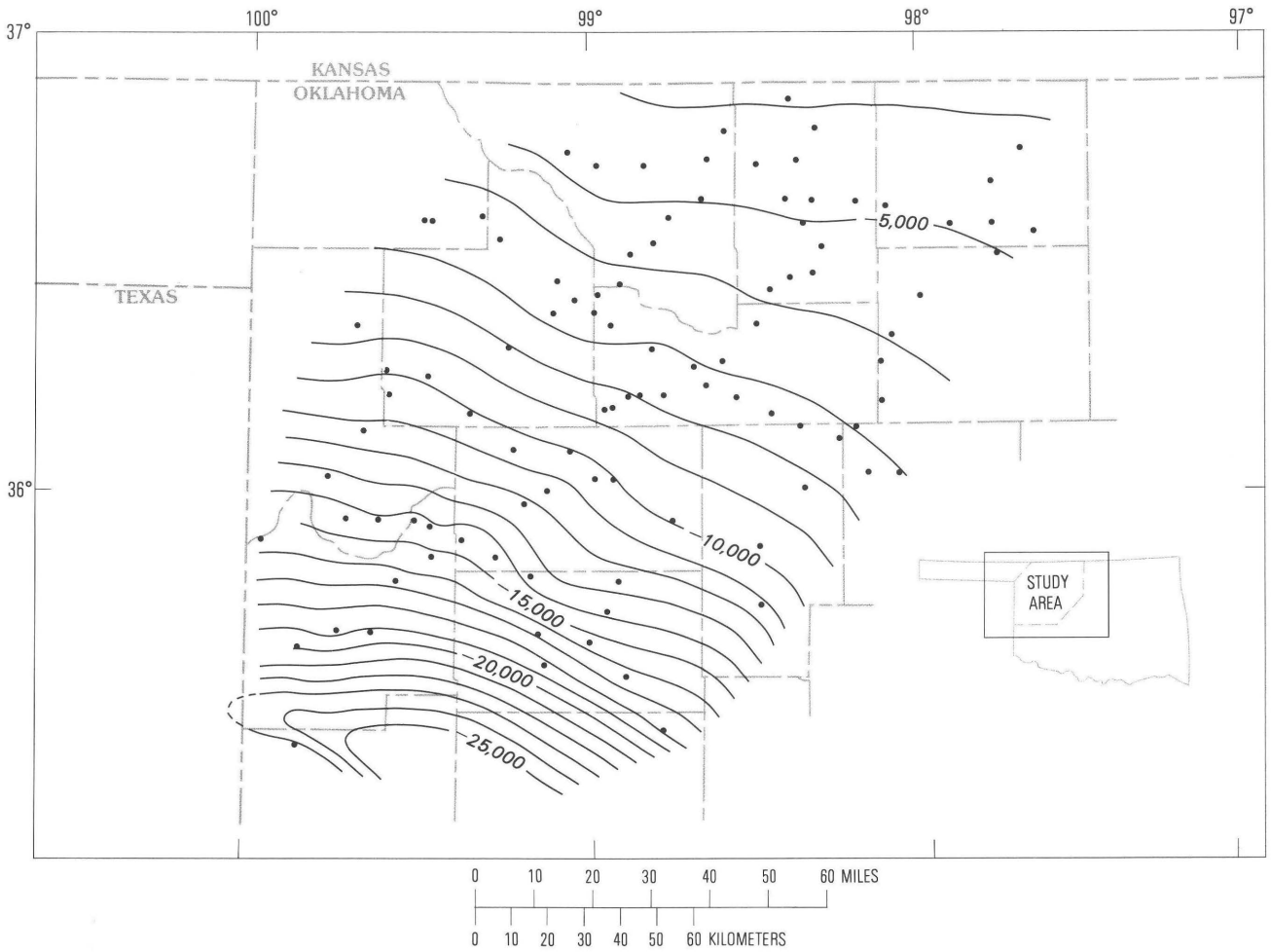

Figure 3. Depth below sea level of top of Woodford Shale. Contour interval 1,000 ft (305 m). Solid circles show locations of wells used in this study. Modified from Hester and others (1990).

Because deposition of the lower member covered surface irregularities of the pre-Woodford unconformity, the thickness of the middle member of the Woodford (fig. 5) is locally more uniform than that of the lower member. Like the lower member, the maximum thickness of the middle member in the northeastern part of the study area is only about 25 ft (8 m). The thickness of the middle member increases toward the axis of the Southern Oklahoma Aulacogen to more than 75 ft (23 m). Figure 5 indicates continued stability of the northeastern part of the study area relative to the central trough of the Southern Oklahoma Aulacogen, which was subsiding during middle Woodford time but apparently more slowly than during deposition of the lower member.

The thickness of the upper member of the Woodford Shale in the northeastern part of the study area (fig. 6) is more than 75 ft (23 m). In contrast to the lower and middle members, isopachs of the upper member show significant thickening to the northeast toward Kansas. Also in contrast to the lower and middle members, the upper member thickens only slightly to the southwest. Figure 6 shows a shift in tectonic pattern; during upper Woodford time regional subsidence of the northeastern part of the study area was coupled with continued slowing of subsidence along the axis of the Southern Oklahoma Aulacogen.

Depositional relations between the three members of the Woodford Shale, depicted in the regional cross sections of figure 7, show that the influence of the first stage of Anadarko Basin tectonic evolution continued at least into Mississippian time. To the southwest, each member of the Woodford thickens, reflecting subsidence along the central trough of the Southern Oklahoma Aulacogen and relative uplift along the axis of the paleotopographic high shown in figure 2. To the northeast, the almost uniform thickness of the lower and middle members records deposition on a relatively stable shelf, whereas increasing thickness of the upper member records downwarping toward the Sedgwick Basin of south-central Kansas.

As a result of the tectonic influence discussed above, thickness of the Woodford Shale in the northeastern part of the study area is dominated by the upper member and

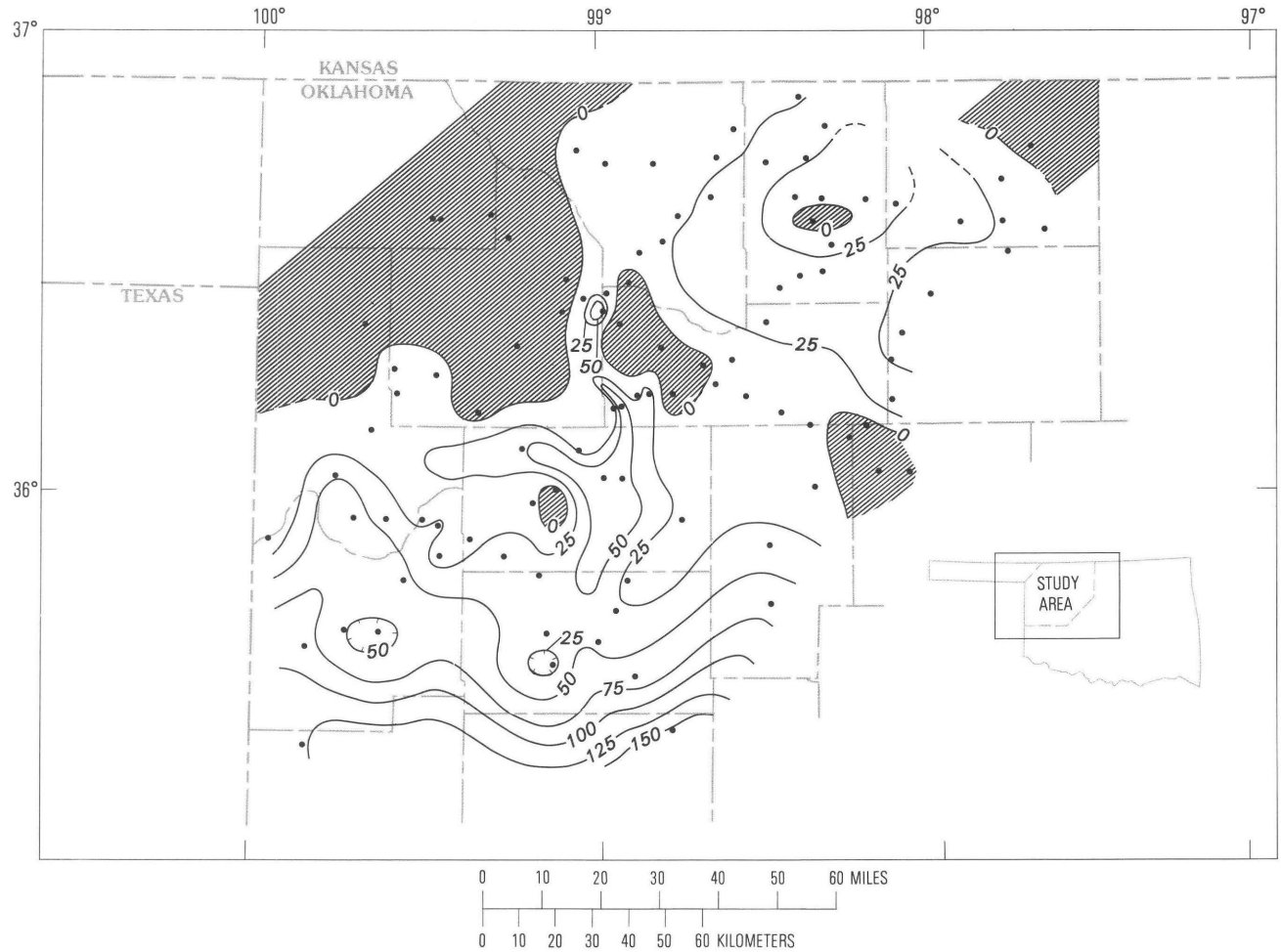

Figure 4. Thickness of lower member of Woodford Shale. Areas where lower member is absent are hachured. Contour interval 25 ft (7.6 m). Solid circles show locations of wells used in this study. Modified from Hester and others (1990).

thickness of the Woodford Shale in the southwestern part of the study area is dominated by the lower and middle members. The effect of these depositional patterns on the source-rock properties of the Woodford Shale is significant when coupled with the thermal-maturity patterns discussed in the following section.

THERMAL-MATURITY PATTERNS

Depositional patterns of the Woodford Shale were mostly shaped by evolution of the first-stage Southern Oklahoma Aulacogen, whereas thermal-maturity patterns were shaped by development of the second-stage foreland-style Anadarko Basin. Subsidence of the Woodford Shale during Mississippian through Permian time produced a large range of burial depths (fig. 3) and thus an unusually broad range of thermal maturities (Cardott and Lambert, 1985). Vitrinite reflectance (Ro) ranges from slightly less than 0.5 percent on the northern shelf to well over 2.0 percent in the deep basin (fig. 8).

The Woodford Shale on the northeast shelf, where thickness is dominated by the upper member, is generally immature to marginally mature with respect to oil generation (Schmoker, 1986). In contrast, the Woodford Shale in the deep Anadarko Basin to the southwest, where thickness is dominated by the lower and middle members, is generally mature to postmature with respect to oil generation. Thus, most hydrocarbons sourced by the Woodford Shale have been generated by the lower and middle members.

STRUCTURAL IMPLICATIONS

Burial histories of Feinstein (1981) indicate very gradual subsidence of the Southern Oklahoma Aulacogen after Ordovician time; however, progressive thickening of the Hunton Group (Late Ordovician, Silurian, and Early Devonian) and the Woodford Shale toward the deep basin (Amsden, 1975)(figs. 2, 4–7) shows that differential subsidence between the central trough of the Southern Oklahoma Aulacogen and the northern margin of the basin persisted

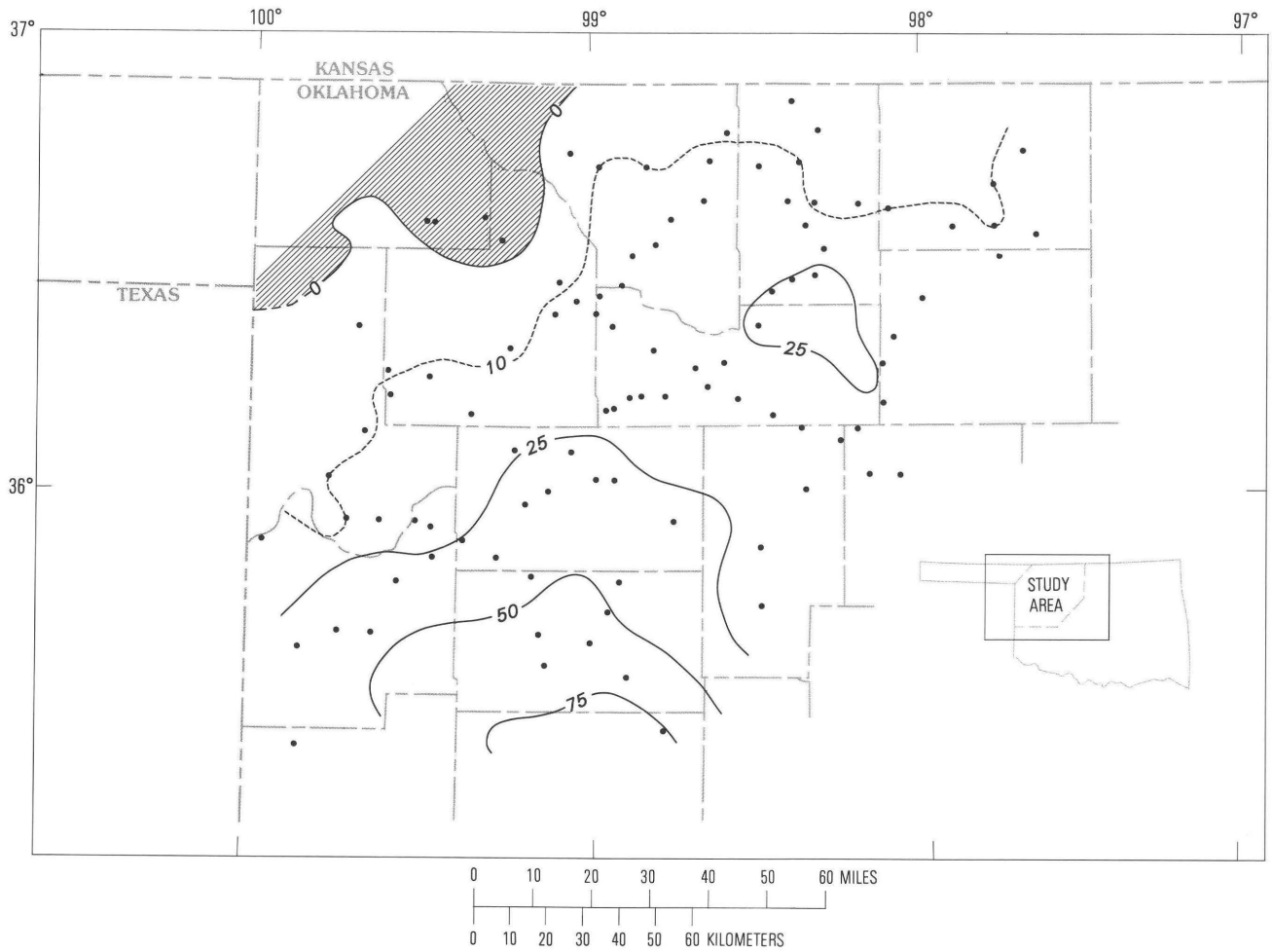

Figure 5. Thickness of middle member of Woodford Shale. Area where middle member is absent is hachured. Contour interval 25 ft (7.6 m). Solid circles show locations of wells used in this study. Modified from Hester and others (1990).

during Hunton and Woodford time. This fact suggests that the basin's fundamental loading mechanisms continued to operate at least into Mississippian time even as the sedimentary record was being overprinted by pre-Woodford regional erosion.

Several lines of evidence suggest that the paleotopographic high apparent in Woodford isopach maps (figs. 2, 4, 5) and cross sections (fig. 7) was an active tectonic feature that was rising during Late Devonian–Early Mississippian time even as the central trough of the aulacogen was subsiding. This evidence, discussed in the following paragraphs, falls into three categories: (1) post-Hunton to pre-Woodford erosional patterns, (2) distribution of the Misener Sandstone (Late Devonian), and (3) Woodford Shale depositional patterns.

The post-Hunton to pre-Woodford erosional channels shown in figure 9 are drawn on the assumption that the lower member of the Woodford is thicker where it fills depressions on the unconformity surface. The shape and continuity of these depressions thus define the erosional channels of figure 9. Channels mapped by Amsden (1975)(inset map, fig. 9), southeast of the present study area, appear to conform with the channels mapped here. The erosional channels of this report are separated by the paleotopographic high into two distinct drainages (fig. 9). To the southwest, the channels emanate from the flank of the paleotopographic high and trend generally southward. To the northeast, the course of the channels deviates roughly 90° to parallel the northeast flank. The drainages do not merge within the study area nor do the erosional channels cross the axis of the paleotopographic high (fig. 9). These facts suggest that the paleotopographic high was flexing upward before and during the pre-Woodford episode of regional erosion.

The Misener Sandstone, a basal facies of the Woodford, is thought to have been derived from eroded Simpson Group (Middle Ordovician) sandstones and deposited in topographic lows at the beginning of the marine transgression that also deposited the Woodford Shale (Amsden and Klapper, 1972). In the study area, the Misener Sandstone is discontinuous across the paleotopographic high and essentially

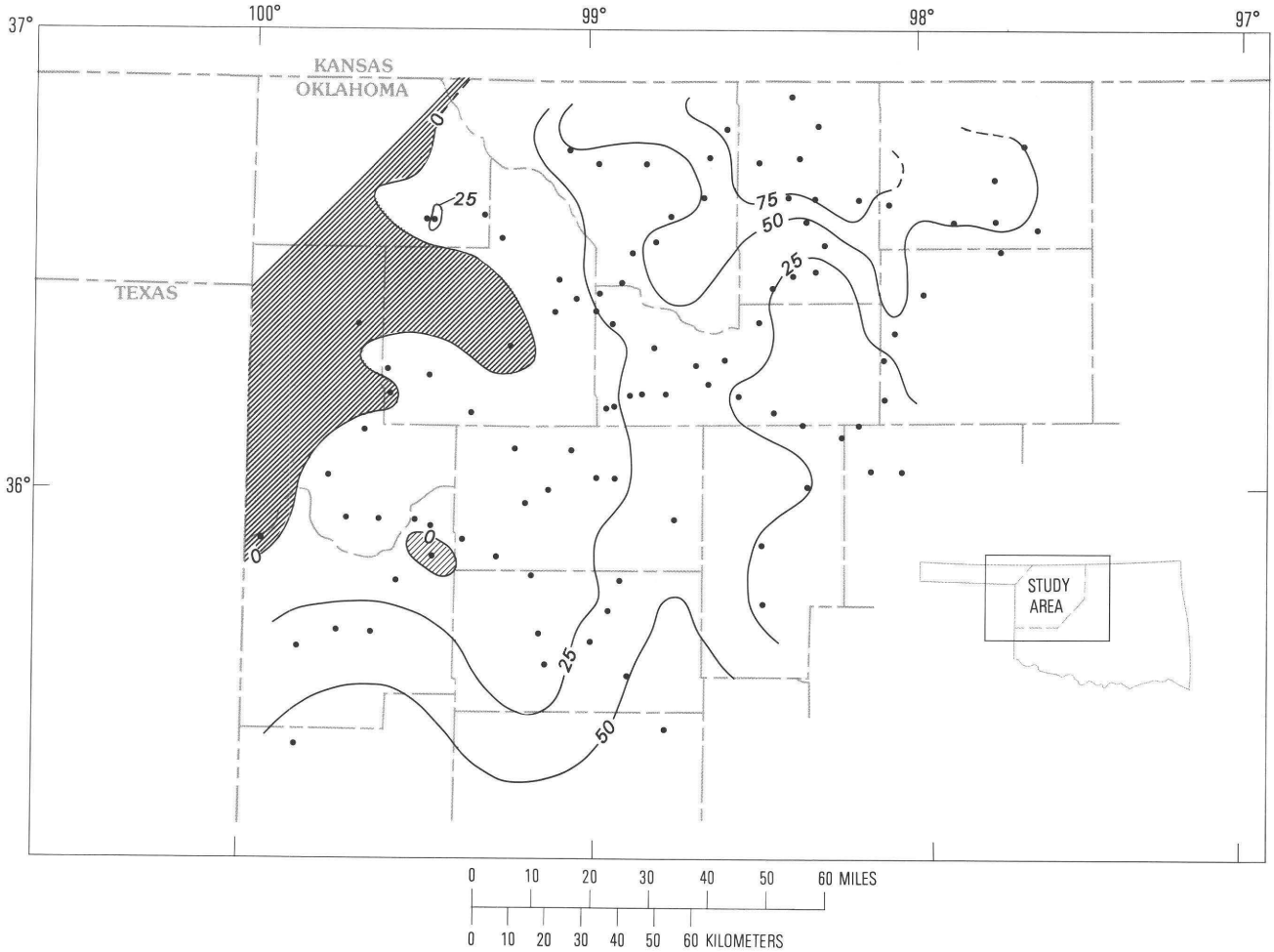

Figure 6. Thickness of upper member of Woodford Shale. Areas where upper member is absent are hachured. Contour interval 25 ft (7.6 m). Solid circles show locations of wells used in this study. Modified from Hester and others (1990).

absent along its southwest slope (fig. 9). The distribution of the Misener Sandstone reflects positive topography at the beginning of marine transgression and suggests continued tectonic uplift of the paleotopographic high.

The paleotopographic high significantly influenced Woodford deposition through Late Devonian and into Early Mississippian time (fig. 7). Cross section *C–C′* (fig. 7), in particular, indicates that the paleotopographic high was rising with respect to both the southwest and northeast depocenters throughout Woodford deposition. This observation again favors uninterrupted tectonic uplift of the paleotopographic high.

The three points of evidence discussed above indicate that the paleotopographic high was in fact a tectonic element that rose steadily from post-Hunton through Woodford time. During the same period, the central trough of the Southern Oklahoma Aulacogen was subsiding. It is suggested here that the paleotopographic high was a forebulge that developed as a direct result of loading and subsidence along the central trough of the Southern Oklahoma Aulacogen.

As described by Turcotte and Schubert (1982), the behavior of the Earth's lithosphere on a geologic time scale is that of an elastic plate floating on a viscous fluid. Downward deflection of the plate in response to loading creates an upwarp or forebulge adjacent to the depression caused by the applied load. Tensional stresses in the upper part of the plate and compressional stresses in the lower part of the plate, coupled with restoring buoyancy forces, produce the forebulge (Peterman and Sims, 1988). The height and position of the forebulge are dependent on the magnitude of downward deflection and the thickness and strength of the lithospheric plate. As a rule of thumb, the ratio of downward deflection along the load axis to uplift of the forebulge is about 15 to 1 (Turcotte and Schubert, 1982).

In theory, a forebulge is an integral part of basin development in response to loading, but clear examples are not common in the ancient subsurface. A well-documented example that is somewhat analogous to the present case is given by Peterman and Sims (1988), who recognized the Goodman Swell in northern Wisconsin as a forebulge of the

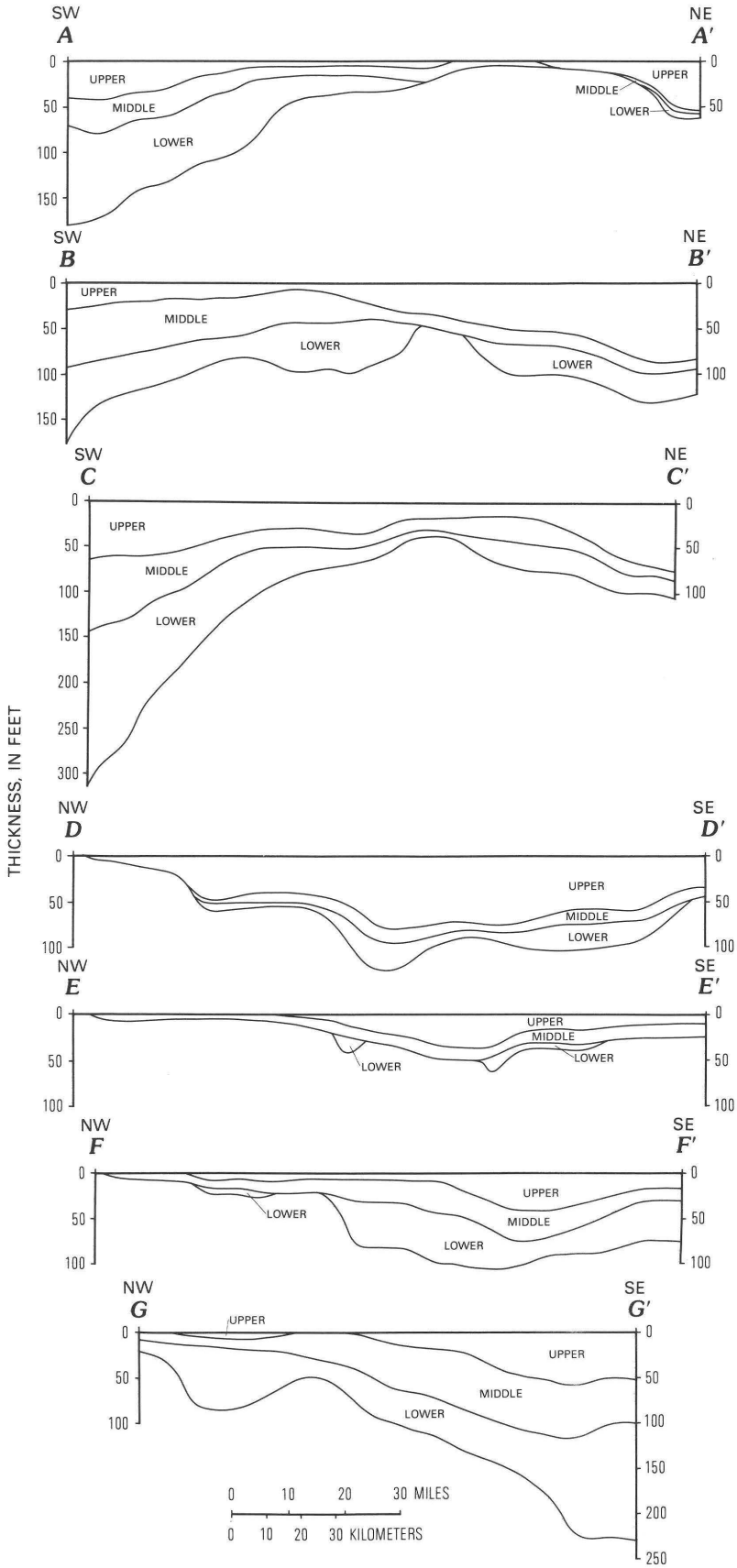
SW
A
NE
A′
UPPER
MIDDLE
LOWER
SW
B
NE
B′
SW
C
NE
C′
NW
D
SE
D′
NW
E
SE
E′
NW
F
SE
F′
NW
G
SE
G′
THICKNESS, IN FEET
0
50
100
150
200
250
300
0 10 20 30 MILES
0 10 20 30 KILOMETERS

Figure 7 (facing page). Cross sections drawn from contoured thicknesses (in feet) of lower, middle, and upper members of Woodford Shale showing influence of tectonic evolution of Anadarko basin on distribution of sediments. Datum is top of upper member. Lines of section shown in figure 1. Modified from Hester and others (1990).

Midcontinent Rift System. The distance between the Goodman Swell and the nearest load axis of the Midcontinent Rift System is comparable to the distance between the paleotopographic high of this report and the axis of the Southern Oklahoma Aulacogen. The flexural uplift of the Goodman Swell is enhanced by a tightly curved arrangement of rift axes and is therefore anomalously large compared to uplift of the paleotopographic high identified here.

Measuring flexural uplift of the paleotopographic high is not straightforward. An estimate of flexural uplift during a limited span of geologic time is based on the decompacted thickness of the middle member of the Woodford Shale at the crest of the paleotopographic high and at the northeast depocenter (fig. 10). Because the thickness of the lower member is affected by topographic relief on the pre-Woodford unconformity and the thickness of the upper member is affected by subsidence of the Sedgwick Basin north of the study area, only the thickness of the middle member was used to estimate flexural uplift.

The thickness of the middle member of the Woodford is controlled by a combination of three penecontemporaneous processes, as shown in figure 10. Thickness due to compactional subsidence (Schmoker and Gautier, 1989) of the underlying Woodford member and to regional sediment accumulation is independent of forebulge development.

Figure 10 indicates that the paleotopographic high, which is interpreted here as a possible forebulge, was uplifted about 30 ft (9 m) during middle Woodford time. Based on a subsidence to uplift ratio of 15 to 1 (Turcotte and Schubert, 1982), the central trough of the Southern Oklahoma Aulacogen would then be expected to have subsided roughly 450 ft

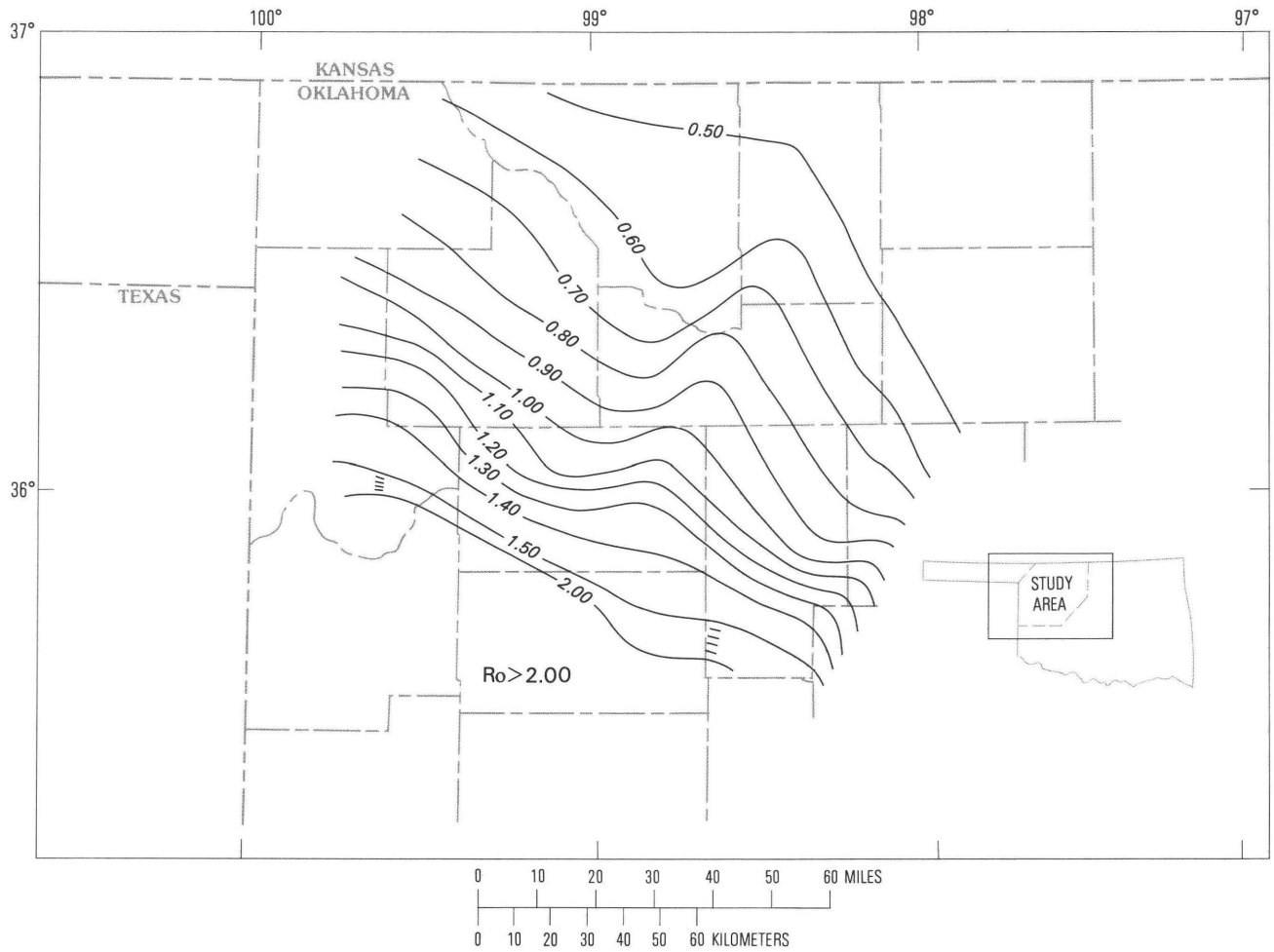

Figure 8. Vitrinite reflectance (Ro, in percent) of Woodford Shale contoured using data of Cardott and Lambert (1985) and B.J. Cardott (written commun., 1987). Contour interval 0.10 percent. Modified from Hester and others (1990).

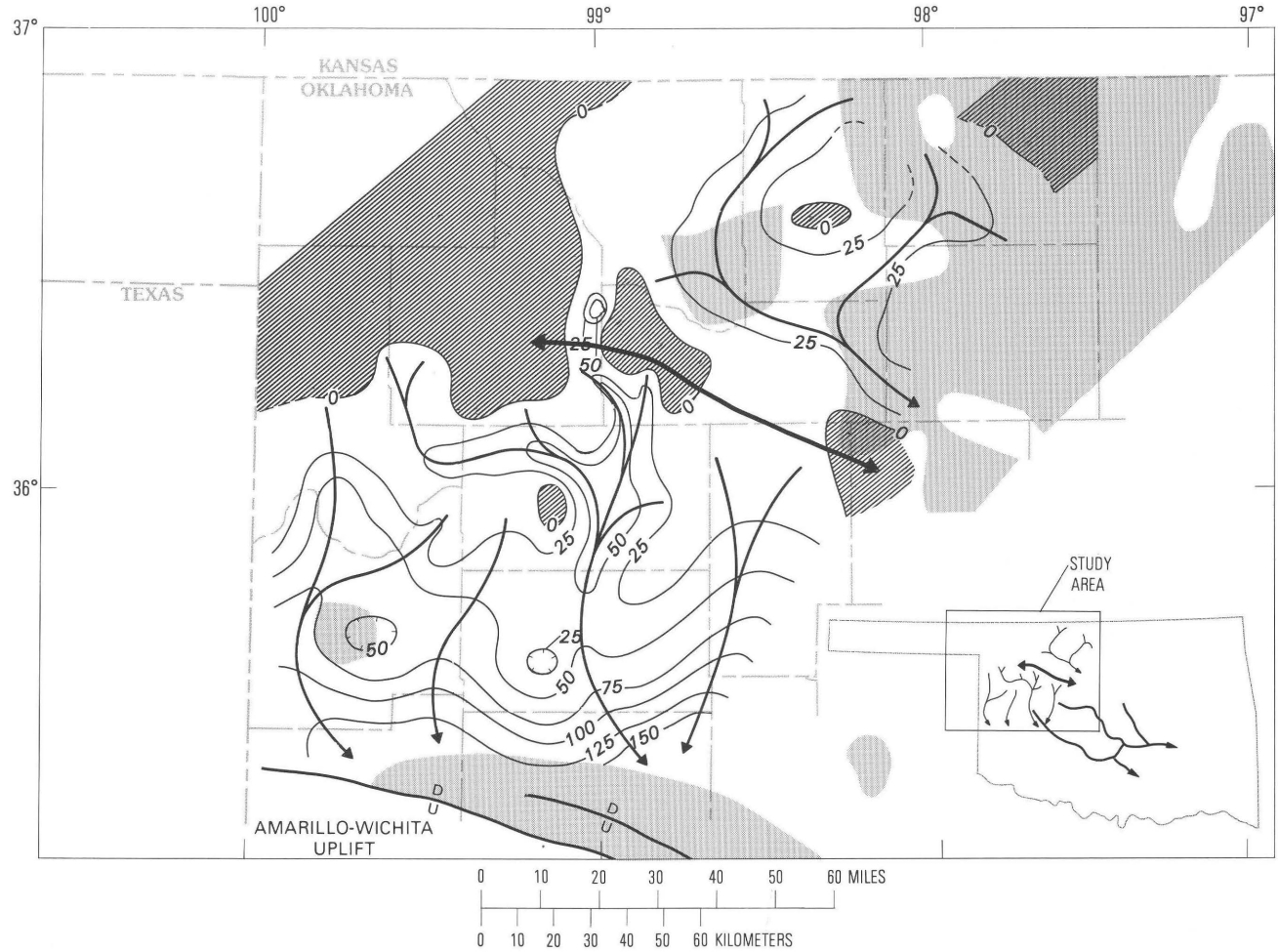

Figure 9. Thickness of lower member of Woodford Shale, major erosional channels on pre-Woodford surface inferred from thickness of lower member (medium lines with arrows), and distribution of Misener Sandstone (screened) as depicted by Amsden (1975). Heavy line with arrows marks axis of paleotopographic high. Areas where Woodford Shale is absent are hachured. Contour interval 25 ft (7.6 m). Inset map of study area shows stream channels of Amsden (1975) (heavier lines to southeast).

(140 m) during the same time interval. The thickness of the middle member of the Woodford projected south of the study area along cross section *C–C'* (fig. 7) to the approximate axis of the aulacogen suggests that the central trough probably subsided at least 430 ft (130 m) during middle Woodford time. Thus the ratio of basin subsidence to uplift of the paleotopographic high during middle Woodford time is in reasonable agreement with that predicted by a theoretical forebulge model.

In view of the tectonic interpretations presented here, sedimentation of the Woodford Shale and thus Woodford source-rock properties have been directly influenced by crustal loading during the terminal stages of the Southern Oklahoma Aulacogen. Subsidence along the axis of the load and the resulting upward flexure of the forebulge at the basin margin explain the observed regional depositional patterns of the Woodford Shale.

SUMMARY AND CONCLUSIONS

Source-rock properties of the Woodford Shale are in large part controlled by original depositional patterns shaped by evolution of the first-stage Southern Oklahoma Aulacogen and by thermal-maturation patterns shaped by development of the second-stage Anadarko Basin. This report emphasizes the influence of subsidence along the axis of the Southern Oklahoma Aulacogen and uplift at the basin margin upon the depositional patterns of the Woodford Shale.

A positive paleotopographic feature parallel with and about 75 mi (120 km) north of the Amarillo-Wichita Uplift divided the Woodford Shale into northeast and southwest depocenters and was a hinge line separating areas of regional basement subsidence and flexure during Woodford time. Three lines of evidence suggest that this positive feature was tectonically rising during post-Hunton through Woodford

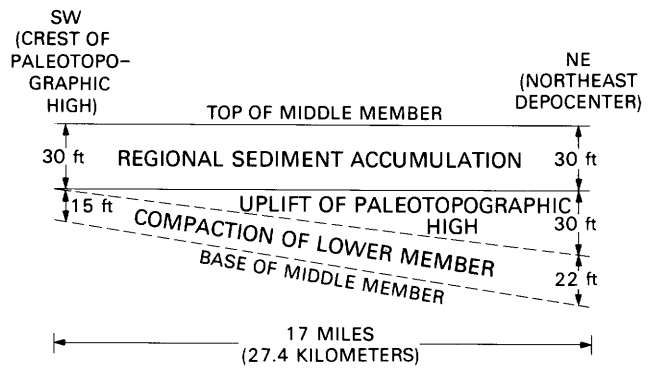

Figure 10. Decompacted thickness of middle member of Woodford Shale along line of section *C–C'* (fig. 7) at crest of paleotopographic high and at northeast depocenter. Subdivisions do not represent stratigraphic units or time-sequential events but show contributions of three penecontemporaneous processes to middle-member thickness. Decompaction based on shale-compaction curves of Baldwin and Butler (1985).

time: (1) erosional channels on the pre-Woodford surface do not cross the axis of the paleotopographic high; (2) the Misener Sandstone, which was deposited in topographic lows, is not present along the axis of the paleotopographic high; and (3) Woodford sediments thicken from the paleotopographic high toward the southwest and northeast depocenters.

In view of this evidence, it is suggested here that the paleotopographic high is a forebulge that developed on the basin margin as a direct result of loading and subsidence along the central trough of the Southern Oklahoma Aulacogen. Subsidence along the rift axis coupled with simultaneous development of a forebulge can account for the Woodford Shale depositional patterns described here.

The Woodford Shale was deposited near the end of the evolution of the Southern Oklahoma Aulacogen, during a relatively short interval of geologic time. The evidence developed in this study regarding a possible forebulge associated with the aulacogen is thus limited to a very narrow phase of the aulacogen's development. An investigation of selected pre-Woodford sediments, analogous to that reported here for the Woodford, is suggested as an approach to further elucidate the nature and development through time of the paleotopographic high interpreted here as a forebulge.

REFERENCES CITED

Amsden, T.W., 1975, Hunton Group (Late Ordovician, Silurian, and Early Devonian) in the Anadarko Basin of Oklahoma: Oklahoma Geological Survey Bulletin 121, 214 p.

Amsden, T.W., and Klapper, Gilbert, 1972, Misener Sandstone (Middle–Upper Devonian), north-central Oklahoma: American Association of Petroleum Geologists Bulletin, v. 56, no. 12, p. 2323–2334.

Baldwin, Brewster, and Butler, C.O., 1985, Compaction curves: American Association of Petroleum Geologists Bulletin, v. 69, no. 4, p. 622–626.

Cardott, B.J., and Lambert, M.W., 1985, Thermal maturation by vitrinite reflectance of Woodford Shale, Anadarko Basin, Oklahoma: American Association of Petroleum Geologists Bulletin, v. 69, no. 11, p. 1982–1998.

Feinstein, Shimon, 1981, Subsidence and thermal history of Southern Oklahoma Aulacogen—Implications for petroleum exploration: American Association of Petroleum Geologists Bulletin, v. 65, no. 12, p. 2521–2533.

Hester, T.C., Sahl, H.L., and Schmoker, J.W., 1988, Cross sections based on gamma-ray, density, and resistivity logs showing stratigraphic units of the Woodford Shale, Anadarko Basin, Oklahoma: U.S. Geological Survey Miscellaneous Field Studies Map MF–2054, 2 plates.

Hester, T.C., Schmoker, J.W., and Sahl, H.L., 1990, Log-derived, regional source-rock characteristics of the Woodford Shale, Anadarko Basin, Oklahoma: U.S. Geological Survey Bulletin 1866–D, 38 p.

Perry, W.J., Jr., 1989, Tectonic evolution of the Anadarko Basin region, Oklahoma: U.S. Geological Survey Bulletin 1866–A, 19 p.

Peterman, Z.E., and Sims, P.K., 1988, The Goodman Swell—A lithospheric flexure caused by crustal loading along the Midcontinent Rift System: Tectonics, v. 7, no. 5, p. 1077–1090.

Schmoker, J.W., 1986, Oil generation in the Anadarko Basin, Oklahoma and Texas—Modeling using Lopatin's method: Oklahoma Geological Survey Special Publication 86–3, 40 p.

Schmoker, J.W., and Gautier, D.L., 1989, Compaction of basin sediments—Modeling based on time-temperature history: Journal of Geophysical research, v. 94, no. B6, p. 7379–7386.

Turcotte D.L., and Schubert, Gerald, 1982, Geodynamics, applications of continuum physics to geological problems: John Wiley, New York, 450 p.

Chapter C

Sequential Laramide Deformation of the Rocky Mountain Foreland of Southwestern Montana, Wyoming, and North-Central Colorado

By WILLIAM J. PERRY, JR., DOUGLAS J. NICHOLS, THADDEUS S. DYMAN, and CHRISTOPHER J. HALEY

U.S. GEOLOGICAL SURVEY BULLETIN 2012

APPLICATION OF STRUCTURAL GEOLOGY TO MINERAL AND ENERGY RESOURCES OF THE CENTRAL AND WESTERN UNITED STATES

CONTENTS

FIGURES

Sequential Laramide Deformation of the Rocky Mountain Foreland of Southwestern Montana, Wyoming, and North-Central Colorado

By William J. Perry, Jr.[1], Douglas J. Nichols[2], Thaddeus S. Dyman[1], *and* Christopher J. Haley[1]

Abstract

Basement-involved compressional and transpressional deformation of the Rocky Mountain foreland began at about 90 Ma in the Lima region of southwestern Montana. In the Lima region, Laramide-style foreland deformation culminated prior to mid-Campanian time (approximately 80 Ma), based on palynostratigraphically dated sediments shed from the early Laramide Blacktail–Snowcrest Uplift. The Madison-Gravelly Uplift, located immediately northwest of Yellowstone Park, is the next youngest Laramide uplift of the northern Rocky Mountain foreland in Montana. Laramide deformation in this area began soon after 79 Ma and was apparently completed by 68–69 Ma, before the close of Cretaceous time. Laramide deformation of the Wind River Uplift, which may have been initiated about 85 Ma based on independent fission-track evidence, culminated in late Paleocene to Eocene time. Available data on timing from Montana and Wyoming suggests that Laramide deformation proceeded eastward and southward from southwestern Montana, reaching the Colorado Front Range by latest Maastrichtian time.

Economic implications of this newly recognized sequence of deformation of the Rocky Mountain foreland include progressive blockage by structural disruption of eastward migration paths for hydrocarbons generated from Paleozoic source rocks in east-central and southeastern Idaho, southwestern Montana, and Wyoming.

INTRODUCTION

Beginning about 1978, the thinking and structural concepts of many structural geologists working in the Rocky Mountains began to converge on regional compression and crustal shortening as the primary mode for Laramide deformation of the Rocky Mountain foreland (fig. 1) (Smithson and others, 1978, 1979; Brewer and others, 1980; Gries, 1981, 1983a, b; Hamilton, 1981, 1988; Petersen, 1983; Schmidt and Garihan, 1983; Brown, 1984, 1988; Kulik and Schmidt, 1988). This concept was first championed by Chamberlin (1919, 1923) and later by Berg (1962) and Blackstone (1963).

The relationship between plate tectonics and Laramide deformation was first explored by Lowell (1974), whose analysis incorporated Lipman and others' (1971) concept of low-angle subduction. The low-angle subduction model was further developed by Dickinson and Snyder (1978), who believed that sufficient shear developed between the base of the continental lithosphere and the top of the underlying subhorizontal "Laramide-style" oceanic crustal slab to facilitate Laramide crustal shortening in the Rocky Mountain foreland. How and when Laramide crustal shortening occurred is still controversial (see, for example, conflicting views by Hamilton, 1981, 1988; Gries, 1983b; Kulik and Schmidt, 1988).

The theme espoused by Armstrong (1968) that the Laramide orogeny did not begin until latest Cretaceous time has led to a virtual disregard by some workers of early Laramide events in the Rocky Mountain foreland (for example, Dickinson and others, 1988). In the Lima region of southwestern Montana (fig. 2), Nichols and others (1985) dated beds in the fining-upward sequence near the top of the foreland-derived conglomerates as middle Campanian (78–81 Ma). The tectonic implications of this date were discussed by Perry and others (1988) and are expanded upon in this report. Numerous other examples of pre–latest Cretaceous Laramide-style deformation of the Rocky Mountain foreland exist, as mentioned by Wilson (1936), Tweto (1975), Schmidt and Garihan (1983), and Tysdal (1986, 1988). In this report we demonstrate that there is a definite sequence of development of Laramide deformation in the Rocky Mountain foreland of

[1]U.S. Geological Survey, Box 25046, MS 940, Denver, Colorado 80225

[2]U.S. Geological Survey, Box 25046, MS 919, Denver, Colorado 80225

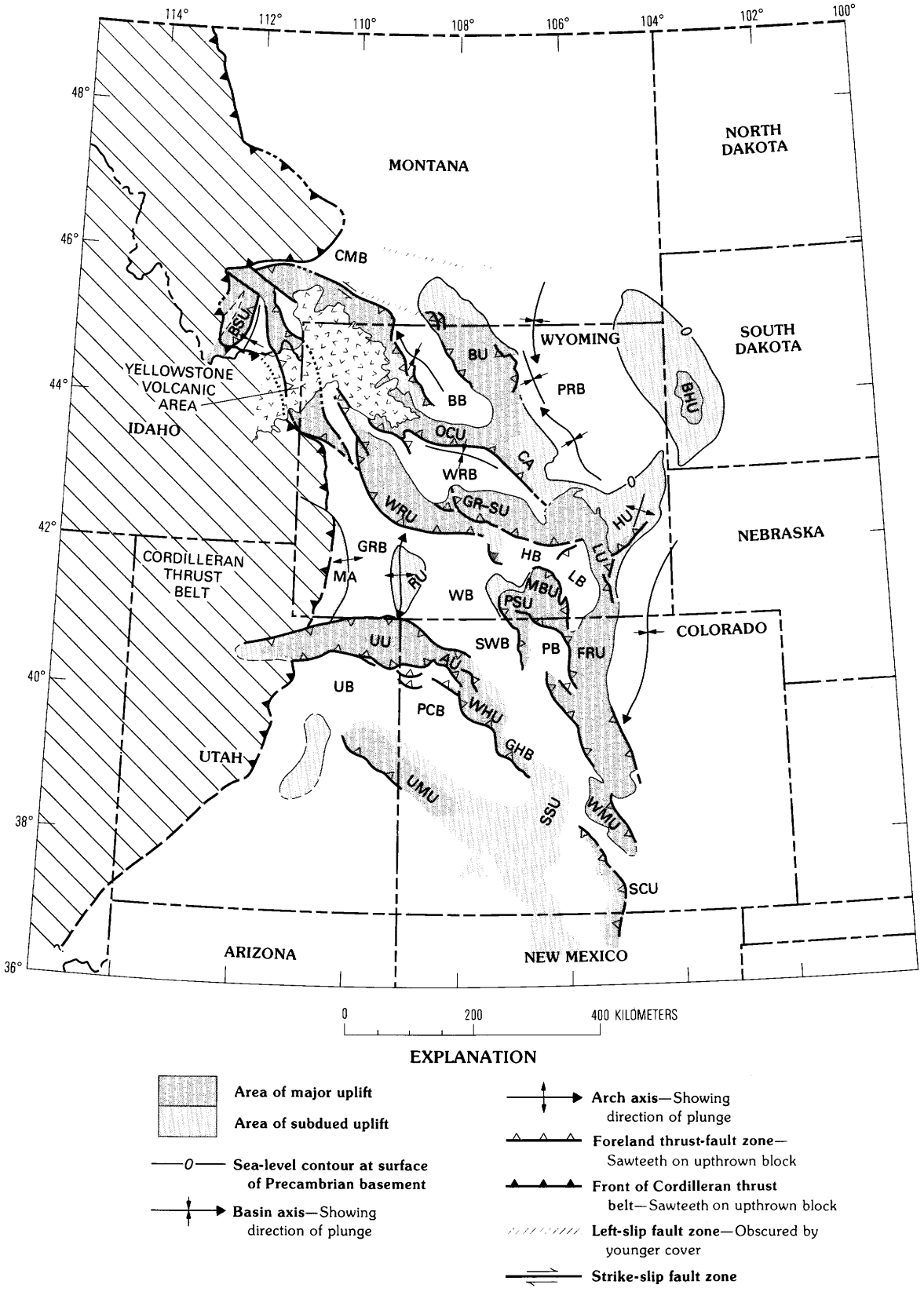
114°
112°
110°
108°
106°
104°
102°
100°
48°
46°
44°
42°
40°
38°
36°
MONTANA
NORTH DAKOTA
SOUTH DAKOTA
WYOMING
NEBRASKA
COLORADO
NEW MEXICO
ARIZONA
UTAH
IDAHO
YELLOWSTONE VOLCANIC AREA
CORDILLERAN THRUST BELT
CMB
BSU
BU
BB
PRB
BHU
OCU
CA
WRB
WRU
GR-SU
HU
HB
LU
LB
GRB
MA
RU
WB
MBU
PSU
UU
SWB
PB
FRU
AU
UB
PCB
WHU
GHB
UMU
SSU
WMU
SCU
0
200
400 KILOMETERS
EXPLANATION
Area of major uplift
Area of subdued uplift
0 Sea-level contour at surface of Precambrian basement
Basin axis—Showing direction of plunge
Arch axis—Showing direction of plunge
Foreland thrust-fault zone—Sawteeth on upthrown block
Front of Cordilleran thrust belt—Sawteeth on upthrown block
Left-slip fault zone—Obscured by younger cover
Strike-slip fault zone

Figure 1(facing page). Principal Laramide basins and uplifts, Rocky Mountain foreland province. Major uplifts are shown in closely spaced dot pattern; broad positive areas in more widely spaced dot pattern. Sawteeth on thrust faults point into upper plates. AU, Axial Uplift; BB, Bighorn Basin; BHU, Black Hills Uplift; BSU, Blacktail-Snowcrest Uplift; BU, Bighorn Uplift; CA, Casper Arch; CMB, Crazy Mountains Basin; FRU, Front Range Uplift; GHB, Grand Hogback; GRB, Green River Basin; GR–SU, Granite Mountains–Shirley Mountains (Sweetwater) Uplift; HB, Hanna Basin; HU, Hartville Uplift; LB, Laramie Basin; LU, Laramie Uplift; MBU, Medicine Bow Uplift; OCU, Owl Creek Uplift; PB, North and Middle Parks Basin; PCB, Piceance Creek Basin; PRB, Powder River Basin; PSU, Park–Sierra Madre Uplift; RU, Rock Springs Uplift; SCU, Sangre de Cristo Uplift; SSU, Sawatch–San Luis Uplift; SWB, Sand Wash Basin; UB, Uinta Basin; UMU, Uncompahgre Mountains Uplift; UU, Uinta Mountains Uplift; WB, Washakie Basin; WHU, White River Uplift; WMU, Wet Mountains Uplift; WRB, Wind River Basin; WRU, Wind River Uplift. Modified from Bayley and Muehlberger (1968).

Montana and Wyoming, from northwest to southeast. We focus on those Laramide uplifts that have a Cretaceous growth history (fig. 3); other uplifts that show little evidence of growth until the late Laramide (late Paleocene and early to middle Eocene) are not discussed. Welts of a few tens of meters of inferred structural relief such as discussed by Merewether and Cobban (1986), defined chiefly by minor unconformities, are also not discussed. We consider the amount of tectonism represented by the minor partitioning of the Early and early Late Cretaceous foreland basin (Schwartz, 1982; DeCelles, 1986; Schwartz and DeCelles, 1988) to be modest, not a source of significant synorogenic sediments or uplift, and not of the scale discussed here.

Contrasting Models of Laramide Sequence of Deformation

Tweto (1975) marshalled available evidence concerning the age and sequence of Laramide deformation in Colorado and adjacent areas showing that the early Laramide uplifts of central Colorado—the Front Range, Medicine Bow, Park–Sierra Madre, and Wet Mountains Uplifts (fig. 1)—are on the site of the late Paleozoic Front Range highland. These uplifts began in late to very late Maastrichtian time, as indicated by closely dated synorogenic debris deposited on their flanks (Baltz, 1972; Tweto, 1975; Kluth and Nelson, 1988). Tweto (1975) concluded that the Sawatch–San Luis (fig. 1) and Wet Mountains Uplifts are more than 70 million years old, slightly older than the other Colorado Laramide uplifts. He also concluded that the Axial, Grand Hogback, and White River Uplifts (fig. 1) were the latest to develop, in Eocene time, whereas the Laramie and Sangre de Cristo

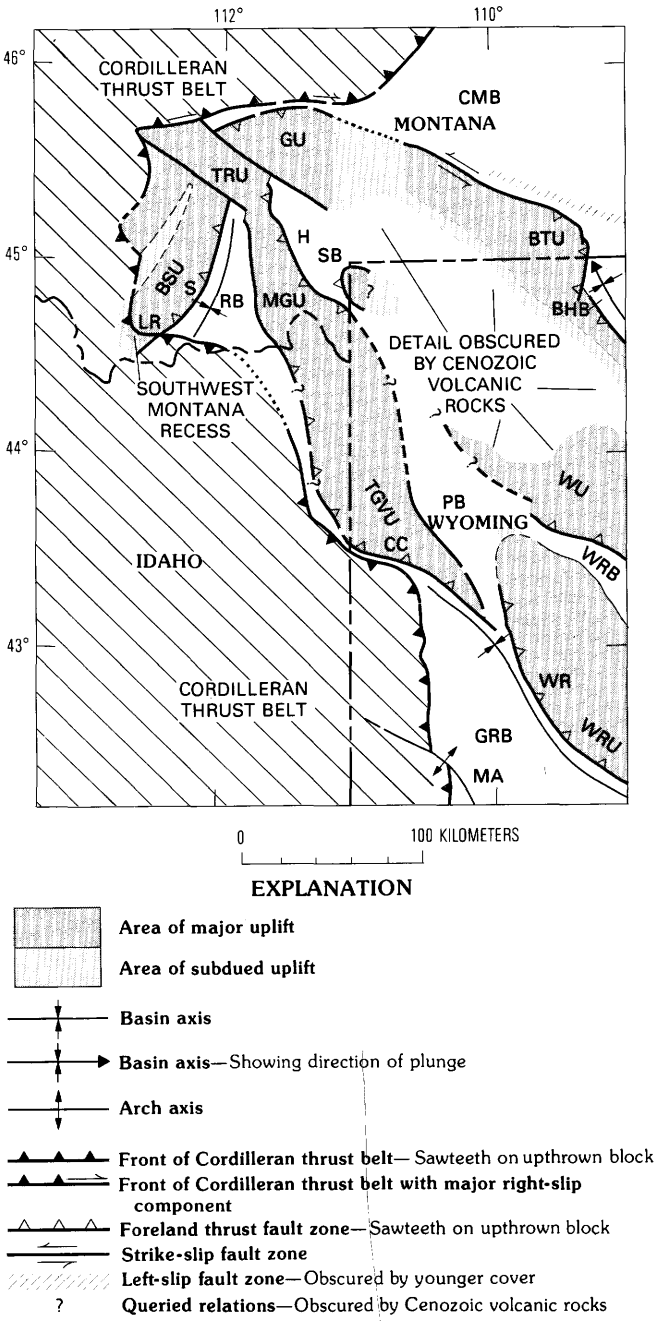

Figure 2. Principal Laramide uplifts (screen pattern), northwestern Wyoming, western Montana, and east-central Idaho. BHB, Bighorn Basin; BSU, Blacktail-Snowcrest Uplift; BTU, Beartooth Uplift; CC, Cache Creek Thrust; CMB, Crazy Mountains Basin; GRB, Green River Basin; GU, Gallatin Uplift; H, Hilgard Thrust System; LR, Lima region; MA, Moxa Arch; MGU, Madison-Gravelly Uplift; PB, Pinyon Basin; RB, Ruby Basin; S, Snowcrest structural terrane and thrust, southeastern margin of Blacktail-Snowcrest Uplift; SB, Sphinx Basin; TGVU, Ancestral Teton–Gros Ventre Uplift; TRU, Tobacco Root Uplift; WR, Wind River Thrust; WRB, Wind River Basin; WRU, Wind River Uplift, WU, Washakie Uplift.

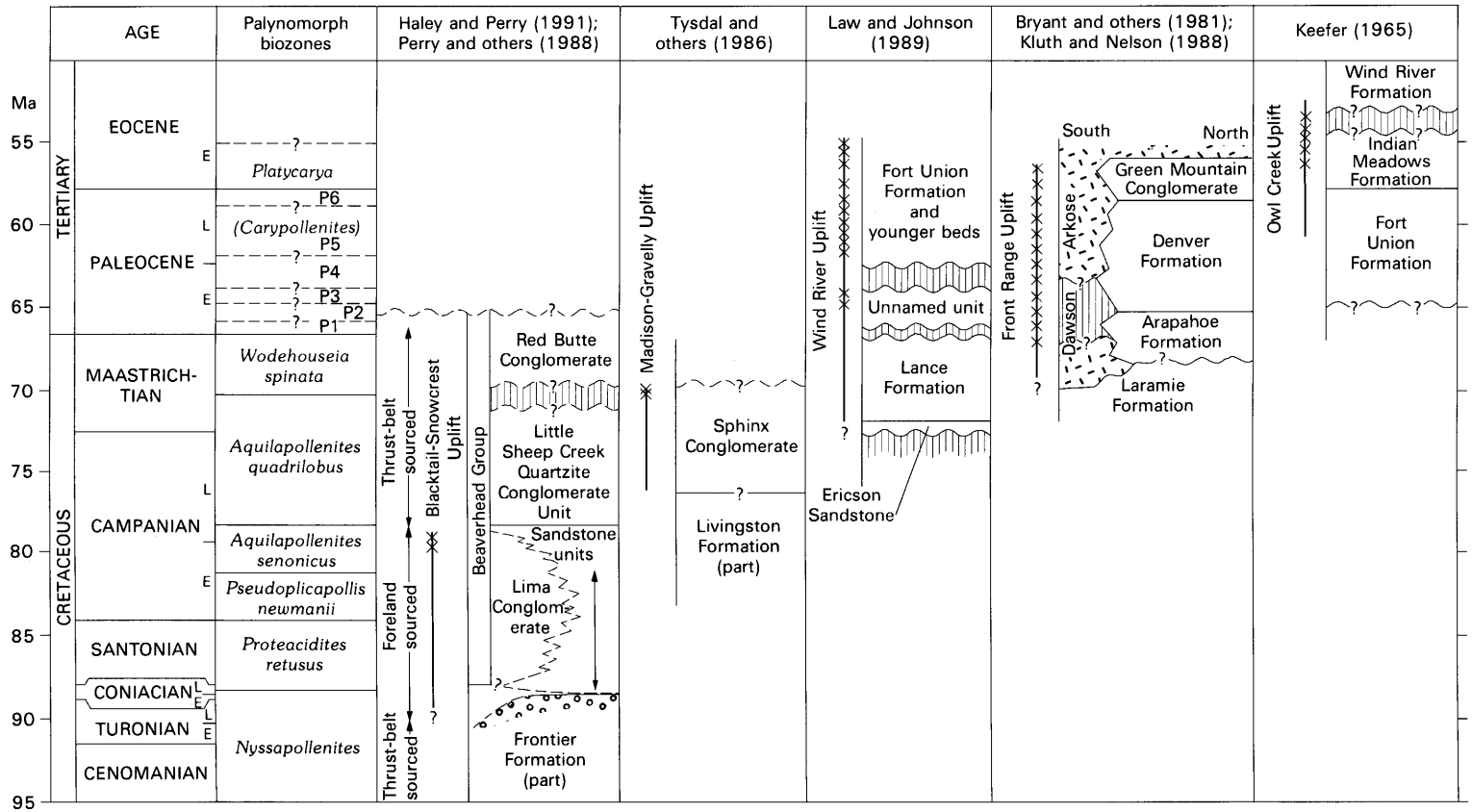

Figure 3. Chart showing duration of intense deformation of Laramide uplifts keyed to age and to palynomorph zones. x's mark times during which Precambrian rocks were exposed on uplifts.

Uplifts (fig. 1) began to develop in Paleocene time. The varying trends of these uplifts require first east-west shortening in late Maastrichtian and Paleocene time, followed by northeast-southwest shortening in early Eocene time, assuming that shortening was dominantly perpendicular to the trends of the ranges.

Hamilton (1981) offered the hypothesis that Laramide compressive deformation was caused by a 2°–4° clockwise rotation of the Colorado Plateau relative to the continental interior during late Late Cretaceous and early Tertiary time. This rotation can be readily eliminated as a cause for all but the latest Laramide events because structures bounding and defining the northern and northeastern margin of the Colorado Plateau (the south flank thrust of the Uinta Mountains, Axial Arch, Grand Hogback, and White River Uplift) are latest Laramide, middle to late Eocene in age (Tweto, 1975). Hamilton's mechanism may explain latest Laramide deformation in the southern and central Rocky Mountains.

Gries (1983b) proposed a multiphase model for Laramide deformation in Colorado and Wyoming. The first phase is characterized by east-west compression in latest Cretaceous time, which she believed was caused by the westward movement of the North American plate during opening of the North Atlantic ocean. The second is characterized by northeast-southwest compression in early Tertiary (chiefly Paleocene) time. The third is characterized by north-south compression in late Laramide (Eocene) time, during the opening of the Arctic Ocean. This is consistent with very young Laramide thrusting along the south flanks of the Granite Mountains and Shirley Mountains in southeastern Wyoming (see also Love, 1971; Blackstone, 1983), the Medicine Bow Mountains in Colorado (Independence Mountain Thrust) (see also Blackstone, 1977; Park, 1977), and the Uinta Mountains in northeastern Utah (see also Ritzma, 1971; Bryant and Nichols, 1988).

Schmidt and Garihan (1983) added another dimension to this controversy by showing evidence of oblique left-reverse Laramide motions along northwest-southeast-trending fault zones. This evidence is consistent with Brown's (1984) observations that a variety of fault styles would be generated with overall east-west shortening if older fault zones of varying trends were reactivated during the Laramide. Kulik and Schmidt (1988) stressed the spatial and temporal overlap between Sevier (thin-skin) thrusting and Laramide basement-involved thrust uplifts. Few of these workers, however, have considered the oldest Laramide events in southwestern Montana, the sequence of events, and the implications of these events, discussed below.

Acknowledgments.—Careful reviews by Chris Potter and Ben Law are appreciated, particularly the insistence by Law that we appreciate the complexity of the Cretaceous rocks in western Wyoming and by Potter that we carefully distinguish between uplift and denudation. The assistance of Marge MacLachlan in reformatting the charts (fig. 3) is most appreciated.

BLACKTAIL-SNOWCREST UPLIFT

Eardley (1960) recognized the Blacktail-Snowcrest Anticline of Scholten and others (1955) as a major Laramide uplift (figs. 1, 2) and, following the mapping by Klepper (1950), showed southeast-directed thrusting along the southeastern margin of this uplift. Eardley (1960, fig. 3, p. 88), however, mistakenly placed the Blacktail-Snowcrest Uplift in his "Paleocene phase (mid-Laramide)."

Ryder (1967), Wilson (1970), and Ryder and Scholten (1973) reexamined the Cretaceous synorogenic conglomerates and related siliciclastic rocks of the Beaverhead Group (Ryder's Beaverhead Formation) of the Lima region and showed that both foreland-sourced and thrust-belt-sourced conglomerates are present (figs. 2, 3). The Lima Conglomerate (fig. 3), the basal conglomerate of the Beaverhead Group, is mostly made up of limestone clasts derived from unroofing of the Blacktail-Snowcrest Uplift. The overlying sequence, characterized by the almost ubiquitous presence of Proterozoic quartzite clasts, was derived from the fold and thrust belt to the west. Based on palynologic work by A.T. Cross, Wilson (1970) showed that the Blacktail-Snowcrest Uplift was a highland during Campanian time. More recently, Nichols and others (1985) determined that the Blacktail-Snowcrest Uplift developed between Coniacian(?) and middle Campanian time. Perry and others (1988) showed that the Blacktail-Snowcrest Uplift had reached its present structural relief prior to middle Campanian time. The middle Campanian palynologic date (78–81 Ma) of Nichols and others (1985) was in the fining-upward sequence near the top of the Lima Conglomerate, which was derived from the Blacktail-Snowcrest Uplift.

Recent field work by Perry, Dyman, and Haley revealed the presence of Mesozoic limestone clasts in conglomerates of the upper part of the Frontier Formation (fig. 3) southeast of Lima Peaks. These clasts are as large as cobble size (20 cm diameter) near the peaks and fine southeastward away from the projected trace of the Blacktail-Snowcrest Uplift. They are composed of Lower Cretaceous gastropod limestone of the Kootenai Formation, micritic limestone of the lower part of the Kootenai, and oolitic limestone of the Jurassic Ellis Group. These clasts within the upper part of the Frontier become less abundant as well as smaller southeastward and generally occur within 17 km southeast of Lima Peaks. The thickness of the limestone-conglomerate-bearing stratigraphic interval also decreases markedly southeastward (Haley and others, 1991). The Frontier-Beaverhead contact is an angular unconformity near Lima Peaks; however, because the two units become conformable to the southeast, the contact is placed at the top of a green porcellanite unit in the Frontier-Beaverhead transition zone, the stratigraphically highest porcellanite (Dyman and others, 1991).

Although the top of the Frontier Formation has not been precisely dated southeast of Lima Peaks, it is unlikely to be younger than Turonian; a carbonaceous siltstone sample

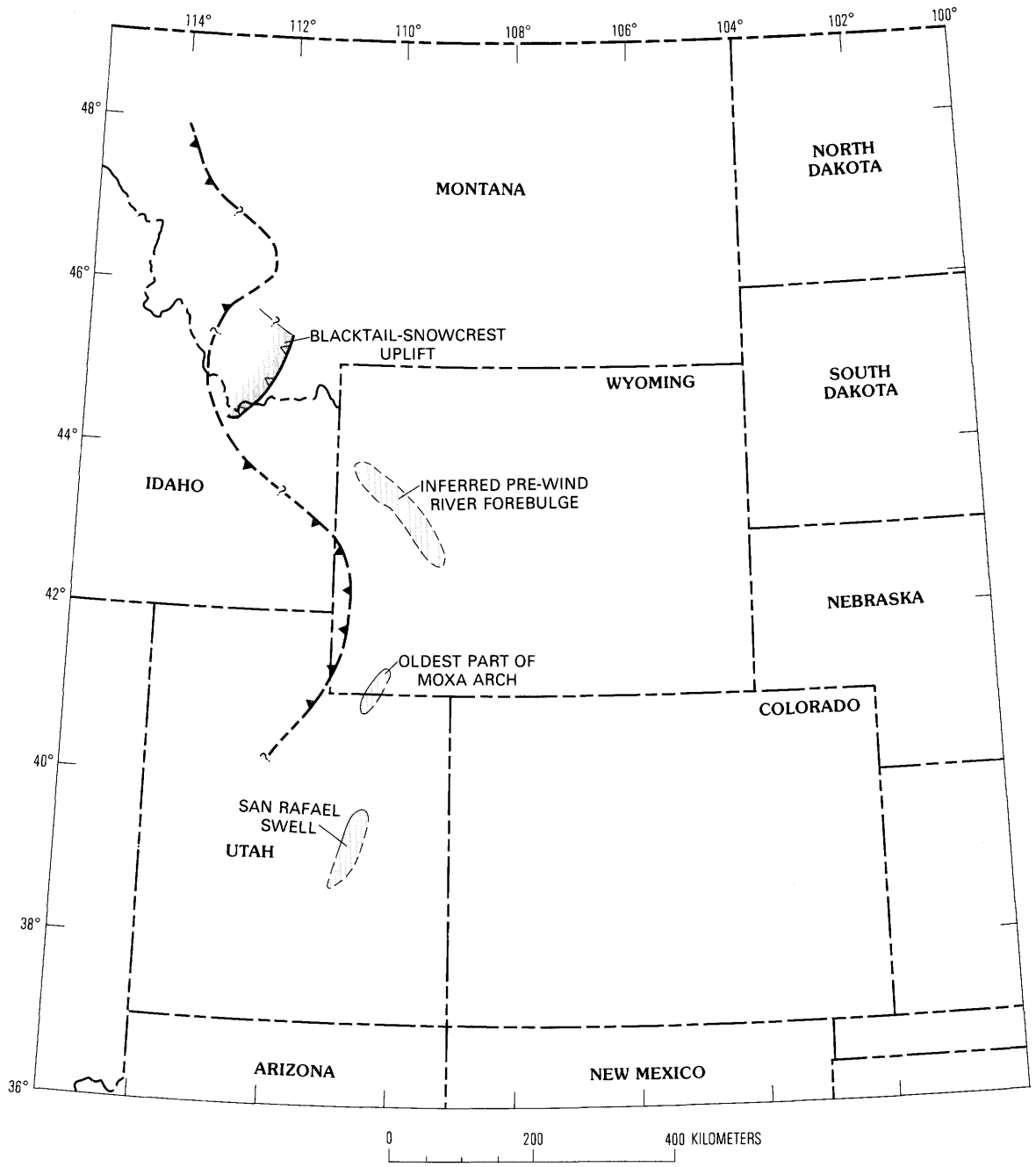

Figure 4. Areas of active Laramide uplifts during period 80–90 Ma. Dark pattern shows area of thrust-bounded uplift with more than 1,500 m of structural relief; light pattern marks area of less than 1,500 but more than 300 m of structural relief generated during this time period.

collected from near the top of the Frontier south of Lima Peaks (Dyman and others, 1991) contained primarily Cenomanian to Turonian palynomorphs typical of the Frontier Formation of Wyoming (Nichols and others, 1982). These rocks near the top of the Frontier are lithologically similar to other Frontier rocks of the region, the lower part of which are definitely Cenomanian. On this basis, Laramide uplift intense enough to have locally sourced conglomerates began about 90 Ma, or slightly earlier in the Lima region of southwestern Montana (fig. 4). The abnormal thickness (more than 2.1 km) of Frontier Formation in the vicinity of Lima Peaks suggests the possibility of a foredeep localized by tectonic loading due to thrusting of the adjacent southeastern margin of the Blacktail-Snowcrest Uplift as well as thin-skin thrusting in the Cordilleran thrust belt to the west (Dyman and others, 1989).

Archean clasts (gneiss, schist, and marble) have been observed in the upper part of the Lima Conglomerate

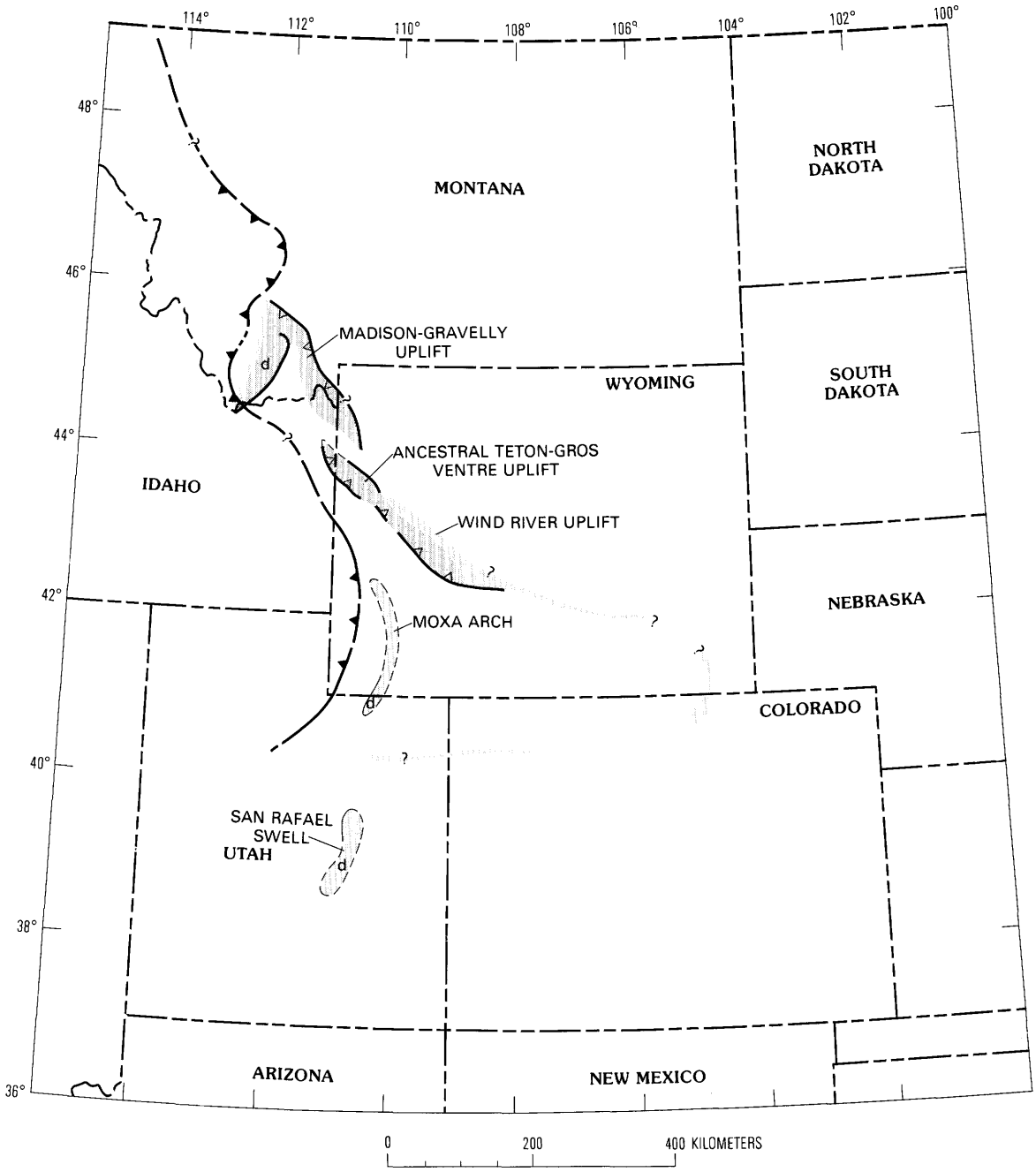

Figure 5. Areas of active Laramide uplifts during period 70–80 Ma. Dark pattern shows area of thrust-bounded uplift with more than 1,500 m of structural relief; light pattern marks area of less than 1,500 but more than 300 m of structural relief generated during this time period. (d) indicates previously active uplift area that is dormant during time period; (?) indicates queried uplift extension.

(Wilson, 1970; Perry and others, 1988) in association with Phanerozoic clasts derived from the uplift. Therefore it is reasonable to conclude that the entire Phanerozoic cover was stripped off at least part of the Blacktail-Snowcrest Uplift by 78–81 Ma (median of 79.5). The median palynologic date for cessation of deposition of Laramide synorogenic sediments eroded from the uplift (79.5 Ma) subtracted from 90 Ma provides an estimate (10.5 Ma) of duration of uplift and erosion.

Based on well data southeast of the uplift (Perry, 1986, drill-holes 1 and 2), a minimum of 2 km of pre-Laramide Cretaceous cover is estimated to have been stripped from the uplift. Similarly, 360 m of lower Mesozoic rocks, 1 km of Upper Paleozoic rocks (the Snowcrest trough sequence, Perry, 1986, fig. 3), and 800 m of Mississippian Madison Formation and older Phanerozoic rocks (Perry, 1986, drill-hole 2) would also have been stripped, a total of 4.16 km of Phanerozoic rocks during approximately 10.5 Ma. From

these data, we calculated an exhumation rate (England and Molnar, 1990) of 0.4 m/10^3 years. England and Molnar (1990) restricted the term "uplift" to mean uplift in terms of the geoid, usage not followed here because of the virtual impossibility of making accurate and precise estimates of the position of the pre-Quaternary geoid. By uplift we mean the uplift of a body of rock with respect to the surrounding land surface. Our calculated exhumation rate obviously underestimates actual uplift rate because it makes no allowance for the topographic relief between crest of uplift and adjacent basin or the depth to which the Precambrian basement was eroded, only the thickness of Phanerozoic strata eroded. To compensate for the second problem, we tried to record the time when basement was first exposed in an uplift, through biostratigraphic data, by bracketing the time when basement clasts, arkose, or metamorphic rock fragments first appear in the sediments shed from that uplift. Because uplift likely occurred chiefly during episodes of stick-slip uplift-margin faulting, a quite variable short-term uplift rate probably existed; we do not intend to imply continuous constant-rate uplift. Variations in rainfall also affect the exhumation rate. Despite these drawbacks, the exhumation rate is a useful comparative measure because it can be calculated for other uplifts farther to the east and southeast, for which first appearance of basement clasts in the material eroded from the uplift can be dated. Therefore the exhumation rate provides a basis for comparison of relative uplift rates, if we are allowed to assume that topographic relief was not vastly different between uplifts and that climatic differences were not so extreme as to overwhelm topographic controls on erosion rates.

MADISON-GRAVELLY UPLIFT

Scholten (1967) recognized that the Madison and Gravelly Ranges comprise the east and west flanks, respectively, of a Laramide uplift that he termed the Madison-Gravelly Uplift (fig. 2). The core of this uplift subsided during Tertiary and Quaternary Basin-Range extension to become the Madison Valley. Tysdal (1986) described the thrust faults and backthrusts of the Hilgard Fault System (fig. 2) along the complexly deformed eastern side of this uplift. This deformed terrane is similar to that along the southeastern limb of the Blacktail-Snowcrest Uplift described by Perry and others (1983, 1988). K-Ar and $^{40}Ar/^{39}Ar$ dating of hornblende from dacitic laccolithic rocks of the same suite as dacite dikes that intruded the Hilgard Fault System yielded ages of 68–69 Ma (Tysdal and others, 1986). These ages indicated to Tysdal and others that Laramide deformation in this area was virtually completed by the close of Cretaceous time, possibly 15 m.y. later than the cessation of growth of the Snowcrest structural terrane to the west (fig. 5). Tysdal and others (1986) reported a palynological age of approximately 79 Ma (early Campanian) from the lower part of the Livingston Formation (fig. 3), just below the oldest locally derived conglomerates (upper part of the Livingston) beneath the Sphinx Conglomerate (fig. 3), the youngest Laramide synorogenic deposit recognized in the Madison Range. If we accept that locally the major episode of Laramide deformation was over by 68–69 Ma and also accept that erosion proceeded synchronous with thrusting to expose Precambrian basement by this time, then primary Laramide growth and exhumation of the Madison-Gravelly Uplift took place during an interval of 10–11 m.y., between 79 Ma and 68–69 Ma. During this time 3.35 km of Phanerozoic cover would have been eroded from the uplift (thickness measured from Tysdal, 1990, section *D–D'*), yielding an estimated exhumation rate of 0.3 m/10^3 years, very close to that for the Blacktail-Snowcrest Uplift. In any case, this estimated rate is only a first approximation because the time of first exposure of the Precambrian basement is unknown for the Madison-Gravelly Uplift.

The contact between the Sphinx Conglomerate and underlying Livingston is conformable almost everywhere. Only the upper member of the Livingston is conglomeratic, consisting of interstratified sandstone and conglomerate (Tysdal and others, 1986). This lithofacies is similar to the much older Cenomanian to Turonian upper part of the Frontier Formation to the west, south of Lima Peaks. The base of the 200-m-thick upper (conglomeratic) member of the Livingston is 300–400 m above the interval dated as 79 Ma (Tysdal and others, 1986, p. 861). Laramide deformation in the Madison Range began probably no more than 76 Ma, about 14 m.y. later than that of the Blacktail-Snowcrest Uplift, based on estimated rapid sedimentation rates in the Livingston. The east-west shortening represented by the Hilgard Thrust System during very late Cretaceous time is consistent with the earliest phase of Laramide deformation in Colorado, described by Tweto (1975).

ANCESTRAL TETON–GROS VENTRE AND WIND RIVER UPLIFTS

Dorr and others (1977) were among the first to point out that the Late Cretaceous rise of the Ancestral Teton–Gros Ventre Uplift (fig. 2) provided a high-standing buttress of Precambrian rocks that deflected later structures in the frontal part of the Cordilleran thrust belt. Wiltschko and Dorr (1983, fig. 2) estimated the age of initial growth of the Ancestral Teton–Gros Ventre–Wind River Arch as about 73 Ma (figs. 3, 5). They showed that this early phase of uplift continued until early Maastrichtian time. In his section nearest the northern flank of the Wind River Range in the northwestern Wind River Basin (fig. 2), southwest of the axis of the basin, Keefer (1965) showed conglomerates in the basal Lance Formation (fig. 3) that he dated only as Late Cretaceous. If this basal Lance is correlative with that described

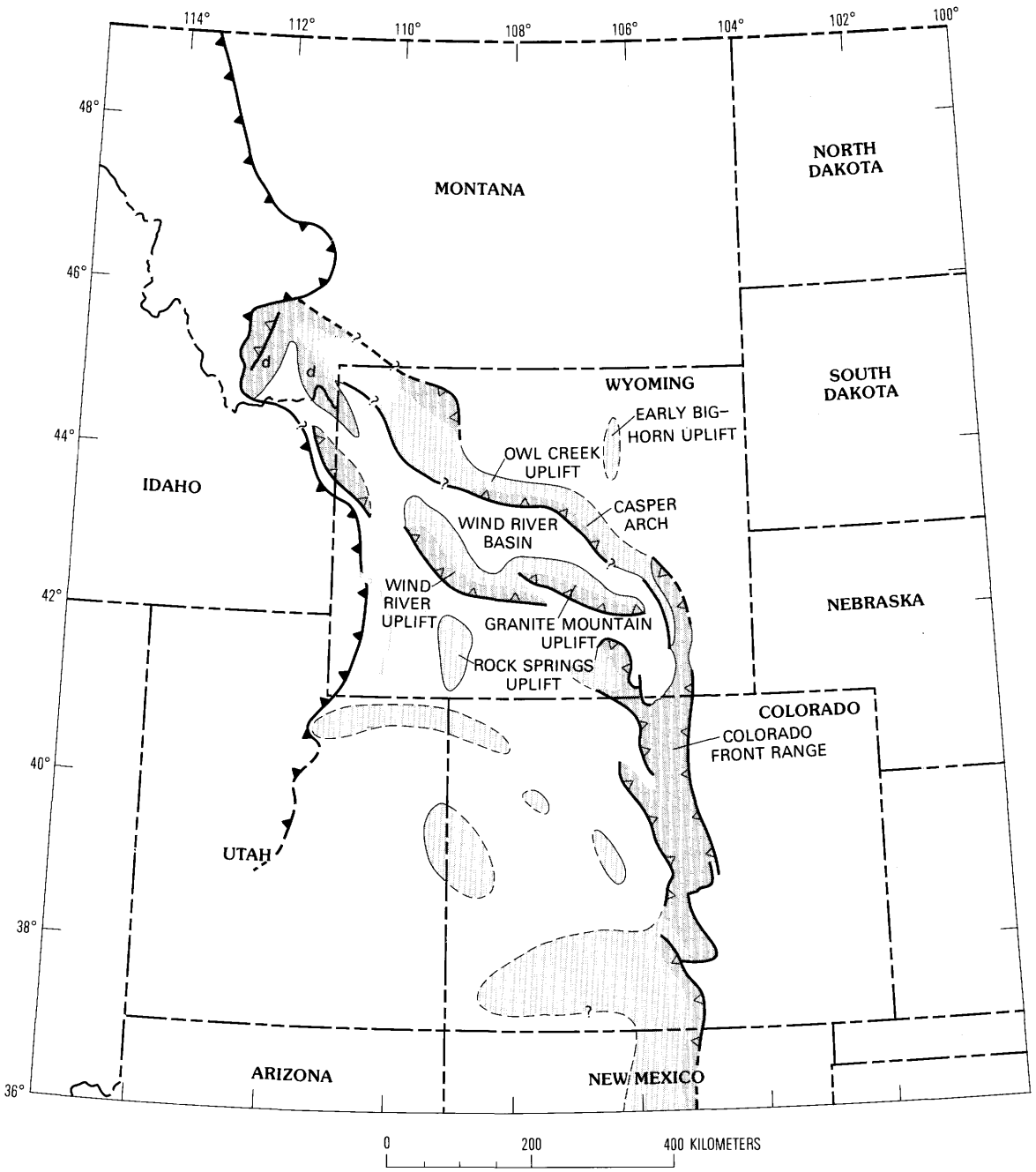

Figure 6. Areas of active Laramide uplifts during period 60–70 Ma. Dark pattern shows area of thrust-bounded uplift with more than 1,500 m of structural relief; light pattern marks area of less than 1,500 but more than 300 m of structural relief generated during this time period. (d) indicates previously active uplift area that is dormant during time period; (?) indicates queried uplift extension.

by Law and Johnson (1979) from the subsurface west of the Wind River Uplift, then the presence of these conglomerates is compatible with the 73-Ma estimate of initiation of uplift by Wiltschko and Dorr (1983). Keefer (1965) also showed the Lance pinching out along the northeastern flank of the Ancestral Teton–Gros Ventre and Wind River Uplifts.

More recently, Shuster and Steidtmann (1988) developed a growth history of the Wind River Uplift based on burial history curves, sandstone provenance studies, and inferred thrust-loading along the northeastern margin of the Green River Basin (adjacent to the Wind River Uplift). They concluded that a "subsidence event at approximately 90 Ma may indicate initial uplift of the Wind River block." They also identified a very rapid subsidence event in the area of the Pinedale Anticline (adjacent to the Wind River Uplift) during Maastrichtian time, which they considered to be

probably due to tectonic loading by the growing Wind River Thrust. Apatite fission-track studies by Shuster (1986) indicate "that the Wind River uplift began between 80 and 90 Ma and moved upward about 8 km."

More extensive, recent apatite fission-track studies by Cerveny (1990) indicate that growth of the Wind River Uplift may have begun by 85 Ma but was clearly underway by 75 Ma, in reasonably good agreement with Wiltschko and Dorr (1983). Cores of the Late Cretaceous Lance Formation from wells drilled in the northeastern Green River Basin contain detrital limestone and dolomite grains (Law and others, 1986) probably derived from Paleozoic limestones being eroded from the adjacent Wind River Uplift during Maastrichtian time, consistent with the results of Cerveny (1990). Ages of uplift in the 80–90-Ma time period in the Wind River Uplift area may relate to a broad forebulge that encompassed the present area of the Rock Springs Uplift as well as the Ancestral Teton–Gros Ventre and Wind River Uplifts and not to the time of initiation of these Laramide structures.

In contrast to the Madison-Gravelly Uplift, which apparently lacks a Tertiary growth history, Cerveny (1990) showed that the northern part of the Wind River Uplift underwent most rapid cooling (presumably uplift) between 60 and 57 Ma, soon after Precambrian basement was exposed based on the first appearance of arkose derived from the Wind River Uplift in the northern Green River Basin (Prensky, 1989). The arkose is in an unnamed lower Tertiary unit (fig. 3) dated palynologically as early to middle Paleocene in age (Law and Johnson, 1989).

EASTWARD PROGRESSION OF LARAMIDE DEFORMATION IN WYOMING

Wind River Basin

The Wind River Basin in west-central Wyoming (figs. 1, 6) occupies a critical position with respect to the sequential development of Laramide structure in Wyoming. Our discussion of the tectonic development of the Wind River Basin is summarized from Keefer (1965) unless otherwise stated. Conglomerate in the Late Cretaceous Lance Formation in the northwestern part of the Wind River Basin, nearest the Wind River Uplift, contains granule-size fragments and scattered pebbles of chert, silicious shale, and porcellanite. Here the Lance is about 350 m thick (Keefer, 1965, p. A17), and only the lower part is conglomeratic. Keefer found no definite evidence for uplift of the Wind River Range during Cretaceous time, but his control was inadequate along the southwestern margin of the basin (contours dashed, no control points within 48 km of the northeastern flank of the Wind River Mountains, see his fig. 9). Perry suggests that the above described conglomerate in the lower part of the Lance was probably eroded from Frontier and older Mesozoic rocks exposed on the growing Wind River Uplift.

Murphy and Love (1958) inferred that a broad, domal uplift developed in latest Cretaceous time on the southeastern flank of the Wind River Basin in the area of the present Granite Mountains. Keefer (1965) reached similar conclusions. In a summary of the Laramide history of the Granite Mountains area, Love (1971) indicated that uplift of this area did not begin until latest Cretaceous time and culminated in earliest Eocene time. He suggested that the early phase of this uplift may have been coextensive with that of the south-central part of the Wind River Range.

Keefer (1965) concluded that the Cretaceous-Tertiary boundary in the Wind River Basin is generally conformable, but that extensive downwarping occurred at this time along the present-day northern margin of the basin. Along the northeastern margin of the Wind River Basin, Keefer (1965) observed that the oldest conglomerate zones are in the lower Eocene Indian Meadows Formation. The oldest arkosic conglomerate in this part of the basin is at the base of the Lost Cabin Member of the overlying Eocene Wind River Formation. The presence of extensive lacustrine sediments, which first appeared in the Wind River Basin in late Paleocene time (Nichols and Ott, 1978; Phillips, 1983), is indicative of internal drainage that likely reflects initial growth of the Casper Arch and Owl Creek Uplift (figs. 1, 6) that closed the outlets of the basin.

Keefer (1965) estimated 2.7 km of middle to late Paleocene uplift in the Owl Creek Mountains and 3.2 km of subsidence in the adjacent Wind River Basin; these amounts indicate a cumulative vertical separation (uplift+subsidence) rate of about 1.3 m/10^3 years using the time scale shown in figure 3. Keefer estimated an additional 2.6 km of uplift and an additional 1.7 km of subsidence in early Eocene time, a cumulative vertical separation rate of about 1.2 m/10^3 years. He showed that thrust faults of the Casper Arch cut the lower Eocene Indian Meadows Formation and that the rocks deformed by this thrusting are erosionally truncated by the overlying lower Eocene Wind River Formation. These relations date the cessation of major Laramide deformation in the area as early Eocene. For comparability with exhumation rates calculated for uplifts in southwestern Montana (approximately 0.4 m/10^3 years for the Blacktail-Snowcrest Uplift and 0.3 m/10^3 years for Madison-Gravelly Uplift derived above), the middle to late Paleocene uplift rate for the Owl Creek Mountains is 0.46 m/10^3 years and the early Eocene rate 0.6 m/10^3 years, based on Keefer's estimates of topographic relief and exhumation and our time scale (fig. 3). We find it remarkable how similar these generalized rates are, calculated from different data sets for different Laramide uplifts. The amount of surface relief shown by Keefer (1965) is merely a guess, of course.

Hanna Basin Region

Blackstone (1983) and Hansen (1986) summarized, respectively, the complex structural geometry and tectonic

history of the Hanna Basin region southeast of the Granite Mountains–Sweetwater Uplift (fig. 1) and suggested that the major west-northwest-trending thrust fault bounding the northern flank of the Hanna Basin is late Paleocene to early Eocene in age. A major unconformity between the Late Cretaceous Pierre Shale and middle Paleocene part of the Coalmont Formation in the North Park Basin south of the Medicine Bow Uplift indicates that the entire area from the Medicine Bow Mountains (and Park Range to the south) eastward to the Colorado Front Range may have been a single broad highland in latest Cretaceous time (Hail, 1965; Wellborn, 1977; Madden, 1979; S.B. Roberts, U.S. Geological Survey, oral commun., 1990).

COLORADO FRONT RANGE

Laramide basement faulting in the Front Range began at 69.3±1.1 Ma (Wallace, 1988). Kluth and Nelson (1988) detailed the uplift history of the Colorado Front Range based on proprietary fission-track and palynologic investigations that are compatible with unpublished data of Nichols. They stated that the basement was exposed in the core of the Front Range by 68 Ma, as indicated by the first appearance of arkosic sediments and basement clasts in the Upper Cretaceous to Eocene Dawson Arkose (fig. 3). Three kilometers of Phanerozoic cover (estimated by Wallace, 1988) was removed from the Front Range during a strikingly brief period of one (or at most two) million years. Based on these values an exhumation rate of 3 m/10^3 years (or minimally 1.5 m/10^3 years) can be calculated. These rates are much greater than Laramide exhumation rates calculated for the Owl Creek Mountains in south-central Wyoming and almost an order of magnitude greater than rates calculated for the older Laramide uplifts of southwestern Montana.

ECONOMIC IMPLICATIONS

A relatively simple unpartitioned Cretaceous foreland basin was envisioned by Dickinson and Snyder (1978, fig. 1) and Cross (1986), although Schwartz (1982), DeCelles (1986), Merewether and Cobban (1986), and Schwartz and DeCelles (1988) indicated that broad tectonic welts of probably low amplitude were present in the Rocky Mountain foreland during late Early and early Late Cretaceous time. The rise of the Blacktail-Snowcrest Uplift, beginning about 90 Ma, would have provided a barrier to eastward updip migration of hydrocarbons generated in the rapidly subsiding foredeep developed in front of the eastward-advancing Helena and Wyoming Salients of the Cordilleran Thrust Belt (fig. 4). Beginning about 75 Ma, a perhaps continuous structural barrier to eastward migration of hydrocarbons would have developed from the northeastern tip of the Blacktail-Snowcrest Uplift, southward through the Madison-Gravelly Uplift, and southeastward through the Ancestral Teton–Gros Ventre–Wind River Uplifts. As a consequence of this structural barrier, hydrocarbons generated farther to the west may have migrated into the southern Green River Basin–Hanna Trough region of southern Wyoming, a major fairway of hydrocarbon production in Wyoming.

SUMMARY

Intense Laramide deformation of the Rocky Mountain foreland began in southwestern Montana at about 90 Ma. The Madison-Gravelly Uplift to the east and Ancestral Teton–Gros Ventre–Wind River Uplifts in western Wyoming began intense growth about 75 Ma. These two uplifts may have been originally coextensive (fig. 2). Near the close of Cretaceous time, intense Laramide deformation spread eastward to the Granite Mountains and Colorado Front Range. This sequence of events cannot be related directly to either Eocene rotation or displacement of the Colorado Plateau but may be related to a southeastward-advancing zone of decoupling in the lower to middle crust that was initiated in southwestern Montana about 90 Ma.

REFERENCES CITED

Armstrong, R.L., 1968, Sevier orogenic belt in Nevada and Utah: Geological Society of America Bulletin, v. 79, p. 429–458.

Baltz, E.H., 1972, Geologic map and cross-sections of the Gallinas Creek area, Sangre de Cristo Mountains, San Miguel County, New Mexico: U.S. Geological Survey Miscellaneous Geological Investigations Map I–673.

Bayley, R.W., and Muehlberger, W.R. 1968, Basement rock map of the United States: U.S. Geological Survey, scale 1:2,500,000.

Berg, R.R., 1962, Mountain flank thrusting in Rocky Mountain Foreland, Wyoming and Colorado: American Association of Petroleum Geologists Bulletin, v. 46, no. 11, p. 2029–2032.

Blackstone, D.L., Jr., 1963, Development of geologic structure in central Rocky Mountains, *in* Childs, O.E., and Beebe, B.W., eds., Backbone of the Americas: American Association of Petroleum Geologists Memoir 2, p. 160–179.

_____ 1977, Independence Mountain thrust fault, North Park basin, Colorado: Contributions to Geology, University of Wyoming, v. 16, p. 1–15.

_____ 1983, Laramide Compressional tectonics, southeastern Wyoming: Contributions to Geology, University of Wyoming, v. 22, p. 1–38.

Brewer, J.A., Smithson, S.B., Oliver, J.E., Kaufman, S., and Brown, L.D., 1980, The Laramide orogeny—Evidence from COCORP deep crustal seismic profiles in the Wind River Mountains, Wyoming: Tectonophysics, v. 62, p. 165–189.

Brown, W.G., 1984, Basement involved tectonics, foreland areas: American Association of Petroleum Geologists Continuing Education Course Note Series, no. 26, 92 p.

_____ 1988, Deformational style of Laramide uplifts in the Wyoming foreland, *in* Schmidt, C.J., and Perry, W.J., Jr., eds., Interaction of the Rocky Mountain foreland and Cordilleran

thrust belt: Geological Society of America Memoir 171, p. 1–25.

Bryant, B., McGrew, L.W., and Wobus, R.A., 1981, Geologic map of the Denver 1°×2° Quadrangle, north-central Colorado: U.S. Geological Survey Miscellaneous Investigations Series Map I–1163, sheet 1, scale 1:250,000.

Bryant, B., and Nichols, D.J., 1988, Late Mesozoic and early Tertiary reactivation of an ancient crustal boundary along the Uinta trend and its interaction with the Sevier orogenic belt, *in* Schmidt, C.J., and Perry, W.J., Jr., eds., Interaction of the Rocky Mountain foreland and Cordilleran thrust belt: Geological Society of America Memoir 171, p. 411–430.

Cerveny, P., 1990, Fission-track thermochronology of the Wind River Range and other basement cored uplifts in the Rocky Mountain foreland: Laramie, University of Wyoming, Ph.D thesis, 189 p.

Chamberlin, R.T., 1919, The building of the Colorado Rockies: Journal of Geology, v. 27, p. 145–164.

_____ 1923, On the crustal shortening of the Colorado Rockies: American Journal of Science, 5th Series, v. 6, p. 215–221.

Cross, T.A., 1986, Tectonic controls of foreland basin subsidence and Laramide style deformation, western United States, *in* Allen, P.A., and Homewood, P., eds., Foreland basins: International Association of Sedimentologists Special Publication 8, p. 15–39.

DeCelles, P.G., 1986, Sedimentation in a tectonically partitioned, nonmarine foreland basin; the Lower Cretaceous Kootenai Formation, southwestern Montana: Geological Society of America Bulletin, v. 97, p. 911–931.

Dickinson, W.R., Klute, M.A., Hayes, M.J., Janecke, S.U., Lundin, E.R., McKittrick, M.A., and Olivares, M.D., 1988, Paleogeographic and paleotectonic setting of Laramide sedimentary basins in the central Rocky Mountain region: Geological Society of America Bulletin, v. 100, p. 1023–1039.

Dickinson, W.R., and Snyder, W.S., 1978, Plate tectonics of the Laramide orogeny, *in* Matthews, V., ed., Laramide folding associated with basement block faulting in the western United States: Geological Society of America Memoir 151, p. 355–366.

Dorr, J.A, Jr., Spearing, D.R., Steidtmann, J.R., 1977, Deformation and deposition between a foreland uplift and an impinging thrust belt—Hoback basin, Wyoming: Geological Society of America Special Paper 177, 82 p.

Dyman, T.S., Haley, J.C., and Perry, W.J., Jr., 1991, Revision of Frontier Formation–Beaverhead Group contact, Lima Peaks area, southwestern Montana and southeastern Idaho, *in* Contributions to Late Cretaceous stratigraphy and paleontology, western Montana: U.S. Geological Survey Bulletin 1962, p. 1–7.

Dyman, T.S., Perry, W.J., Jr., Nichols, D.J., Davis, L.E., and Haley, J.C., 1989, Stratigraphy, petrology, and provenance of the Cenomanian to Turonian Frontier Formation near Lima, southwestern Montana, *in* French, D.E., and Grabb, R.F., eds., Geologic resources of Montana: Montana Geological Society 1989 Field Conference Guidebook, p. 103–114.

Eardley, A.J., 1960, Phases of orogeny in the deformed belt of southwestern Montana and adjacent areas of Idaho and Wyoming, *in* Campau, D.E., and Anisgard, H.W., eds., West Yellowstone earthquake area: Billings Geological Society 11th Annual Field Conference Guidebook, p. 86–91.

England, P., and Molnar, P., 1990, Surface uplift, uplift of rocks, and exhumation of rocks: Geology, v. 18, p. 1173–1177.

Gries, R., 1981, Oil and gas prospecting beneath the Precambrian of foreland thrust plates in the Rocky Mountains: The Mountain Geologist, v. 18, no. 1, p. 1–18.

_____1983a, Oil and gas prospecting beneath Precambrian of foreland thrust plates in Rocky Mountains: American Association of Petroleum Geologists Bulletin, v. 67, p. 1–28.

_____ 1983b, North-south compression of Rocky Mountain foreland structures, *in* Lowell, J.D., and Gries, R., eds., Rocky Mountain foreland basins and uplifts: Rocky Mountain Association of Geologists, p. 9–32.

Hail, W.J., Jr., 1965, Geology of northwestern North Park, Colorado: U.S. Geological Survey Bulletin 1188, 133 p.

Haley, J.C., Dyman, T.S., and Perry, W.J., Jr., 1991, The Frontier Formation—A record of mid-Cretaceous foreland uplift in southwestern Montana: Geological Society of America Abstracts with Programs, v. 23, no. 4, p. 29.

Haley, J.C., and Perry, W.J., Jr., 1991, The Red Butte Conglomerate—A thrust-belt derived conglomerate of the Beaverhead Group, southwestern Montana: U.S. Geological Survey Bulletin 1945, 19 p.

Hamilton, W.B., 1981, Plate-tectonic mechanism of Laramide deformation: University of Wyoming, Contributions to Geology, v. 19, p. 87–92.

_____ 1988, Laramide crustal shortening, *in* Schmidt, C.J., and Perry, W.J., Jr., eds., Interaction of the Rocky Mountain foreland and Cordilleran thrust belt: Geological Society of America Memoir 171, p. 27–39.

Hansen, D.E., 1986, Laramide tectonics and deposition of the Ferris and Hanna Formations, south-central Wyoming, *in* Peterson, J.A., Paleotectonics and sedimentation: American Association of Petroleum Geologists Memoir 41, p. 481–495.

Keefer, W.R., 1965, Stratigraphy and geologic history of the uppermost Cretaceous, Paleocene, and lower Eocene rocks in the Wind River basin, Wyoming: U.S. Geological Survey Professional Paper 495–A, 77 p.

Klepper, M.R., 1950, A geologic reconnaissance of parts of Beaverhead and Madison Counties, Montana: U.S. Geological Survey Bulletin 969–C, 85 p., 1 sheet, scale 1:250,000.

Kluth, C.F., and Nelson, S.N., 1988, Age of the Dawson Arkose, southwestern Air Force Academy, Colorado, and implications for the uplift history of the Front Range: The Mountain Geologist, v. 25, p. 29–35.

Kulik, D.M., and Schmidt, C.J., 1988, Region of overlap and styles of interaction of the Cordilleran thrust belt and Rocky Mountain foreland, *in* Schmidt, C.J., and Perry, W.J., Jr., Interaction of the Rocky Mountain foreland and the Cordilleran thrust belt: Geological Society of America Memoir 171, p. 75–98.

Law, B.E., and Johnson, R.C., 1989, Structural and stratigraphic framework of the Pinedale anticline, Wyoming, and the Multiwell Experiment site, Colorado, *in* Law, B.E., and Spencer, C.W., eds., Geology of tight gas reservoirs in the Pinedale anticline area, Wyoming, and at the Multiwell Experiment site, Colorado: U.S. Geological Survey Bulletin 1886, p. B1–B11.

Law, B.E., Pollastro, R.M., and Keighin, C.W., 1986, Geologic characterization of low-permeability gas reservoirs in selected wells, Greater Green River Basin, Wyoming, Colorado, and Utah, *in* Spencer, C.W., and Mast, R.F., eds., Geology of tight gas reservoirs: American Association of Petroleum Geologists Studies in Geology 24, p. 253–270.

Lipman, P.W., Prostka, H.J., and Christiansen, R.L., 1971, Evolving subduction zones in the western United States, as interpreted from igneous rocks: Science, v. 174, p. 821–825.

Love, J.D., 1971, Relation of Cenozoic geologic events in the Granite Mountains area, central Wyoming, to economic deposits, *in* Renfro, A. R., ed., Symposium on Wyoming tectonics and

their economic significance: Wyoming Geological Association 23rd Annual Field Conference Guidebook, p. 74–80.

Lowell, J.D., 1974, Plate tectonics and foreland basement deformation: Geology, v. 2, no. 6, p. 275–278.

Madden, D.R., 1979, Biostratigraphy of the Pierre Shale in North Park, Colorado, and correlation with sections in Boulder, Middle Park, and northwest Colorado: U.S. Geological Survey Open-File Report 79–729, 17 p, scale 1:62,500.

Merewether, E.A., and Cobban, W.A., 1986, Biostratigraphic units and tectonism in the mid-Cretaceous foreland of Wyoming, Colorado, and adjoining areas, *in* Peterson, J.A., ed., Paleotectonics and sedimentation: American Association of Petroleum Geologists Memoir 41, p. 443–468.

Murphy, J.F., and Love, J.D., 1958, Tectonic development of the Wind River Basin, central Wyoming [abs.]: American Association of Petroleum Geologists Rocky Mountain Section, p. 126–127.

Nichols, D.J., Jacobson, S.R., and Tschudy, R.H., 1982, Cretaceous palynomorph biozones for the central and northern Rocky Mountain region of the United States, *in* Powers, R.B., ed., Geologic studies of the Cordilleran thrust belt—1982: Rocky Mountain Association of Geologists, p. 721–733.

Nichols, D.J., and Ott, H.L., 1978, Biostratigraphy and evolution of the *Momipites-Caryapollenites* lineage in the Early Tertiary in the Wind River basin, Wyoming: Palynology, v. 2, p. 93–112.

Nichols, D.J., Perry, W.J., Jr., and Haley, J.C., 1985, Reinterpretation of the palynology and age of Laramide syntectonic deposits, southwestern Montana, and revision of the Beaverhead Group: Geology, v. 13, p. 149–153.

Park, G.M., 1977, Oil potential of Mesozoic sediments beneath the Independence Mountain thrust fault, North Park, Colorado, *in* Veal, H.K., ed., Exploration frontiers of the central and southern Rockies: Rocky Mountain Association of Geologists, p. 61–66.

Perry, W.J., Jr., 1986, Critical deep drillholes and indicated paleotectonic features north of the Snake River downwarp in southern Beaverhead County, Montana, and adjacent Idaho: U.S. Geological Survey Open-File Report 86–413, 16 p.

Perry, W.J., Jr., Haley, J.C., Nichols, D.J., Hammons, P.M., and Ponton, J. D., 1988, Interactions of Rocky Mountain foreland and Cordilleran thrust belt in Lima region, southwest Montana, *in* Schmidt, C.J., and Perry, W.J., Jr., eds., Interaction of the Rocky Mountain foreland and Cordilleran thrust belt: Geological Society of America Memoir 171, p. 267–290.

Perry, W.J., Jr., Wardlaw, B.R., Bostick, N.H., and Maughan, E.K., 1983, Structure, burial history, and petroleum potential of the frontal thrust belt and adjacent foreland, southwest Montana: American Association of Petroleum Geologists Bulletin, v. 67, no. 5, p. 725–743.

Petersen, F.A., 1983, Foreland detachment structures, *in* Lowell, J.D., and Gries, R., eds., Rocky Mountain foreland basins and uplifts: Rocky Mountain Association of Geologists, p. 65–77.

Phillips, S.T., 1983, Tectonic influence on sedimentation, Waltman Member, Fort Union Formation, Wind River Basin, Wyoming, *in* Lowell, J.D., and Gries, R., eds., Rocky Mountain foreland basins and uplifts: Rocky Mountain Association of Geologists, p. 149–160.

Prensky, S.E., 1989, Gamma-ray well-log anomaly in the northern Green River basin of Wyoming, *in* Law, B.E., and Spencer, C.W., eds., Geology of tight gas reservoirs in the Pinedale anticline area, Wyoming, and at the Multiwell Experiment site, Colorado: U.S. Geological Survey Bulletin 1886, p. H1–H21.

Ritzma, H.R., 1971, Faulting on the north flank of the Uinta Mountains, Utah and Colorado, *in* Renfro, A.R., Madison, L.V., and Jarre, G.A., eds., Symposium on Wyoming tectonics and their economic significance: Wyoming Geological Association 23rd Annual Field Conference Guidebook, p. 145–150.

Ryder, R.T., 1967, Lithosomes in the Beaverhead Formation, Montana-Idaho, a preliminary report: Montana Geological Society 18th Annual Field Conference Guidebook, p. 63–70.

Ryder, R.T., and Scholten, Robert, 1973, Syntectonic conglomerates in southwest Montana; their nature, origin, and tectonic significance: Geological Society of America Bulletin, v. 84, p. 773–796.

Schmidt, C.J., and Garihan, J.M., 1983, Laramide tectonic development of the Rocky Mountain foreland of southwestern Montana, *in* Lowell, J.D., ed., Rocky Mountain basins and uplifts: Rocky Mountain Association of Geologists, p. 271–294.

Scholten, R., 1967, Structural framework and oil potential of extreme southwestern Montana: Montana Geological Society 18th Annual Field Conference Guidebook, p. 7–19.

Scholten, R., Keenmon, K.A., and Kupsch, W.O., 1955, Geology of the Lima region, Montana-Idaho: Geological Society of America Bulletin, v. 66, p. 345–404.

Schwartz, R.K., 1982, Broken Cretaceous foreland basin in southwestern Montana—Sedimentation related to tectonism, *in* Powers, R.B., ed., Geologic studies of the Cordilleran thrust belt—1982: Rocky Mountain Association of Geologists, v. 1, p. 159–183.

Schwartz, R.K., and DeCelles, P.G., 1988, Cordilleran foreland basin evolution in response to interactive Cretaceous thrusting and foreland partitioning, southwestern Montana, *in* Schmidt, C.J., and Perry, W.J., Jr., eds., Interaction of the Rocky Mountain foreland and Cordilleran thrust belt: Geological Society of America Memoir 171, p. 489–513.

Shuster, M.W., 1986, The origin and sedimentary evolution of the northern Green River basin, western Wyoming: Laramie, University of Wyoming, Ph.D. thesis, 323 p.

Shuster, M.W., and Steidtmann, J.R., 1988, Tectonic and sedimentary evolution of the northern Green River basin, western Wyoming, *in* Schmidt, C.J., and Perry, W.J., Jr., eds., Interaction of the Rocky Mountain foreland and Cordilleran thrust belt: Geological Society of America Memoir 171, p. 515–529.

Smithson, S.B., Brewer, J.A., Kaufman, S., Oliver, J.E., and Hurich, C.A., 1978, Nature of the Wind River thrust, Wyoming, from COCORP deep-reflection data and from gravity data: Geology, v. 6, p. 648–652.

_____ 1979, Structure of the Laramide Wind River uplift, Wyoming, from COCORP deep-reflection data and from gravity data: Journal of Geophysical Research, v. 84, p. 5955–5972.

Tweto, Ogden, 1975, Laramide (Late Cretaceous–early Tertiary) orogeny in southern Rocky Mountains: Geological Society of America Memoir 155, p. 1–43.

Tysdal, R.G., 1986, Thrust faults and backthrusts in Madison Range of southwestern Montana foreland: American Association of Petroleum Geologists Bulletin, v. 70, p. 360–376.

_____ 1988, Deformation along the northeast side of Blacktail Mountains salient, southwestern Montana, *in* Schmidt, C.J., and Perry, W.J., Jr., eds., Interaction of the Rocky Mountain foreland and Cordilleran thrust belt: Geological Society of America Memoir 171, p. 203–215.

_____ 1990, Geologic map of the Sphinx Mountain Quadrangle and adjacent parts of the Cameron, Cliff Lake, and Hebgen Dam Quadrangles, Montana: U.S. Geological Survey Miscellaneous Investigations Map I–1815, scale 1:62,500.

Tysdal, R.G., Marvin, R.F., and DeWitt, E., 1986, Late Cretaceous stratigraphy, deformation, and intrusion in the Madison Range of southwestern Montana: Geological Society of America Bulletin, v. 97, p. 859–868.

Tysdal, R.G., Nichols, D.J., and Winkler, G.R., 1987, The Livingston Formation in the Madison Range of southwestern Montana: U.S. Geological Survey Bulletin 1665, 15 p.

Wallace, A.R., 1988, Comment on "Age of the Dawson Arkose, southwestern Air Force Academy, Colorado, and implications for the uplift history of the Front Range": The Mountain Geologist, v. 25, p. 37–38.

Wellborn, R.E., 1977, Structural style in relation to oil and gas exploration in North Park–Middle Park basin, Colorado, *in* Veal, H.K., ed., Exploration frontiers of the central and southern Rockies: Rocky Mountain Association of Geologists, p. 41–60.

Wilson, C.W., Jr., 1936, Geology of Nye-Bowler lineament, Stillwater and Carbon Counties, Montana: American Association of Petroleum Geologists Bulletin, v. 20, p. 1161–1188.

Wilson, M.D., 1970, Upper Cretaceous–Paleocene synorogenic conglomerates of southwestern Montana: American Association of Petroleum Geologists Bulletin, v. 54, p. 1843–1867.

Wiltschko, D.V., and Dorr, J.A., Jr., 1983, Timing of deformation in overthrust belt and foreland of Idaho, Wyoming, and Utah: American Association of Petroleum Geologists Bulletin, v. 67, p. 1304–1322.

Chapter D

Influence of Crustal Structure on the Course of the Arkansas River, South-Central Colorado

By KEN WATSON, DANIEL H. KNEPPER, JR., and MICHAEL W. WEBRING

U.S. GEOLOGICAL SURVEY BULLETIN 2012

APPLICATION OF STRUCTURAL GEOLOGY TO MINERAL AND ENERGY RESOURCES OF THE CENTRAL AND WESTERN UNITED STATES

CONTENTS

FIGURES

Influence of Crustal Structure on the Course of the Arkansas River, South-Central Colorado

By Ken Watson[1], Daniel H. Knepper, Jr.[1], *and* Michael W. Webring[1]

Abstract

On small-scale aerial photos, satellite images, topographic maps, and digital terrain images, the linear northeast-trending segment of the Arkansas River between Coaldale and Parkdale, south-central Colorado, and the somewhat longer associated topographic lineament suggest to even the casual observer an element of geologic control. This segment of the river is generally considered to be a superposed stream established during regional uplift and incised in late Pliocene and Pleistocene time. Although joints in Proterozoic crystalline rocks probably exert control on the path of the river on a local scale, evaluation of geologic maps indicates that the regional trend and location of the river and its associated topographic lineament are not controlled by a single structural feature (fault, shear zone, broad-scale folding).

Examination of published geophysical maps and processing and analysis of digital geophysical data for the western half of the Pueblo, Colorado, 1°×2° Quadrangle indicate that the Arkansas River and its topographic lineament spatially correspond approximately to a northeast-trending boundary between contrasting crustal blocks of the southern Front Range to the north and the Wet Mountains and DeWeese Plateau to the south. Exposed Cambrian alkalic plutonic rocks and associated carbonatites, which are restricted to the Wet Mountains–DeWeese Plateau block, and granodiorites account for some of the observed geophysical contrasts; however, a geophysical contrast in the vicinity of the Arkansas River topographic lineament is difficult to explain based on exposed rock types.

Possible surface expression of the block boundary includes northeast-trending geologic features within an anomalous zone extending from the Pikes Peak batholith southwestward to the Sangre de Cristo Mountains. The dimensions of this zone are controlled by an anomalous northeast-trending zone of northeast- trending faults. Within the zone a northeast-trending contact between granodiorite of the Routt Plutonic Suite and metamorphic rocks follows within 2 km of the Arkansas River for much of the distance between Coaldale and Parkdale, Colorado.

The northeast-trending course of the Arkansas River and its topographic lineament are interpreted as being loosely controlled by the northeast-trending zone of faults and the Precambrian lithologic contact that reflects the boundary between the southern Front Range and Wet Mountains–DeWeese Plateau crustal blocks. Extensive vertical and lateral erosion of the Arkansas River canyon during late Pliocene and Pleistocene time has removed any physical evidence of the topography of the exhumed late Eocene erosion surface upon which the original course of the river was established; however, some combination of differential uplift or erosion along the northeast-trending zone of faults and the granodiorite-metamorphic contact could have influenced establishment of the linear northeast trend of the river before downcutting. Indirectly, then, the modern course of the Arkansas River between Coaldale and Parkdale and its associated topographic lineament reflect the northeast-trending boundary between the southern Front Range and Wet Mountains–DeWeese Plateau crustal blocks.

Understanding structural controls in the vicinity of this northeast-trending boundary is important because the boundary is near mineral deposits that are conspicuously outside the Colorado Mineral Belt.

[1]U.S. Geological Survey, Box 25046, MS964, Denver, Colorado 80225.

INTRODUCTION

The Arkansas River in south-central Colorado includes a northeast-trending segment, approximately 40 km long, between Coaldale and Parkdale. At a regional scale the topographic lineament associated with the river extends southwest to Hayden Pass in the Sangre de Cristo Mountains. Hayden Pass is the lowest point (3,567 m) along the crest of the rugged Sangre de Cristo Mountains between Methodist Mountain 32 km to the northwest and Mendano Pass 72 km to the southeast (fig. 1*A*). In addition, Hayden Pass marks a conspicuous northwestward narrowing of the Sangre de Cristo Mountains (fig. 1*B*). On digital terrain data of the State (fig. 2*A*) a somewhat longer (60 km) topographic lineament is apparent.

The Arkansas River between Salida and Canon City, Colorado (fig. 2*B*), has been interpreted as a superposed

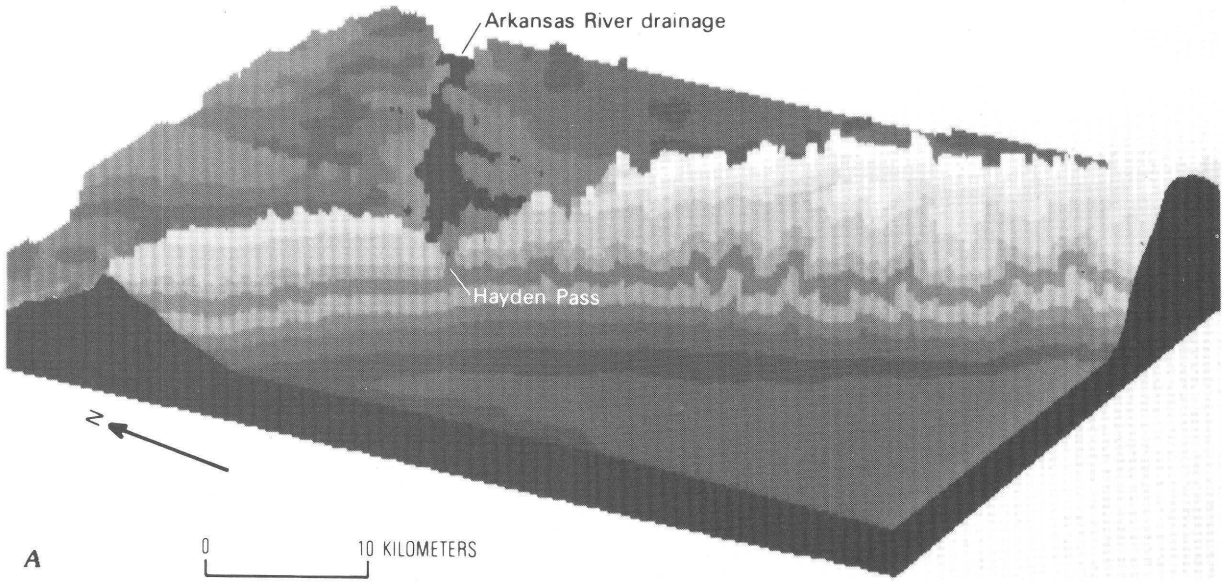

Figure 1(above and facing page). Study area in south-central Colorado. *A,* Three-dimensional view of the Sangre de Cristo Mountains (looking northeast) showing Hayden Pass and Arkansas River drainage. Vertical exaggeration about 6:1. Data from 1:250,000 topographic map of Pueblo 1°×2° Quadrangle. *B,* Plan view of area shown in *A.*

drainage, although the covering rocks from which it was superposed are not preserved (Thornbury, 1965, p. 349). The present course of the river was probably established in late Oligocene or early Miocene time on the extensive exhumed late Eocene erosion surface of low relief in south-central Colorado (Epis and Chapin, 1975). Paleochannels containing gravel deposits and remnants of Oligocene ash-flow tuffs are preserved on the late Eocene erosion surface immediately north and south of the present Arkansas River canyon, but extensive lateral and vertical erosion by the Arkansas River and its tributaries have removed any physical evidence of the early history of the Arkansas River itself.

Steeply dipping Precambrian metamorphic and igneous rocks exposed in and along the Arkansas River canyon, although complexly deformed, do not indicate that a geologic structure (shear zone?) controls the exceptionally straight course of the river; indeed, the regional metamorphic foliation is at a high acute angle to the N. 60° E. trend of the river, such that the canyon exposes an extensive cross section of these steeply dipping rocks.

This segment of the Arkansas River is in an area established as an airborne geophysics demonstration area for testing new geophysical instrumentation and methods and extending integrated interpretation techniques (Watson and others, 1989). The Geophysics Environmental and Minerals (GEM) demonstration area (fig. 2*B*) includes most of the western half of the Pueblo 1°×2° Quadrangle. Several digital data sets have been compiled for the GEM area, including gravity, aeromagnetic, radiometric, geologic, remote sensing (Landsat Thematic Mapper; Heat Capacity Mapping Mission), and digital elevation model terrain data. Numerous other geologic and geophysical maps provide additional local and regional information.

This report summarizes the results of a preliminary investigation to determine whether available data might provide some insights to the nature and cause of the linearity of the Arkansas River between Coaldale and Parkdale, Colorado. These results are preliminary but provide some observations that suggest possible structural and lithologic controls of the river, as well as broad-scale crust-mantle influence on the geologic evolution in this area of the Front Range–Wet Mountains junction.

Acknowledgment.—The authors would like to acknowledge the assistance of Adel Zohdy in providing illustrations of the three-dimensional and plan views of the Sangre de Cristo Mountains.

GENERAL GEOLOGY

The GEM area is roughly centered on Canon City, Colorado, at the junction between the southern Front Range and the northern Wet Mountains (fig. 2*B*). These Precambrian-cored uplifts are flanked by a well-exposed section of Phanerozoic sedimentary strata deformed by diverse types of mountain-flank structures. Precambrian rocks include a variety of Proterozoic igneous and metamorphic rocks. In the northern Wet Mountains, Precambrian crystalline rocks were intruded by Cambrian alkalic and carbonatite rocks prior to deposition of the Phanerozoic sedimentary cover rocks. Oligocene volcanic rocks in various parts of the study area are related to local eruptive centers or are distal deposits

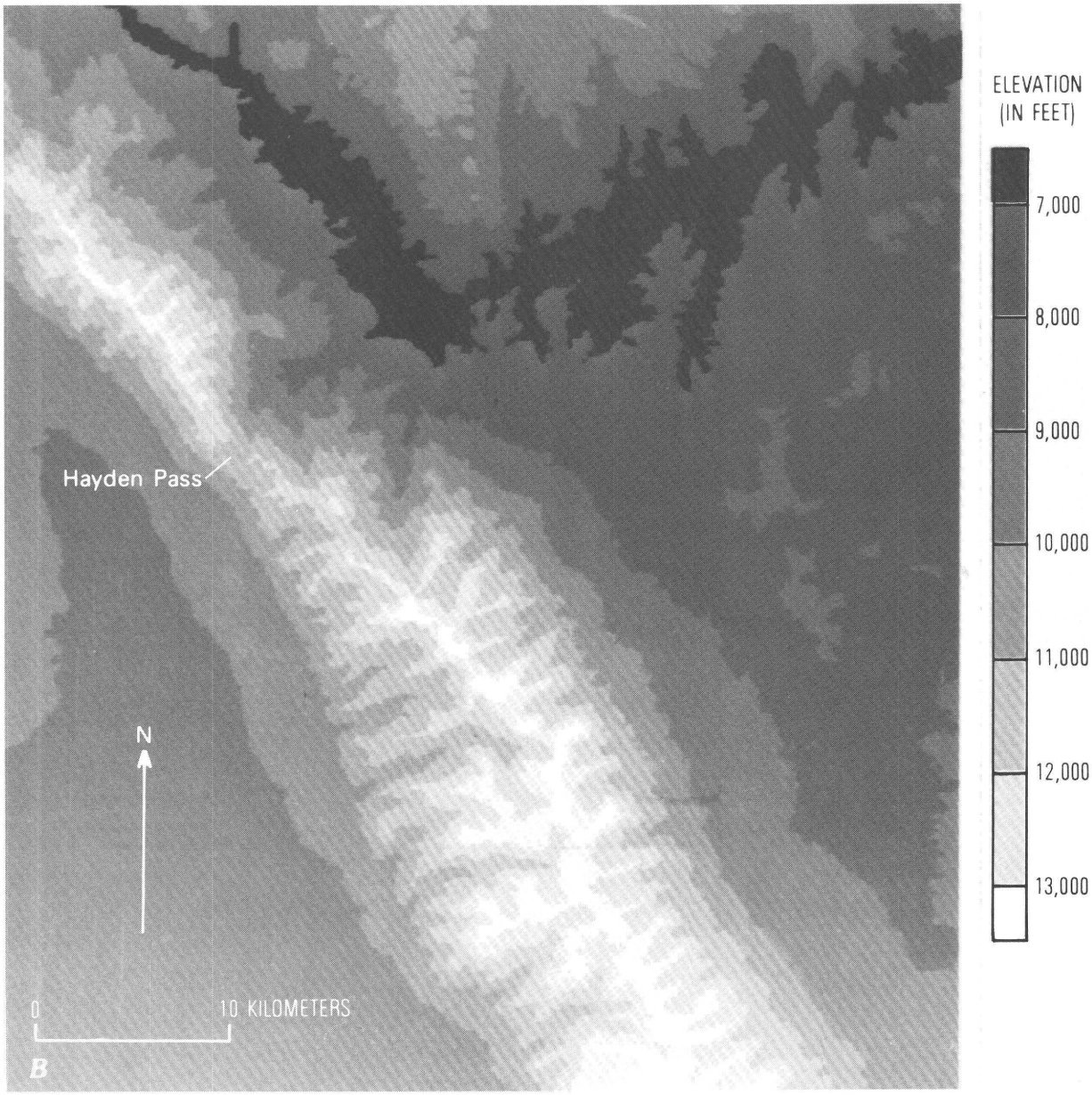

in early Tertiary paleochannels. Miocene and Pliocene sediments and sedimentary rocks occupy several north- to northwest-trending grabens formed during the evolution of the Rio Grande Rift Zone, and gravels locally lie on pediment surfaces and in terraces formed during various stages of the Pleistocene.

The largest and most important mineral deposit in the GEM area is the world-class gold-telluride deposit associated with hydrothermally altered Miocene alkalic volcanic rocks at Cripple Creek, Colorado (Lovering and Goddard, 1950, p. 289). Smaller precious- and base-metal deposits are present at several Oligocene volcanic centers in the region. Lead, zinc, and copper sulfide ores and minor gold and silver have been reported in Precambrian rocks at various places; copper sulfide ore was mined from Pennsylvanian redbeds at Cotopaxi (Vanderwilt, 1947, p. 83–87). Small amounts of placer gold have been produced from the Arkansas River between Salida and Florence. Iron and small quantities of rare-earth elements are associated with Cambrian alkalic and carbonatite rocks in the northern Wet Mountains and DeWeese Plateau (Shawe and Parker, 1967; Armbrustmacher, 1988), and a small uranium deposit is in sediments deposited at the base of a paleovalley at Tallahassee Creek. Precambrian pegmatites in the area have been mined for beryl, columbite-tantalite, muscovite, and feldspar, and gypsum and fire clay have been produced in the area (Vanderwilt, 1947). Cretaceous coals have been mined south of Canon City, and a producing oil field is located near Florence. Because of normal faulting during the evolution of the Rio Grande Rift Zone, the area may have undiscovered

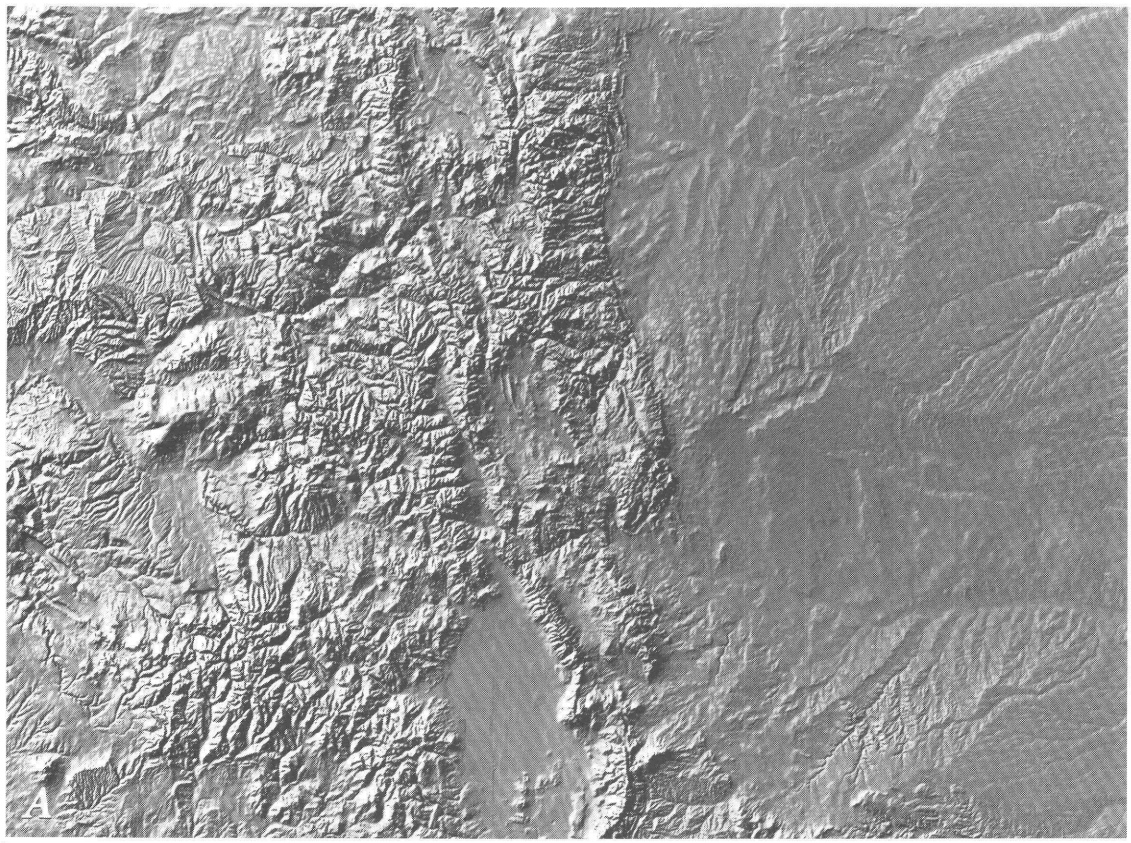

Figure 2 (above and facing page). Digital terrain image (*A*), illumination from northwest, and location map (*B*) showing features mentioned in text and boundaries of GEM study area, Colorado.

mineral deposits on downdropped blocks that are now concealed by upper Tertiary sedimentary rocks and Quaternary alluvial materials.

NEAR-SURFACE EXPRESSION

The courses of modern drainages are commonly controlled by geologic phenomena such as geomorphic features reflecting differential erosion along structures or lithologic units of varying resistance and active faulting and uplift. Detailed and reconnaissance geologic maps (1:62,500 and 1:250,000 scale) of the southern Front Range, South Park, Wet Mountains, and DeWeese Plateau were examined to determine if geologic features exposed at the surface could be related to the trend of the Arkansas River between Coaldale and Parkdale and the associated topographic lineament. Both the pattern of faulting and the distribution of Precambrian granodiorite and metamorphic rocks in the vicinity of the Arkansas River suggest possible surficial controls on the course of the river.

Detailed and reconnaissance geologic mapping shows that the present course of the Arkansas River between Coaldale and Parkdale does not follow a fault or shear zone (Scott and others, 1978; Taylor, Scott, Wobus, and Epis, 1975a); however, the pattern of faults in the area suggests that faulting may have played a major part in establishing the straight course of the river. The major faults in the Wet Mountains–DeWeese Plateau block trend northwesterly northward to the vicinity of Hillside and the Cambrian McClure Mountain Complex, an alkalic complex, where a northeast-trending zone of northeast-trending faults subparallel with the Arkansas River signals a rather abrupt change in structural style (fig. 3). The northeast-trending fault zone extends northeastward across the Canon City embayment and the southern Front Range to the Pikes Peak batholith. Rocks of Precambrian, Paleozoic, and Mesozoic age are cut by the northeast-trending faults; lower Eocene sediments of the Echo Park Alluvium, rocks of the Oligocene Gribbles Park Tuff (Taylor, Scott, and Wobus, 1975), and sodic granite of the Miocene Slide Rock Mountain stock (Taylor, Scott, and Wobus, 1975) are the youngest rocks cut by northeast-trending faults in the zone.

Prior to Neogene movements on the Ilse fault and the uplift of the Wet Mountains and southern Front Range blocks, Oligocene to Miocene low-gradient streams flowed generally eastward across an exhumed, relatively flat Eocene erosion surface (Taylor, 1975). Most of the faults having demonstrated Neogene movement trend north or northwesterly (Epis and Chapin, 1975, fig. 19; Taylor, 1975, fig. 1);

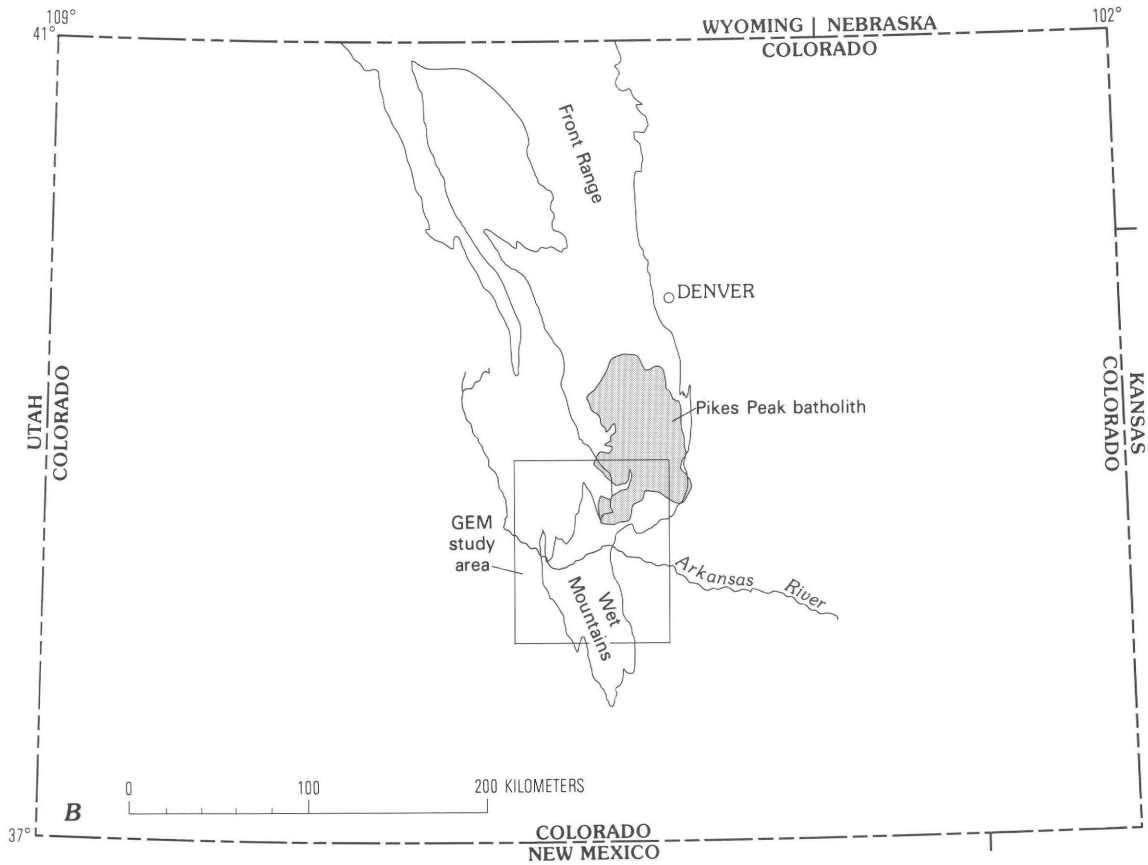

the northeast-trending faults in the northeast-trending fault zone may have also had minor movement in the Neogene, although they were probably in existence prior to the major Neogene tectonism that segmented the paleochannels. The northeasterly trend of Oligocene to Miocene paleochannels identified within or near the northeast-trending fault zone (Goat Creek–Hillside and Oak Creek, Taylor, Scott, Wobus, and Epis, 1975a; Tanner Peak, Taylor, Scott, and Wobus, 1975; Howard, Taylor, Scott, and Wobus, 1975) suggests either a uniform gradient direction on the late Eocene erosion surface or a northeast-trending grain to the subtle topography on the erosion surface. The presence of so many northeast-trending faults within this area suggests the possibility that low ridge and valley topography, perhaps reflecting differential erosion or movement along the abundant northeast-trending faults, may have influenced the course of the paleovalleys. The Arkansas River, now deeply incised through the late Eocene erosion surface, may have originated as another paleochannel before uplift and deep incision in the Pliocene and Pleistocene; however, subsequent downcutting and lateral erosion by the Arkansas River and its tributaries have removed any evidence of the original shape and trend of the early Arkansas River drainage channel and any deposits that may have accumulated in the channel.

Two major Precambrian rock types are exposed in the area of the southern Front Range and northern Wet Mountains and DeWeese Plateau—metamorphic rocks and granodiorite (Scott and others, 1978; Tweto, 1979). The oldest and most widespread rocks are quartzite, biotite schist, gneiss and migmatite, and other metavolcanic and metasedimentary rocks older than about 1,700 Ma (fig. 4). These rocks were intruded by abundant granodioritic magmas at catazonal to mesozonal depths (Hutchinson, 1976) about 1,700 Ma (Routt Plutonic Suite of Tweto (1987)).

Smaller granitic and quartz monzonitic plutons emplaced about 1,400 Ma (Berthoud Plutonic Suite age) at mesozonal depths are exposed in a few areas of the southern Front Range–northern Wet Mountains area. Granitic rocks of the extensive Pikes Peak batholith (about 1,000 Ma) make up much of the southern Front Range north of the study area.

Along the 35-km-long, northeast-trending segment of the Arkansas River between Coaldale and Parkdale, Colorado, granodioritic rocks of Routt Plutonic Suite age to the north are in contact with older Proterozoic metasedimentary and metavolcanic rocks to the south (Taylor, Scott, Wobus, and Epis, 1975a). The regional trend of this contact is essentially parallel with the Arkansas River and for 25 km along this stretch of the river the contact is within 2 km of the river and commonly within 1 km. This spatial relationship strongly suggests that the granite-metamorphic contact may have influenced the ultimate course of the river, although the nature of this influence is unknown.

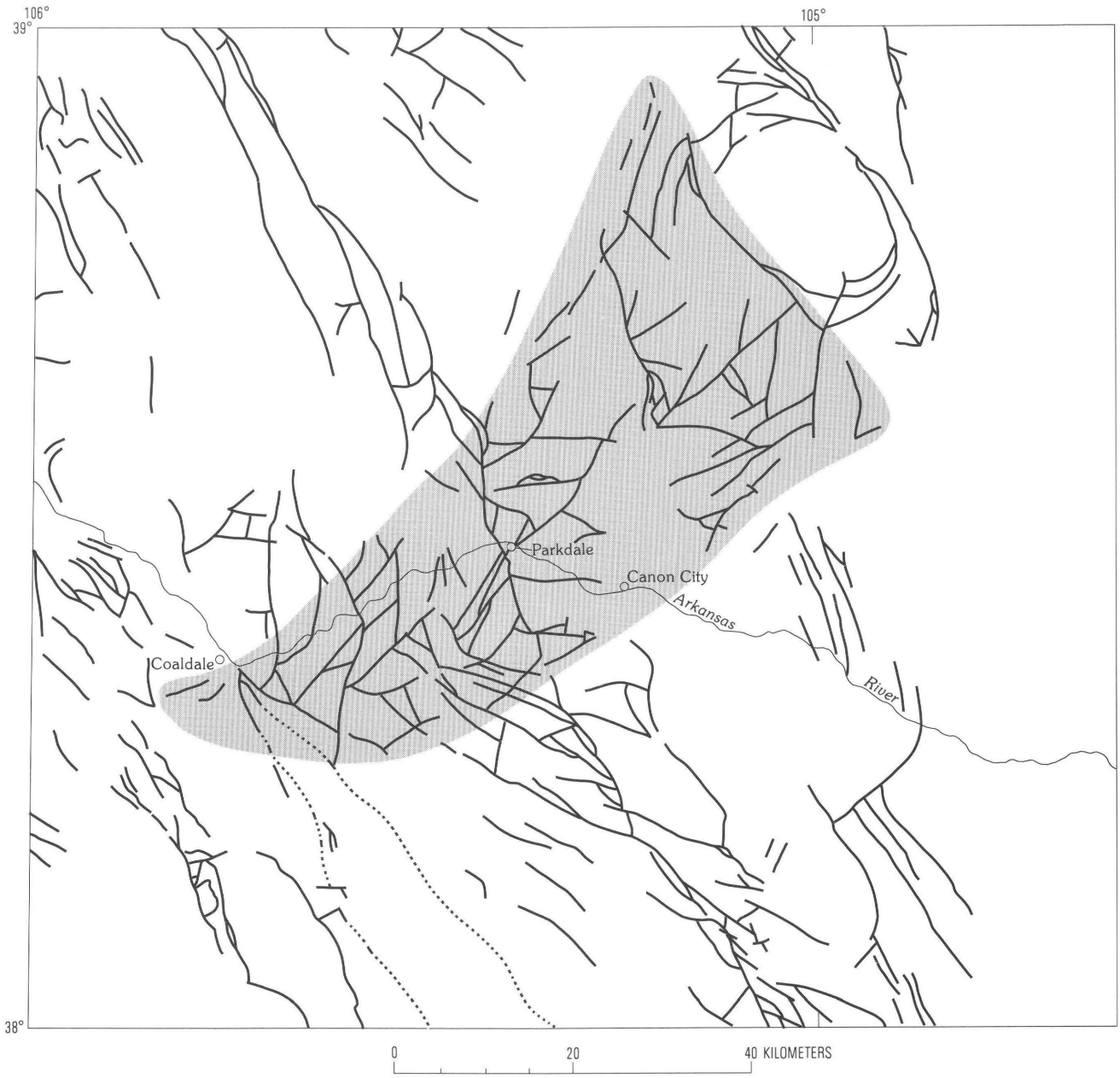

Figure 3. Northeast-trending zone of northeast-trending faults (dashed where inferred) (after Tweto, 1979) in study area, south-central Colorado.

CRUSTAL EXPRESSION

Because geologic maps of the southern Front Range–Wet Mountains/DeWeese Plateau areas (Taylor, Scott, and Wobus, 1975; Taylor, Scott, Wobus, and Epis, 1975a, b; Scott and others, 1978) clearly show that the course of the Arkansas River between Coaldale and Parkdale is not controlled by a fault or shear zone, potential-field data were examined to see if there are any magnetic or gravity characteristics in the area that might suggest a possible controlling influence.

Aeromagnetic Data

Residual total-field magnetic data (1-mi and some 3-mi line spacing, acquired 400 ft above mean terrain) were digitally processed for display in image format at 1:250,000 scale to examine geologic structure. The data were then reduced to the pole using a 0.25-km grid size (fig. 5*A*) to remove inclination errors and place anomalies above their sources. Two distinct areas (areas I and II) having similar high spatial frequency pattern signatures were identified. These two areas are characterized by anomalies having max-

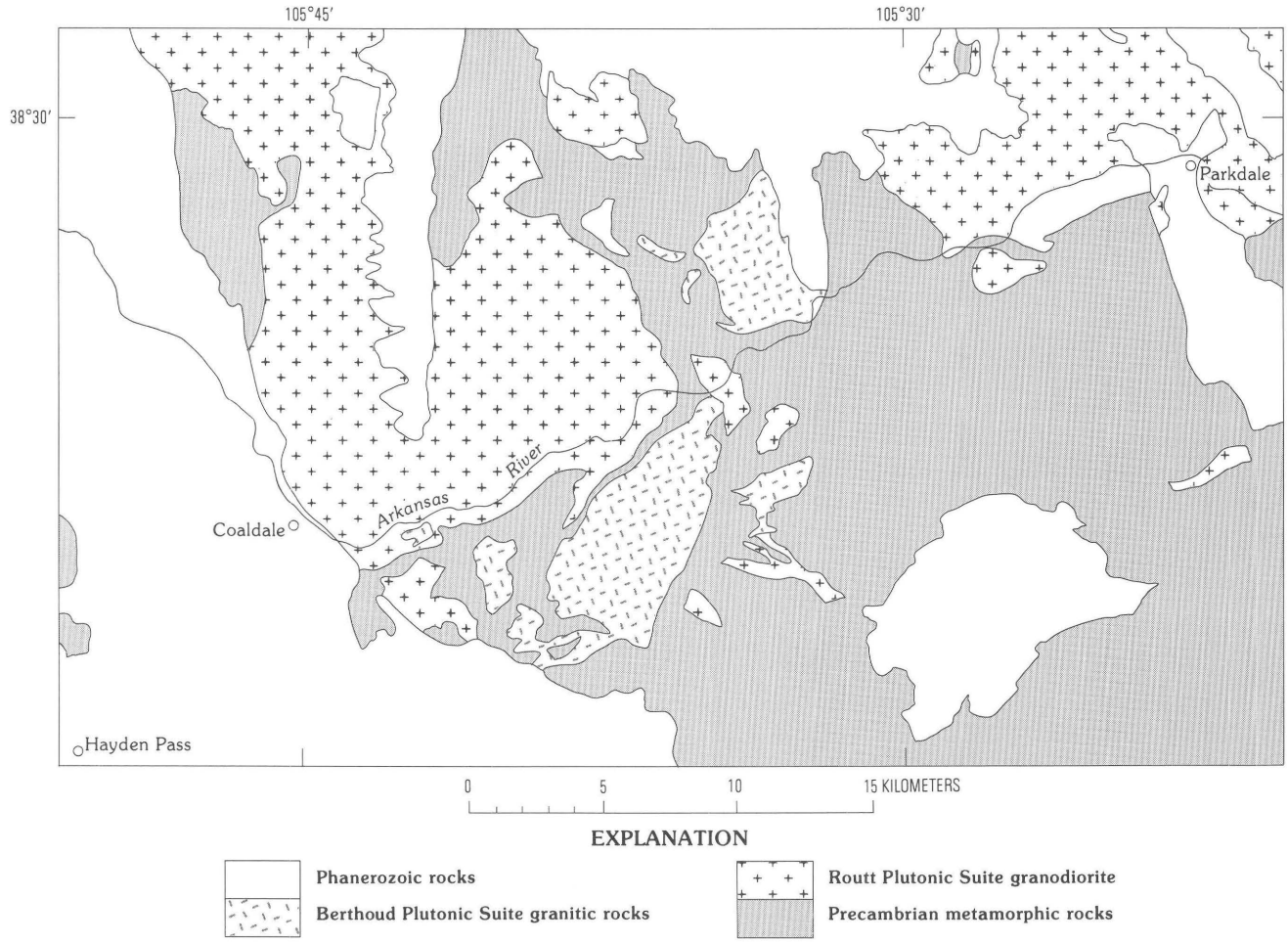

Figure 4. Generalized lithology of Proterozoic rocks along Arkansas River between Coaldale and Parkdale, south-central Colorado. Modified from Scott and others (1978).

imum dimensions of 8 km or less (Boler and Klein, 1990a), although the eastern boundary of area I and the southern boundary of area II differ somewhat from the Front Range area as mapped by Boler and Klein (1990a).

Area I, covering the Wet Mountains and DeWeese Plateau, corresponds at the surface to predominantly migmatitic gneiss older than Routt Plutonic Suite. Most of the magnetic anomalies have been interpreted to be caused by a Cambrian alkalic intrusive complex having mafic derivatives (Boler and Klein, 1990a). Anomalies on the northeastern side of area I, along the crest of the Wet Mountains, are caused by Precambrian granodiorite (Boler and Klein, 1990a). The boundaries of area I generally coincide with the Wet Mountains Fault on the east, the Westcliff Fault on the west, and a zone of northeast-trending faults near the Arkansas River canyon on the north. The cause of the northern truncation of area I is not readily apparent. Rocks to the north of area I, in a magnetic quiet zone, are mostly Precambrian granodiorite (Routt Plutonic Suite) and are the source of magnetic anomaly highs in both areas I and II. Because the zone is similar in outcrop pattern, elevation, and topography to magnetic rocks of the DeWeese Plateau and because there is no evidence for alteration, Boler and Klein were unable to identify the cause of this magnetically quiet area. To the north a series of magnetic highs are associated with Precambrian basement highs covered by Tertiary sedimentary and volcanic rocks (Boler and Klein, 1990a). The quiet area, which contains a number of northeast-trending faults, also includes the northeast-trending segment of the Arkansas River described previously.

The second area of magnetic anomalies (area II, fig. 5*A*) is northeast of area I. The surface rocks are predominantly granodiorite of the Routt Plutonic Suite. Area II is bounded on the east by the Pikes Peak batholith (figs. 2*B*, 5*A*), on the southeast by Paleozoic sediments, and on the west by the Elkhorn–Current Creek–Ilse Fault Zone. Area II corresponds approximately to Boler and Klein's (1990a) feature H. Although volcanic cover rocks are present west of area II, their influence on the boundary is not evident. The sources of the magnetic anomalies in area II are Precambrian

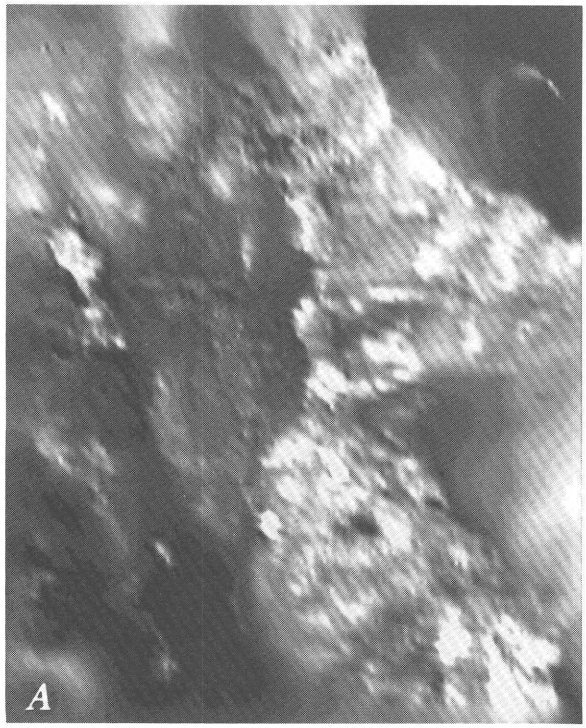

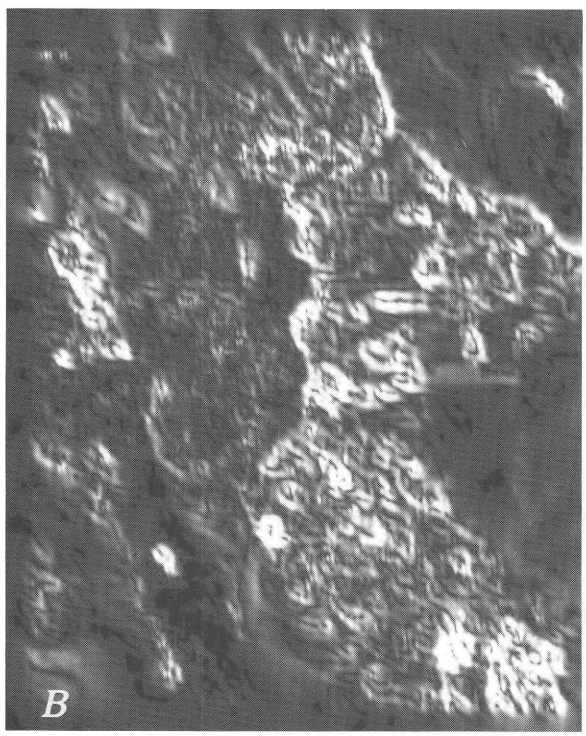

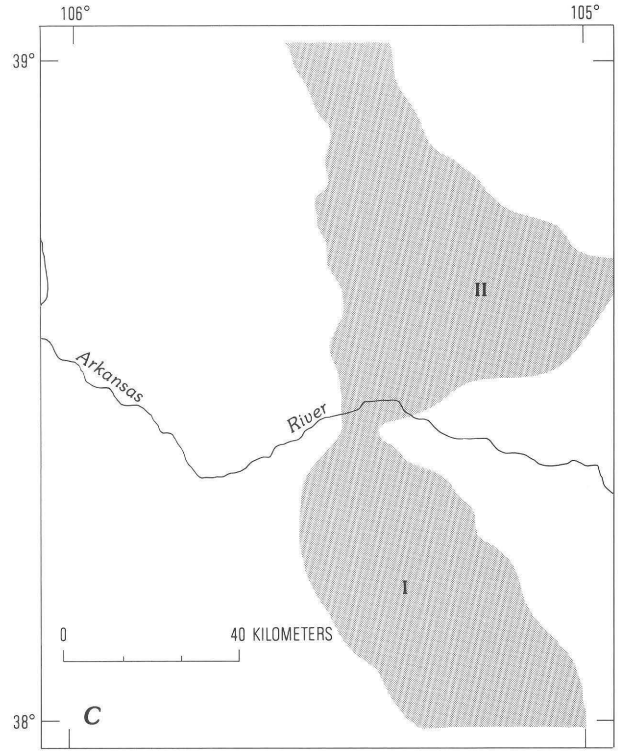

Figure 5 (above and facing column). Magnetic data for western half of Pueblo, Colorado, 1°×2° Quadrangle. *A*, Image of reduced-to-pole magnetic data. Original grid was produced using minimum curvature (Briggs, 1974) with elliptical weights to enhance N. 45° W. direction (M.W. Webring, U.S. Geological Survey, 1990, oral commun.). Areas of magnetic highs are bright on image. *B*, Image of horizontal gradient of reduced-to-pole magnetic data (upward continued 200 m). Aeromagnetic highs are bright and correspond to edges of bodies. *C*, Map showing magnetic signature patterns (see text) (dotted line patterns) and areas (I,II) of magnetic anomalies.

granodiorite (Routt Plutonic Suite) and Precambrian quartz monzonite (Berthoud Plutonic Suite). To the east a pronounced magnetic low is associated with Precambrian Pikes Peak Granite (1,000 Ma); this association is based on the low magnetization of the granite, not on reverse magnetization (Boler and Klein, 1990a).

To examine the boundaries of areas I and II more fully, the horizontal gradient of the reduced to the pole field was computed and upward continued 200 m to smooth high-frequency artifacts (fig. 5*B*). In this representation, magnetic gradient highs are associated with the edges of bodies thus making it easier to infer subtle trends and structural alignments. Two prominent zones are evident. One, in the north-central part of the image, corresponds to the edge of the Pike Peak batholith. The other, a north-trending magnetic gradient high at approximately long 105.5° W., corresponds to the western edges of both areas I and II. From south to north this high coincides with the northwest-trending Westcliffe Fault, passes through a regional grain of northwest-trending faults (locally coinciding with numerous northeast-trending faults), then to the Current Creek–Ilse Fault Zone, and then north-northwest along the fault zone to the Guffey volcanic center.

Although the northern boundary of area I and the southern boundary of area II suggest some spatial coincidence

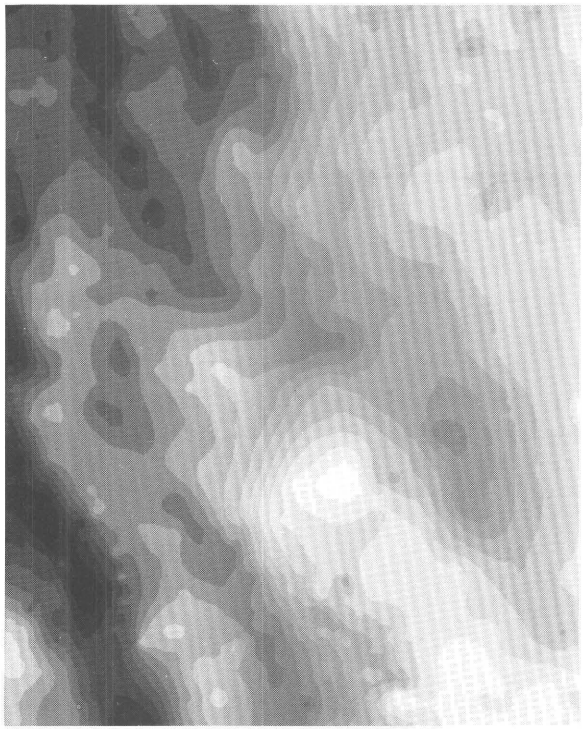

Figure 6. Gravity map of western half of Pueblo 1°×2° Quadrangle. Areas of gravity highs are light on image. Map area is same as figure 5.

with the straight segment of the Arkansas River drainage, the reasons are not directly evident. Why are the granodiorites of the quiet zone less magnetic? Hydrothermal alteration could result in destruction of magnetite, but Boler and Klein (1990a) found no evidence for alteration. One hypothesis is that the magma source here contained less magnetite than did sources to the south and to the east. Another explanation is that during the cooling of this batholith reverse magnetism could have been captured and this remanence would have reduced the total magnetic field. A last hypothesis is that the granodiorite in the quiet zone is much thinner than elsewhere, thereby reducing the mass of magnetic minerals and thus the total field. Field sampling and extensive drilling are required to establish the correct cause with a high confidence level. At this time we are left with fairly strong evidence that anomalies along the boundary between area I and the quiet zone are fault controlled, that Cambrian intrusive rocks are not at the surface north of area I, and that possible explanations of the magnetic quiet zone are lithologic or tectonic differences, or possibly both.

Gravity Data

Bouguer gravity data for the Pueblo Quadrangle (Boler and Klein, 1990b) were examined in the vicinity of the straight segment of the Arkansas River between Coaldale and Parkdale (fig. 6). Area I identified on the magnetic data is a gravity high, the boundaries of which closely approximate the –220-mGal contour and the steepest gradient. Adjacent to and east of area I a northwest-trending gravity low is associated with the Florence basin that cuts across the southwestern end of area II. The northeastern boundary of area II is controlled by the Pikes Peak batholith, which appears as a weak, but very broad, gravity high. The western edge of area II corresponds to a gravity gradient (roughly along the –237-mGal contour). Southeast of Pikes Peak a broad northeast trend to the gravity contours parallels the southeast boundary of area II due to variations in crustal thickness. These contours strike northeast along a 100-km-long segment before swinging to the north parallel with the front of the Front Range.

The gravity data confirm that the areas identified on the basis of the magnetic data correspond to crustal differences, but they provide no additional evidence as to the nature of the boundary between the Wet Mountains–DeWeese Plateau and southern Front Range blocks.

DISCUSSION

The zone of northeast-trending faults and the northeast-trending granodiorite-metamorphic contact are possible elements of geologic control of the location and trend of the Arkansas River between Coaldale and Parkdale, Colorado. It is clear, however, that these features are not related to a simple shear zone such as the shear zones ancestral to the Colorado Mineral Belt to the north in central Colorado (Tweto and Sims, 1963; Warner, 1978). Aeromagnetic and gravity data, as well as the restricted distribution of Cambrian alkalic rocks, indicate that the anomalous northeast-trending zone, including the northeast-trending faults, the granodiorite-metamorphic contact, and the Arkansas River topographic lineament, may be the relatively subtle expression of a deeper seated boundary between contrasting blocks of Proterozoic crust.

The Proterozoic crust of Colorado and northern New Mexico was accreted to the southern margin of the Archean craton in Wyoming between 1,790 and 1,660 Ma (Reed and others, 1987). The suture between Archean and Proterozoic crust is well marked by the northeast-trending Proterozoic Cheyenne Belt of Proterozoic crustal blocks bounded by shear zones (Duebendorfer and Houston, 1987) in southern Wyoming (fig. 7). Southward into Colorado, numerous northeast-trending shear zones and faults of Early Proterozoic ancestry mark conspicuous changes in regional structure (Tweto and Sims, 1963; Reed and others, 1987) and controlled the emplacement of Laramide granitic intrusive bodies of the Colorado Mineral Belt (Tweto and Sims, 1963). Bowring and Karlstrom (1990) suggested that these structures may reflect the boundaries between relatively thin lithospheric fragments assembled into the Proterozoic crust that maintained their identity through subsequent orogenic

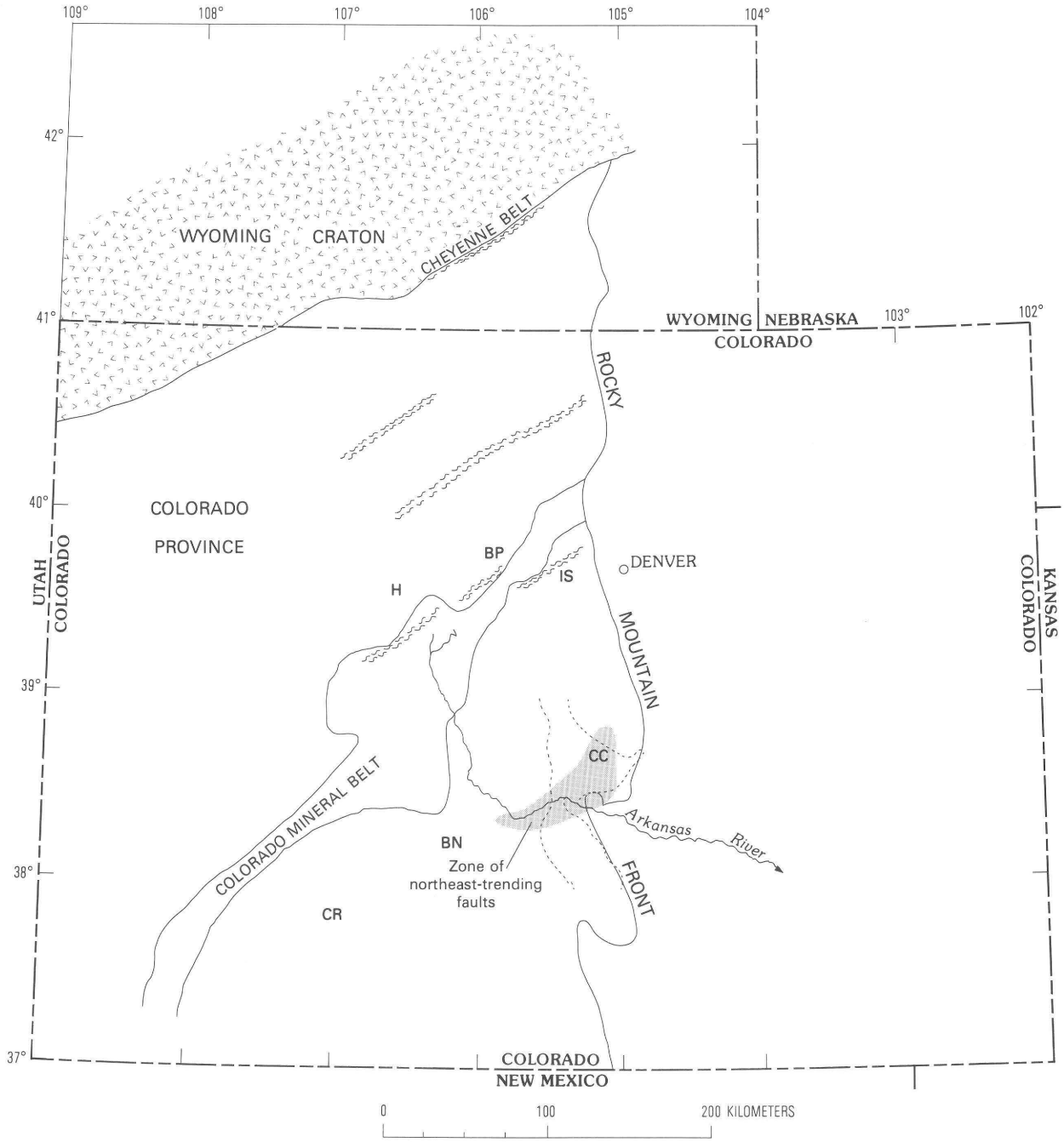

Figure 7. Map showing structural features, mineral deposits, and magnetic anomalies, Colorado and southeastern Wyoming. Double-wavy lines indicate shear zones: H, Homestake; BP, Berthoud Pass; IS, Idaho Springs. Mineral deposits: CC, Cripple Creek; BN, Bonanza; CR, Creede. Dotted lines indicate magnetic anomalies. Compiled from Reed and others (1987) and Duebendorfer and Houston (1987).

plutonism (Routt Plutonic Suite, 1.75–1.6 Ga) and anorogenic plutonism and differential uplift and erosion (Berthoud Plutonic Suite and Pikes Peak Granite, 1.4–1.1 Ga) and were reactivated repeatedly through Tertiary time. It is likely that such structures would be variously modified by metamorphic and plutonic activity but might still maintain a subtle influence on subsequent tectonic events.

Geophysical expression of the Proterozoic crust in south-central Colorado suggests a boundary between contrasting blocks in the vicinity of the Arkansas River topographic lineament. Possible surface expression of this boundary is limited to a northeast-trending zone of northeast-trending faults, a northeast-trending contact between granodiorite of the Routt Plutonic Suite and older metamorphic rocks, and the

Arkansas River topographic lineament itself. If this boundary originated during the Early Proterozoic assembly of heterogeneous crustal blocks, it was either irregular and complex or it has been greatly modified by subsequent plutonism and metamorphism. Nevertheless, this crustal boundary may account for the en echelon pattern of uplift during orogenesis in late Paleozoic (Ancestral Rockies) and Late Cretaceous–Eocene (Laramide) times, as well as during uplift of the Front Range and Wet Mountains in Neogene time (fig. 7).

Based on observations over an admittedly limited geographic area, the modern course of the Arkansas River between Coaldale and Parkdale, Colorado, and the associated Arkansas River topographic lineament probably are indirectly controlled by geologic features expressing a northeast-trending boundary between contrasting Proterozoic crustal blocks. This interpretation is preliminary at best, and additional geological and geophysical studies are necessary to understand the nature of the block boundary, particularly its lateral extent, and the effects it may have had on Precambrian and Phanerozoic events including the formation of mineral deposits. The location of several major mineral deposits (Cripple Creek, Bonanza, Creede) conspicuously outside the Colorado Mineral Belt (fig. 7) provides additional motivation for understanding crustal structure in this region.

REFERENCES CITED

Armbrustmacher, T.J., 1988, Geology and resources of thorium and associated elements in the Wet Mountains area, Fremont and Custer Counties, Colorado: U.S. Geological Survey Professional Paper 1049–F, 34 p.

Briggs, I.C., 1974, Machine contouring using minimum curvature: Geophysics, v. 39, p. 39–48.

Boler, F.M., and Klein, D.P., 1990a, Residual aeromagnetic and interpretative maps of the Pueblo 1°×2° Quadrangle, south-central Colorado: U.S. Geological Survey Miscellaneous Investigations Series Map I–1419–C, scale 1:250,000.

_____1990b, Residual Bouguer gravity and interpretative maps of the Pueblo 1°×2° Quadrangle, south-central Colorado: U.S. Geological Survey Miscellaneous Investigations Series Map I–1419–B, scale 1:250,000.

Bowring, S.A., and Karlstrom, K.E., 1990, Growth, stabilization, and reactivation of Proterozoic lithosphere in the southwestern United States: Geology, v. 8, p. 1203–1206.

Duebendorfer, E.M., and Houston, R.S., 1987, Proterozoic accretionary tectonics at the southern margin of the Archean Wyoming craton: Geological Society of America Bulletin, v. 98, p. 554–568.

Epis, R.C., and Chapin, C.E., 1975, Geomorphic and tectonic implications of the post-Laramide, Late Eocene erosion surface in the southern Rocky Mountains: Geological Society of America Memoir 144, p. 45–74.

Hutchinson, R.M., 1976, Precambrian geochronology of western and central Colorado and southern Wyoming, *in* Epis, R.C., and Weimer, R.J., eds., Studies in Colorado field geology: Professional Contributions of Colorado School of Mines, no. 8, p. 73–77.

Lovering, T.S., and Goddard, E.N., 1950, Geology and ore deposits of the Front Range, Colorado: U.S. Geological Survey Professional Paper 223, 319 p.

Reed, J.C., Jr., Bickford, M.E., Premo, W.R., Aleinikoff, J.N., and Pallister, J.S., 1987, Evolution of the early Proterozoic Colorado province—Constraints from U-Pb geochronology: Geology, v. 15, p. 861–865.

Scott, G.R., Taylor, R.B., Epis, R.C., and Wobus, R.A., 1978, Geologic map of the Pueblo 1°×2° Quadrangle, south-central Colorado: U.S. Geological Survey Miscellaneous Investigations Map I–1022, scale 1:250,000.

Shawe, D.R. and Parker, R.L., 1967, Mafic-ultramafic layered intrusion at Iron Mountain, Fremont County, Colorado: U.S. Geological Survey Bulletin 1251–A, p. A1–A28.

Taylor, R.B., 1975, Neogene tectonism in south-central Colorado: Geological Society of America Memoir 144, p. 211–226.

Taylor, R.B., Scott, G.R., and Wobus, R.A., 1975, Reconnaissance geologic map of the Howard Quadrangle, central Colorado: U.S. Geological Survey Miscellaneous Investigations Map I–892, scale 1:62,500.

Taylor, R.B., Scott, G.R., Wobus, R.A., and Epis, R.C., 1975a, Reconnaissance geologic map of the Cotopaxi 15-minute Quadrangle, Fremont and Custer Counties, Colorado: U.S. Geological Survey Miscellaneous Investigations Map I–900, scale 1:62,500.

_____1975b, Reconnaissance geologic map of the Royal Gorge 15-Minute Quadrangle, Fremont and Custer Counties, Colorado: U.S. Geological Survey Miscellaneous Investigations Map I–869, scale 1:62,500.

Thornbury, W.D., 1965, Regional geomorphology of the United States: New York, John Wiley and Sons, 609 p.

Tweto, Ogden, 1979, Geologic map of Colorado: U.S. Geological Survey, scale 1:500,000.

_____1987, Rock units of the Precambrian basement of Colorado: U.S. Geological Survey Professional Paper 1321–A, 54 p.

Tweto, Ogden, and Sims, P.K., 1963, Precambrian ancestry of the Colorado mineral belt: Geological Society of America Bulletin, v. 74, no. 8, p. 991–1014.

Vanderwilt, J.W., 1947, Mineral resources of Colorado: State of Colorado, Mineral Resources Board, 547 p.

Warner, L.A., 1978, The Colorado lineament—A middle Precambrian wrench fault system: Geological Society of America Bulletin, v. 89, p.161–171.

Watson, Ken, Knepper, D.H., Jr., Clark, R.N., Pitkin, J.A., Labson Vic, Campbell, D.L., Rowan, L.C., Kruse, F.A., Lee, Keenan, and Livo, K.E., 1989, Plans for integrated airborne geophysical study of the Geophysics Environmental and Minerals demonstration area, south-central Colorado, *in* USGS Research on Mineral Resources—1989 Program and Abstracts, Fifth Annual V.E. McKelvey Forum on Mineral and Energy Resources: U.S. Geological Survey Circular 1035, p. 77–78.

Chapter E

Implications of Gravity and Seismic Reflection Data for Laramide Mountain Ranges and Basins of Wyoming and Southern Montana

By STEPHEN L. ROBBINS and JOHN A. GROW

U.S. GEOLOGICAL SURVEY BULLETIN 2012

APPLICATIONS OF STRUCTURAL GEOLOGY TO MINERAL AND ENERGY RESOURCES OF THE CENTRAL AND WESTERN UNITED STATES

CONTENTS

PLATES

[Plates are in pocket]

FIGURES

Implications of Gravity and Seismic Reflection Data for Laramide Mountain Ranges and Basins of Wyoming and Southern Montana

By Stephen L. Robbins[1] *and* John A. Grow[2]

Abstract

Gravity profiles and seismic reflection profiles indicate low-angle thrusting of several Laramide mountain ranges onto basins in Wyoming and southern Montana. Examples include thrusting of the Bighorn Mountains northeastward onto the western Powder River Basin, the Wind River Mountains southwestward onto the Green River Basin, the Owl Creek Mountains southward onto the Wind River Basin, the Shirley Mountains southward onto the Hanna Basin, the Granite Mountains southwestward toward the Great Divide Basin, and the Beartooth Mountains northeastward onto the Bighorn Basin. Interpretations of the profiles contain several similarities: (1) thrust angles of 20°–30°; (2) thrust distances onto the basins of 10–20 km; and (3) thrusts that appear to sole in the middle or lower crust.

Isostatic residual anomaly (IRA) values range from –77 mGal over the Hanna Basin to +75 mGal over the Laramie Mountains but average near zero. Large positive IRA values (+40 to +70 mGal) over all of the Laramide mountain ranges indicate that local roots are absent beneath these mountain ranges. IRA lows of –20 to –70 mGal over the deeper basins are primarily a reflection of low-density basin-fill deposits. The fact that the IRA values average near zero indicates that the longer wavelength elevation changes (greater than 100 km) must be isostatically compensated; that is, the crustal thickness compensates for regional elevation changes but not for local mountain ranges.

Positive gravity anomalies within some of the basins in areas of little structural relief (areas such as the central Powder River Basin where some borehole and seismic data are available) suggest that density varies laterally significantly within Precambrian basement rocks, probably because of differences in basement rock types. Aeromagnetic patterns within these basins also support this interpretation.

A better understanding of the geometry of thrust faults that have carried mountain ranges over the edges of adjacent sedimentary basins, and of the structural relief within these basins, is needed in order to effectively explore for future hydrocarbon resources.

INTRODUCTION

The Laramide orogeny uplifted Precambrian basement blocks throughout the western United States during Late Cretaceous and early Cenozoic time (Hamilton, 1988; Perry and others, this volume). Vertical uplifts of 13 km and crustal shortening of more than 20 km have been demonstrated in the Wind River Mountains (plates 1, 2) (Smithson and others, 1978; Sharry and others, 1986; Blackstone, 1990). Within northern Wyoming and southern Montana, the basement blocks are composed of Archean granite, gneiss, amphibolite, and minor mafic dikes (Love and Christensen, 1986). Cratonic sedimentary rocks of Cambrian through Jurassic age unconformably overlie the basement and thin from 2½ km in western Wyoming (Lamerson, 1982) to less than 1 km in northeastern Wyoming (Rocky Mountain Association of Geologists, 1972) with no evidence of any significant pre-Laramide relief on the basement. Although thin-skinned sedimentary thrusts formed along the Utah-Wyoming border area during the Cretaceous Sevier orogeny, the Laramide orogeny is the only significant tectonic event during Phanerozoic time in northern Wyoming that involved major disruptions in the basement. Therefore, northern Wyoming offers a unique opportunity to study the processes involved in compressional deformation of the continental crust and lithosphere in an area relatively uncomplicated by either earlier or later Phanerozoic tectonic events.

Debate over whether Laramide mountain ranges are bordered by thrust faults or vertical faults goes back almost a century (Darton, 1906). Berg (1963) published a seismic line over the west flank of the Wind River Mountains that shows

[1]U.S. Geological Survey, Box 25046, MS939, Denver, Colorado 80225.

[2]U.S. Geological Survey, Box 25046, MS960, Denver, Colorado 80225.

a thrust fault flattening to the northeast. Subsequently, however, Prucha and others (1965) introduced the concept of concave-downward (upthrusting) faults for which the dip increases downward to near vertical at basement level. Variations on the vertical fault theme were dominant into the late 1970's (Matthews, 1978). A combination of multifold seismic reflection profiles, gravity models, and drill holes through Precambrian overhangs, especially in the last dozen years, confirms that thrust faulting was the dominant mode of deformation along Laramide mountain fronts (Berg, 1963; Berg and Romberg, 1966; Smithson and others, 1978; Blackstone, 1981; Gries, 1981, 1983; Bally, 1983; Lowell, 1983; Skeen and Ray, 1983; Gries and Dyer, 1985). Furthermore, a gravity model and a reprocessed version of the COCORP (Consortium for Continental Reflection Profiling) seismic profile over the Wind River Mountains indicates that the Wind River Thrust flattens within the lower crust at depths of about 22 km (Hurich and Smithson, 1982; Sharry and others, 1986).

Gravity data recently collected in the Powder River Basin and the Bighorn Mountains of northeastern Wyoming (Robbins and Grow, 1990) and seismic profiles along the east flank of the Bighorn Mountains (Grow and others, 1988) indicate that low-angle faults (20°–30° W. dip) that flatten within the middle or lower crust are also dominant in northeastern Wyoming. Therefore, thrusts that flatten within the middle and lower crust probably are dominant across most of the Laramide province of Wyoming from the Wind River Mountains eastward for a distance of 300 km to the Bighorn Mountains.

In this paper, we present new compilations of complete Bouguer gravity anomaly, isostatic gravity anomaly, and horizontal gravity gradient maps for Wyoming and southern Montana in color at a scale of 1:1,500,000. Although data are missing for some parts of this region, these are the first color gravity maps at a large enough scale to allow discussion of individual Laramide mountain fronts as well as regional trends across the entire province. We also review some of the previously published key seismic reflection lines and gravity models for the area. Finally, we discuss the implications of the new gravity maps for tectonic models of the Wyoming Laramide province and for applications of these types of maps for improved mineral, oil, and gas exploration techniques.

GEOLOGIC SETTING

Elevations in southern Montana and Wyoming range from about 1,100 m in the northeast to almost 4,200 m in the Wind River Mountains (plate 1). The Bighorn Mountains (4,000 m), Beartooth Mountains (3,800 m), and Medicine Bow Mountains (3,700 m) are the other major ranges in the area. The intermontane basins have a systematic topographic gradient from 1,100 m in the high plains of the northeast to more than 2,000 m in the Green River Basin of western Wyoming.

Structural relief on the Precambrian basement surface extends from more than 9 km below sea level to more than 4 km above sea level along the northeast flank of the Green River Basin and the west flank of the Wind River Mountains (plate 2) (Blackstone, 1990).

Paleozoic cratonic shallow-marine sedimentary rocks that lie unconformably on Archean basement rocks are 1 km thick in western Wyoming and thin to less than 1 km in northeastern Wyoming; there is no evidence for any significant pre-Laramide relief on the basement surface (Rocky Mountain Association of Geologists, 1972; Lamerson, 1982; Peterson, 1983). Cratonic deposition continued in Triassic and Jurassic time; about 1.5 km of rock was deposited in the western part of Wyoming and about 0.3 km in the eastern part. In the Early Cretaceous, Sevier thrusting along the Utah-Wyoming border resulted in debris being shed to the east; as much as 1.6 km of rock was deposited in the western part of Wyoming and 0.2 km in the eastern part. Amounts of synorogenic clastic debris increased rapidly in the Late Cretaceous; this debris was fed into a broad marine seaway that connected the Gulf of Mexico with the Arctic Ocean (McGookey, 1972). Upper Cretaceous sedimentary rocks range from 3.6 km thick in western Wyoming to about 1.5 km thick in eastern Wyoming except along the flanks of the Wind River Mountains, which began to rise in the Late Cretaceous, where Upper Cretaceous rocks are only 1.2 km thick (McGookey, 1972, fig. 22). The rapid rise of Laramide uplifts resulted in thick lower Cenozoic nonmarine deposits of the Fort Union (Paleocene) and Wasatch (Paleocene and Eocene) Formations that have combined thicknesses of more than 3 km in western Wyoming and as much as 2 km in northeastern Wyoming.

Central and northern Wyoming and southern Montana have been subjected to limited basement-involved deformation since Precambrian time, whereas southern Wyoming and Colorado were subjected to more intense late Paleozoic tectonic activity; we focus our attention in this paper on northern Wyoming where Laramide deformation is far more significant.

GRAVITY DATA

Complete Bouguer anomaly (CBA), isostatic residual anomaly (IRA), and horizontal gradient anomaly (HGA) gravity maps of Wyoming and southern Montana are presented on plates 3–5; 21,206 data points were used to generate these maps. Most of these data are from U.S. Defense Mapping Agency files (St. Louis, Missouri), but 1,386 stations in eastern Wyoming and southeastern Montana were collected by us. Principal facts for 1,040 of these gravity

stations are in Williamson and Robbins (1991) and were used together with the Defense Mapping Agency data to compile CBA gravity maps of the Sheridan and Gillette 1°×2° quadrangles (Robbins, in press; Robbins and Williamson, in press). Principal facts for our 346 stations in the Arminto, Newcastle, and Torrington 1°× 2° quadrangles are unpublished.

All gravity values are based on the IGSN–1971 datum (Morelli, 1974), and the data were reduced using the GRS–1967 formulas (International Association of Geodesy, 1971) and an assumed average crustal density of 2.67 g/cm^3. The terrain effect to a distance 167 km from each station was removed using a computer program based on Plouff (1977). The terrain effect for the stations established by the authors was removed by manually making corrections to a distance of 0.59 km and using the computer program from 0.59 to 167 km. Isostatic corrections were made using a computer program by Simpson and others (1983) assuming an Airy-Heiskanen compensation model where the parameters used are (1) density of the topographic load, 2.72 g/cm^3, (2) depth of compensation below sea level, 40 km, and (3) density contrast at the crust-mantle boundary, +0.35 g/cm^3. The CBA and IRA gravity maps were generated by first gridding the scattered data using a computer program by Webring (1981) and then plotting the gridded data using the program COLOR by Godson (1980). A 2.5-km grid interval was used to plot the CBA and IRA maps (plates 3, 4). The HGA map (plate 5) was generated from the IRA grid file using a package of programs called BOUNDARY based on Blakely and Simpson (1986).

The maps are plotted at a scale of 1:1,500,000. Station spacing is quite variable, and the blank areas are where the station spacing is greater than 10 km. The CBA and IRA maps are contoured at 5 mGal, and the HGA map is contoured at 1 mGal/km.

The CBA values range from –75 mGal in southeastern Montana to –285 mGal in the Green River Basin in western Wyoming (plate 3). The most dominant feature on the CBA map is the regional gradient from northeast to southwest, which is a direct reflection of the topographic gradient (plate 1). The mountain ranges are associated with relative highs that are 30–50 mGal above the regional trends and the basins with relative lows that are 30–50 mGal below the regional trend.

The IRA values are as much as +75 mGal in the Laramie Mountains, the deepest low is –77 mGal in the Hanna Basin (plate 4). The average IRA value of near zero indicates that the region is isostatically compensated at longer wavelengths (>100 km). The basins have low IRA values of from –35 mGal in the Powder River Basin to –77 mGal in the Hanna Basin; these low values are caused mainly by low-density sedimentary fill within the basins. The high IRA values in the Laramie, Bighorn, and Wind River Mountains (+75, +65, and +45 mGal, respectively) and other lesser mountain ranges are not associated with dense, mafic Precambrian basement rocks. This implies that the local Airy-Heiskanen compensation model assumed deeper roots under the mountain ranges than are actually present. In other words, the mountains either do not have local roots or the roots are significantly shallower than assumed by the Airy-Heiskanen model.

PREVIOUS GEOPHYSICAL STUDIES

The first known published gravity study is by Chamberlin (1935), who demonstrated that the isostatic character of the region is anomalous. Later, Malahoff and Moberly (1968), in a regional gravity study of the State of Wyoming recognized that the mountain blocks within the State were rootless. In this section, we briefly discuss the most significant previously published gravity and seismic studies. The locations of the studies and appropriate references are shown on plate 1.

Wind River Mountains–Green River Basin

The Wind River Mountains are the most extensively studied of any Laramide mountain range, and a careful review of key studies there illustrates the evolution of structural concepts during recent decades. Berg (1963) published a line-drawing interpretation of a single-fold analog seismic profile across the southwest flank of the range beneath which he interpreted a thrust fault flattening to the northeast. Berg and Romberg (1966) published a gravity model consistent with this seismic interpretation. The COCORP deep-crustal seismic-reflection line was acquired in 1977 and is the first published multifold seismic line across the Wind River Mountain front (Smithson and others, 1978). It confirms Berg's thrust fault model, and following its publication a number of multifold seismic profiles across the Wind River Mountains (Lowell, 1983; Basham and Martin, 1985) and other ranges (Gries, 1981, 1983; Skeen and Ray, 1983; Gries and Dyer, 1985) were published that confirm crustal shortening was dominant over vertical uplift.

Lowell's (1983) multifold seismic line shows a wedge of granite thrust over the Green River Basin with the fault flattening to the northeast and at least 16 km of overhang (fig. 1). Lowell did not give the precise location of this profile, but the structure shown is so similar to that shown by Berg (1963) that the two are probably very close to each other.

Smithson and others' (1978) publication of the COCORP deep-crustal seismic line across the Wind River Mountains is probably the most important single seismic profile in advancing evidence for thrusting (30°–35°) in the upper crust within the Laramide province. A reprocessed version of this COCORP line (Sharry and others, 1986) has significantly improved the section in the middle and lower crust and suggests that imbricated thrusts flatten out to the northeast between 20 and 30 km depth with the main thrust at a

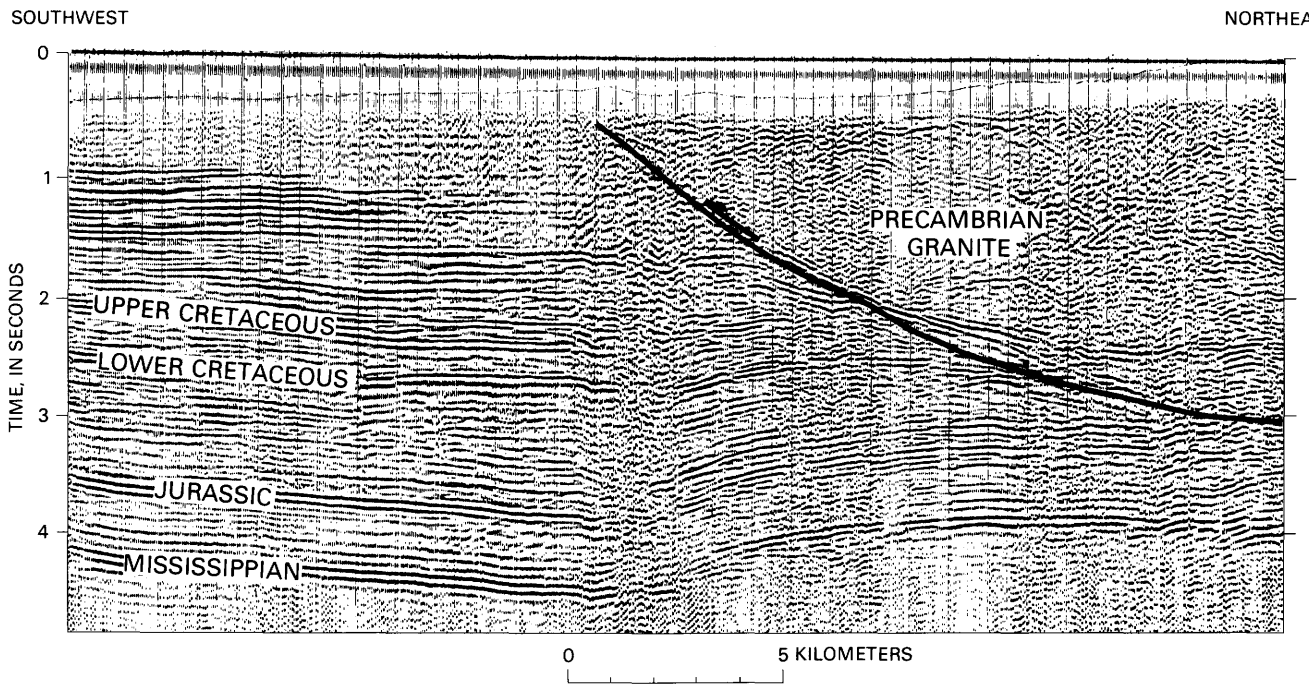

Figure 1. Seismic line across the Wind River Thrust. Reprinted with permission from Lowell (1983, fig. 2, p. 5). Approximate location of seismic line shown on plate 1.

depth of 22 km (fig. 2). This seismic profile is 140 km long and shows data to a depth of 40 km. Strong reflectors in the southwest were observed to the base of the Paleozoic sedimentary fill in the Green River Basin; the Pinedale Anticline is just west of the main thrust fault, and the reflector at 33 km depth is interpreted as the Moho.

A two-dimensional gravity model along the COCORP profile (Hurich and Smithson, 1982) suggests that the Wind River Thrust flattens out in the lower crust and that the thrust uplifted higher density lower crust (2.88 g/cm^3) into the middle crust but did not penetrate below the Moho (fig. 3). The flattening of the thrust in the middle to lower crust demonstrated in both Sharry and others' (1986) version of the COCORP seismic line and the Hurich and Smithson gravity model is consistent with the positive isostatic gravity anomalies across the range discussed in the previous section that imply the range is rootless.

Owl Creek Mountains/Casper Arch–Wind River Basin–Granite Mountains–Great Divide Basin

Case and Keefer (1966) published two gravity models that cross the north flank of the Wind River Basin (fig. 4*A*). These show that the fault at this northern boundary is a high-angle reverse fault dipping to the north. The eastern of the two profiles continues southward across the Granite Mountains and into the Great Divide Basin, where a low-angle fault dips northward beneath the south flank of the Granite Mountains (fig. 4*B*). Karasa (1976) showed two profiles over the Granite Mountains that he also interpreted as being underlain by low-angle north-dipping faults.

Ray and Berg (1985) published a high-quality multifold seismic profile over the northeast flank of the Wind River Basin and Owl Creek–Casper Arch Thrust, which they interpreted as flattening to the northeast with at least 16 km of overhang (fig. 5).

Although not as spectacular as the Wind River Mountains COCORP deep-crustal seismic line and gravity model, gravity models and seismic lines across the Owl Creek Mountains, Granite Mountains, and Casper Arch all support the low-angle thrust fault model in which faults flatten out within the crust.

Beartooth Mountains–Bighorn Basin

Bonini and Kinard (1983) showed two alternative gravity models over the northeast flank of the Beartooth Mountains into the Bighorn Basin (fig. 6). Model 1 is an upthrust model similar to that of Prucha and others (1965); model 2 is a 30° thrust that has approximately 12 km of overhang and is a much closer fit to the residual curve than the high-angle thrust. Proprietary magneto-telluric and seismic exploration methods (Smith, 1987), as well as drilling into the Precambrian rocks and an underlying sedimentary section, have been employed in this area.

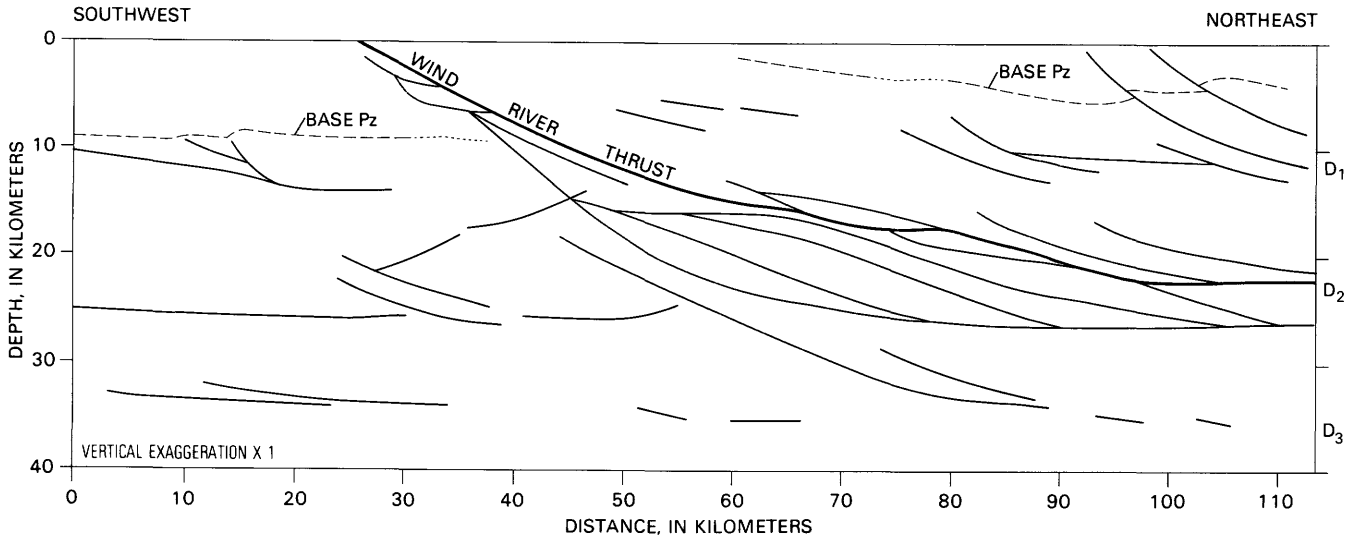

Figure 2. Interpretation of reprocessed version of COCORP deep-crustal seismic-reflection line across the Wind River Mountains. (Sharry and others, 1986) showing imbricate listric thrust fault systems that splay off three decollement zones (D_1, D_2, and D_3). The main thrust appears to flatten onto a decollement (D_2) between 17 and 26 km depth. The original seismic displays, given in Sharry and others (1986), are the best seismic evidence to date for the thrust flattening in the lower crust. Location of line shown on plate 1.

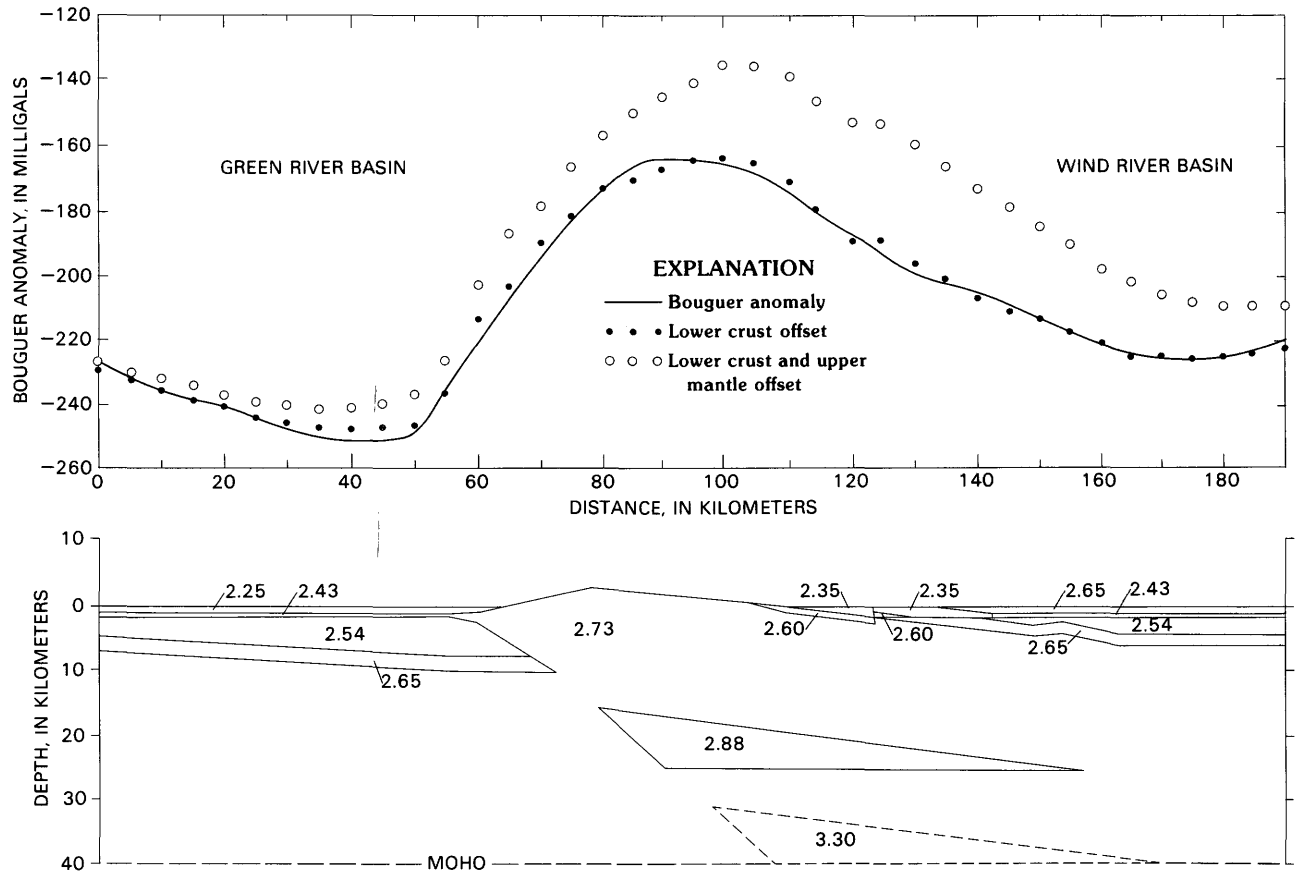

Figure 3. Gravity profile across the Wind River Mountains. Reprinted with permission from Hurich and Smithson (1982, fig. 4b, p. 1555). Location of gravity profile shown on plate 1.

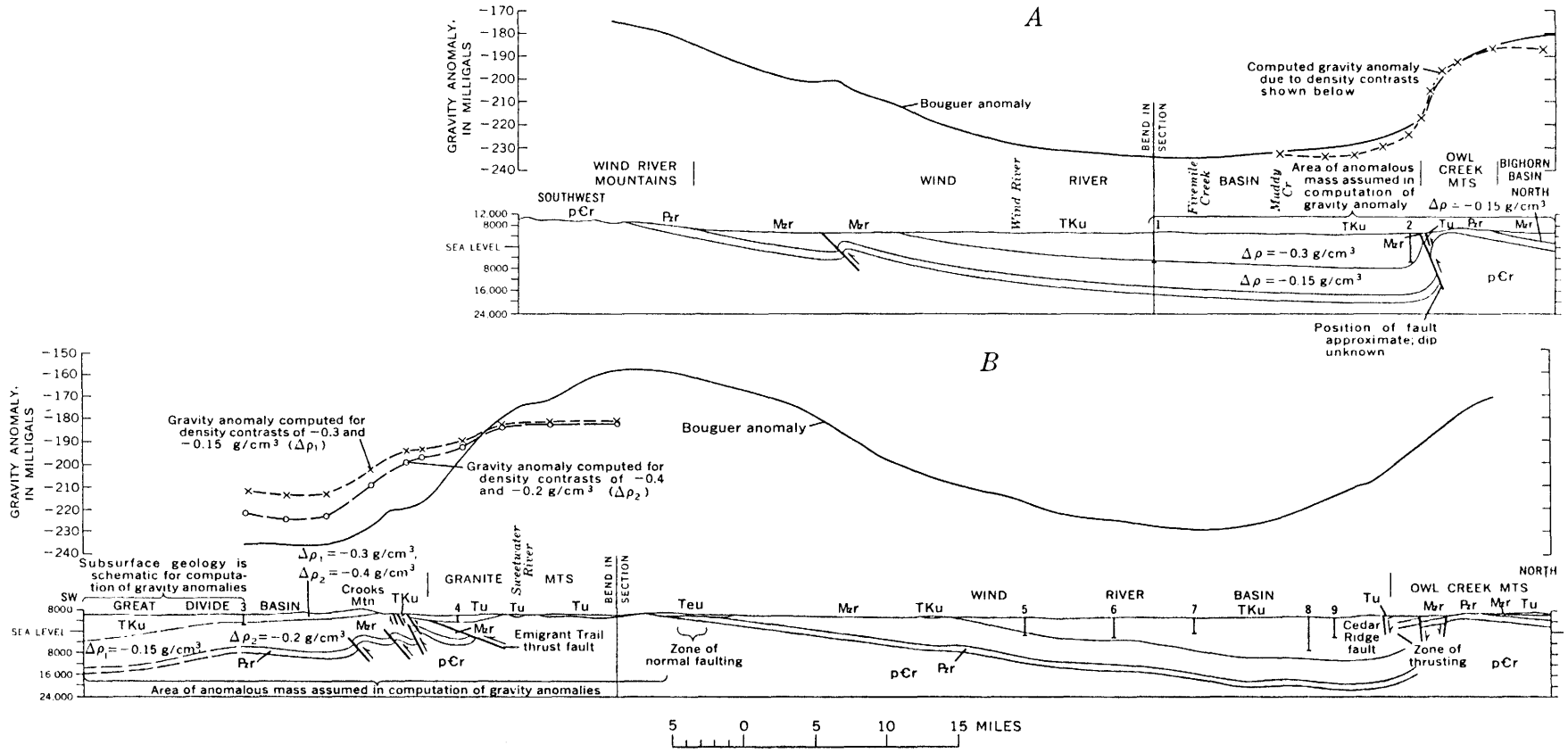
A
GRAVITY ANOMALY, IN MILLIGALS
−170
−180
−190
−200
−210
−220
−230
−240
Bouguer anomaly
Computed gravity anomaly due to density contrasts shown below
BEND IN SECTION
WIND RIVER MOUNTAINS
WIND
RIVER
BASIN
Fivemile Creek
Muddy Cr
Wind River
Area of anomalous mass assumed in computation of gravity anomaly
OWL CREEK MTS
BIGHORN BASIN
NORTH
Δρ = −0.15 g/cm³
SOUTHWEST
pCr
Pzr
Mzr
TKu
Tu
1
2
12,000
8000
SEA LEVEL
16,000
24,000
Δρ = −0.3 g/cm³
Δρ = −0.15 g/cm³
Position of fault approximate; dip unknown
B
GRAVITY ANOMALY, IN MILLIGALS
−150
−160
−170
−180
−190
−200
−210
−220
−230
−240
Gravity anomaly computed for density contrasts of −0.3 and −0.15 g/cm³ (Δρ1)
Gravity anomaly computed for density contrasts of −0.4 and −0.2 g/cm³ (Δρ2)
Bouguer anomaly
Δρ1 = −0.3 g/cm³,
Δρ2 = −0.4 g/cm³
Subsurface geology is schematic for computation of gravity anomalies
GRANITE
Sweetwater River
MTS
BEND IN SECTION
NORTH
SW
GREAT DIVIDE BASIN
Crooks Mtn
TKu
3
4
Tu
Teu
Mzr
WIND
RIVER
BASIN
5
6
7
8
9
OWL CREEK MTS
Pzr
SEA LEVEL
8000
16,000
24,000
Δρ1 = −0.15 g/cm³
Δρ2 = −0.2 g/cm³
Emigrant Trail thrust fault
Zone of normal faulting
Cedar Ridge fault
Zone of thrusting
pCr
Area of anomalous mass assumed in computation of gravity anomalies
5 0 5 10 15 MILES

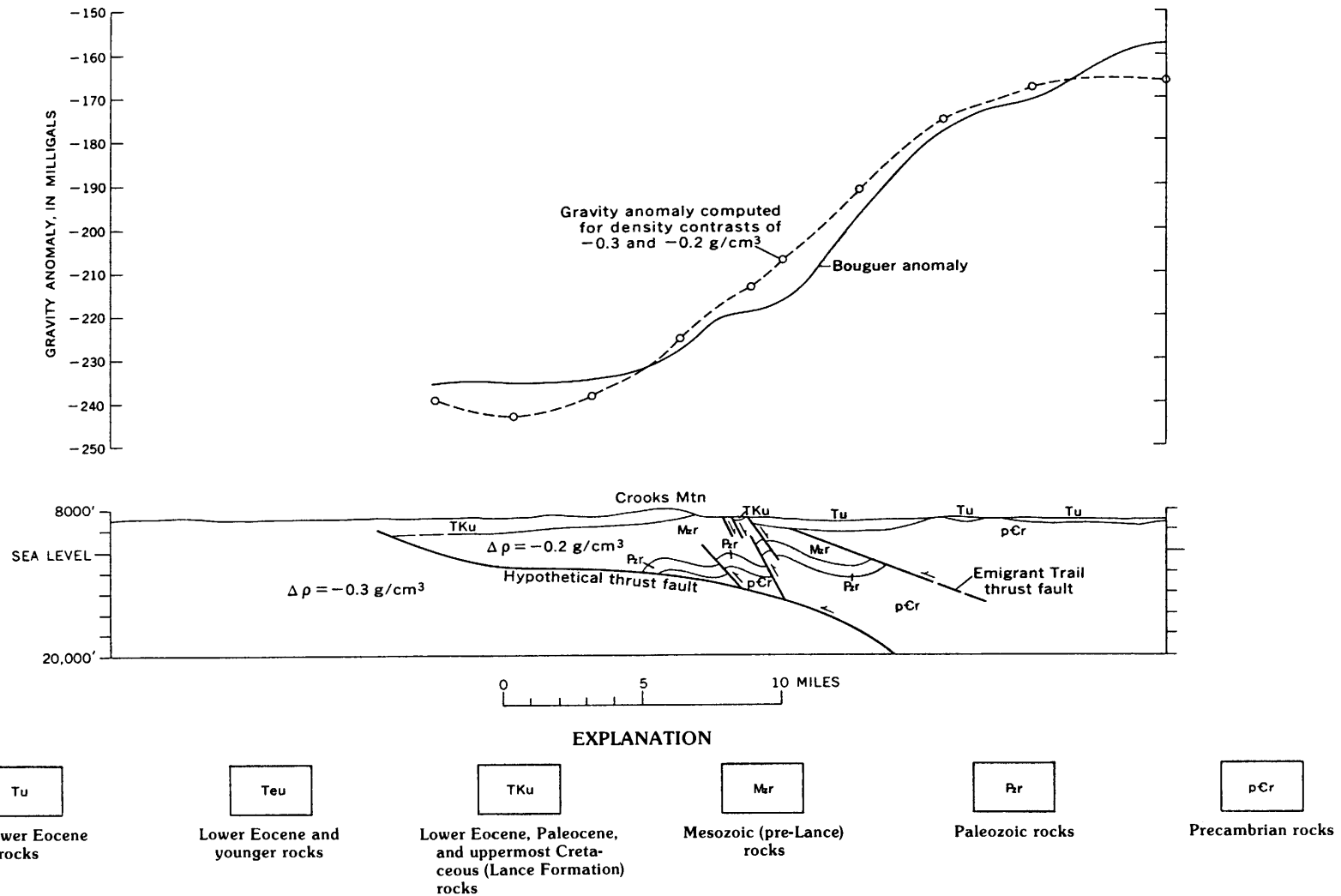

Figure 4. Gravity profiles across the Wind River Basin. Reprinted from Case and Keefer (1966, figs. 4 and 5, p. C125 and C127). Location of gravity profiles shown on plate 1. Note that the top of figure is an expanded version of the southern end of profile B.

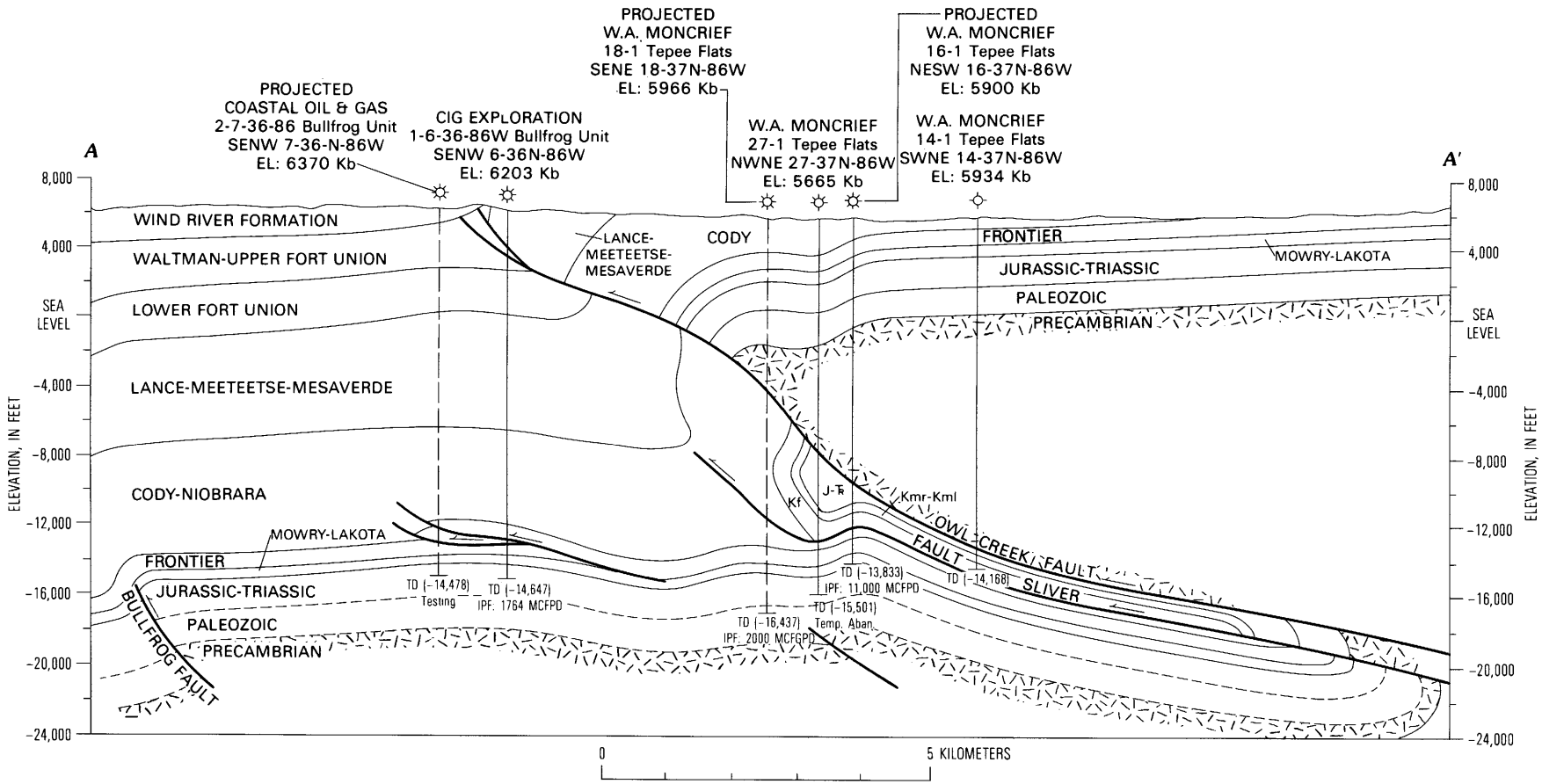

Figure 5. Interpreted cross section across the Casper Arch Thrust. Kf, Frontier Formation; Kmr-Kml, Mowry Shale to Lakota clastics (informal unit). Reprinted with permission from Ray and Berg (1985, fig. 3, p. 52). Line of cross section shown on plate 1.

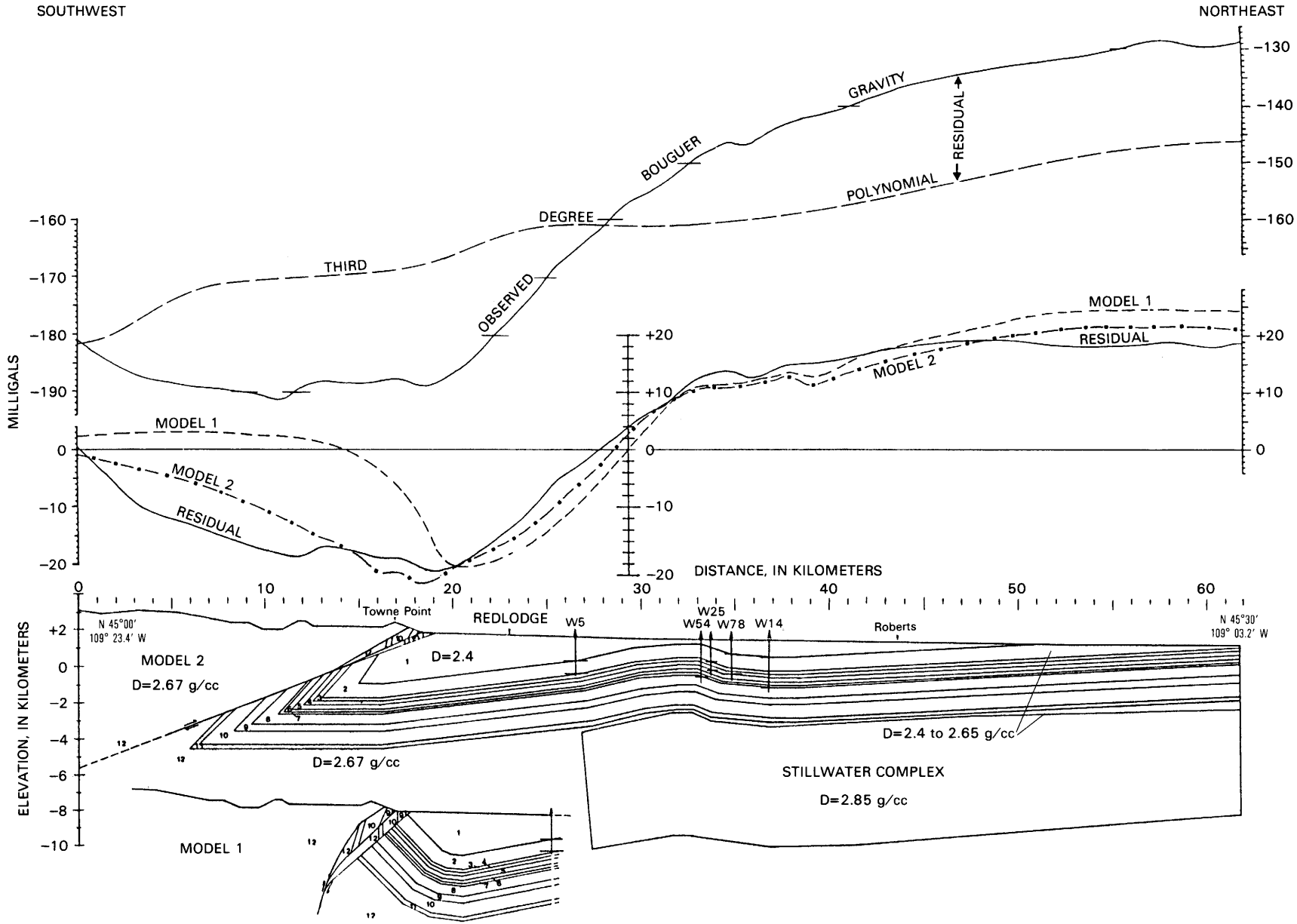

Figure 6. Gravity profile across the Beartooth Mountain front. Residual curve is the observed Bouguer gravity minus a third-degree polynomial estimate of the regional field. Reprinted with permission from Bonini and Kinard (1983, fig 4, p. 93). Location of gravity profile shown on plate 1.

Farther to the south, Stone (1985a, b) presented seismic profiles (plate 1) on both the east and west flanks of the Bighorn Basin that show a number of west-dipping thrusts which offset basement by less than 1 km of displacement on individual faults.

Bighorn Mountains–Powder River Basin–Black Hills

Seismic profiles across the east flank of the Bighorn Mountains show that two major west-dipping thrust faults are present just west of Buffalo, Wyoming (Grow and others, 1988). The dominant thrust dips 20°–30° to the west and has 6–11 km of basement overhang. The lesser fault (Buffalo Deep) (Blackstone, 1981) is a few kilometers east of the main mountain front and has less than 1 km of offset. A seismic line just west of Buffalo shows both faults clearly (fig. 7). This line was provided by Chevron USA, Inc., and was reprocessed by the U.S. Geological Survey (Miller and others, 1988). This profile shows a fault with 30° west dip and 6 km of overhang. The Arco Kenney Ranch well located near this profile penetrated about 1 km of granite before entering sedimentary rocks of the Powder River Basin. A second seismic profile from about 20 km north of Buffalo shows a fault with 20° west dip and about 11 km of overhang (Grow and others, 1988). The Gulf Granite Ridge exploration well, within 1 km of this line, penetrated 1.8 km of granite before entering sedimentary rocks of the Powder River Basin.

A gravity and magnetic profile and models across the Powder River Basin (fig. 8) synthesize the structure of the Precambrian basement from the Bighorn Mountains to the Black Hills (Robbins and Grow, 1990). Constraints on the model include the Buffalo seismic line (fig. 7), seismic lines in the Powder River Basin by Moore (1985), the structure contour map of the basement (plate 2) by Blackstone (1990), and modeling along the east flank of the Bighorns by Jenkins (1986). The normal density of the basement is assumed to be 2.73 g/cm^3, based on measurements of Hurich and Smithson (1982). Short-wavelength gravity and magnetic highs and lows are observed over the main part of the Powder River Basin in contrast to the very gently west dipping basement surface. High and low density (2.58–3.01 g/cm^3) and magnetic ($I=20\times10^{-6}$–$3{,}200\times10^{-6}$ emu/cm^3) bodies within the upper basement must be assumed in order to fit observed gravity and magnetic curves over the Powder River Basin. This implies that significant lithologic heterogeneity exists in the upper part of the basement beneath this basin.

Densities of sedimentary rocks in the basin range from 2.23 to 2.58 g/cm^3, based on a limited review of well logs and bore-hole gravity measurements (Jenkins, 1986). The average density is about 2.45 g/cm^3, in the deepest part of the basin. These density values for the Powder River Basin are somewhat lower than density values for sedimentary rocks used by Hurich and Smithson (1982) in the Green River Basin of from 2.25 to 2.65 g/cm^3 and an average of more than 2.50 g/cm^3. The greater thickness of the entire section is to the west, especially for Paleozoic and Mesozoic rocks, and the greater proportion of Tertiary rocks is in the east, which may account for the lower average density values for sedimentary rocks in the Powder River Basin. Although rock density studies of more regional extent are needed in the Powder River Basin, the values used in our gravity model (fig. 8) are the best currently available.

The excellent fit between the calculated and observed gravity curves using a model in which density anomalies are confined to the upper 8 km (fig. 8) implies that additional density bodies or offsets are not required beneath the Bighorn Mountains; that is, the main thrust fault flattens out in the middle crust without cutting the Moho or a major density boundary within the crust. No deep-crustal reflection data are available for the Bighorn Basin or Bighorn Mountains at this time, but both our shallow seismic data and gravity model for the Bighorn Mountains suggest that the main west-dipping thrust fault is analogous to the Wind River Thrust except that it has about half as much displacement and a detachment zone somewhat shallower in the crust.

Other Geophysical Studies Supporting Low-Angle Thrusting

Three studies in southern Wyoming also support the low-angle thrusting model; however, pre-Laramide basement-involved deformation in the southern Wyoming mountains during the Paleozoic adds complications beyond the scope of this study. A COCORP seismic profile over the Laramie Range in southeastern Wyoming (plate 1) shows smaller scale thrust faults dipping 30°–35° that can be traced to depths of 10 km and have offsets of approximately 3 km (Brewer and others, 1982; Johnson and Smithson, 1986). A gravity study of the Shirley Mountains and Hanna basin also concludes that low-angle north-dipping thrusts underlie the south flank of the Shirley Mountains (Oliver, 1970). An east-west gravity model over the Rock Springs and Sierra Madre Uplifts in southwestern Wyoming by Bankey and Merewether (1990) shows a smaller scale listric thrust deep beneath the basin deposits.

HORIZONTAL GRAVITY GRADIENT

In deciding how to interpret the HGA gravity map (plate 5), we assumed a simple two-body fault-contact model (fig. 9) for which we computed the response for six different fault dip angles. The model assumes a 6-km-deep basin in which the sedimentary rocks have a -0.2 g/cm^3 density contrast with respect to surrounding basement rocks. The six fault dip

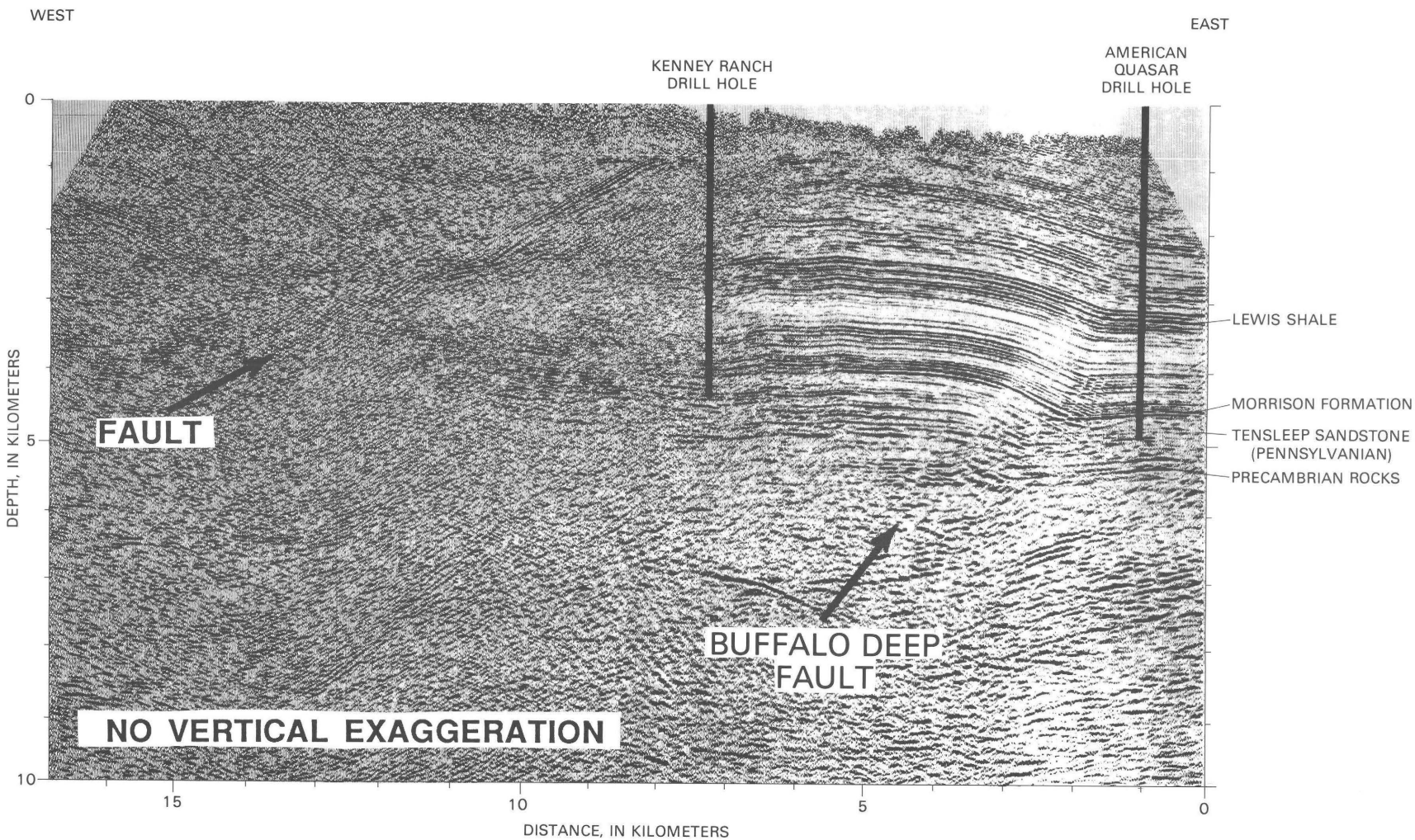

Figure 7. Seismic line 4557 across the east flank of the Bighorn Mountains. UJ, Upper Jurassic rocks; UK, Upper Cretaceous rocks. Migrated depth. From Chevron USA, Inc., used with permission; reprocessed by Miller and others (1988). Location of seismic line shown on plate 1.

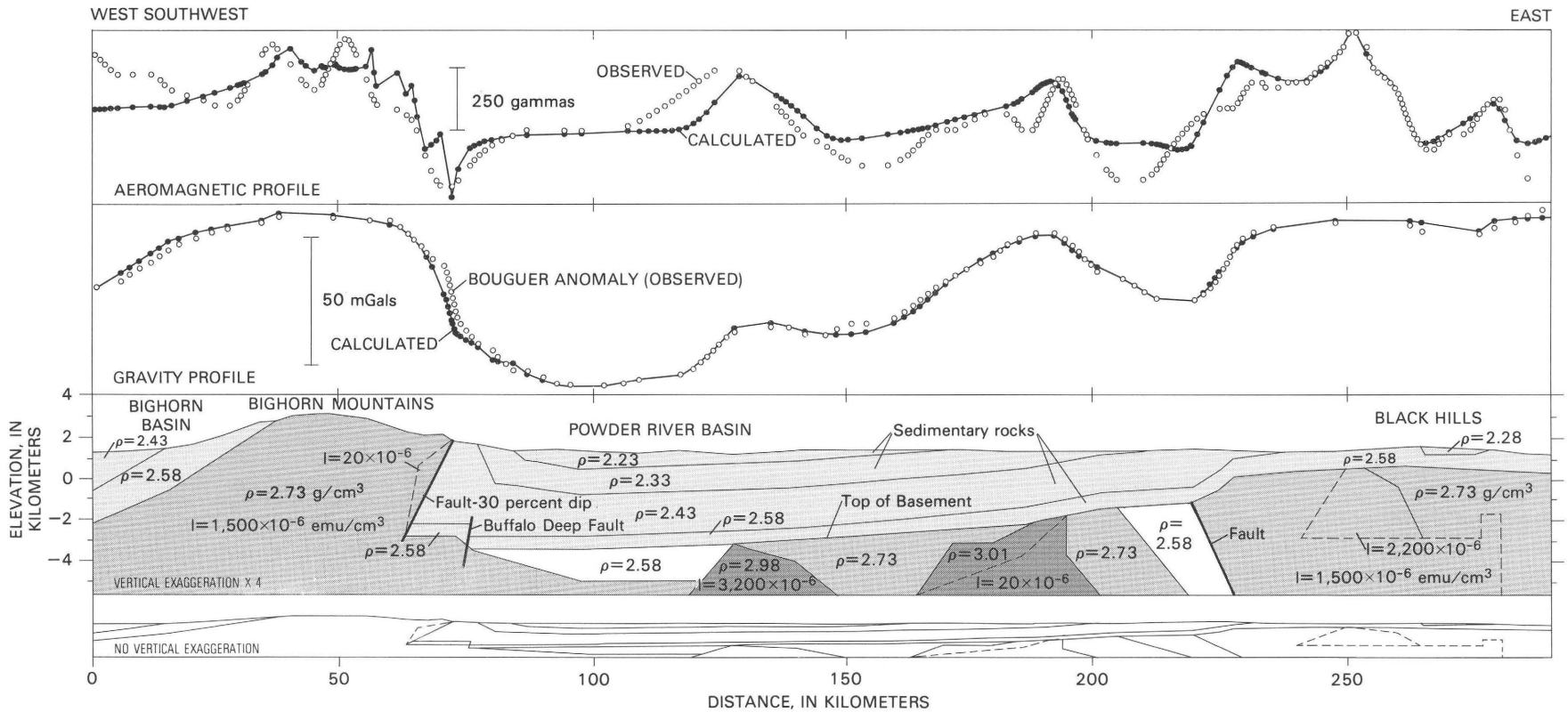

Figure 8. Gravity and magnetic profiles across the Powder River Basin. Location of profile shown on plate 1.

angles are 70° normal, vertical, and 20°, 30°, 45°, and 60° reverse (thrust faults). Although the amplitude of the anomalies over such faults will vary depending on the actual density contrasts and depth of basin fill, the position of the maximum gravity gradient is dependent solely on the fault angle. Whereas the position of the maximum gradient is directly over a vertical fault, the maximum gradient position is displaced toward the mountain range (with respect to the surface trace of a fault) for reverse faults and toward the basin for normal faults. Although the maximum gradients are within 2 km of the surface trace in all six cases, intermediate gradients are displaced 10–20 km toward the range for the low-angle thrusts (20° and 30°).

The surface traces of the major range-bounding faults (plate 2) are plotted on the HGA map (plate 5) in order to compare gravity gradients with fault-trace positions. Examination of plate 5 reveals that intermediate gradients are displaced toward the ranges by 20 km or more in the Bighorn, Wind River, Owl Creek, and Granite Mountains and most of the other mountain ranges. Complications may arise where shallow density variations exist within uplifted basement blocks, where the core of the uplift has later collapsed, or where postorogenic debris has onlapped the leading edge of the eroded mountain front. Interference patterns between multiple faults could also confuse the interpretation. In spite of these complications, the overall pattern of asymmetric displacement of the maximum and intermediate gradients toward the mountain ranges provides additional evidence that the Laramide mountain ranges in this region are dominated by low-angle thrust faults.

If the gravity data are of uniform quality and close enough spacing, the HGA map can be a valuable reconnaissance tool for estimating whether a particular range front fault is dominantly normal, vertical, or reverse. We have already mentioned the significant gaps in station spacing within this region, and caution should be exercised in using the HGA map in areas where these gaps exist. Two-dimensional modeling of the gravity profiles with constraints from seismic reflection and magneto-telluric profiles would be desirable to confirm inferences based on the HGA map. As more gravity stations with close spacing become available in the future, the value of the HGA maps for structural reconnaissance studies in the oil, gas, and mineral industry will increase significantly.

ISOSTATIC COMPENSATION

The purpose in generating an IRA gravity map (plate 4) is to preserve the signatures of anomalous densities within the upper crust while removing the effects of mountain roots assumed to lie directly beneath the elevated topography in the Airy-Heiskanen model. Because IRA values in the study area range from a high of +75 mGal to a low of –77 mGal and average near zero, the technique appears to have successfully removed the long-wavelength effects of the regional topographic gradient (plate 1) from the CBA values (plate 3), which range from –75 to –285 mGal. This near-zero average implies that the area is isostatically compensated at regional scales, but that the Airy-Heiskanen model is not the dominant isostatic system involved in the compensation of this area and is not the optimum model for computing IRA maps. With average IRA values near zero and a total range of 152 mGal (versus 210 mGal for the CBA map), the IRA map is a significant improvement, however, over the CBA map in terms of its resolution for emphasizing upper crustal structures.

In order to assess the magnitude of the gravitational effect of the mountain roots in the IRA map, we computed a two-dimensional Airy-Heiskanen isostatic model from the Green River Basin to the northern Powder River Basin (fig. 10). The model crosses the highest peaks in the Wind River and Bighorn Mountains (also in Wyoming) and traverses the main topographic gradient from southeastern Montana to western Wyoming (plate 1). In making an Airy-Heiskanen isostatic correction, the weight of the topography above sea level is compensated for by an assumed local depression of the crust-mantle boundary. The weight of the topography above sea level must be balanced by the buoyancy of the crustal root beneath the depth of compensation. We assumed a density of 2.67 g/cm^3 for the topography above sea level, a depth of compensation of 30 km, and a density contrast of –0.4 g/cm^3 at the Moho. Note that the computed depth to Moho increases from 38 km in the northeast to 47 km in the southwest and has local maximums of about 58 km beneath the Wind River and Bighorn Mountains (fig. 10).

The calculated effect of the assumed isostatic root varies from –160 to –260 mGal from northeast to southwest and is a reasonably good first-order fit to the observed CBA profile in the high plains and intermontane basins; however, CBA values are 75–100 mGal higher than the effect of the roots over the Wind River and Bighorn Mountains; that is, the two-dimensional IRA values are +75 to +100 mGal over the main range, slightly higher values than those on the IRA map due to differences between two- and three-dimensional models as well as to slight differences in density contrast and depth of compensation. The values used for the IRA map result in slightly smaller anomalies, but the main conclusions are not affected by these minor differences between the two- and three-dimensional models or the assumed densities and depths of compensation.

The local root beneath the Bighorn Mountains causes a local downwarp of more than 40 mGal below the regional trend of the effect of the isostatic root (fig. 10). In the previous section, where we reviewed the seismic profiles and two-dimensional gravity models for the Wind River and Bighorn Mountains, we noted evidence for flattening of the thrust faults within the crust; that is, these Laramide mountains probably lack local roots. Therefore, the Airy-Heiskanen or

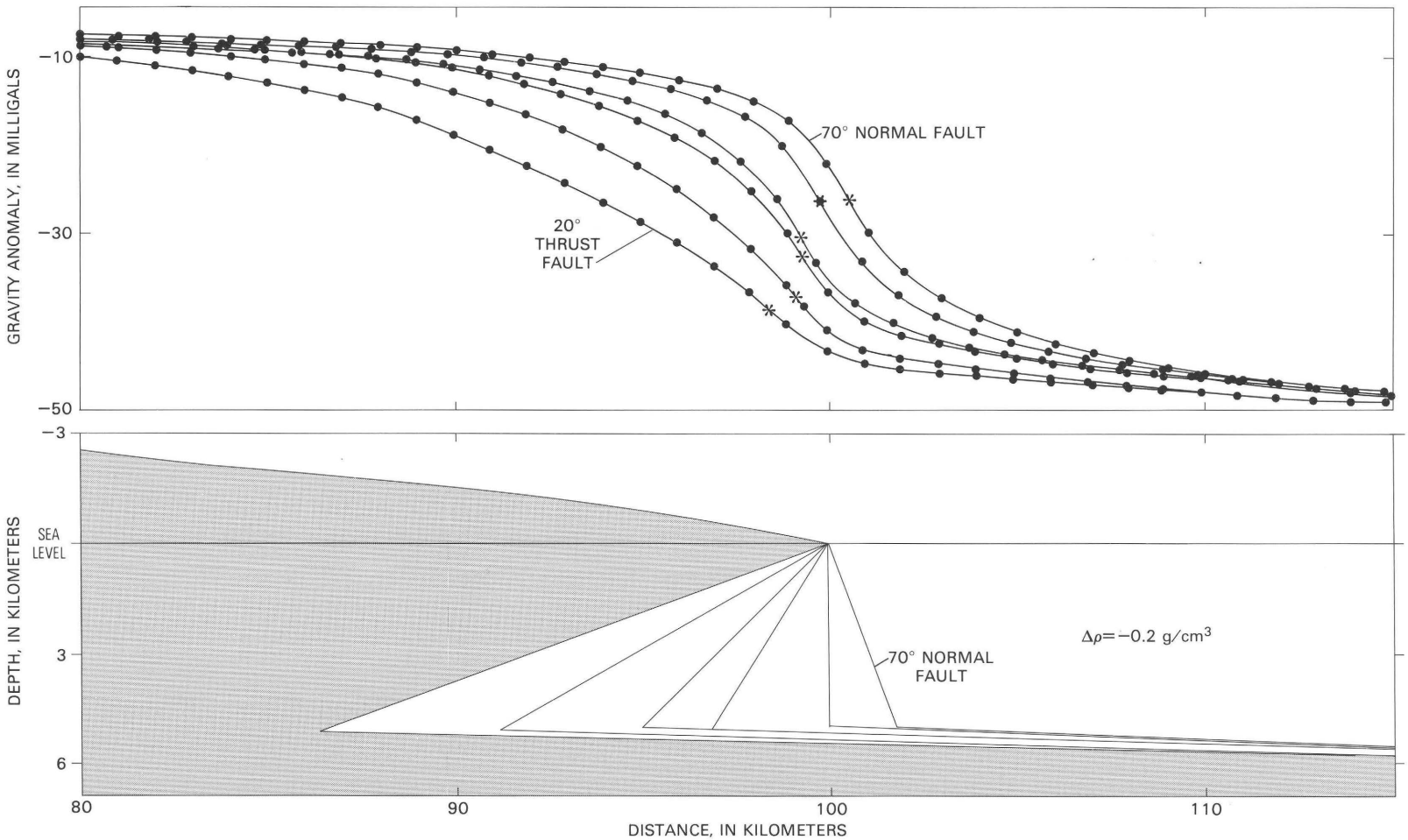

Figure 9. Gravity anomaly–fault dip comparison model. Asterisks indicate maximum gradient.

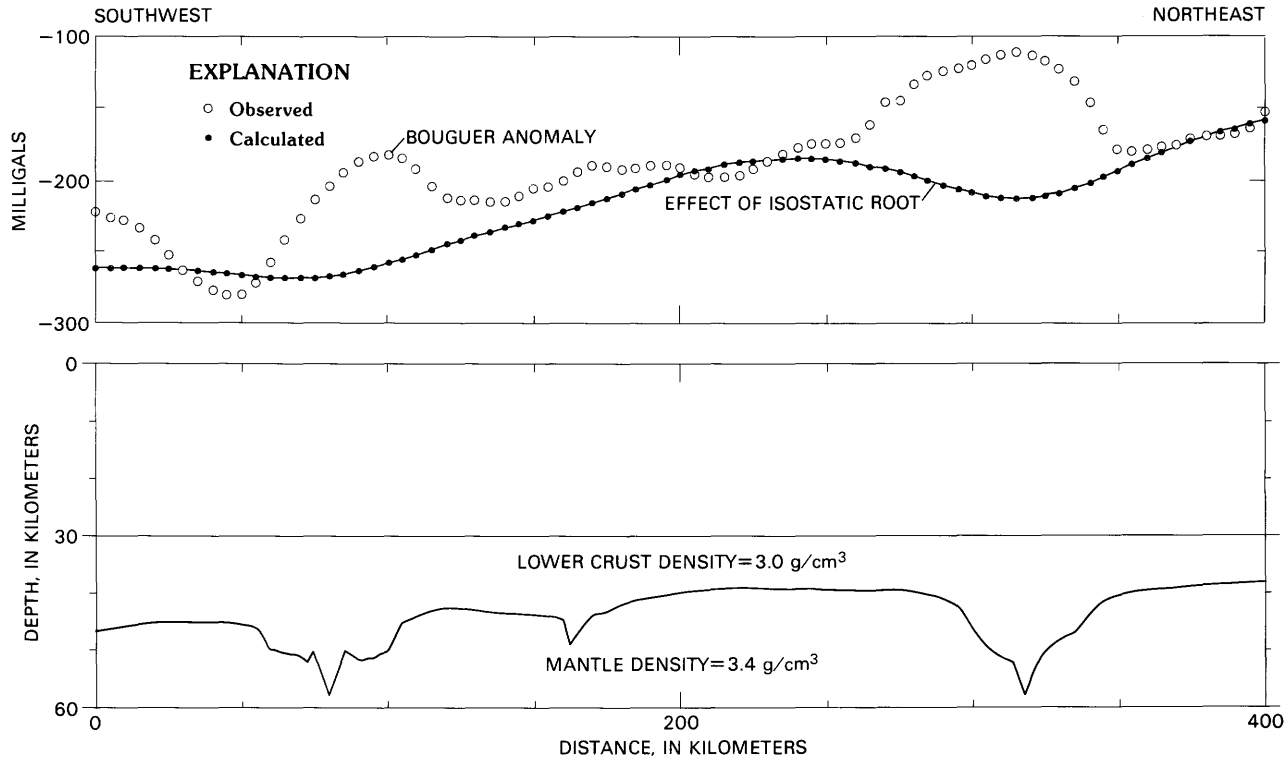

Figure 10. Airy-Heiskanen isostatic compensation model across Wyoming. Line of section shown on plate 1.

local mechanism for compensation is not the optimum system, at least for shorter wavelength mountain ranges such as the Wind River and Bighorn ranges where their widths (or wavelengths) are less than 100 km. A modified Airy-Heiskanen algorithm that would average the regional topography for wavelengths greater than 100 km would smooth out the effect of isostatic root curve (fig. 10), and this would result in smaller isostatic anomalies. With a smaller range of IRA anomalies, the resolution for discriminating anomalies caused by upper crustal structure would be enhanced. Such maps would be considerably more valuable for oil, gas, and mineral exploration than the present CBA or IRA maps and would also increase the resolution in the derivative HGA maps. Alternatively, Jachens and others (1989) suggested that the IRA maps can be filtered to remove the longer wavelength effects. This important area for future gravity research could yield valuable insight in areas of energy-rich basins like the Laramide province of Wyoming.

The most important conclusion from the IRA map (plate 4) and two-dimensional gravity model (fig. 10) is that the Laramide province of Wyoming is near isostatic equilibrium at regional scales; that is, at wavelengths longer than 100 km. The large local positive values over the mountain ranges imply, however, either that the ranges are underlain by high-density crust or that the assumption in the IRA model of local roots beneath the ranges is, in fact, erroneous. Because most outcrops of basement rocks in the region lack evidence for large volumes of dense mafic rocks, the IRA map implies that the mountain ranges are rootless and not in local isostatic balance. This local imbalance happens because the local weight of the ranges on the crust and lithosphere is distributed over wavelengths longer than 100 km.

ROCK DENSITY

Hurich and Smithson (1982) could not model the entire gravity anomaly over the Wind River Mountains using only contributions from contrasts between basin-fill deposits and basement blocks in the ranges. They had to include an uplifted dense lower crustal layer (2.88 g/cm^3) into the upper crust (2.73 g/cm^3) along the Wind River Fault (fig. 3). Smithson and others (1978) and Karasa (1976) encountered the same difficulty. The contribution from these uplifted lower crustal rocks (fig. 3) is as much as +22 mGal over the range and decreases to less than 2 mGal at distances of 100 km on either side of the mountain range. At least two alternative explanations (or combinations) can provide approximately +20 mGal.

1. If the average density contrast between basin-fill deposits and the basement was slightly larger than that determined by Hurich and Smithson (1982), then a smaller contribution from the lower crust would be necessary. For example, a simple model using a basin-fill contrast of −0.06 g/cm^3 relative to the basement also produces a positive of

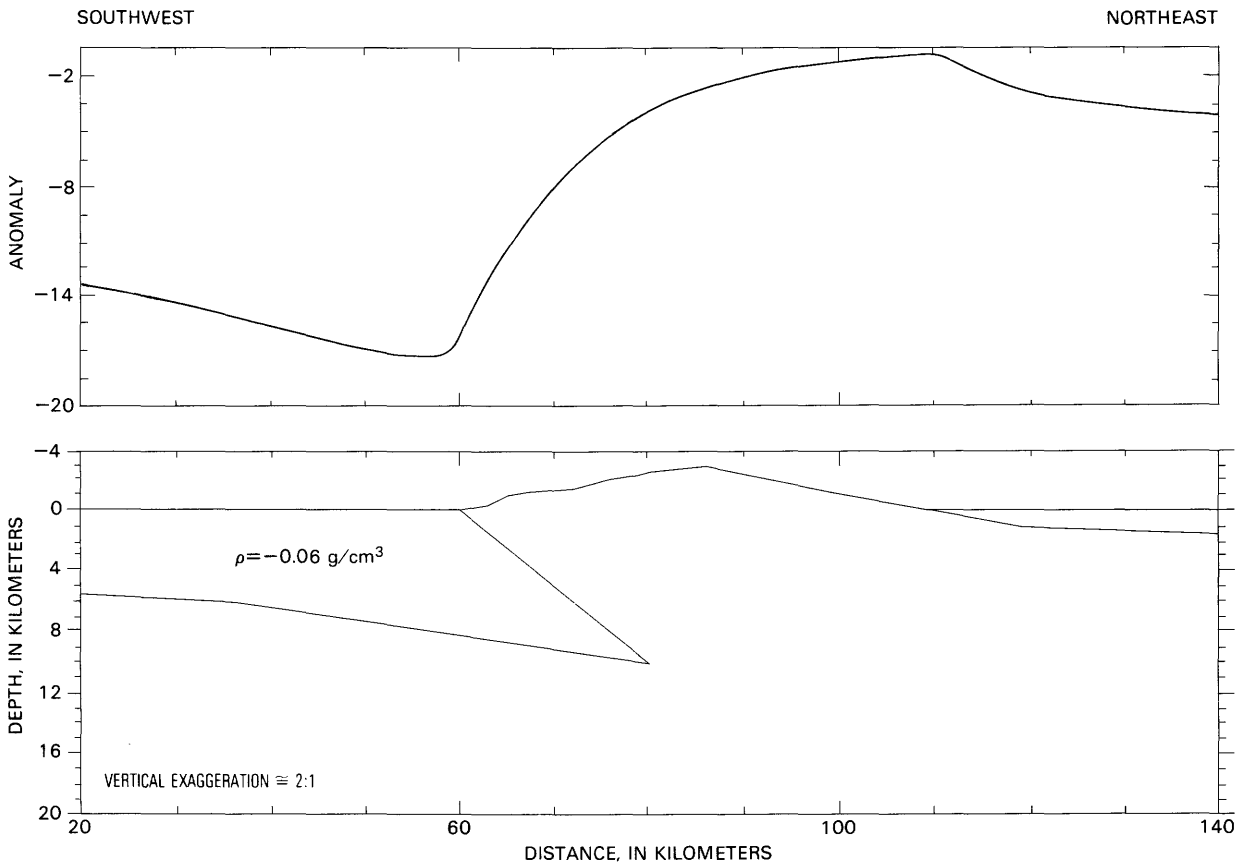

Figure 11. Sediment density contrast model across Wind River Thrust.

approximately 20 mGal (fig. 11). Therefore, the models are sensitive to relatively small changes in average sediment or basement density. Our gravity model over the Bighorn Mountain front and the Powder River Basin used basin-fill density values about 0.05 g/cm^3 lower than those used by Hurich and Smithson, and we did not need a contribution from the lower crust.

2. Our gravity and magnetic model of the Powder River Basin demonstrates that significant short-wavelength (<50 km) lateral density and magnetization anomalies are present within the upper few kilometers of the basement (fig. 8). Longer wavelength (>50 km) lateral density variations averaging +0.05 g/cm^3 in the upper 10 km of the basement could also provide contributions of approximately +20 mGal.

Although we agree with Hurich and Smithson that the gravity models require that the thrust faults flatten before reaching the Moho, we are not convinced that the thrusts uplift dense lower crust. Very small differences in basement and basin-fill densities could alter this conclusion.

A thorough discussion of rock density measurements is beyond the scope of this paper, and the reader is referred to the following references: Smithson (1971), Karasa (1976), Beyer and Clutsom (1978, 1980), Kososki and Robbins (1979, 1980a, b), Parks (1979), Hurich and Smithson (1982), Wagoner (1985), and Bankey and Merewether (1990). Although the density studies of Hurich and Smithson (1982) and Bankey and Merewether (1990) are probably the most comprehensive to date, additional studies using bore-hole gravity and (or) a larger sample of density logs throughout Wyoming are needed to confirm those results.

STRUCTURAL SYNTHESIS

A 400-km-long cross section from the Green River Basin to the Powder River Basin synthesizes the major geological and geophysical observations across Wyoming (fig. 12). The section is slightly modified from Peterson (1983) and shows the basic concept for flattening of the thrusts within the middle crust. Gries (1981, 1983), Lowell (1983), and Stone (1988) have proposed similar models.

The maximum thrust displacement is approximately 20 km in the Wind River Mountains and about 10 km in the Bighorn Mountains. Uplift in the Wind River Mountains started in Late Cretaceous time and in the Bighorn Mountains in Paleocene time, and major deformation ceased in Eocene time in both ranges (Perry and others, this volume). This difference in onset times may account for differences in relative amounts of deformation in the two ranges. Smaller thrust

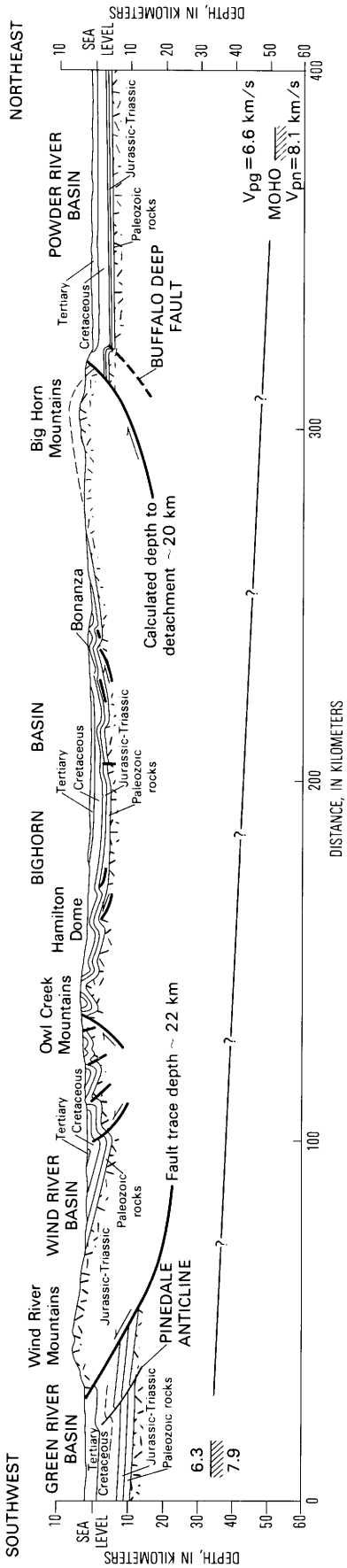

Figure 12. Interpreted cross section across Wyoming. Modified from Peterson (1983, fig. 2, p. 68, 69). The Wind River thrusts have been modified to conform with the Sharry and others (1986) version of the COCORP profile (fig. 2), and the east flank of the Bighorn Mountains is consistent with the Chevron 4557 seismic profile (fig. 7). Moho depths at the northeastern and southwestern ends of the profile and the crustal and mantle velocities are from Braile and others (1989).

faults are in the Wind River and Bighorn Basins and an intermediate thrust is along the southwest flank of the Owl Creek Mountains.

The cross section also shows Moho depths and crustal and mantle velocities based on seismic refraction studies (Braille and others, 1989). In the southwestern part of Wyoming, the Moho is at a depth of about 35 km, in good agreement with the Moho reflector on the Wind River COCORP profile (Sharry and others, 1986). In northeastern Wyoming, the Moho is at a depth of approximately 50 km. Although no deep-crustal refraction measurements are available in the central region of the section, we have dashed in a Moho dipping gently to the northeast with no local mountain roots beneath the mountain ranges. Note that the inferred regional dip of the Moho based on refraction data is opposite to the regional dip calculated for the two-dimensional Airy-Heiskanen isostatic profile (fig. 10). Therefore, although the Airy-Heiskanen model is a good first approximation to the long-wavelength components of the Bouguer gravity field, the actual mechanism for isostatic compensation must be dominated by lateral density variations in the crust and mantle that allow the actual Moho to rise to the southwest. Both crustal and upper mantle compressional velocities are lower in the southwest than in the northeast and support the inference of lateral density changes in the crust and upper mantle. Lateral density variation is a Pratt isostatic mechanism (Heiskanen and Vening Meinesz, 1958), and probably is the more dominant isostatic mechanism in the Laramide province of Wyoming.

The CBA, IRA, and HGA gravity maps herein add to the body of geophysical and geologic data in the Laramide province that demonstrates the dominance of low-angle thrusts that probably flatten within the crust. Understanding the crustal structure and mechanism of isostatic compensation will ultimately allow improved isostatic algorithms to be developed, which will further enhance the resolution of IRA and HGA gravity maps for hydrocarbon and mineral exploration.

CONCLUSIONS

1. The +50 to +75 mGal isostatic residual anomaly (IRA) gravity values over Laramide mountain ranges imply that the mountains have much smaller roots than assumed in the local Airy-Heiskanen model; that is, they are rootless.

2. The –50 to –77 mGal IRA values over the foreland basins in front of the Laramide mountain ranges are caused by the low-density basin fill.

3. The near-zero average IRA values across Wyoming and southern Montana indicate that the Airy-Heiskanen model is a good first approximation to the complete Bouguer anomaly (CBA) gravity values and that the region is near isostatic equilibrium for wavelengths longer than 100 km.

4. Modified IRA maps based on topography averaged over wavelengths longer than 100 km would correct for the erroneous roots assumed in the local Airy-Heiskanen model and thus reduce the peak to trough range of values and enhance the resolution for smaller geologic features of importance in energy and mineral exploration. Further research is needed in this area.

5. Lateral variations in crustal and upper mantle compressional velocities imply that densities also vary laterally. Therefore, actual isostatic compensation must involve a combination of both Airy-Heiskanen and Pratt systems.

6. The IRA and horizontal gradient anomaly (HGA) gravity maps support previous seismic reflection, two-dimensional gravity modeling, and exploration drilling data indicating that low-angle (20°–30°) faulting is the dominant style of Laramide deformation. Basement overhangs of 10–20 km are documented in some ranges, such as the Bighorn and Wind River Mountains.

7. The high gravity gradients are displaced toward the mountain ranges on the HGA maps and further support the concept of low-angle thrust faulting.

8 The COCORP Wind River seismic profile, as well as two-dimensional gravity models there and in the Bighorn Mountains, indicate that the thrust flattens out in the middle or lower crust and that the mountains are rootless, as proposed by Peterson (1983).

9. Energy and mineral exploration can benefit from the gravity maps presented in this paper, and when the numerous gaps in the field data are filled the value of the maps will improve significantly.

REFERENCES CITED

Bally, A.W., 1983, Seismic expression of structural styles—A picture and work atlas, v. 3; Tectonics of compressional provinces/strike slip provinces: American Association of Petroleum Geologists Studies in Geology Series 15, 414 p.

Bankey, Viki, and Merewether, E.A., 1990, Bouguer gravity anomaly map of southwestern Wyoming, northeastern Utah, and northwestern Colorado: U.S. Geological Survey Geophysical Investigations Map GP–993, 1 sheet, scale 1:500,000.

Basham, W.L., and Martin, W.F., 1985, Seismic line across the Wind River thrust, Wyoming, *in* Gries, R.R., and Dyer, R.C., eds., Seismic exploration of the Rocky Mountains: Rocky Mountain Association of Geologists and Denver Geophysical Society, p. 59–66.

Berg, R.R., 1963, Laramide sediments along the Wind River thrust, Wyoming, *in* Childs, O.E., and Beebe, B.W., eds., Backbone of the Americas: American Association of Petroleum Geologists Memoir 2, p. 220–230.

Berg, R.R., and Romberg, F.E., 1966, Gravity profile across the Wind River Mountains, Wyoming: Geological Society of America Bulletin, v. 77, p. 647–656.

Beyer, L.A., and Clutsom, F.G., 1978, Density and porosity of oil reservoirs and overlying formations from borehole gravity measurements, Gebo oil field, Hot Springs County, Wyoming: U.S. Geological Survey Oil and Gas Investigations Chart OC–88, 16 p., 3 sheets.

——1980, Density and porosity of Upper Cretaceous through Permian formations from borehole gravity measurements, Big Polecat oil and gas field, Park County, Wyoming: U.S. Geological Survey Oil and Gas Investigations Chart OC–103, 14 p., 3 sheets.

Blackstone, D.L., Jr., 1981, Compression as an agent in deformation of the east-central flank of the Bighorn Mountains, Sheridan and Johnson Counties, Wyoming: Contributions to Geology, v. 19, p. 105–122.

——1990, Precambrian basement map of Wyoming; outcrop and structural configuration: Wyoming Geological Survey Map Series MS–27, scale 1:1,000,000.

Blakely, R.J., and Simpson, R.W., 1986, Approximating edges of source bodies from magnetic or gravity anomalies: Geophysics, v. 51, no. 7, p. 1494–1498.

Bonini, W.E., and Kinard, R.E., 1983, Gravity anomalies along the Beartooth front Montana; evidence for a low-angle thrust: Wyoming Geological Association 34th Annual Field Conference Guidebook, p. 89–94.

Braile, L.W., Hinze, W.J., von Frese, R.R.B., and Keller, G.R., Jr., 1989, Seismic properties of the crust and uppermost mantle of the conterminous United States and adjacent Canada, *in* Pakiser, L.C., and Mooney, W.D., eds., Geophysical framework of the continental United States: Geological Society of America Memoir 172, p. 655–680.

Brewer, J.A., Allmendinger, R.W., Brown, L.D., Oliver, J.E., and Kaufman, S., 1982, COCORP profiling across the Rocky Mountain front in southern Wyoming, part 1; Laramide structure: Geological Society of America Bulletin, v. 93, no. 12, p. 1242–1252.

Brewer, J.A., Smithson, S.B., Oliver, J.E., Kaufman, S., and Brown, L.D., 1980, The Laramide orogeny; evidence from COCORP deep crustal seismic profiles in the Wind River Mountains, Wyoming: Tectonophysics, v. 62, p. 165–189.

Case, J.E., and Keefer, W.R., 1966, Regional gravity survey, Wind River basin, Wyoming: U.S. Geological Survey Professional Paper 550–C, p. C120–C128.

Chamberlin, R.T., 1935, Geologic analysis of the gravity anomalies for the Black Hills–Bighorn–Beartooth region: Geological Society of American Bulletin v. 46, p. 393–408.

Darton, N.H., 1906, Geology of the Bighorn Mountains: U.S. Geological Survey Professional Paper 51, 129 p.

Godson, R.H., 1980, Program COLOR: U.S. Geological Survey unpublished report, 13 p.

Gries, R.R., 1981, Oil and gas prospecting beneath the Precambrian of foreland thrust plates in the Rocky Mountains: The Mountain Geologist, v. 18, p. 1–18.

——1983, Oil and gas prospecting beneath the Precambrian of foreland thrust plates in the Rocky Mountains: American Association of Petroleum Geologists Bulletin, v. 67, p. 1–26.

Gries, R.R., and Dyer, R.C., 1985, Seismic exploration of the Rocky Mountains: Rocky Mountain Association of Geologists and Denver Geophysical Society Atlas, 300 p.

Grow, J.A., Hinrichs, E.N., Miller, J.J., Lee, M.W., and Robbins, S.L., 1988, Laramide thrusting of the Bighorn Mountains onto the Powder River basin near Buffalo, Wyoming [abs]: U.S. Geological Survey Circular 1025, p. 18.

Hamilton, W.B., 1988, Laramide crustal shortening: Geological Society of America Memoir 171, p. 27–39.

Heiskanen, W.A., and Vening Meinesz, 1958, The Earth and its gravity field: New York, McGraw-Hill, 470 p.

Hurich, C.A., 1981, Gravity interpretation of the southern Wind River Mountains, Wyoming: Laramie, University of Wyoming, M.S. thesis, 42 p., 3 plates.

Hurich, C.A., and Smithson, S.B., 1982, Gravity interpretation of the southern Wind River Mountains, Wyoming: Geophysics, v. 47, no. 11, p. 1550–1561.

International Association of Geodesy, 1971, Geodetic reference system 1967: International Association of Geodesy Special Publication 3, 116 p.

Jachens, R.C., Simpson, R.W., Blakely, R.J., and Saltus, R.W., 1989, Isostatic residual gravity and crustal geology of the United States, *in* Pakiser, L.C., and Mooney, W.D., eds., Geophysical framework of the continental United States: Geological Society of America Memoir 172, p. 405–424.

Jenkins, C.D., Jr., 1986, A preliminary tectonic analysis of the northeastern margin of the Bighorn uplift, Buffalo to Dayton, Wyoming: Rapid City, South Dakota School of Mines and Technology, M.S. thesis, 121 p., 3 plates.

Johnson, R.A., and Smithson, S.B., 1986, Interpretive processing of crustal seismic reflection data: examples from the Laramie Range COCORP data, *in* Barazangi, M., and Brown, L. eds., Reflection seismology–A global perspective: American Geophysical Union Geodynamics Series, v. 13, p. 197–208.

Karasa, N.L., 1976, A gravity interpretation of the structure of the Granite Mountains area, central Wyoming: Laramie, University of Wyoming, M.S. thesis, 63 p., 2 plates.

Kososki, B.A., and Robbins, S.L., 1979, In situ bulk density and porosity estimates from borehole gravity data in limestones of the Madison Group, test well no. 1, Crook County, Wyoming: U.S. Geological Survey Open-File Report 79–1514, 14 p.

_____1980a, In-situ bulk-density estimates from borehole gravity data in the Madison Group test well no. 3, Yellowstone County, Montana: U.S. Geological Survey Open-File Report 80–784, 11 p.

_____1980b, In-situ density estimates from borehole gravity data from the Madison Group test well no. 2, Custer County, Montana: U.S. Geological Survey Open-File Report 80–982, 11 p.

Lamerson, P.R., 1982, The Fossil basin and its relationship to the Absaroka thrust system, Wyoming and Utah, *in* Powers, R.B., ed., Geologic studies of the Cordilleran thrust belt: Rocky Mountain Association of Geologists, v. 1, p. 279–340.

Love, J.D., and Christensen, A.C., 1985, Geologic map of Wyoming: U.S. Geological Survey, 2 sheets, scale 1:500,000.

Lowell, J.D., 1983, Foreland deformation, *in* Lowell, J.D., and Gries, R.R., eds., Rocky Mountain foreland basins and uplift: Rocky Mountain Association of Geologists, p. 1–8.

Malahoff, Alexander, and Moberly, Ralph, Jr., 1968, Effects of structure on the gravity field of Wyoming: Geophysics, v. 33, no. 5, p. 781–804.

Matthews, Vincent, III, ed., 1978, Laramide folding associated with basement block faulting in the western United States: Geological Society of America Memoir 151, 376 p.

McGookey, D.P., 1972, Cretaceous system, *in* Geologic atlas of the Rocky Mountains: Rocky Mountain Association of Geologists, p. 190–228.

Miller, J.J., Lee, M.W., Grow, J.A., Hinrichs, E.N., and Robbins, S.L., 1988, Seismic reflection profiles across the eastern Bighorn Mountains between Buffalo and Story, Wyoming [abs]: U.S. Geological Survey Circular 1025, p. 36–37.

Moore, W.R., 1985, Seismic profiles of the Powder River basin, Wyoming, *in* Gries, R.R., and Dyer, R.C., eds., Seismic exploration of the Rocky Mountains: Rocky Mountain Association of Geologists and Denver Geophysical Society, p. 187–199.

Morelli, C., ed., 1974, The international gravity standardization net 1971: International Association of Geodesy Special Publication 4, 194 p.

Oliver, K.L., 1970, Gravity study of the Hanna basin: Laramie, University of Wyoming, M.S. thesis, 46 p., 3 plates.

Parks, P.H., 1979, Gravity interpretation of the Wind River Mountains, Wyoming: College Station, Texas A & M University, M.S. thesis, 107 p., 1 plate.

Peterson, F.A., 1983, Foreland detachment structures, *in* Lowell, J.D., and Gries, R.R., eds., Rocky Mountain foreland basins and uplift: Rocky Mountain Association of Geologists, p. 65–77.

Plouff, Donald, 1977, Preliminary documentation for a FORTRAN program to compute gravity terrain corrections based on topography digitized on a geographic grid: U.S. Geological Survey Open-File Report 77–535, 45 p.

Prucha, J.J., Graham, J.A., and Nickelson, R.P., 1965, Basement-controlled deformation in Wyoming Province of Rocky Mountain foreland: American Association of Petroleum Geologist Bulletin v. 49, p. 966–992.

Ray, R.R., and Berg, C.R., 1985, Seismic interpretation of the Casper Arch thrust, Tepee Flats Field, Wyoming, *in* Gries, R.R., and Dyer, R.C., eds., Seismic exploration of the Rocky Mountains: Rocky Mountain Association of Geologists and Denver Geophysical Society, p. 51–58.

Ray, R.R., and Keefer, W.R., 1985, Wind River basin, central Wyoming, *in* Gries, R.R., and Dyer, R.C., eds., Seismic exploration of the Rocky Mountains: Rocky Mountain Association of Geologists and Denver Geophysical Society, p. 201–212.

Robbins, S.L., in press, Complete Bouguer anomaly gravity map of the Sheridan 1°×2° Quadrangle, northern Wyoming: Wyoming Geological Survey Map Series 25, scale 1:250,000.

Robbins, S.L., and Grow, J.A., 1990, Structural and basement lithological implications of gravity and seismic reflection data across the central Powder River basin from the Black Hills to the Bighorn Mountains [abs.]: U.S. Geological Survey Circular 1060, p. 71.

Robbins, S.L., and Williamson, Courteney, in press, Complete Bouguer anomaly gravity map of the Gillette 1°×2° Quadrangle, northeastern Wyoming: Wyoming Geological Survey Map Series 25–G, scale 1:250,000.

Rocky Mountain Association of Geologists, 1972, Geologic atlas of the Rocky Mountain region: Rocky Mountain Association of Geologists, 331 p.

Sharry, J., Langan, R.T., Jovanivich, D.B., Jones, G.M., Hill, N.R., and Guidish, T.M., 1986, Enhanced imaging of the COCORP seismic line, Wind River Mountains, *in* Barazangi, Muawia, and Brown, Larry, eds., Reflection seismology; a global perspective: American Geophysical Union Geodynamics Series, v. 13, p. 223–236.

Simpson, R.W., Jachens, R.C., and Blakely, R.J., 1983, AIRYROOT; a FORTRAN program for calculating the gravitational attraction of an Airy isostatic root out to 166.7 km: U.S. Geological Survey Open-File Report 83–883, 66 p.

Skeen, R.C., and Ray, R.R., 1983, Seismic models and interpretation of the Casper arch thrust—Application to Rocky Mountain foreland structure: The Mountain Geologist, v. 20, p. 99–124.

Smith, R.D., 1987, Rocky Mountain foreland uplifts; an exploration case history on the Beartooth Mountains, Montana [abs.]: Denver Geophysical Society Record, March, p. 2–3.

Smithson, S.B., 1971, Densities of metamorphic rocks: Geophysics, v. 36, no. 4, p. 690–694.

Smithson, S.B., Brewer, J.A., Kaufman, S., Oliver, J.E. and Hurich, C.A., 1978, Nature of the Wind River thrust, Wyoming, from COCORP deep-reflection data and from gravity data: Geology, v. 6, p. 648–652.

_____1979, Structure of the Laramide Wind River uplift, Wyoming, from COCORP deep reflection data and from gravity data: Journal of Geophysical Research, v. 84, no. B11, p. 5955–5972.

Stone, D.S., 1985a, Geologic interpretation of seismic profiles, Bighorn basin, part I; east flank, *in* Gries, R.R., and Dyer, R.C., eds., Seismic exploration of the Rocky Mountains: Rocky Mountain Association of Geologists and Denver Geophysical Society, p. 165–176.

_____1985b, Geologic interpretation of seismic profiles, Bighorn basin, Wyoming, part II; west flank, *in* Gries, R.R., and Dyer, R.C., eds., Seismic exploration of the Rocky Mountains: Rocky Mountain Association of Geologists and Denver Geophysical Society, p. 175–186.

_____1988, Seismic line across Wyoming [abs.]: Denver Geophysical Society Record, p. 2–3.

Wagoner, Colin, 1985, Gravity models of the Wyoming overthrust belt: Golden, Colorado School of Mines, M.S. thesis, 81 p.

Webring, Michael, 1981, MINC; a gridding program based on minimum curvature: U.S. Geological Survey Open-File Report 81–1224, 43 p.

Williamson, Courteney, and Robbins, S.L., 1991, Principal facts for 1,040 gravity stations in the Gillette and Sheridan 1°×2° Quadrangles, Wyoming and in the northern Bighorn Mountains, Montana: U.S. Geological Survey Open-File Report 91–287, 59 p.

Woodward, L.A., 1988, Tectonic map of the Rocky Mountain region of the United States, *in* Sloss, L.L., ed., The geology of North America; sedimentary cover—North American craton: U.S.: Geological Society of America Decade of North American Geology, v. D–2, plate 2.

Chapter F

Pre-Late Eocene Structures and their Control of Gold Ore at the Drum Mine, West-Central Utah

By C.J. NUTT and C.H. THORMAN

U.S. GEOLOGICAL SURVEY BULLETIN 2012

APPLICATION OF STRUCTURAL GEOLOGY TO MINERAL AND
ENERGY RESOURCES OF THE CENTRAL AND WESTERN UNITED STATES

CONTENTS

FIGURES

TABLE

Pre-Late Eocene Structures and their Control of Gold Ore at the Drum Mine, West-Central Utah

By C.J. Nutt[1] *and* C.H. Thorman[1]

Abstract

The Drum Mine in west-central Utah exploited disseminated gold from two orebodies in Middle Cambrian carbonate rocks and shale and Eocene to Oligocene igneous rocks and related pebble dikes and sills. The mine is in the central part of the Drum Mountains and in the Detroit Mining District, which is in part underlain by late Eocene to Oligocene porphyry. Ore deposition at the mine was controlled by faults parallel with or at low angles to bedding and their associated ramp structures and by high-angle fractures and faults with little offset. The low-angle structures are primarily younger-over-older faults that thin units and are concentrated in or near shale units. Igneous and pebble sills, many of which are ore bearing, follow the bedding-parallel faults and ramps. East-west- to northeast-trending faults bound the mine area and are postulated to be tear faults associated with low-angle faulting. These high-angle faults controlled, and therefore predate, a paleovalley filled with flows of 42-Ma Drum Mountains Rhyodacite. A pre–late Eocene age of low-angle faulting is based on the post–low-angle-fault age of Eocene to Oligocene sills and pebble sills localized along low-angle faults and the pre–42-Ma age of the associated high-angle faults that controlled the paleovalley.

INTRODUCTION

The Drum Mine in the eastern Great Basin of west-central Utah (fig. 1) exploited two orebodies of disseminated gold hosted by sedimentary and igneous rocks. The orebodies were mined in two pits, herein referred to as the northeast and southwest pits (fig. 2). At the time of our study from 1987 to 1989, part of the main orebody in the southwest pit and pods of ore in the northeast pit were exposed; the rest of the ore had been removed. Our work shows that ore deposition was controlled by faults parallel with or at low angles to bedding and their associated ramp structures and by high-angle fractures and faults. The low-angle to bedding-parallel faults are mostly younger-over-older faults that thin units; rarely units are thickened. Although thinning of units in the Great Basin is commonly interpreted as the result of middle Tertiary or younger extension, we interpret the low-angle to bedding-parallel faults to be older than late Eocene and probably related to Jurassic or Late Cretaceous to early Tertiary (Sevier-age) deformation.

[1]U.S. Geological Survey, Box 25046, MS905, Denver, Colorado 80225.

GEOLOGIC SETTING

The Drum Mine is in the central part of the Drum Mountains, in an area underlain by Upper Proterozoic to Lower Cambrian quartzite and subordinate shale and siltstone, Middle Cambrian carbonate rocks and subordinate shale, and Tertiary igneous rocks and minor fanglomerate and conglomerate. A late Eocene to Oligocene quartz monzonite porphyry system underlies the central part of the Drum

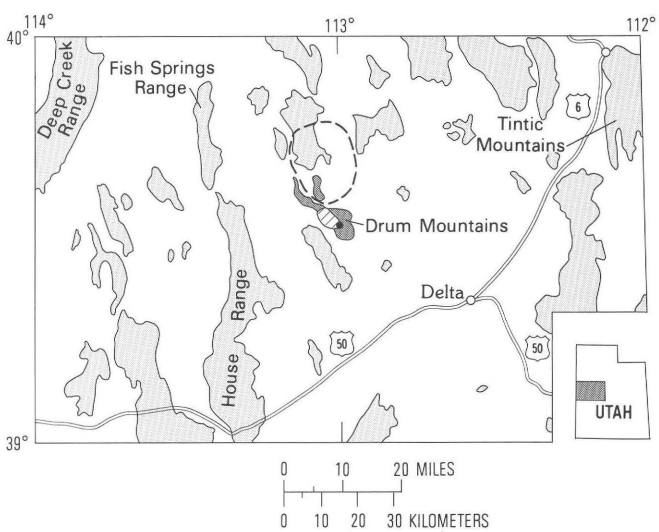

Figure 1. Location of Drum Mine (solid circle), Detroit Mining District (diagonal line pattern), and Drum Mountains (dark screen) in west-central Utah. Mountain ranges are shown by light shading; approximate outline of Thomas Caldera is shown by dashed line.

EXPLANATION

QUATERNARY
- Alluvium

TERTIARY
- Tuff
- Mt. Laird porphyry dike
- Drum Mountain Rhyodacite
- Fanglomerate

MIDDLE CAMBRIAN
- Wheeler Shale
- Swasey Limestone
- Whirlwind Formation
- Dome Limestone

- Chisholm Formation, undifferentiated south of Drum Peak Fault
- 3 Upper shale
- 2 Middle thin-bedded limestone
- 1 Lower shale
- Brown-weathering altered Howell Limestone and Tatow Member of Pioche Formation, undifferentiated
- Howell Limestone
- Marker shale shown by dotted line
- Tatow Member of Pioche Formation

LOWER CAMBRIAN
- Lower member of Pioche Formation and upper part of Prospect Mountain Quartzite, undifferentiated

- **Contact**—Dashed where approximately located
- **Fault**—Dashed where approximately located, dotted where concealed
- **Low angle to bedding-parallel fault that thins and locally thickens beds**—Hachures on upper plate, dashed where approximately located
- 20 **Strike and dip of beds**
- **Pebble dike**
- **Breccia**
- **Jasperoid**
- **Approximate outline of the Drum Mine property; includes pits, tailings, and buildings**

Figure 2. Geology of Drum Mine area. Modified from Nutt and others (1991).

Table 1. Age determinations of igneous rocks in the Detroit Mining District, west-central Utah
[nd indicates not determined]

Unit	Age (Ma)		Comment
	Fission track	$^{40}Ar/^{39}Ar$	
Felsite dike	[1]35.6	nd	Minimum age because zircon may have been reset during alteration.
Mt. Laird Tuff	[2]39	[3]36.5	Extrusive equivalent of porphyry in mining district. Ar-Ar age from what is called Mt. Laird Tuff in Keg Mountains, Utah.
Drum Mountains Rhyodacite	[2]42	nd	None.

[1]Robert A. Zimmermann (U.S. Geological Survey, written commun., 1989).
[2]Lindsey (1982).
[3]Shubat and Snee (this volume).

Mountains, also known as the Detroit Mining District, and is expressed at the surface by dikes and plugs of altered porphyry and numerous pebble dikes. Gold- and copper-bearing veins and manganese replacement deposits mined from the late 1800's to the mid-1900's are related to this porphyry system. Nutt and others (1991) proposed that the Drum gold deposit is also porphyry related.

The Drum Mountains are in the Cretaceous to early Tertiary Sevier Thrust Belt, typified by easterly directed thrusting and folding. In addition, the Drum Mountains are in the eastern Great Basin part of the Cenozoic Basin and Range Province, a region that has undergone considerable extension. Typically, ranges in this part of the Great Basin are tilted blocks of unmetamorphosed rocks that appear little deformed; however, Hintze (1978) documented stratigraphic thinning that he attributed to Sevier-age bedding-parallel faults in the House and Fish Springs Ranges west of the Drum Mountains (fig. 1).

The Drum Mountains are in the midst of Eocene to Oligocene calc-alkaline and Miocene bimodal volcanic fields that extend west from the Tintic Mountains to the eastern side of the Deep Creek Range (fig. 1). In the vicinity of the Drum Mountains, volcanism commenced with the eruption of flows of the Drum Mountains Rhyodacite (about 42 Ma), followed by voluminous eruption of tuffs and caldera formation from about 39 Ma to 35 Ma (Lindsey, 1982). The Detroit Mining District is just south of the ring fracture fault of the Eocene to Oligocene Thomas caldera (fig. 1). Lindsey (1982) proposed that the porphyry in the Drum Mountains is an intrusive phase of the caldera-related Mt. Laird Tuff. Table 1 shows age determinations of some igneous rocks in the Detroit Mining District.

DRUM MINE

The Drum Mine is in the lower part of the Cambrian miogeoclinal carbonate section, just above the transition from Late Proterozoic and Early Cambrian siliciclastic sedimentation to Cambrian carbonate sedimentation (fig. 2). A southwest-dipping section of Cambrian rocks cropping out in the mine includes, from oldest to youngest, the lower member of the Pioche Formation (quartzite, siltstone, and shale), the Tatow Member of the Pioche Formation (dolomitic limestone), and the Howell Limestone (thick-bedded limestone) in the northeast pit and the Chisholm Formation (shale and thin-bedded limestone) and Dome Limestone (thick-bedded limestone) in the southwest pit (figs. 3, 4). The best exposed orebody in the mine is in the Chisholm Formation, which consists of a lower shale, middle thin-bedded limestone, and an upper shale (fig. 4). Gold-bearing clay-altered rock and jasperoid are concentrated in the shale units, primarily near contacts with overlying and underlying limestone.

At least five types of igneous rocks, as well as numerous pebble dikes and sills, crop out near or in the mine (figs. 2, 3): the Drum Mountains Rhyodacite (about 42 Ma) forms the edge of the northeast pit and probably once covered the entire mine area; Mt. Laird porphyry sills and dike (39–36.5 Ma) cut the sedimentary rocks in the mine and surrounding area; felsite dikes and sills (35.6 Ma or older) crop out in the mine and to the north; a muscovite-bearing tuff (unknown age) is exposed in the northeast pit; and a vent-facies tuff (unknown age) is present east of the mine. Igneous-related breccias and pebble dikes and sills, mostly associated with Mt. Laird porphyry and felsite, are common in the mine area. Pebble dikes and sills range from almost completely granulated quartzite fragments to scattered quartzite clasts in clay matrix. Clay-altered Mt. Laird porphyry is present both as fragments and as matrix material. The abundance of igneous and pebble dikes and sills suggests that the mine area is underlain by porphyry.

The mine area is in a present-day topographically low area, partly filled with Drum Mountains Rhyodacite, that is interpreted to be an exhumed paleovalley in Paleozoic rocks. Fanglomerate containing Cambrian carbonate clasts crops out along the northern margin of the paleovalley, and conglomerate overlies Paleozoic rocks in part of the mine area. The paleotopography had a trellis geometry similar to the present drainage, as demonstrated by the presence of flow rocks in one of the present-day trellis tributaries to the main valley.

Figure 3 (above and facing page). Detailed geology of Drum Mine. Modified from Nutt and others (1991).

LOW-ANGLE AND BEDDING-PARALLEL FAULTS

Previously undetected faults that are parallel with or at a low angle to bedding are throughout the Drum Mountains. These faults, herein referred to as bedding-parallel or low-angle faults, are mostly younger-over-older structures and are primarily in shaly and thin-bedded units that are poorly exposed. Faults are most prominent in shales near the contact between the Upper Proterozoic to Lower Cambrian quartzite section and the overlying Cambrian carbonate section and in shale-rich units such as the Chisholm Formation.

In the Drum Mountains, domains of extremely attenuated rocks are bounded by high-angle faults. The mine area is an

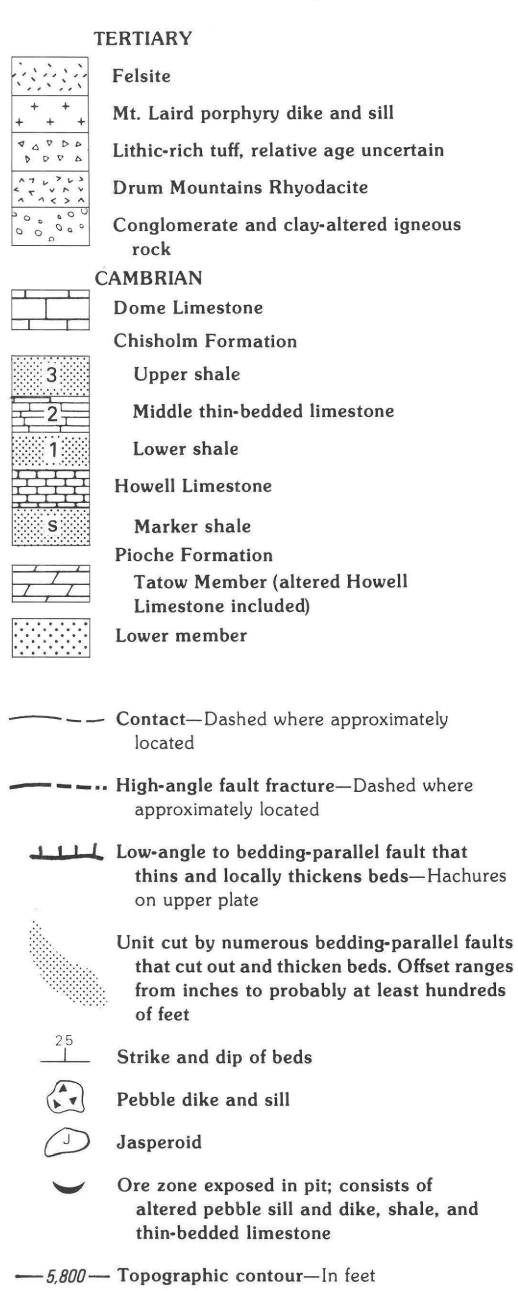

example of these highly attenuated domains. The Chisholm Formation thins dramatically in the vicinity of the Drum Mine (figs. 2, 3), and the upper shale, about 45 ft (14 m) thick, is cut out southeast of the mine. The fault block that includes the mine area is bounded by two east-west- to northeast-trending faults about three-quarters of a mile (1 km) apart (fig. 2). The southern fault, the Drum Peak Fault, is well exposed, whereas the northern fault, the PV Fault, is not exposed but is interpreted to underlie the northern margin of the paleovalley based on small-scale folding along its edge. We propose that the Drum Peak and PV Faults are tear faults bounding the deformed block that contains the mine and that this deformation prepared the area structurally for mineralization.

Low-angle to bedding-parallel faults are widespread in the Drum Mine (fig. 3). Most are in shale units and near contacts separating units of contrasting competency—the lower member of the Pioche Formation, at and near the contact separating the clastic rocks from the overlying carbonate section, and the Chisholm Formation. In many cases, it is difficult to identify one main fault; rather, numerous faults having offsets ranging from inches to at least hundreds of feet are in favorable intervals such as near the upper and lower contacts of shale units.

The best examples of low-angle to bedding-parallel faults and associated structures are in the Chisholm Formation in the southwest pit. Both the upper and lower shales are folded, broken, and cut by low-angle faults. Breccia is most extensive near shale-limestone contacts and in the limestone hanging wall. At the bottom of the southwest pit, where the shale is cut out, the fault is marked by folded thin-bedded limestones. Ramps are associated with the faults and uniformly step up to the northeast. Pebble sills, most of which are ore bearing, are concentrated along low-angle faults at shale-limestone contacts and particularly above ramps. In general, the best ore was mined from ramp areas (Jumbo Mining Company, oral commun., 1989). Figure 5, a photograph of the bottom of the southwest pit, shows some of these features.

High-angle structures that show little to no displacement were important conduits for gold-bearing fluids. Many of these structures are filled with pebble dikes. The most prominent of these is the King Tut Fault, marked at the surface by a pebble dike and at depth by ore at its intersection with shale units. Flexure zones above ramps typically have arrays of radiating fractures, but the fractures generally do not extend more than a hundred feet or so. We observed no high-angle faults that sole into the low-angle faults nor any rotation of blocks above the highly attenuated shale units.

DISCUSSION

Gold ore at the Drum Mine was localized both by the low-angle to bedding-parallel faults and by high-angle faults and fractures. Ore remaining in the southwest pit is concentrated along low-angle and bedding-parallel faults and associated ramps that are best developed in and near shales in the Chisholm Formation.

The timing of the low-angle and bedding-parallel faulting is mainly constrained by crosscutting igneous rocks. Pebble sills, primarily associated with the 39–36.5-Ma Mt. Laird porphyry and 35.6-Ma or older felsic dikes, were localized along low-angle faults and ramps and therefore postdate faulting. The sills are undeformed except for minor postemplacement shears. Also, pebble dikes are along

MIDDLE CAMBRIAN	Chisholm Formation		365 ft (111 m)	Cliff-forming thin-bedded to massive gray limestone. Oncolitic and oolitic locally.
	Dome Limestone		200 ft (61 m)	Upper olive-green to brown shale, red-weathering oncolitic limestone; middle ledge-forming thin-bedded gray limestone; basal olive-green to tan shale, *Glossopleura*-bearing limestone.
	Howell Limestone		330 ft (101 m)	Cliff-forming thin-bedded to massive gray limestone, oncolitic locally, oolitic limestone at top. Green shale locally in part.
	Pioche Formation	Tatow Member	55 ft (17 m)	Brown-weathering dolomitic limestone.
LOWER CAMBRIAN		Lower member	360 ft (110 m)	Black-weathering fine-grained quartzite and micaceous quartzite, green to brown micaceous shale and siltstone.

Figure 4. Generalized stratigraphy of Cambrian rocks at the Drum Mine.

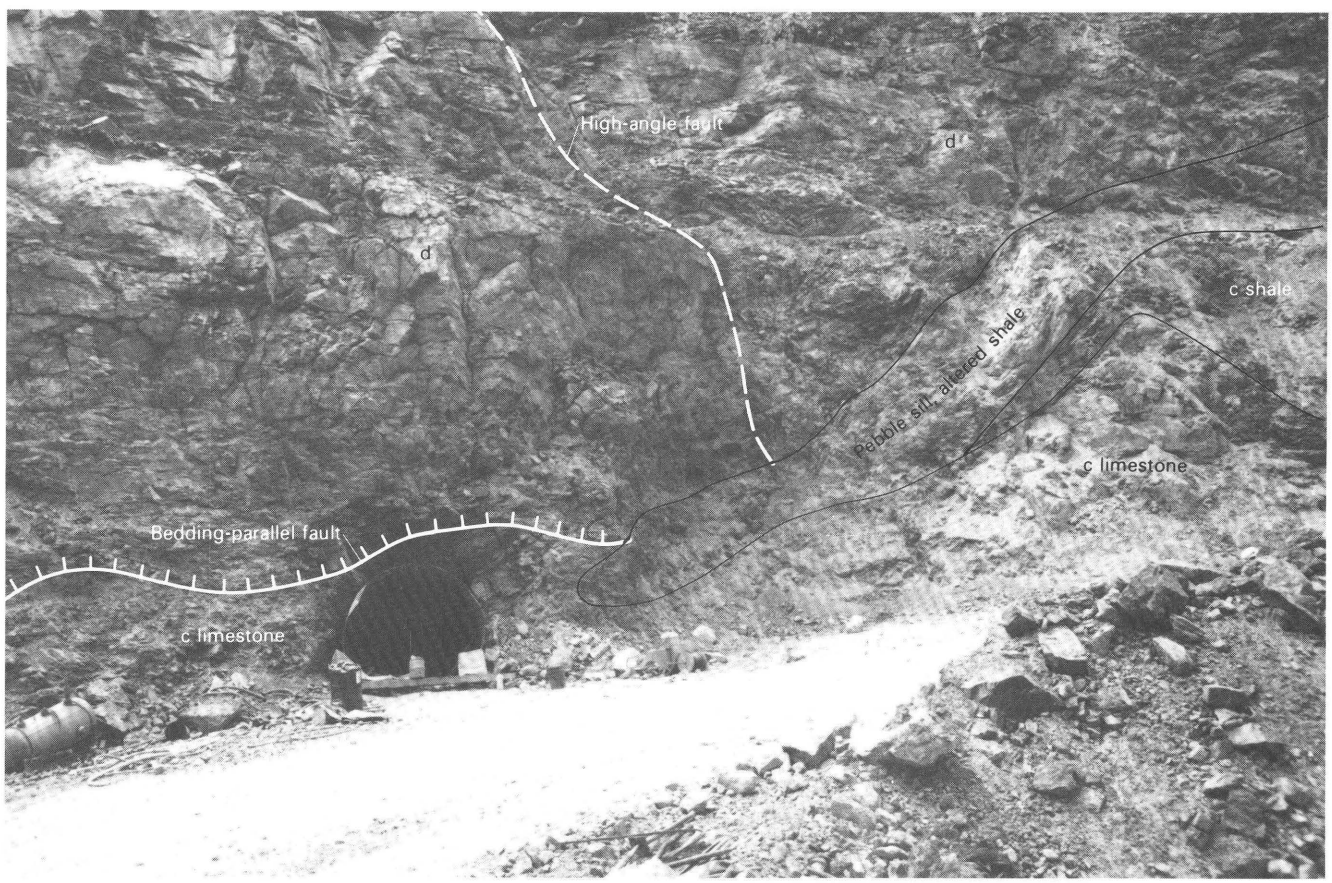

Figure 5. Photograph showing southwest pit, Drum Mine. Bedding-parallel fault cuts out upper shale of Chisholm Formation (c) and places Dome Limestone (d) on middle limestone of the Chisholm Formation (c). Limestone beds are folded where shale is attenuated. On right side of photograph, gold-bearing pebble sill is localized above ramp. Bench is about 25 ft (7.6 m) above road.

high-angle faults and fractures, many of which are associated with low-angle faults, although some probably formed or reopened during porphyry intrusion.

A second and more tenuous constraint on the formation of low-angle faults is based on the age of the paleovalley that includes the mine area. The paleovalley must be older than the Drum Mountains Rhyodacite that filled it at about 42 Ma. If, as we postulate, the paleovalley is controlled by tear faults related to the low-angle faults, then low-angle faults predate erosion of the paleovalley as well as later 42-Ma flows. Erosion followed a period of uplift, probably forming the paleovalley in the Late Cretaceous to early Tertiary. It should be noted that Anderson (1983) believed that throughout this part of Utah the basal volcanic rocks are detached and that what has been interpreted as the base of the paleovalleys is a detachment surface. This interpretation would negate our argument on age constraint and imply that all low-angle faults are middle Tertiary or younger in age. The presence of fanglomerate, which does not contain volcanic clasts and underlies the volcanic rocks, is consistent, however, with the paleovalley interpretation. Also, volcanic flow rocks that are depositional on Cambrian limestones in a paleotributary of the trellis paleodrainage strongly support our interpretation of a normal, undisturbed basal Tertiary unconformity. We believe that little, if any, movement has occurred at the base of the Tertiary volcanic sequence in this area.

These age constraints date the low-angle faults and associated ramps as being older than late Eocene. Although not necessarily of common origin, younger-over-older faults of probable Mesozoic age have been documented to the north by Allmendinger and Jordan (1984) in the Newfoundland Mountains, Utah, and by Miller and others (1987) in the Pilot Range, Utah and Nevada. Recognition of younger-over-older faults similar to those in the Drum Mountains is, as of now, restricted to the hinterland of the Sevier Thrust Belt, a distribution that suggests they are related to Sevier deformation. However, Jurassic deformation, variably included in the Sevier orogeny or considered a separate event, is increasingly being recognized in the Great Basin (Allmendinger and Jordan, 1984; Miller, 1987; Thorman and others, 1990) and may have occurred in this part of Utah. Regardless of exact timing, these low-angle faults predate middle Tertiary extension and imply significant pre–late Eocene deformation in the area.

REFERENCES CITED

Allmendinger, R.W., and Jordan, T.E., 1984, Mesozoic structure of the Newfoundland Mountains, Utah—Horizontal shortening and subsequent extension in the hinterland of the Sevier belt: Geological Society of America Bulletin, v. 95, p. 1280–1292.

Anderson, R.E., 1983, Cenozoic structural history of selected areas in the eastern Great Basin, Nevada-Utah: U.S. Geological Survey Open-File Report 83–504, 47 p.

Hintze, L.F., 1978, Sevier orogenic attenuation faulting in the Fish Springs and House ranges, western Utah: Brigham Young University Geology Studies, v. 25, pt. 1, p. 11–24.

Lindsey, D.A., 1982, Tertiary volcanic rocks and uranium in the Thomas Range and northern Drum Mountains, Juab County: U.S. Geological Survey Professional Paper 1221, 71 p.

Miller, D.M., Hillhouse, W.C., Zartman, R.E., and Lanphere, M.A., 1987, Geochronology of intrusive and metamorphic rocks in the Pilot Range, Utah and Nevada, and comparison with regional patterns: Geological Society of America Bulletin, v. 99, p. 866–879.

Nutt, C.J., Thorman, C.H., Zimbelman, D.R., and Gloyn, R.W., 1991, Geologic setting and trace-element geochemistry of the Detroit mining district and Drum gold mine, Drum Mountains, west-central Utah, *in* Raines, G.L., Lisle, R.E., Schafer, R.W., and Wilkinson, W.H., eds., Geology and ore deposits of the Great Basin, Symposium Proceedings, 1990, Reno, Nevada: Geological Society of Nevada and U.S. Geological Survey, v. 1, p. 491–509.

Thorman, C.H., Ketner, K.B., and Peterson, Fred, 1990, The Elko orogeny—Late Jurassic orogenesis in the Cordilleran miogeocline: Geological Society of America Abstracts with Program, v. 22, no. 3, p. 88.

Chapter G

High-Precision $^{40}Ar/^{39}Ar$ Geochronology, Volcanic Stratigraphy, and Mineral Deposits of Keg Mountain, West-Central Utah

By MICHAEL A. SHUBAT and LAWRENCE W. SNEE

U.S. GEOLOGICAL SURVEY BULLETIN 2012

APPLICATION OF STRUCTURAL GEOLOGY TO MINERAL AND ENERGY RESOURCES OF THE CENTRAL AND WESTERN UNITED STATES

CONTENTS

FIGURES

TABLES

High-Precision $^{40}Ar/^{39}Ar$ Geochronology, Volcanic Stratigraphy, and Mineral Deposits of Keg Mountain, West-Central Utah

By Michael A. Shubat[1] *and* Lawrence W. Snee[2]

Abstract

High-precision $^{40}Ar/^{39}Ar$ age-spectrum dates combined with results of geologic mapping define the Eocene and Oligocene history of Keg Mountain, which straddles the center of the Deep Creek–Tintic mineral belt in west-central Utah. The chronology of volcanic events consists of (1) eruption of the tuff of Dead Ox and subsidence to form the Flint Spring cauldron (undated but presumed to be late Eocene), (2) eruption of the dacitic tuff of Keg Mountain (36.77±0.12 Ma) and subsidence of the Keg cauldron, followed by resurgent doming, (3) eruption of the Mt. Laird Tuff (36.54±0.06 Ma), collapse of the Thomas caldera, and intrusion of hypabyssal dacite (36.49±0.15 Ma), and (4) eruption of the Joy Tuff (34.88±0.06 Ma), collapse of the Dugway Valley cauldron and possibly coeval Picture Rock caldera, and intrusion of rhyolite porphyry (35.14±0.15 Ma), (5) eruption of the Dell Tuff (approximately 32 Ma) from an unknown source, and (6) eruption of late Miocene alkali rhyolite.

These calderas and cauldrons, the margins of which are poorly defined and mostly inferred, outline the eastern part of a large, late Eocene to early Oligocene igneous complex that encompasses the Thomas Range, Keg Mountain, and northern Drum Mountains area. Associated with eruptive members of the igneous complex are hypabyssal intrusive rocks and mineral deposits. In detail, however, spatial relationships between inferred caldera margins, associated hypabyssal intrusions, and mineral deposits are not well understood. Mineral deposits in the area consist of volcanic-hosted gold prospects, polymetallic veins, and precious-metal-enriched jasperoid bodies that are along high-angle, small-displacement normal faults apparently unrelated to inferred caldera margins.

[1]Utah Geological Survey, 2363 South Foothill Drive, Salt Lake City, Utah 84109–1491.

[2]U.S. Geological Survey, Box 25046, MS 963, Denver, Colorado 80225.

INTRODUCTION

Keg Mountain in west-central Utah (fig. 1) is underlain by a diverse assemblage of volcanic and subvolcanic rocks that span the interval from the late Eocene to late Miocene. The Eocene and Oligocene history of this area is of particular interest because it provides a view of the onset and development of one of western Utah's enigmatic east-trending mineral (and magmatic) belts, the Deep Creek–Tintic mineral belt (Shawe and Stewart, 1976). New dates and results of geologic mapping presented in this study show that hypabyssal intrusions related to caldera-forming events extend many kilometers (>10) from known or inferred caldera margins. Comparison of results from this study with preliminary results from the adjacent Simpson Mountains (Yambrick and Snee, 1989) suggests that high-precision $^{40}Ar/^{39}Ar$ age-spectrum dates can be used to correlate non-ash-flow volcanic and subvolcanic rocks related to caldera-forming events between adjacent ranges.

Previous regional geologic studies by Erickson (1963), Shawe (1972), Lindsey and others (1975), Lindsey (1982), and Morris (1987) note the complex volcanic geology of Keg Mountain and stress the need for detailed mapping. Some unresolved problems stemming from these investigations are location of the eastern sides of the Thomas caldera and Dugway Valley cauldron (Lindsey, 1982), verification of Shawe's (1972) proposed Keg caldera, and location of suspected caldera margins related to the Joy and Dell Tuffs (Lindsey, 1982). The locations of these caldera and cauldron margins are of increasing economic interest because of the possible genetic link between hypabyssal intrusions related to caldera-forming events and epithermal gold mineralization in the Keg and Drum Mountains. This report presents the results of a joint Utah Geological and Mineral Survey–U.S. Geological Survey investigation of the geology and mineral potential of Keg Mountain as part of the Delta 1°×2° quadrangle study of the Conterminous United States Mineral Assessment Program (CUSMAP).

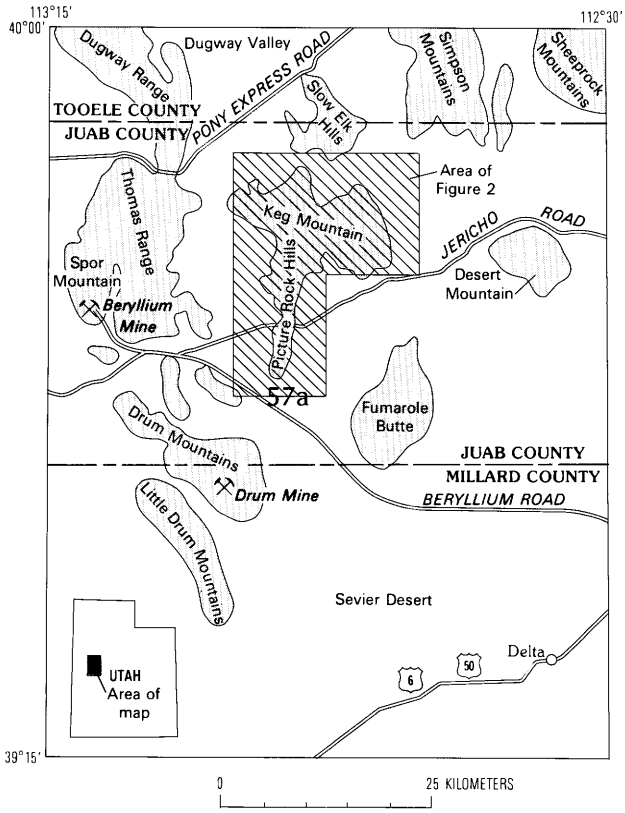

Figure 1. Location of Keg Mountain, west-central Utah.

GEOLOGIC SETTING

Within the Keg Mountain area is limited exposure of the Cambrian, upper part of the Prospect Mountain Quartzite and Middle Cambrian carbonate rocks, typical of these units exposed elsewhere in the region. These units record an Early Cambrian marine transgression and Middle Cambrian deposition of miogeoclinal carbonate strata. During the Cretaceous Sevier orogeny the Prospect Mountain Quartzite was thrust over the carbonate rocks; this thrust fault is exposed in Keg Mountain. Geologically, however, Keg Mountain is primarily composed of Cenozoic volcanic rocks and subvolcanic intrusive rocks. These Cenozoic rocks lie near the axis of the broad, east-trending Deep Creek–Tintic mineral belt (Shawe and Stewart, 1976; Stewart and others, 1977). Numerous high-angle normal faults that formed during regional extension in the late Eocene to late Miocene control the location of many of the mineral deposits at Keg Mountain and in surrounding districts.

Lindsey (1982), Lindsey and others (1975), and Shawe (1972) separated volcanism and related mineralization in the Thomas Range, Drum, Keg, and Desert Mountains into three stages. Using fission-track dates, Lindsey (1982) quantified the following stages. The oldest stage of activity (late Eocene, 42–39 Ma) consisted of eruptions of calc-alkaline, intermediate composition (rhyodacite–quartz latite) volcanic rocks and related intrusive rocks. In the Thomas Range and Drum Mountains, this oldest stage culminated with the eruption of the Mt. Laird Tuff and the formation of the Thomas caldera (Lindsey, 1982). Mineral deposits related to this stage include those of copper, manganese, and gold in the Drum Mountains and may include polymetallic vein and replacement and gold at Keg Mountain. Eruptions of rhyolitic ash-flow tuffs, continued caldera subsidence, and intrusion of felsic stocks and plugs characterize the middle stage of activity (early to middle Oligocene, 38–32 Ma). In the Thomas Range, Lindsey (1982) related subsidence of the Dugway Valley cauldron with eruption of the Joy Tuff. The middle stage apparently lacks associated mineral deposits. The youngest stage of activity (Miocene, 21 to 7–6 Ma) consists of bimodal alkali rhyolite–basalt volcanism. Lithophile mineral deposits that formed during this stage include the world-class beryllium deposit at Spor Mountain (fig. 1) (Lindsey, 1977) and uranium (Lindsey, 1982) and fluorspar deposits in the Thomas Range.

GEOCHRONOLOGY

$^{40}Ar/^{39}Ar$ Dating Methods

Samples from the Keg Mountains were dated using the $^{40}Ar/^{39}Ar$ age-spectrum technique, a variant of the conventional K/Ar method. To obtain a date using this technique, the sample of unknown age and a standard of known age are irradiated together in a nuclear reactor to produce ^{39}Ar from ^{39}K by fast-neutron bombardment. After irradiation, the $^{40}Ar_{Radiogenic}/^{39}Ar_{Potassium}$ ratios of sample and standard are determined. An $^{40}Ar/^{39}Ar$ isotopic date of a sample is calculated according to the relationship

$$t_u = 1/\lambda \ln(JF+1),$$

where t_u is the calculated date of the sample, λ is the decay constant for radioactive decay of ^{40}K to ^{40}Ar and ^{40}Ca, J is related to neutron flux during irradiation, and F is the ratio of $^{40}Ar_R$ (radiogenic ^{40}Ar) to $^{39}Ar_K$ (potassium-derived ^{39}Ar) of the sample. The decay constants used in this study are those recommended by Steiger and Jäger (1977): $\lambda_\varepsilon = 0.581\times10^{-10}$/yr, $\lambda_\beta = 4.962\times10^{-10}$/yr, and $\lambda = \lambda_\varepsilon + \lambda_\beta = 5.543\times10^{-10}$/yr. The flux parameter, J, is calculated according to the relationship $J = (e^{\lambda t_m} - 1)/(^{40}Ar_R/^{39}Ar_K)_m$ where t_m is the age of the primary flux "monitor" (that is, standard) and $(^{40}Ar_R/^{39}Ar_K)_m$ is the measured and corrected ratio of the standard. The standard for this experiment was hornblende MMhb–1 with %K=1.555, $^{40}Ar_R = 1.624\times10^{-9}$ mol/g, and K–Ar date=520.4 Ma (Alexander and others, 1978; Samson and Alexander, 1987). In order to determine the actual $^{40}Ar_R/^{39}Ar_K$ ratio of a sample or standard, however, it is necessary to correct for the presence of atmospheric ^{40}Ar and irradiation-produced interfering isotopes such as ^{40}Ar (from ^{40}K), ^{39}Ar (from ^{42}Ca), and ^{36}Ar (from ^{40}Ca and ^{35}Cl).

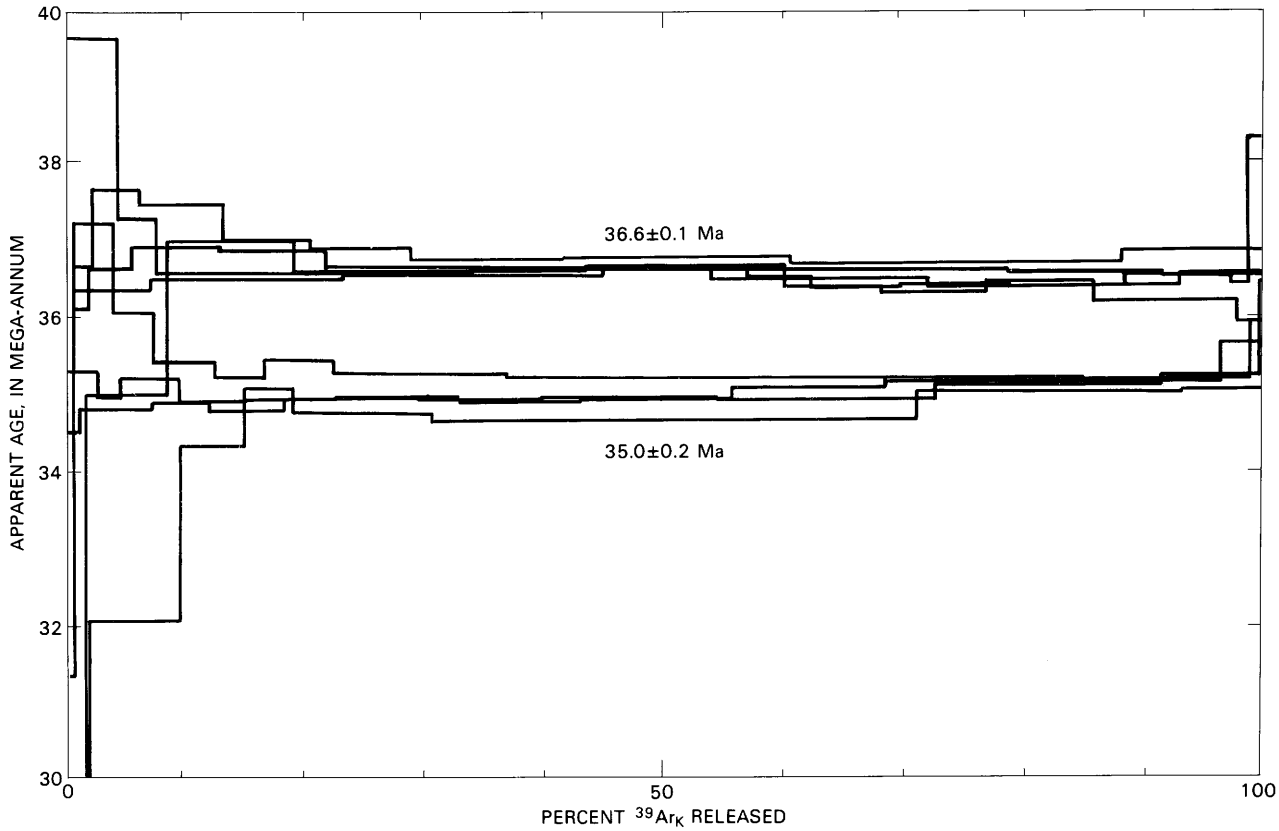

Figure 2. Composite age-spectrum diagram for nine mineral separates from six rocks, Keg Mountain, Utah, showing two statistically distinct groups of $^{40}Ar/^{39}Ar$ plateau dates, the younger at 35.0±0.2 and the older at 36.6±0.1 Ma. The plateau dates of all samples within each group are statistically identical within 2σ analytical precision. Samples of the younger group include sanidine and biotite from the basal vitrophyre of the Joy Tuff (KMR–1–3) and sanidine and biotite from a hypabyssal rhyolite intrusion (KMR–4–6). Samples of the older group include hornblende and biotite from the base of the Mt. Laird Tuff (KMR–4–8), biotite from the Mt. Laird Tuff (NKM–21–12), biotite from the basal vitrophyre of the tuff of Keg Mountain (KP–6–5), and biotite from a hypabyssal dacite porphyry intrusion (NKM–6–3).

These corrections are well defined, but, because the mathematical formulation for F is complex, it is not presented here. (Our formulation of F is modified from Dalrymple and others, 1981, to include corrections for all interferences.)

We selected six samples from Keg Mountain that yielded nine mineral separates used for detailed high-precision $^{40}Ar/^{39}Ar$ dating. The samples include hornblende and biotite from the basal Mt. Laird Tuff, biotite from the middle part of the Mt. Laird Tuff, biotite from the basal vitrophyre of the tuff of Keg Mountain, biotite from a hypabyssal dacite porphyry, sanidine and biotite from a hypabyssal rhyolite porphyry, and sanidine and biotite from the basal vitrophyre of the Joy Tuff. Minerals were separated using standard techniques and are greater than 99.9 percent pure. Detailed $^{40}Ar/^{39}Ar$ data are listed in table 1, and a summary of the dates is given in table 2. A composite age-spectrum diagram for samples analyzed in this study is shown in figure 2, and sample localities are shown on figure 3 and included in table 1.

The isotopic composition of argon was measured at the U.S. Geological Survey, Denver, Colorado, using a MAP215 Series rare-gas mass spectrometer made by Mass Analyzer Products Limited. Abundances of five isotopes of argon (^{40}Ar, ^{39}Ar, ^{38}Ar, ^{37}Ar, and ^{36}Ar) were measured for every sample. Argon was released from the samples in 12–14 temperature steps; abbreviated results are listed in table 1. Radiogenic ^{40}Ar is total ^{40}Ar derived from natural radioactive decay of ^{40}K after all corrections for non-decay-derived ^{40}Ar, including atmospheric ^{40}Ar and ^{40}K-derived ^{40}Ar, have been made. K-derived ^{39}Ar is total ^{39}Ar derived from the epithermal neutron-induced reaction $^{39}K(n,p)^{39}Ar$ after corrections for non-^{39}K-derived ^{39}Ar, including ^{42}Ca-derived ^{39}Ar, are made. F is the quantity resulting from the division of radiogenic ^{40}Ar by the amount of K-derived ^{39}Ar. Quantities for radiogenic ^{40}Ar and K-derived ^{39}Ar are given in volts of signal measured on a Faraday detector by a digital voltmeter. These quantities can be converted to moles, using the mass spectrometer sensitivity at time of

Table 1. $^{40}Ar/^{39}Ar$ age-spectrum data for Keg Mountain, Utah

[Sample localities shown in figure 3. $^{40}Ar_R$ is radiogenic ^{40}Ar; $^{39}Ar_K$ is potassium-derived ^{39}Ar]

Temperature (°C)	$^{40}Ar_R$	$^{39}Ar_K$	F	$^{39}Ar/^{37}Ar$	$^{40}Ar_R$ (percent)	$^{39}Ar_K$ (percent)	Apparent age and error (Ma at 1σ)
Sample KMR–1–3/23/DD13; Joy Tuff, basal vitrophyre; sanidine; 102.1 mg; measured $^{40}Ar/^{36}Ar_a$=299.5; *J*-value=0.007431±0.25% (1σ); lat 39°50'48.73" N., long 112°52'22.18" W.							
500	0.06512	0.02860	2.277	15.87	17.5	0.2	30.26±2.80
600	0.21056	0.08308	2.534	30.96	78.7	0.5	33.66±0.82
700	0.54243	0.20856	2.601	40.54	60.6	1.2	34.53±0.51
750	1.03892	0.39621	2.622	45.76	93.3	2.2	34.81±0.15
800	1.63759	0.62452	2.622	51.82	95.5	3.5	34.81±0.14
850	2.36865	0.89993	2.632	61.46	93.9	5.0	34.94±0.18
900	2.95837	1.12915	2.620	73.84	97.3	6.2	34.78±0.10
950	5.24909	1.99358	2.633	93.42	98.2	11.0	34.96±0.10
1,000	4.80260	1.82517	2.631	115.43	98.1	10.1	34.93±0.10
1,050	6.93128	2.63075	2.635	131.75	98.2	14.5	34.98±0.10
1,100	8.64343	3.28430	2.632	149.34	98.3	18.2	34.94±0.10
1,150	8.99432	3.40018	2.645	156.17	98.1	18.8	35.12±0.10
1,250	3.89366	1.46577	2.656	129.61	93.2	8.1	35.26±0.10
1,400	0.33891	0.12319	2.751	69.78	47.3	0.7	36.51±0.38
Total-gas date			2.635				34.98±0.11
Plateau date (700–1,100°C)						71.8	34.92±0.16
Sample KMR–1–3/25/DD13; Joy Tuff, basal vitrophyre; biotite; 50.2 mg; measured $^{40}Ar/^{36}Ar_a$=299.5; *J*-value=0.007426±0.25% (1σ); lat 39°50'48.73"N., long 112°52'22.18"W.							
500	0.03568	0.03102	1.150	19.73	11.9	0.4	15.34±2.61
600	0.20935	0.14345	1.459	41.29	31.7	2.0	19.44±0.48
700	1.26122	0.52197	2.416	94.19	60.7	7.4	32.08±0.19
750	0.99149	0.38304	2.588	105.05	81.9	5.4	34.35±0.14
800	0.77367	0.29221	2.648	106.61	85.1	4.1	35.13±0.20
850	0.75824	0.28920	2.622	94.91	83.8	4.1	34.79±0.27
900	1.35843	0.51814	2.622	118.87	84.0	7.3	34.78±0.16
950	3.15754	1.20841	2.613	112.43	85.0	17.1	34.67±0.10
1,000	4.25305	1.62684	2.614	84.75	88.3	23.0	34.69±0.10
1,050	4.08619	1.54554	2.644	62.32	91.2	21.9	35.08±0.10
1,150	1.27066	0.48007	2.647	11.74	91.0	6.8	35.11±0.13
1,300	0.06602	0.02544	2.595	7.38	27.4	0.4	34.43±5.89
Total-gas date			2.579				34.22±0.17
Preferred date (850–1,150°C)						80.2	34.84±0.14

measurement of 9.736×10^{-13} moles argon per volt of signal. The detection limit for argon at the time of this experiment was 2×10^{-17} moles. The measured $^{40}Ar/^{36}Ar$ ratio used for mass discrimination correction is 299.5.

All samples were irradiated in a single irradiation package for 30 hours at 1 megawatt in the U.S. Geological Survey TRIGA reactor in Denver. The *J*-value for each sample was determined from adjacent standards; errors of 0.25 percent (68 percent confidence level) in the calculated *J*-value were determined experimentally by calculating the reproducibility of multiple monitors. Corrections for irradiation-produced, interfering isotopes of argon were made by measuring production ratios for the interfering isotopes of argon produced in pure K_2SO_4 and CaF_2 irradiated simultaneously with the samples of this study. Those ratios, as determined from four measurements of each salt, with errors at 68-percent confidence level, are

$(^{36}Ar/^{37}Ar)_{Ca}=2.69\pm0.01\times10^{-4}$,
$(^{39}Ar/^{37}Ar)_{Ca}=7.08\pm0.03\times10^{-4}$,
$(^{38}Ar/^{37}Ar)_{Ca}=2.90\pm0.18\times10^{-5}$,
$(^{40}Ar/^{39}Ar)_{K}=8.76\pm0.37\times10^{-3}$,
$(^{37}Ar/^{39}Ar)_{K}=1.39\pm0.57\times10^{-4}$, and
$(^{38}Ar/^{39}Ar)_{K}=1.30\pm0.01\times10^{-2}$.

Corrections were made for additional interfering isotopes of argon produced from irradiation of chlorine using the method described by Roddick (1983). Measured quantities of ^{37}Ar and ^{39}Ar were corrected for radioactive decay, and in table 1 the $^{39}Ar/^{37}Ar$ ratios were corrected for this decay as well as for interfering argon isotopes. By multiplying the $^{39}Ar/^{37}Ar$ ratios by approximately 0.5, the relative approximate K/Ca distribution of the samples may be obtained. Error estimates for apparent ages of individual temperature steps were assigned by using the equations of Dalrymple and others (1981); however, the equations were modified to

Table 1. $^{40}Ar/^{39}Ar$ age-spectrum data for Keg Mountain, Utah—Continued

[Sample localities shown in figure 3. $^{40}Ar_R$ is radiogenic ^{40}Ar; $^{39}Ar_K$ is potassium-derived ^{39}Ar]

Temperature (°C)	$^{40}Ar_R$	$^{39}Ar_K$	F	$^{39}Ar/^{37}Ar$	$^{40}Ar_R$ (percent)	$^{39}Ar_K$ (percent)	Apparent age and error (Ma at 1σ)
Sample KMR–4–6/22/DD13; Hypabyssal rhyolite porphyry; sanidine; 112.3 mg; measured $^{40}Ar/^{36}Ar_a$=299.5; *J*-value=0.007380±0.25% (1σ); lat 39°48'3.40" N., long 112°52'26.95" W.							
600	0.38830	0.14676	2.646	5.29	72.3	0.8	34.89±0.35
700	1.18169	0.44145	2.677	6.87	72.1	2.3	35.29±0.15
750	1.01737	0.38392	2.650	63.83	95.8	2.0	34.94±0.18
800	2.54557	0.95339	2.670	81.86	93.7	4.9	35.20±0.14
850	2.75714	1.04152	2.647	105.60	97.3	5.3	34.90±0.10
900	3.93424	1.48459	2.650	123.56	98.2	7.6	34.94±0.10
950	5.32784	2.00846	2.653	137.12	98.3	10.3	34.98±0.10
1,000	5.17896	1.95629	2.647	153.88	98.3	10.0	34.91±0.10
1,050	6.54139	2.46716	2.651	156.27	98.1	12.6	34.96±0.10
1,100	6.63168	2.49090	2.662	148.85	96.9	12.7	35.10±0.10
1,150	14.51355	5.44169	2.667	151.64	91.8	27.8	35.16±0.10
1,250	1.88149	0.69523	2.706	120.40	82.9	3.6	35.67±0.14
1,400	0.13923	0.05151	2.703	50.40	31.9	0.3	35.63±1.21
Total-gas date			2.660				35.07±0.11
Plateau date (850–1,150°C)						86.3	35.04±0.15
Sample KMR–4–6/27/DD13; Hypabyssal rhyolite porphyry; biotite; 62.1 mg; measured $^{40}Ar/^{36}Ar_a$=299.5; *J*-value=0.007409±0.25% (1σ); lat 39°48'3.40" N., long 112°52'26.95" W.							
500	0.02788	0.02762	1.009	13.80	6.3	0.3	13.44±3.28
600	0.21071	0.08909	2.365	15.45	34.1	1.0	31.34±0.60
700	0.83796	0.29766	2.815	102.93	63.4	3.4	37.24±0.18
750	0.78662	0.28854	2.726	232.15	87.9	3.2	36.08±0.58
800	1.21031	0.45221	2.676	202.17	89.7	5.1	35.42±0.17
850	0.94621	0.35555	2.661	157.91	88.3	4.0	35.22±0.17
900	1.35650	0.50591	2.681	132.03	88.8	5.7	35.49±0.13
950	3.42385	1.28393	2.667	162.36	87.6	14.5	35.30±0.13
1,000	5.56171	2.09056	2.660	153.11	89.8	23.5	35.21±0.10
1,050	5.71675	2.15001	2.659	77.66	90.9	24.2	35.19±0.10
1,150	3.28766	1.23540	2.661	28.15	90.6	13.9	35.22±0.14
1,300	0.27950	0.10264	2.723	21.83	51.4	1.2	36.04±0.66
Total-gas date			2.663				35.25±0.16
Plateau date (800–1,150°C)						90.9	35.25±0.13

allow the option of choosing the larger of separately derived errors in the *F*-value—either a calculated error from differential equations or an experimental error determined from the reproducibility of identical samples. Age plateaus were determined by comparing contiguous gas fractions using the critical value test of Dalrymple and Lanphere (1969), and the error was determined using equations of Dalrymple and others (1981).

$^{40}Ar/^{39}Ar$ Data

Age spectra for the nine dated minerals are relatively uncomplicated and are summarized in table 2. The minor amounts of excess argon or argon loss displayed by most spectra had no effect on apparent age interpretations. Eight of nine spectra have apparent age plateaus defined by 70–99 percent of the released ^{39}Ar from the sample. The age spectrum for biotite sample KMR–1–3 is slightly disturbed and displays minor excess argon but yields a preferred date, defined by weight-averaging the 850°C–1,150°C temperature steps, that is statistically indistinguishable from the plateau date for the coexisting sanidine. Two other samples from which two minerals were dated are KMR–4–6 and KMR–4–8. In both cases the coexisting minerals yielded statistically indistinguishable dates. Without discriminating data, there is no reason to select the apparent age of either mineral over the other in a pair; therefore, the best estimates of crystallization age for samples KMR–1–3, KMR–4–6, and KMR–4–8 are the averages of the dates for each pair; that is, 34.88±0.06, 35.14±0.15, and 36.58±0.06 Ma, respectively.

Dates for the nine minerals fall into two statistically distinct groups (fig. 2), 36.6±0.1 and 35.0±0.2 Ma, that define two distinct periods of magmatism. The tuff of Keg Mountain, Mt. Laird Tuff, and a hypabyssal dacite porphyry were

Table 1. $^{40}Ar/^{39}Ar$ age-spectrum data for Keg Mountain, Utah—Continued

[Sample localities shown in figure 3. $^{40}Ar_R$ is radiogenic ^{40}Ar; $^{39}Ar_K$ is potassium-derived ^{39}Ar]

Temperature (°C)	$^{40}Ar_R$	$^{39}Ar_K$	F	$^{39}Ar/^{37}Ar$	$^{40}Ar_R$ (percent)	$^{39}Ar_K$ (percent)	Apparent age and error (Ma at 1σ)
Sample NKM–6–3/29/DD13; Hypabyssal dacite porphyry; biotite; 67.4 mg; measured $^{40}Ar/^{36}Ar_a$=299.5; *J*-value=0.007395±0.25% (1σ); lat 39°49'24.53" N., long 112°53'34.35" W.							
500	0.06138	0.06406	0.958	15.16	9.4	0.8	12.74±0.87
600	0.17083	0.10871	1.571	4.59	35.9	1.3	20.84±0.81
700	1.50395	0.56855	2.645	78.93	54.6	6.9	34.95±0.11
750	2.42808	0.86649	2.802	185.50	88.3	10.5	37.00±0.12
800	5.52870	1.99433	2.772	320.71	96.1	24.2	36.61±0.10
850	3.74547	1.34822	2.778	277.33	96.0	16.3	36.69±0.10
900	1.82843	0.66352	2.756	100.62	87.6	8.0	36.39±0.13
950	1.98268	0.72116	2.749	6.45	86.8	8.7	36.31±0.14
1,000	2.05554	0.74390	2.763	9.71	89.0	9.0	36.49±0.11
1,050	2.68882	0.97950	2.745	66.45	89.6	11.9	36.25±0.17
1,150	0.49706	0.18255	2.723	14.64	82.7	2.2	35.96±0.31
1,300	0.00887	0.00594	1.492	3.24	3.2	0.1	19.79±8.48
Total-gas date			2.728				36.03±0.15
Plateau date (800–1,150°C)						80.4	36.49±0.15
Sample KP–6–5/28/DD13; Tuff of Keg Mountain, basal vitrophyre; biotite; 55.0 mg; measured $^{40}Ar/^{36}Ar_a$=299.5; *J*-value=0.007420±0.25% (1σ); lat 39°47'46.00" N., long 112°53'29.96" W.							
500	0.06530	0.03487	1.873	12.80	11.8	0.5	24.89±1.97
600	0.11228	0.04253	2.640	19.66	45.8	0.6	35.00±1.70
700	0.30849	0.11201	2.754	43.96	41.9	1.5	36.49±0.61
750	0.86382	0.30429	2.839	85.27	75.8	4.0	37.60±0.13
800	1.47215	0.52130	2.824	136.63	90.3	6.9	37.41±0.13
850	1.49688	0.53668	2.789	159.41	93.1	7.1	36.95±0.16
900	1.78396	0.64114	2.782	230.13	94.1	8.5	36.87±0.12
950	2.62071	0.94540	2.772	265.82	92.1	12.5	36.73±0.13
1,000	3.97124	1.43109	2.775	88.47	90.8	18.9	36.77±0.11
1,050	5.74289	2.07489	2.768	235.51	90.2	27.4	36.67±0.10
1,150	2.52579	0.90807	2.782	140.48	89.0	12.0	36.85±0.12
1,300	0.02514	0.00969	2.595	16.05	13.0	0.1	34.40±7.45
Total-gas date			2.776				36.78±0.14
Plateau date (850–1,150°C)						86.4	36.77±0.12

emplaced during the first episode. Within the resolution of the data for these three units, the differences in emplacement history as recognized in the field (see later section) are not distinguishable in the argon data. The Joy Tuff and a hypabyssal rhyolite porphyry plug were emplaced during the later magmatic episode. Again, within the resolution of the argon data, an isotopic age difference for these two units cannot be resolved.

VOLCANIC STRATIGRAPHY AND IGNEOUS ROCKS

Andesite of Keg Spring

The oldest volcanic unit at Keg Mountain, based on field relations, is the andesite of Keg Spring (M.A. Shubat and G.E. Christenson, 1989, unpublished mapping). It consists of a heterogeneous sequence of dark-colored andesite flows and andesitic mudflow breccia. Erickson (1963) originally named the unit the Keg Spring andesite and latite, and Shawe (1972) and Staub (1975) referred to it as the Keg Spring andesite. The andesite of Keg Spring probably is a constructional volcanic high that was formed from multiple vents. Apparent interfingering of units indicates that eruption of the andesite of Keg Spring spanned the interval from pre-tuff of Dead Ox (late Eocene) to post–Mt. Laird Tuff (<36.54±0.06 Ma) eruption.

Tuff of Dead Ox

The tuff of Dead Ox (M.A. Shubat and G.E. Christenson, 1989, unpublished mapping) consists of three intercalated lithostratigraphic units: (1) a stratified tuff member, (2) a megabreccia member, and (3) a lithic-crystal ash-flow tuff member. The stratified tuff consists of thin-bedded to laminated volcanic sandstone, siltstone, and ash-rich tuff. Lithic-crystal tuff is present as distinct beds and also as the matrix of megabreccia. Coarsely lithic portions (20–40 cm diameter

Table 1. $^{40}Ar/^{39}Ar$ age-spectrum data for Keg Mountain, Utah—Continued

[Sample localities shown in figure 3. $^{40}Ar_R$ is radiogenic ^{40}Ar; $^{39}Ar_K$ is potassium-derived ^{39}Ar]

Temperature (°C)	$^{40}Ar_R$	$^{39}Ar_K$	F	$^{39}Ar/^{37}Ar$	$^{40}Ar_R$ (percent)	$^{39}Ar_K$ (percent)	Apparent age and error (Ma at 1σ)
Sample NKM–21–12/26/DD13; Mt. Laird Tuff; biotite; 57.3 mg; measured $^{40}Ar/^{36}Ar_a$=299.5; *J*-value=0.007430±0.25% (1σ); lat 39°48'55.99" N., long 112°55'51.93" W.							
500	0.02223	0.01927	1.154	10.58	5.8	0.3	15.40±5.62
600	0.10302	0.04913	2.097	12.66	28.2	0.7	27.89±1.26
700	1.19991	0.43847	2.737	46.37	50.4	6.6	36.31±0.17
750	2.93219	1.06674	2.749	112.40	84.1	15.9	36.47±0.10
800	3.96776	1.44129	2.753	190.38	89.8	21.5	36.53±0.10
850	2.18086	0.78986	2.761	188.57	83.1	11.8	36.63±0.13
900	0.99403	0.36113	2.753	68.38	68.1	5.4	36.52±0.27
950	1.32051	0.48162	2.742	3.31	69.1	7.2	36.38±0.11
1,000	1.68199	0.61257	2.746	1.11	73.3	9.2	36.43±0.12
1,050	2.59559	0.94584	2.744	8.77	82.3	14.1	36.41±0.10
1,150	1.32329	0.48045	2.754	3.54	77.0	7.2	36.55±0.18
1,300	0.01956	0.00480	4.071	0.22	4.7	0.1	53.75±9.61
Total-gas date			2.741				36.37±0.16
Plateau date (700–1,150°C)						98.9	36.48±0.14
Sample KMR–4–8/21/DD13; Mt. Laird Tuff, base; hornblende; 310 mg; measured $^{40}Ar/^{36}Ar_a$=299.5; *J*-value=0.007357±0.25% (1σ); lat 39°51'00.09" N., long 112°52'41.43" W.							
500	0.02351	0.01087	2.163	0.39	3.5	0.3	28.48±3.37
700	0.21900	0.06423	3.409	1.29	24.3	1.5	44.69±1.11
800	0.19170	0.06208	3.088	1.44	63.0	1.4	40.53±0.92
850	0.10858	0.03586	3.028	1.47	63.7	0.8	39.74±2.90
900	0.10127	0.03260	3.106	0.96	57.5	0.8	40.76±1.95
950	0.38293	0.13478	2.841	0.24	65.6	3.1	37.32±0.56
1,000	3.09179	1.11026	2.785	0.17	84.2	25.9	36.59±0.14
1,050	5.34234	1.91651	2.788	0.16	90.2	44.6	36.62±0.10
1,100	1.52856	0.54926	2.783	0.14	88.1	12.8	36.56±0.16
1,150	0.68760	0.24725	2.781	0.13	85.1	5.8	36.54±0.30
1,200	0.19654	0.07082	2.775	0.13	70.3	1.6	36.46±0.75
1,400	0.17336	0.05950	2.914	0.14	13.3	1.4	38.26±0.79
Total-gas date			2.806				36.86±0.31
Plateau date (1,000–1,200°C)						90.7	36.59±0.29

clasts) of the lithic-crystal tuff resemble "mesobreccia" described by Lipman (1976) and weather to form cobble- and boulder-strewn slopes with poorly exposed matrix.

The megabreccia member of the tuff of Dead Ox consists of clasts of Paleozoic rocks, conglomerate, andesitic mudflow breccia, and andesite set in poorly welded lithic tuff matrix. Lithic-crystal tuff matrix is poorly exposed because of mantling of megabreccia by Quaternary Lake Bonneville lacustrine deposits but is seen as a thin rind of tuff coating megabreccia clasts. Clast sizes are from less than 0.2 to 240 m in diameter, but most clasts are between 3 and 60 m. Most quartzite and some limestone clasts in the megabreccia are pervasively brecciated. In places clasts are monolithologic, angular, matrix-supported breccia with a fine-grained matrix of comminuted material, whereas in other places clasts are intact but highly fractured and sheared. The former textures could have been produced in a subvolcanic environment by "gas-explosion" and hydrothermal activity, as reviewed by Shawe and Snyder (1988). The latter textures could represent blocks deformed during thrusting and later incorporated into the megabreccia. In contrast to the Paleozoic clasts, andesite clasts are only locally brecciated. The juxtaposition of surficially derived andesite (debris-flow facies) clasts and shattered Paleozoic clasts argues for an origin involving the mixing of eruptive megabreccia (Shawe and Snyder, 1988) and landslide megabreccia (Lipman, 1976). Such mixing could occur during an Aira-type eruption (Aramaki, 1984), during which a volcanic depression is filled with megabreccia and tuff and lacks distinct ring-faults.

Field relations suggest that the tuff of Dead Ox underlies the tuff of Keg Mountain and predominantly overlies, but in part interfingers with, the andesite of Keg Spring.

Table 1. $^{40}Ar/^{39}Ar$ age-spectrum data for Keg Mountain, Utah—Continued
[Sample localities shown in figure 3. $^{40}Ar_R$ is radiogenic ^{40}Ar; $^{39}Ar_K$ is potassium-derived ^{39}Ar]

Temperature (°C)	$^{40}Ar_R$	$^{39}Ar_K$	F	$^{39}Ar/^{37}Ar$	$^{40}Ar_R$ (percent)	$^{39}Ar_K$ (percent)	Apparent age and error (Ma at 1σ)
Sample KMR–4–8/24/DD13; Mt. Laird Tuff, base; biotite; 78.2 mg; measured $^{40}Ar/^{36}Ar_a$=299.5; *J*-value=0.7424±0.25% (1σ); lat 39°51'00.09" N., long 112°52'41.43" W.							
500	0.06137	0.05137	1.195	11.53	9.0	0.5	15.93±0.97
600	0.12916	0.05911	2.185	19.41	42.0	0.6	29.03±1.54
700	0.36972	0.13581	2.722	27.57	48.1	1.3	36.10±0.49
750	1.06817	0.38646	2.764	55.93	76.4	3.7	36.64±0.14
800	2.01958	0.72495	2.786	103.09	89.4	7.0	36.93±0.13
850	2.59186	0.93159	2.782	139.57	92.8	9.0	36.88±0.12
900	3.62307	1.30943	2.767	162.10	93.8	12.6	36.68±0.10
950	5.48573	1.98479	2.764	45.77	92.1	19.2	36.64±0.10
1,000	5.12590	1.86121	2.754	4.41	88.5	18.0	36.51±0.10
1,050	4.66806	1.69934	2.747	18.34	87.3	16.4	36.42±0.10
1,150	3.27674	1.18838	2.757	12.98	86.6	11.5	36.56±0.12
1,300	0.08719	0.03137	2.780	1.93	37.6	0.3	36.85±2.69
Total-gas date			2.751				36.47±0.13
Plateau date (900–1,150°C)						77.6	36.56±0.11

Table 2. Summary of $^{40}Ar/^{39}Ar$ age-spectrum dates for Keg Mountain, Utah

Sample no.	Unit	Mineral	Date (Ma±1σ)	Character of age spectrum
KMR–1–3	Joy Tuff, basal vitrophyre	Sanidine	34.92±0.16	Plateau; minor inherited argon.
		Biotite	34.84±0.14	Preferred date; disturbed with minor argon loss.
KMR–4–6	Hypabyssal rhyolite porphyry	Sanidine	35.04±0.15	Plateau; minor excess argon.
		Biotite	35.25±0.13	Plateau; minor excess argon.
NKM–6–3	Hypabyssal dacite porphyry	Biotite	36.49±0.15	Plateau; minor excess argon.
KP–6–5	Tuff of Keg Mountain, basal vitrophyre	Biotite	36.77±0.12	Plateau; minor excess argon.
NKM–21–12	Mt. Laird Tuff	Biotite	36.48±0.14	Plateau.
KMR–4–8	Mt. Laird Tuff, base	Hornblende	36.59±0.29	Plateau; minor excess argon.
		Biotite	36.56±0.11	Plateau; minor excess argon.

Constraints on the minimum age of the unit are the observations that (1) the tuff of Dead Ox is cut by a dacite porphyry plug dated at 36.49±0.15 Ma (sample NKM–6–3) and (2) the megabreccia member contains no clasts of tuff of Keg Mountain or Mt. Laird Tuff. A constraint on the maximum age of the unit is the observation that clasts of the andesite of Keg Spring are common in the megabreccia member.

Tuff of Keg Mountain

The tuff of Keg Mountain (M.A. Shubat and G.E. Christenson, unpublished mapping, 1989) consists of dark-colored, densely welded, moderately crystal-rich ash-flow tuff of dacitic composition that has a local black vitrophyric base. Abundant bronze-weathering biotite, prominent on surfaces parallel with layering, characterizes the unit. As discussed above, our dates show a slightly older age for the tuff of Keg Mountain compared to the Mt. Laird Tuff but do not provide statistically unambiguous eruption ages. Field relations, discussed below, suggest that the tuff of Keg Mountain is older than the Mt. Laird Tuff. First, several dacite porphyry plugs, one of which we dated at 36.49±0.15 Ma (sample NKM–6–3, table 2), that are compositionally similar to the Mt. Laird Tuff cut the tuff of Keg Mountain. Second, there is a consistent stratigraphic succession from the tuff of Keg Mountain to Mt. Laird to Dell Tuff with increasing elevation in the north-central part of Keg Mountain; this stratigraphic superposition supports the suggested age sequence. Third, the tuff of Keg Mountain is absent south of an arcuate fault in the Picture Rock Hills Quadrangle (the northern edge of the Picture Rock caldera(?), fig. 3). Therefore, if the tuff of Keg Mountain is younger than the Mt. Laird Tuff, then its absence south of the fault requires confinement of the tuff of Keg Mountain to the Keg cauldron or stratigraphic thinning of the tuff of Keg Mountain from almost 200 m to zero over a distance of 2 km. If the tuff of Keg Mountain is older, then the Mt. Laird Tuff covers the tuff of Keg Mountain south of this fault.

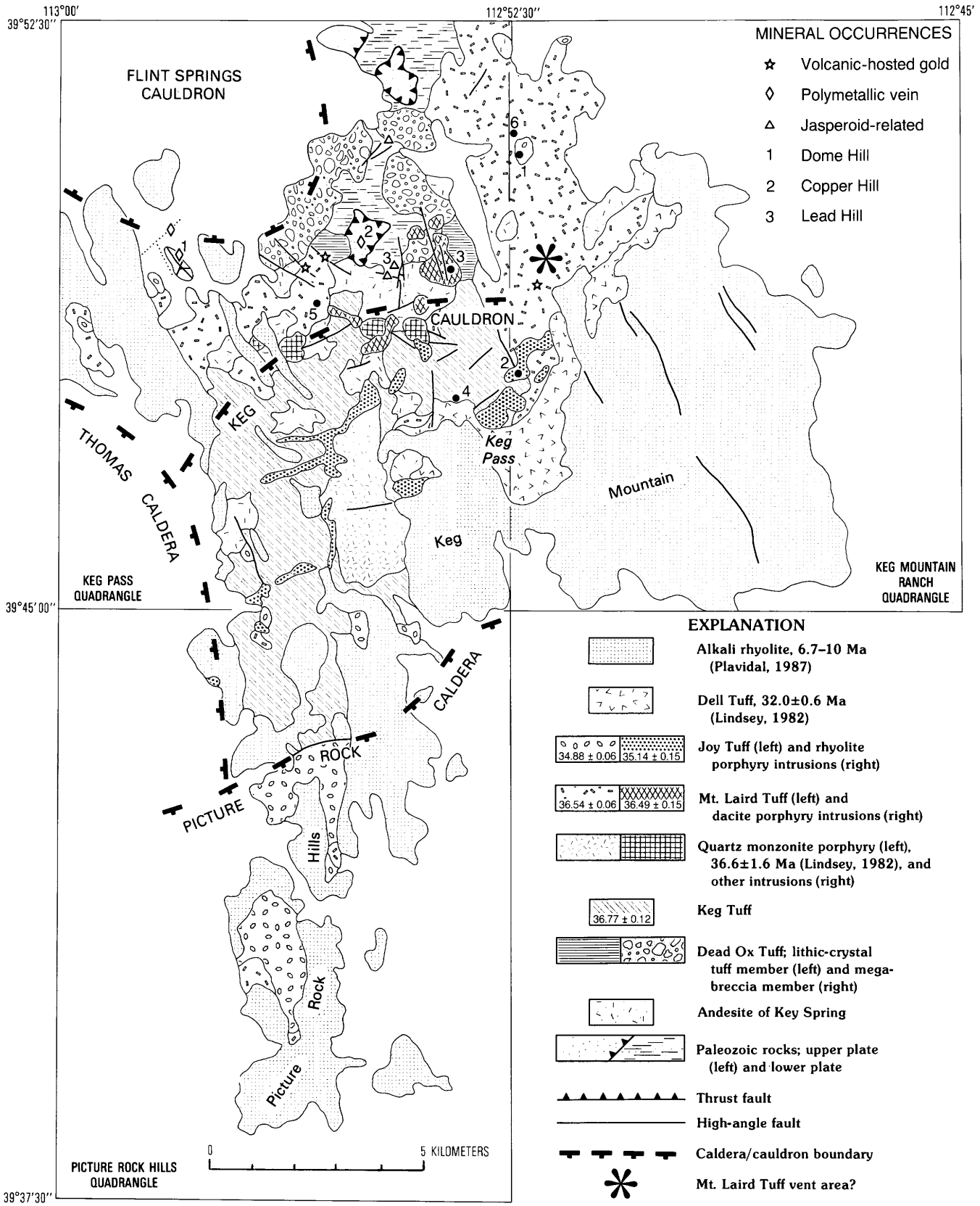

Figure 3. Simplified geology of Keg Mountain, west-central Utah. Solid numbered circles are locations of dated samples listed in table 2: 1, KMR–1–3; 2, KMR–4–6; 3, NKM–6–3; 4, KP–6–5; 5, NKM–21–12; 6, KMR–4–8.

Quartz Monzonite Porphyry

The quartz monzonite porphyry is a holocrystalline intrusive rock containing coarse (2–12 mm) phenocrysts of plagioclase, quartz, biotite, hornblende, pyroxene, and magnetite set in a fine-grained hypidiomorphic-granular matrix of quartz, plagioclase, and potassium feldspar. The porphyry forms a stock about 4.8 km long by 1.6 km wide in the south-central part of the Keg Pass Quadrangle (fig. 3). Lindsey and others (1975) dated the porphyry by the fission-track method at 36.6±1.6 Ma.

Mt. Laird Tuff

The Mt. Laird Tuff (Lindsey, 1979, 1982) is a regionally extensive unit consisting of moderately welded ash-flow tuff, tuff breccia, lapilli tuff, accretionary lapilli-block tuff, probable flow rocks, and hypabyssal intrusive rocks of rhyodacitic to quartz latitic composition. Its most distinctive characteristic is the presence of abundant, coarse (2–12 mm) phenocrysts of white plagioclase in all facies. Our dates indicate an extrusion age of 36.54±0.06 Ma for the Mt. Laird Tuff (samples KMR–4–8 and NKM–21–12, table 2), which is statistically identical to a 36.4±1.6 Ma date reported by Lindsey (1982). Because the fission-track date of the overlying Joy Tuff is about 38 Ma, Lindsey considered the true age of the Mt. Laird Tuff to be about 39 Ma. Over most of Keg Mountain, the Mt. Laird Tuff appears to be outflow from the Thomas caldera; however, mapping indicates an apparent Mt. Laird vent in the north-central part of Keg Mountain (fig. 3). Rocks in this apparent vent consist of an accretionary lapilli-block tuff facies that grades into a hypabyssal porphyry facies; these are cut by pebble dikes containing fragmented and unfragmented Mt. Laird clasts. In addition, within the vent the tuff has steeply dipping layering.

Dacite Porphyry Intrusive Rocks

The hypabyssal dacite porphyry consists of abundant, coarse (2–10 mm) phenocrysts of plagioclase, quartz, biotite, hornblende, and magnetite set in a matrix of plagioclase, quartz, and potassium feldspar microphenocrysts and aphanitic material. Dacite porphyry forms several small plugs, each less than 900 m in diameter, in the center of the Keg Pass Quadrangle (fig. 3). Our date of 36.49±0.15 Ma (sample NKM–6–3, table 2), as well as mineralogic and petrologic similarities, indicates that these rocks are comagmatic with the Mt. Laird Tuff.

Regional aeromagnetic data (Kucks, 1991) show a circular, high-amplitude magnetic high (with a paired dipole low to the north) that straddles the northern part of the east-central edge of the Keg Pass Quadrangle (fig. 4). We interpret this anomaly to represent a buried dacite porphyry stock because of its proximity to several mapped dacite porphyry plugs and the possible Mt. Laird vent area described above (fig. 3). Magnetotelluric resistivity data (D. Campbell, oral commun., 1990) support this interpretation. This interpretation has significance for exploration because anomalous amounts of gold are commonly detected in argillic-pyritic alteration halos around this type of intrusion.

Joy Tuff

The Joy Tuff (Lindsey, 1979) is a regionally extensive unit that consists of moderately to densely welded, moderately crystal-rich, rhyolitic ash-flow tuff that locally has a black basal vitrophyre and overlying black fiamme-rich zone. Several exposures of the basal vitrophyre of the Joy Tuff resting on the Mt. Laird Tuff show that it clearly overlies the Mt. Laird Tuff; therefore, field relations are consistent with our date of 34.88±0.06 Ma (sample KMR–1–3, table 2). Our date shows a marked discordance with nine fission-track ages reported by Lindsey (1982) that average 38.0±0.7 Ma. Although the improved accuracy of the $^{40}Ar/^{39}Ar$ age-spectrum dating method may be solely responsible for this discrepancy, it is possible that the unit mapped as Joy Tuff at Keg Mountain is lithologically similar to but younger than the Joy Tuff at the type locality. The exposed thickness of the Joy Tuff is thin (<24 m) in most of the Keg Mountain area, but south of an arcuate fault (figs. 2, 3) it abruptly thickens to more than 180 m. Lindsey (1982) believed the source of the Joy Tuff to be within the Dugway Valley cauldron (fig. 4).

Rhyolite Porphyry

The rhyolite porphyry consists of coarse (as large as 1 cm) phenocrysts of orthoclase, quartz, plagioclase, and biotite set in an aphanitic matrix. Rhyolite porphyry forms plugs that lie within two linear, subparallel, northeast-trending belts, one of which is about 14 km long, that cut through the west-central part of Keg Mountain. Lithology and our date of 35.14±0.15 Ma (sample KMR–4–6, table 2) for one of these plugs are similar to those of the Joy Tuff and suggest that the rhyolite porphyry unit is comagmatic with and a hypabyssal equivalent of the Joy Tuff. A fission-track age of 30.8±1.8 Ma reported by Lindsey and others (1975) for another rhyolite porphyry plug raises the possibility that more than one age of rhyolite intrusions may be present.

Figure 4 (facing page). Complete Bouguer gravity map of the north-central part of the Delta 1°X2° quadrangle, Utah (from Bankey and Cook, 1989). Stippled areas are magnetic highs (from Kucks, 1991). Thick lines are known or inferred caldera margins as discussed in text. Contour interval 2 mGal.

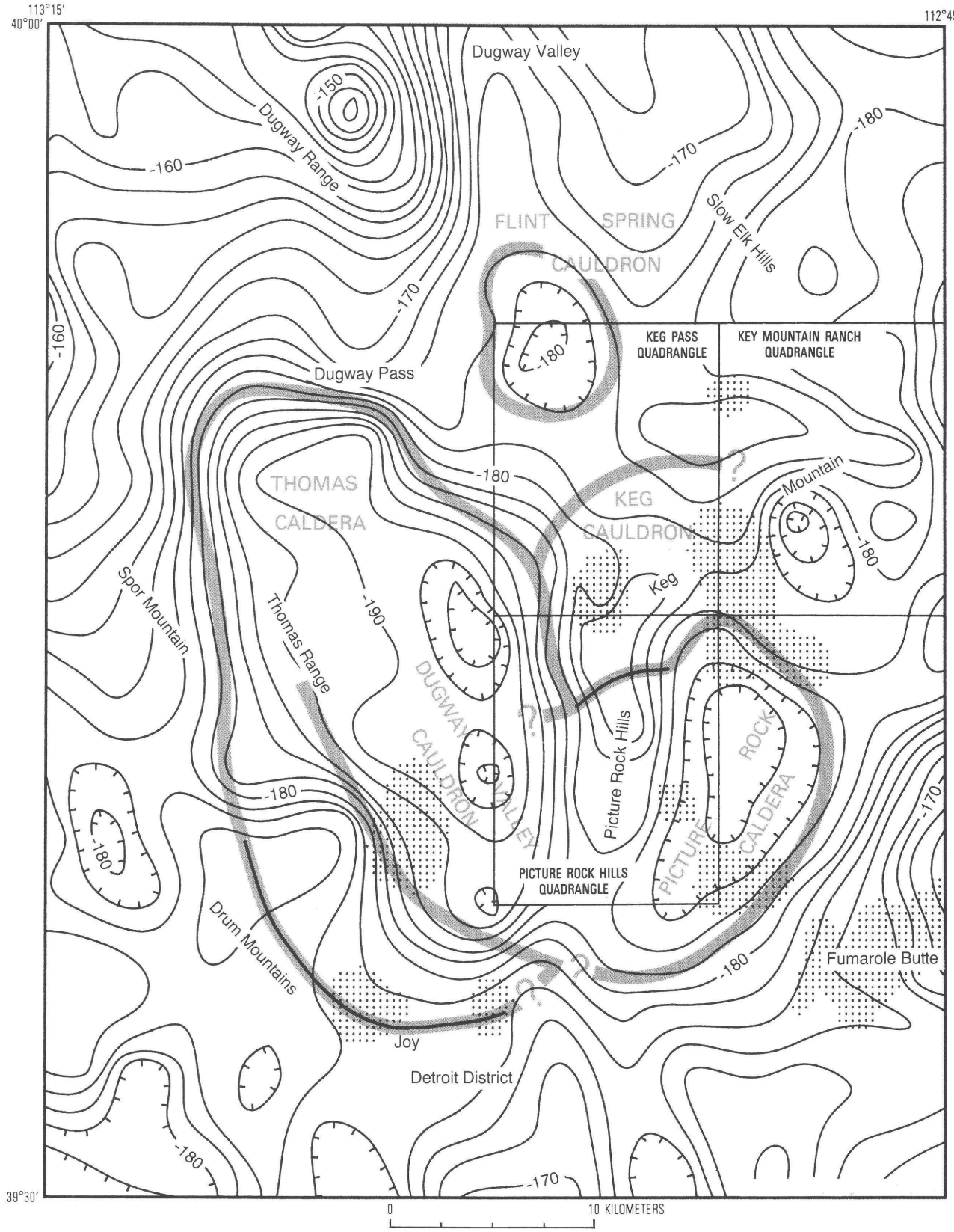
113°15′
40°00′
112°45′
39°30′
Dugway Valley
Dugway Range
Slow Elk Hills
FLINT SPRING CAULDRON
KEG PASS QUADRANGLE
KEY MOUNTAIN RANCH QUADRANGLE
Dugway Pass
THOMAS CALDERA
KEG CAULDRON
Mountain
Keg
Spor Mountain
Thomas Range
DUGWAY VALLEY CAULDRON
Picture Rock Hills
PICTURE ROCK CALDERA
PICTURE ROCK HILLS QUADRANGLE
Drum Mountains
Fumarole Butte
Joy
Detroit District
-150
-160
-170
-180
-190
0
10 KILOMETERS

Several lines of evidence suggest that a buried pluton, which we interpret to be a granitic body related to the rhyolite porphyry plugs exposed at the surface, underlies the Keg Pass area (figs. 2, 3). Deep resistivity (AMT) soundings collected along a north-south profile across Keg Mountain (Campbell and Visnyei, 1989) show a resistive body at depth beneath Keg Pass that has a resistivity signature (>200 ohm-meters) typical of many igneous rocks in the region (D. Campbell, oral commun., 1990). Regional aeromagnetic data (Kucks, 1991) show a high-amplitude magnetic ridge extending from Keg Pass to a point about 8 km to the south (fig. 4). This magnetic signature is similar to the signatures of many known intrusions in the Deep Creek–Tintic mineral belt.

Dell Tuff

The Dell Tuff (Lindsey, 1979) is a pink to tan, poorly to moderately welded, crystal-rich, rhyolitic ash-flow tuff containing 2–8-mm phenocrysts of quartz, sanidine, plagioclase, and biotite. Staatz and Carr (1964) first described the tuff, and Lindsey (1979) formally named it for exposures in the Thomas Range. The minimum thickness of the Dell Tuff at Keg Mountain is 150 m. Recent paleomagnetic work by J.L. Hanna (University of Vermont, oral commun., 1989) shows that the Dell Tuff at the type locality ("The Dell," in the Thomas Range) has a normal magnetic polarity and that the Dell Tuff at Keg Pass has a reverse polarity; the Dell Tuff therefore consists of at least two cooling units. Lindsey and others (1975) dated three samples from Keg Pass, ranging in age from 32.5±1.6 to 33.8±1.3 Ma, and Lindsey (1982) established an average age of 32.0±0.6 Ma for the formation. The source of the Dell Tuff has not been found; however, Lindsey (1982) speculated that the source should lie in or near Keg Mountain or the Thomas Range.

Alkali Rhyolite

Alkali rhyolite at Keg Mountain is present in two units, the lower unit is an unnamed rhyolite (Plavidal, 1987) and the upper unit is the Topaz Mountain Rhyolite (Lindsey, 1979). Work by Plavidal (1987) shows that the two units are compositionally gradational; the Topaz Mountain Rhyolite was probably derived from the older unnamed rhyolite parent through crystal fractionation. Both units consist of flows, domes, and dikelike shallow intrusions of white, gray, and purplish alkali rhyolite. Phenocrysts in the unnamed rhyolite consist of coarse (1 cm), abundant (20–40 percent) plagioclase and sanidine and lesser quartz and biotite. The Topaz Mountain Rhyolite contains sparse (10–15 percent), small (2 mm) phenocrysts of quartz, sanidine, plagioclase, and biotite. Black vitrophyre is at the base of some flows and domes in both formations. Flows and domes probably were erupted from local vents, with dikelike bodies serving as feeders. Stratified tuff horizons are in both formations as discontinuous, wedge-shaped (less than 60 m thick) intercalations between flows. Stratified tuff is pale tan to orange and massive to thin bedded and consists of rhyolitic tuff and volcaniclastic sandstone. Stratified tuff was deposited as air-fall, ash-flow, and ground-surge eruptions and as waterlain deposits (Lindsey, 1979; Bikun, 1980; Plavidal, 1987). The exposed thickness of alkali rhyolite at Keg Mountain is 450 m. Plavidal (1987) reported K-Ar dates of 6.7±0.3 and 6.9±0.3 Ma for the unnamed rhyolite. Fission track ages of 7.8±0.6 and 8.2±0.5 Ma for the Topaz Mountain Rhyolite at Keg Mountain reported by Lindsey and others (1975) indicate a discrepancy in geochronology.

STRUCTURE

Mesozoic Compressional Structures

Morris (1983, 1987) first identified in the northern Keg Mountain area and Slow Elk Hills a Sevier-age thrust that locally consists of several imbricate slivers. Exposed lower plate rocks of this thrust are probable Howell Limestone (Middle Cambrian) (Hintze and Robison, 1975), and upper plate rocks include the Prospect Mountain Quartzite, Pioche Formation, and Howell Limestone. The thrust may represent as little as 350 m or as much as 2,000 m of stratigraphic separation. Upper plate quartzite is pervasively brecciated throughout the area. Lower plate carbonate rocks have been locally altered to jasperoid immediately beneath the thrust. Ubiquitous white calcite veinlets in lower plate carbonate rocks may be related to the thrusting event. Axes of small-amplitude (<60 m), upright, map-scale folds and minor folds (east vergent) in lower plate carbonate rocks plunge gently toward the north-northeast. The thrust surface is sharp and well exposed in many locations, consisting of a thin (<4 cm) cataclasite zone and no ductile deformation on the footwall.

Caldera and Cauldron Structures

Flint Spring Cauldron

The source of the tuff of Dead Ox remains unidentified, but our interpretation of an eruptive origin (or at least an eruptive component) for the megabreccia member of the tuff of Dead Ox suggests a nearby vent. We tentatively propose that the tuff of Dead Ox erupted from the Flint Spring cauldron (M.A. Shubat and G.E. Christenson, unpublished data, 1989) in the northwest part of the Keg Pass Quadrangle (figs. 3, 4). Two lines of evidence support this proposition: (1) the presence of a subtle gravity low in this area and (2) the absence of a mappable caldera margin (structural or topographic wall) bounding the megabreccia terrain. The absence

of a thick section of the tuff of Dead Ox, a pronounced gravity low near the megabreccia terrain, or recognizable ring faults argues against a large local source caldera for the tuff of Dead Ox.

Keg Cauldron

To date, the tuff of Keg Mountain has only been recognized at Keg Mountain and therefore is probably a locally derived unit. We propose that it was erupted from a cauldron, termed the Keg cauldron (M.A. Shubat and G.E. Christenson, unpublished data, 1989), centered on the quartz monzonite porphyry stock in the south-central part of the Keg Pass Quadrangle (figs. 3, 4). As defined here, the Keg cauldron differs substantially from the Keg caldera defined by Shawe (1972). The term "caldera" does not apply because of the absence of clearly defined margins. Evidence for the existence of the Keg cauldron is the thickening of the tuff of Keg Mountain from zero in the center of the Keg Pass Quadrangle to more than 165 m only 3 km to the south. The distribution of, and dips measured in, the tuff of Keg Mountain outlines a broad, low-relief dome centered on the quartz monzonite porphyry stock. Because of similarities in modal composition, age, and spatial distribution, we consider this stock to be comagmatic with the tuff of Keg Mountain and view it as a resurgent intrusion that caused doming.

Thomas Caldera

We place the eastern edge of the Thomas caldera along the western margin of Keg Mountain (figs. 3, 4), as originally drawn by Shawe (1972) and Lindsey (1982), for stratigraphic and geophysical reasons. We interpret the Mt. Laird Tuff at Keg Mountain to be a thin outflow facies of the formation; thus the caldera margin must lie west of Keg Mountain. Detailed mapping shows that where top and bottom contacts are exposed only thin sections of Mt.Laird Tuff are present between the tuff of Keg Mountain and the Joy Tuff and that over the center of the proposed Keg cauldron the Mt. Laird Tuff is missing. We found no stratigraphic or structural evidence indicating that the margin of the Thomas caldera passes through or east of Keg Mountain. Based on geophysical evidence, a likely place to draw the eastern margin of the Thomas caldera is a persistent gravity gradient along the western margin of Keg Mountain (fig. 4); in this case the gravity low of Dugway Valley is interpreted to represent, in part, less dense intracaldera fill. The absence of late Tertiary to Quaternary fault scarps along the western margin of Keg Mountain argues against this gradient being only the result of basin-range faulting. This gradient forms the eastern margin of an oval-shaped, north-elongate gravity low (fig. 4) that we associate with the Thomas caldera. The closure of this gravity anomaly at its northern and southern ends and the presence of bedrock near the axis of the low suggest control by rocks other than basin-fill sediments. The gravity low may represent subvolcanic intrusion of Miocene Topaz Mountain Rhyolite in addition to fill of the Thomas caldera.

Picture Rock Caldera

ARCO geologists identified and named the Picture Rock caldera while exploring for minerals in the Thomas Range and Keg Mountain area during the late 1970's and early 1980's (Anaconda Geological Document Collection, University of Wyoming, Laramie). The caldera is primarily defined by an oval-shaped gravity low (fig. 4) that is coincident with low-resistivity material (Campbell and Visnyei, 1989) that could be intracaldera fill. An arcuate fault, concave to the south, mapped in the north-central part of the Picture Rock Hills Quadrangle (fig. 3), separates a thick section (>180 m) of Joy Tuff to the south from thin sections (<24 m) to the north. We interpret this fault as the structural wall of the Picture Rock caldera and associate the caldera with the eruption of the Joy Tuff. Insufficient data exist to determine the relationship between the Picture Rock caldera and the Dugway Valley cauldron. As discussed above, it is possible that rocks mapped as Joy Tuff in the Thomas Range and at Keg Mountain may be distinct units, in which case the Picture Rock caldera would be the source for the Joy-like ashflow tuff exposed in the Picture Rock Hills.

High-Angle Normal Faults

Many small-displacement, high-angle normal faults at Keg Mountain cut units as young as the 6-Ma Topaz Mountain Rhyolite (Plavidal, 1987) but do not cut Quaternary units. Well-exposed field relations and geochronology tightly constrain the onset of at least some of the high-angle faulting. One north-striking fault in the center of the Keg Pass Quadrangle drops the base of the tuff of Keg Mountain 15 m down to the west and is filled by a dacite porphyry plug. Our dates for the tuff of Keg Mountain and one of the dacite porphyry intrusions indicate that the age of this fault is between 36.77±0.12 and 36.49±0.15 Ma. High-angle faults at Keg Mountain are in all orientations, and the amounts of stratigraphic separation across these faults, where demonstrable, are small (<60 m). Apparently, these faults formed throughout the period of volcanism from the early Oligocene to Pliocene. Examination of slickensides surfaces of some faults yielded a normal sense of slip. Although small in displacement and sparsely distributed, high-angle faults exert a strong control on the localization of mineral deposits at Keg Mountain.

MINERAL DEPOSITS

Morris (1978) first described pyritic alteration in the Keg Mountain area, and since then lead, silver, copper, and gold

have been discovered (fig. 3). These deposits form three main categories: volcanic-hosted gold, sediment-hosted polymetallic (lead-zinc-silver dominated) vein and replacement, and carbonate-hosted jasperoid prospects.

Volcanic-Hosted Gold Deposits

The most explored volcanic-hosted gold deposit at Keg Mountain is about 1 km west of the Copper Hill prospect (fig. 3). Industry geologists discovered the prospect in 1987 and explored it with 14 drill holes in 1988 and 1989. Gold is concentrated along a high-angle, northwest-striking, southwest-dipping normal fault that juxtaposes the Mt. Laird Tuff (hanging wall) against the lithic-crystal tuff member of the tuff of Dead Ox. Within a few meters of the fault the tuff of Dead Ox is intensely argillized and pyritized. The highest values obtained to date average 1.02 ppm Au over a 6-m interval. Other areas in which gold is anomalous (fig. 3) are adjacent to pebble dikes cutting the Mt. Laird Tuff, near contacts of dacite porphyry plugs, and along high-angle faults.

Dome Hill Prospect

The Prospect Mountain Quartzite hosts a polymetallic vein and replacement deposit (Cox and Singer, 1986) at Dome Hill (fig. 3). Dome Hill constitutes the southwestern half of a dome that is cut by several high-angle faults, the most prominent of which consists of a silicified rib along the elongate northwest-trending axis of the hill. On the surface, host rocks are quartzite and lesser interbedded shale; in core, carbonate rocks also form the host. The mineral deposit at Dome Hill consists of highly oxidized stockwork and replacement with anomalous concentrations of silver, lead, copper, gold, and bismuth. Primary sulfide minerals are pyrite, galena, tetrahedrite-tennantite, and rare chalcopyrite. Analyses of mineralized samples show high concentrations of silver (as much as 27 oz/ton in bulk samples) and bismuth (as much as 3.7 percent) and locally high values of gold (6.5 ppm), base metals, arsenic, and antimony.

Faults and fractures control the exposed distribution of mineralized rock at Dome Hill, and highly anomalous samples are along the dominant northwest-trending fault along the crest of the hill. Mineralized rock apparently extends for more than 900 m to the northwest of the hill to an area of buried mineralized rock discovered by drilling (fig. 3). Drill holes in this area tested a northeast-trending self-potential responder coincident with northeast-striking air-photo lineaments. Drill core shows the presence of quartz veinlets in carbonate host rock containing pyrite, galena, and sphalerite and several intercepts of disseminated sulfides in silicified breccia zones. One stockwork zone contains 0.70 oz/ton Ag, 0.55 percent Pb, and 0.54 percent Zn over a 3-m interval.

Lead Hill Prospect

Two types of mineralized rock are present at Lead Hill: (1) carbonate-hosted gold-, silver-, zinc-, and molybdenum-bearing jasperoid and (2) small, massive pods of galena replacing limestone. Jasperoid is along high-angle faults and fracture zones and forms resistant, dark-brown masses about 2–9 m long and 1–3 m wide. Sparse ore minerals in jasperoid are fine-grained pyrite and galena. Gangue minerals are almost entirely microcrystalline, chalcedonic silica with a ubiquitous iron oxide stain and trace of sericite. Geochemical analyses show that the lead, silver, molybdenum, gold, and zinc are contained in the jasperoid. The highest values obtained from jasperoid samples are 1.89 percent Pb, 7.88 oz/ton Ag, 450 ppm Mo, 0.59 ppm Au, and 280 ppm Zn. The second type of mineralized rock at Lead Hill is small (<30 cm diameter) pods of almost massive galena that replaced limestone adjacent to a granodiorite dike exposed in a prospect trench at the north end of Lead Hill. Analyses of the galena-rich pods also show the presence of silver (0.66 oz/ton) and trace amounts of zinc.

CONCLUSIONS

The combination of detailed geologic mapping and high-precision $^{40}Ar/^{39}Ar$ geochronology allowed us to identify the following sequence of Eocene and Oligocene caldera- and cauldron-forming events at Keg Mountain (in order of decreasing age): eruption of the tuff of Dead Ox from the Flint Spring cauldron, the tuff of Keg Mountain from the Keg cauldron, the Mt. Laird Tuff from the Thomas caldera, and the Joy Tuff (or a Joy-like tuff) from the Picture Rock caldera. Geochronology provides a temporal link between the petrographically similar Mt. Laird Tuff and hypabyssal dacite porphyry intrusive rocks, which we take as evidence for a comagmatic origin. Correlation of hypabyssal dacite intrusive rocks with the Mt. Laird Tuff implies that the area affected by this magmatic event is much larger than the areal extent of the Thomas caldera (about 300 km^2). The distance spanned from the dacite intrusions at Keg Mountain to similar intrusions in the Drum Mountains, on the opposite side of the Thomas caldera, is more than 35 km.

Work in the Simpson Mountains (fig. 1) by Yambrick and Snee (1989) resulted in discovery of rocks of similar lithology and age (36.5±0.2 Ma) to the Mt. Laird–related rocks described here. Yambrick and Snee also dated a rhyodacitic ash-flow tuff at 35.1±0.2 Ma, indistinguishable in age from Joy-related rocks dated in this study at 35.0±0.2 Ma. (In addition, R.A. Yambrick and L.W. Snee dated the rhyolite of Judd Creek from the Simpson Mountains and determined that it was extruded at 35.9±0.2 Ma, a time when volcanism apparently did not occur at Keg Mountain.) These similarities suggest that high-precision $^{40}Ar/^{39}Ar$ age-spectrum dating can be used in conjunction with petrochemistry

and petrography to correlate volcanic and subvolcanic rocks between adjacent ranges. For example, at 36.5±0.2 Ma intermediate rocks similar in composition to the Mt. Laird Tuff were erupted and intruded in the area from the Drum to Simpson Mountains and thus affected an area as much as 60 km in one dimension. Assuming the other dimension of this tract to be at least 10 km yields a minimum area of 600 km^2, twice that of the Thomas caldera. Perhaps of equal or more significance, Keg Mountain and the Simpson Mountains were affected by volcanic activity that produced rocks of similar composition (rhyolite, rhyodacite and quartz latite) during the same time interval (36.5–35.0 Ma).

In a gross sense, mineral deposits at Keg Mountain probably are associated with the eastern part of a large, late Eocene to early Oligocene igneous complex that spans the Thomas Range, Keg Mountain, and northern Drum Mountains area. These mineral deposits consist of volcanic-hosted gold prospects, polymetallic veins, and precious-metals-enriched jasperoid bodies that are along high-angle, small-displacement normal faults. In detail, however, there are no clear spatial relationships between inferred caldera margins, associated hypabyssal intrusions, and mineral deposits (fig. 3). The widespread distribution of hypabyssal intrusions related to the Mt. Laird Tuff and Joy Tuff magmatic systems suggests the possibility of concealed, larger intrusions related to these systems. Mineral deposits at Keg Mountain may have been formed by hydrothermal systems induced by possible concealed intrusions.

REFERENCES CITED

Alexander, E.C., Michelson, G.M., and Lanphere, M.A., 1978, A new $^{40}Ar/^{39}Ar$ dating standard: U.S. Geological Survey Open-File Report 78–701, p. 6–8.

Aramaki, Shigeo, 1984, Formation of the Aira caldera, southern Kyushu, ~22,000 years ago: Journal of Geophysical Research, v. 89, no. B10, p. 8485–8501.

Bankey, Viki, and Cook, K.L., 1989, Complete Bouguer gravity map and related geophysical maps of the Delta 1°×2° quadrangle, Utah: U.S. Geological Survey Miscellaneous Field Studies Map MF–2081–A, scale 1:250,000.

Bikun, J.V., 1980, Fluorine and lithophile element mineralization at Spor Mountain, Utah: Tempe, Arizona State University, M.S. thesis, 195 p.

Campbell, D.L., and Visnyei, Andrew, 1989, Audio-magnetotelluric soundings in the Delta Utah 1°×2° quadrangle: U.S. Geological Survey Open-File Report 89–538, 71 p.

Cox, D.P., and Singer, D.A., 1986, eds., Mineral deposit models: U.S. Geological Survey Bulletin 1693, 379 p.

Dalrymple, G.B., Alexander, E.C., Lanphere, M.A., and Kraker, G.P., 1981, Irradiation of samples for $^{40}Ar/^{39}Ar$ dating using the Geological Survey TRIGA reactor: U.S. Geological Survey Professional Paper 1176, 56 p.

Dalrymple, G.B., and Lanphere, M.A., 1969, Potassium-argon dating: San Francisco, W.H. Freeman, 251 p.

Erickson, M.P., 1963, Volcanic geology of western Juab County, Utah, *in* Sharp, B.J., and Williams, N.C., eds., Beryllium and uranium mineralization in western Juab County, Utah: Utah Geological Society, Guidebook to the Geology of Utah, no. 17, p. 23–35.

Hintze, L.F., and Robison, R.A., 1975, Middle Cambrian stratigraphy of the House, Wah Wah, and adjacent ranges in western Utah: Geological Society of America Bulletin, v. 86, p. 881–891.

Kucks, R.P., 1991, Aeromagnetic and related maps of the Delta 1°×2° CUSMAP quadrangle, Utah: U.S. Geological Survey Miscellaneous Field Studies Map MF–2081–B, 7 p., scale 1:250,000.

Lindsey, D.A., 1977, Epithermal beryllium deposits in waterlaid tuff, western Utah: Economic Geology, v. 72, no. 2, p. 219–232.

_____1979, Geologic map and cross sections of Tertiary rocks in the Thomas Range and northern Drum Mountains, Juab County, Utah: U.S. Geological Survey Miscellaneous Investigations Series Map I–1176, scale 1:62,500.

_____1982, Tertiary volcanic rocks and uranium in the Thomas Range and northern Drum Mountains, Juab County, Utah: U.S. Geological Survey Professional Paper 1221, 71 p.

Lindsey, D.A., Naeser, C.W., and Shawe, D.R., 1975, Age of volcanism, intrusion, and mineralization in the Thomas Range, Keg Mountain, and Desert Mountain, western Utah: U.S. Geological Survey Journal of Research, v. 3, no. 5, p. 597–604.

Lipman, P.W., 1976, Caldera-collapse breccias in the western San Juan Mountains, Colorado: Geological Society of America Bulletin, v. 87, p. 1397–1410.

Morris, H.T., 1978, Unprospected zone of pyritic alteration in west-central Utah: U.S. Geological Survey Open-File Report 78–791, 8 p.

_____1983, Interrelations of thrust and transcurrent faults in the central Sevier orogenic belt near Leamington, Utah, *in* Miller, D.M., Todd, V.R., and Howard, K.A., eds., Tectonic and stratigraphic studies in the Great Basin: Geological Society of America Memoir 157, p. 75–81.

_____1987, Generalized geologic map of the Delta 2° quadrangle, Tooele, Juab, Millard, and Utah Counties, Utah: U.S. Geological Survey Open-File Report 87–185, scale 1:250,000.

Plavidal, K.R., 1987, The geology and petrology of the eastern Keg Mountains, Juab County, Utah: Salt Lake City, University of Utah, M.S. thesis, 137 p.

Roddick, J.S., 1983, High precision intercalibration of $^{40}Ar/^{39}Ar$ standards: Geochimica et Cosmochimica Acta, v. 47, p. 887–898.

Samson, S.D., and Alexander, C.E., 1987, Calibration of the interlaboratory $^{40}Ar/^{39}Ar$ dating standard, MMhb–1: Isotope Geoscience, v. 66, p. 27–34.

Shawe, D.R., 1972, Reconnaissance geology and mineral potential of the Thomas, Keg, and Desert calderas, central Juab County, Utah: U.S. Geological Survey Professional Paper 800–B, p. B67–B77.

Shawe, D.R., and Snyder, D.B., 1988, Ash-flow eruptive megabreccias of the Manhattan and Mount Jefferson Calderas, Nye County, Nevada: U.S. Geological Survey Professional Paper 1471, 28 p.

Shawe, D.R., and Stewart, J.H., 1976, Ore deposits as related to tectonics and magmatism, Nevada and Utah: American Institute of Mining Engineers, Annual Meeting, Las Vegas, Nevada, 1977, Transactions, v. 260, p. 225–232.

Staatz, M.H., and Carr, W.J., 1964, Geology and mineral deposits of the Thomas and Dugway Ranges, Juab and Tooele

Counties, Utah: U.S. Geological Survey Professional Paper 415, 188 p.

Staub, A.M., 1975, Geology of the Picture Rock Hills quadrangle, Juab County, Utah: Salt Lake City, University of Utah, M.S. thesis, 87 p.

Steiger, R.H., and Jäger, E., 1977, Subcommission on geochronology; convention on the use of decay constants in geo- and cosmochronology: Earth and Planetary Science Letters, v. 36, p. 359–354.

Stewart, J.H., Moore, W.J., and Zietz, Isidore, 1977, East-west patterns of Cenozoic igneous rocks, aeromagnetic anomalies, and mineral deposits, Nevada and Utah: Geological Society of America Bulletin, v. 88, no. 1, p. 67–77.

Yambrick, R.A., and Snee, L.W., 1989, Early Oligocene calc-alkaline and middle Miocene bimodal volcanism, Simpson Mountains, west-central Utah: Geological Society of America Abstracts with Program, v. 21, no. 7, p. A245.

Chapter H

Structural Setting of the Chief Mining District, Eastern Chief Range, Lincoln County, Nevada

By PETER D. ROWLEY, LAWRENCE W. SNEE, HARALD H. MEHNERT, R. ERNEST ANDERSON, GARY J. AXEN, KELLY J. BURKE, F. WILLIAM SIMONDS, RALPH R. SHROBA, and STEPHEN D. OLMORE

U.S. GEOLOGICAL SURVEY BULLETIN 2012

APPLICATION OF STRUCTURAL GEOLOGY TO MINERAL AND ENERGY RESOURCES OF THE CENTRAL AND WESTERN UNITED STATES

CONTENTS

FIGURES

TABLE

Structural Setting of the Chief Mining District, Eastern Chief Range, Lincoln County, Nevada

By Peter D. Rowley[1], Lawrence W. Snee[2], Harald H. Mehnert[2], R. Ernest Anderson[3], Gary J. Axen[4], Kelly J. Burke[5], F. William Simonds[1], Ralph R. Shroba[1], *and* Stephen D. Olmore[6]

Abstract

The Chief Mining District produced at least 2,000 ounces of gold, 11,000 ounces of silver, and minor amounts of lead and copper between 1870 and the 1960's. The production was from fissure-vein precious-metal deposits containing highly oxidized mineral aggregates within breccia zones of mostly low-angle faults. The main veins consist of scorodite and related minerals that replaced arsenopyrite and of barite, galena, quartz, and iron- and manganese-oxide minerals. The deposits probably represent the lower part of an epithermal gold-silver system that was subsequently deeply eroded. The likelihood of finding additional precious-metal economic orebodies is not good, but the district has potential for a porphyry-copper deposit.

Most veins are in Proterozoic and Cambrian quartzite (Stirling Quartzite, Wood Canyon Formation, Zabriskie Quartzite) and Cambrian limestone (Highland Peak Formation). A large shallow intrusive body of quartz monzonite porphyry, the Cobalt Canyon stock, underlies the district and was the source of the mineralizing fluids, perhaps from convective cells of heated meteoric water. $^{40}Ar/^{39}Ar$ dates for minerals in the stock average 24.8 Ma; the stock may represent an early phase of igneous activity in the Caliente caldera complex, whose boundary is about 4 km south of the mining district.

The Chief Mining District is near the western end of the east-trending Delamar–Iron Springs mineral belt. This belt may have resulted from igneous activity along early Tertiary east-striking faults, which also may have defined other east-striking structural features in the area including the Timpahute Lineament, which intersects the mining district. Other epithermal gold districts in and near the Caliente caldera complex also contain east-striking features that suggest that younger (reactivated) faulting, igneous activity, and mineralization were all locally controlled by east-striking faults.

Recent detailed geologic mapping demonstrates at least three episodes of Tertiary extensional faulting in the district. The oldest episode of faulting was along the low-angle Stampede Detachment Fault Zone, a major east-dipping structure of pre–late Oligocene age (pre-32 Ma), with upper plate movement to the east, that separates Zabriskie Quartzite in the lower plate from Highland Peak Formation in the upper plate. Faults of this episode provided sites for fissure-vein orebodies. The second episode of extensional faulting took place in the Miocene (by at least 19 Ma and continuing to less than 12 Ma) and is characterized by high-angle strike-slip, oblique-slip, and normal faults and, outside the district, by detachment faults. An early phase of this episode may have controlled emplacement of the Cobalt Canyon stock and thus epithermal mineralization. The youngest episode, basin-range faulting, formed much of the present topography; the faults strike north, postdate basalts of 12 Ma, and also cut basin-fill sedimentary rocks of the Panaca Formation (as young as 3 Ma) and Quaternary deposits.

INTRODUCTION

The Chief Mining District in Lincoln County, Nevada, also known as the Caliente Mining District, produced at least 2,000 ounces of gold, 11,000 ounces of silver, and minor amounts of lead and copper between 1870 and the 1960's. The metals came from a cluster of mines (fig. 1) in a 6-km^2 area on the eastern side of the Chief Range, about 8 km north of Caliente, Nevada. Orebodies are in quartzite of Late Proterozoic and Early Cambrian age and limestone and dolomite of Early and Middle Cambrian age; the ore resulted from emplacement of a quartz monzonite porphyry stock of

[1]U.S. Geological Survey, Box 25046, MS 913, Denver, Colorado 80225.
[2]U.S. Geological Survey, Box 25046, MS 963, Denver, Colorado 80225.
[3]U.S. Geological Survey, Box 25046, MS 966, Denver, Colorado 80225.
[4]Department of Earth and Planetary Science, Harvard University, Cambridge, Massachusetts.
[5]Department of Geology, Northern Arizona University, Flagstaff, Arizona.
[6]U.S. Geological Survey, Ciudad Bolivar, Venezuela.

Oligocene age. This report summarizes the structural control on the orebodies based on data collected during detailed bedrock mapping. It also includes preliminary $^{40}Ar/^{39}Ar$ dates that constrain the timing of faulting and mineralization.

The Chief Mining District is in the eastern Great Basin (fig. 2) at the western end of the east-trending Delamar–Iron Springs mineral belt of Shawe and Stewart (1976). The Chief Range is a basin range bounded on the east by the deep Panaca fault-block basin. The main locus of igneous activity in the area is the large Tertiary Caliente caldera complex of Nevada and Utah; the northern rim of this complex is as close as 4 km to the mining district.

Prior to our studies, the only geologic information published on the Chief Mining District was a report based on a reconnaissance study of the orebodies by a master geologist, Eugene Callaghan, that was written in 1936 while production in the district was declining. As far as we know, production ceased in the 1960's and the mining district was subsequently abandoned; few buildings remain standing (fig. 1), and, because most shafts, adits, and tunnels have collapsed, few orebodies are accessible. Even where freshly exposed, most orebodies are extensively oxidized and the ore minerals are complex hydrous oxides that are difficult to identify without extensive microscopic and geochemical study, which we have not done. Thus we cannot contribute much additional information on the orebodies, except for chemical analyses of grab samples (table 1). Much later than Callaghan's study, the geologic setting of the area was established by milestone reconnaissance 1:250,000-scale geologic maps of Lincoln County, Nevada, by Tschanz and Pampeyan (1970) and Ekren and others (1977).

The new data in this report result from two 1:24,000-scale geologic mapping projects. The first, beginning in 1985, involved structural studies by G.J. Axen (University of Northern Arizona and Harvard University) and his students in the Highland Range and nearby areas about 10–15 km north of the Chief Mining District and their collaboration with J.M. Bartley (University of Utah), W.J. Taylor (University of Utah), and D.R. Lux (University of Maine at Orono) who worked in the North Pahroc Range, southern Schell Creek Range, and southern Fairview Range, about 30 km west and north-northwest of the mining district. The purpose of this work was to define geometry, timing, and mechanisms of Tertiary extension in the area, the products of which include two major detachment fault zones, the older Stampede Detachment and the younger Highland Detachment (Axen and others, 1988). In order to understand these fault zones, the Paleozoic stratigraphy of the area was refined. Mapping progressed southward, the most recent being that of Burke (1991) in the northern Chief Range. The second project, beginning in 1986, involved quadrangle mapping by the U.S. Geological Survey (USGS) near Caliente in an effort to understand the evolution of the Caliente caldera complex. This project was later incorporated into a major USGS mapping project that encompasses the Basin and Range–Colorado Plateau (BARCO) transition zone in southeastern Nevada and southwestern Utah. Mapping of the Caliente caldera complex started along its northwestern margin in the Indian Cove quadrangle (Rowley and Shroba, 1990, 1991), just east of the mining district, and in the Eccles (R.E. Anderson, unpub. data, 1988) and Caliente quadrangles (P.D. Rowley, unpub. data, 1988), southeast and south of the mining district. Later mapping of the Chief Mountain quadrangle (Rowley and others, 1991), which embraces the mining district and most of the Chief Range, as well as mapping of the Pahroc Spring SE quadrangle (Swadley and Rowley, 1992) and mapping in progress of the Caliente NW, Delamar, and Dow Mountain quadrangles, provides additional geologic framework for this report.

Six new $^{40}Ar/^{39}Ar$ mineral dates from three samples and one K-Ar mineral date from one sample help to constrain temporal relationships in the Chief Mining District. These data are part of a larger K-Ar and $^{40}Ar/^{39}Ar$ geochronologic study being done within the context of the BARCO project. The $^{40}Ar/^{39}Ar$ isotopic dating method is a variant of the conventional K-Ar method; for $^{40}Ar/^{39}Ar$ analysis, samples are irradiated in a nuclear reactor to produce ^{39}Ar from ^{39}K. In this study, 50–100 mg of sanidine and biotite and about 300 mg of hornblende were irradiated in the USGS Denver TRIGA reactor for 30 hours at 1 megawatt. Each sample was irradiated adjacent to an aliquant of standard MMhb–1 hornblende for which K=1.555 percent, $^{40}Ar_K=1.624\times10^{-9}$ mol/g, and K-Ar date=520.4 Ma (Samson and Alexander, 1987). Samples were experimentally degassed in a double-vacuum resistance furnace via step heating in 12–15 steps under ultra-high vacuum for about 20 minutes at each temperature step. The mass 40, 39, 38, 37, and 36 isotopes of argon were analyzed using a Mass Analyser Products series 215 rare-gas mass spectrometer. Raw isotopic data were corrected for volume, mass discrimination, trap current, radioactive decay of ^{37}Ar and ^{39}Ar, and interfering isotopes of argon. Decay constants of Steiger and Jäger (1977) were used to recalculate dates of any cited samples that were analyzed before 1977. Our preliminary ages were first reported in Rowley, Snee, and others (1990) and Snee and others (1990). Isotopic data are available from the authors.

Classifications of volcanic and plutonic rocks are those of the International Union of Geological Sciences (Le Bas and others, 1986, and Streckeisen, 1976, respectively). Relative offset on some faults that contain slickensides was determined using the methods of Angelier and others (1985) and Petit (1987).

Acknowledgments.—We gratefully acknowledge numerous helpful discussions with R.B. Scott concerning the structural setting and regional stratigraphy, with G.B. Allen and S.P. Bingham (both of Alma American Mining Corporation), J.E. Elliott, and E.B. Ekren regarding epithermal mineral deposits, and with W C Swadley pertaining to surficial deposits. We thank R.B. Blakestad and R.R. Kern (both of Homestake Mining Company) for access to company-

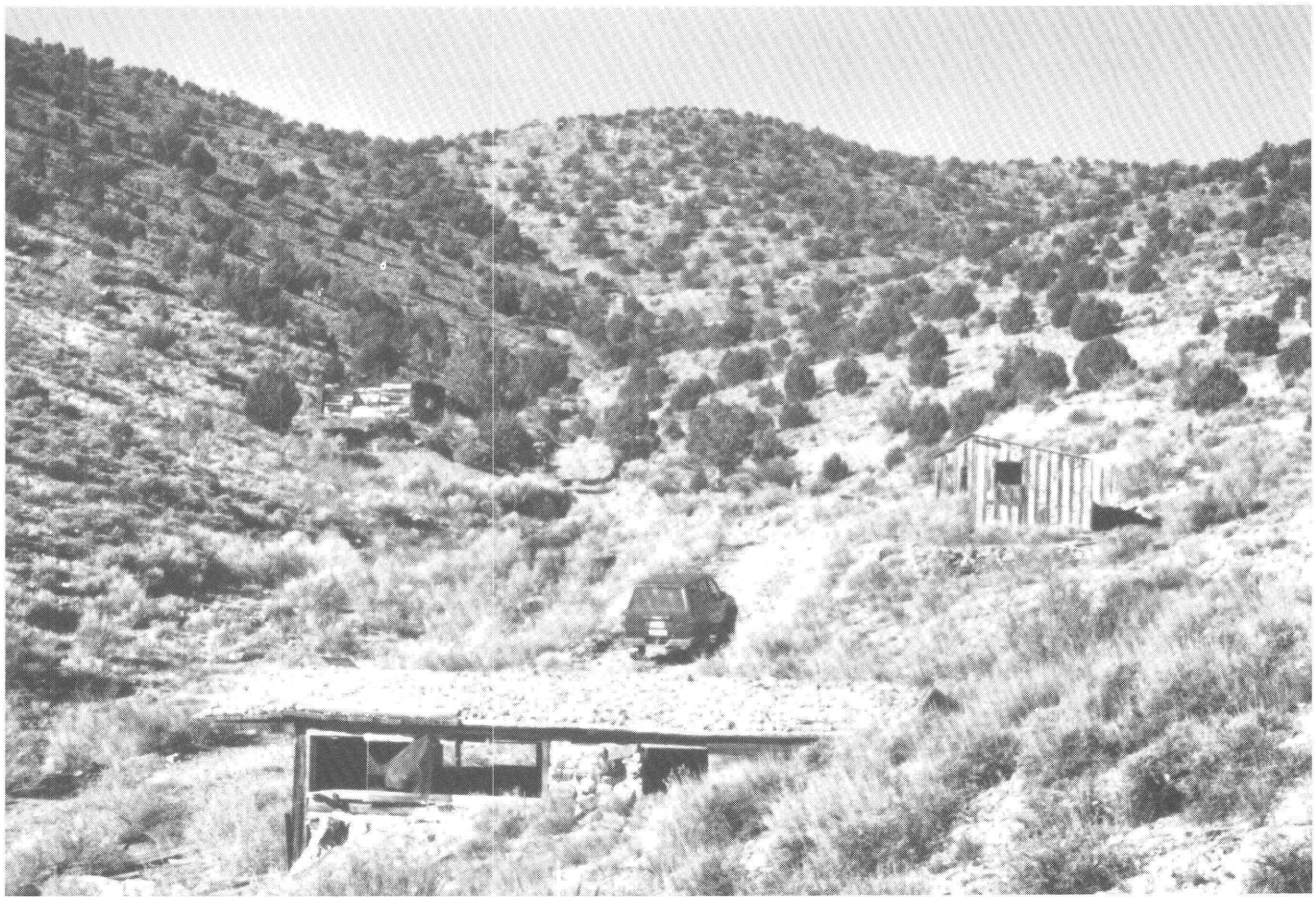

Figure 1. Photograph, looking west, showing mines in upper Cobalt Canyon, Chief Mining District, Lincoln County, Nevada. Building to right of car was a former boarding house, and building farther up the canyon and to left is at entrance to tunnel of the Contact Mine; both are underlain by Highland Peak Formation, beyond which are Stirling Quartzite, Wood Canyon Formation, and Zabriskie Quartzite. A dump at the Gold Stake Mine is farther up canyon. The Advance Mine is in gulch left of central hill on horizon, and the Old Democrat Mine is at bottom of gulch to right of central hill.

confidential data on the Chief Mining District, and we are grateful to these geologists and to Homestake for permission to publish some of those data, as identified in the text. We thank J.L. Askey and J.B. Harlan (both of FMC Gold Company), Charley Martin (Worldwide Resources), and R.R. Kern for information on the Taylor (Easter) Mine. Inclusion of chemical analysis of mineralized and altered rock samples (table1) would not have been possible without the kind cooperation and rapid work of B.M. Adrian, R. Hill, D.E. Detra, R.M. O'Leary, R.W. Leinz, and C.M. McDougal of the USGS, and dating could not have been done without mineral separations by D.M. Cheney. Mapping in the northern Chief Range and adjacent areas by Axen and Burke was partly funded by grants to them from Texaco, Marathon, and Mobil oil companies, by grants to Burke from Sigma Xi and Northern Arizona University, and by National Science Foundation Grant EAR–14455–AC2 to J.M. Bartley (University of Utah). Editorial assistance was provided by C.H. Thorman and K.S. Kellogg. We thank C.H. Thorman for technical review of the manuscript and Ron, Betty, Chad, and Brenda Young of Caliente for help and many kindnesses during our field work.

HISTORY AND PRODUCTION

The date when the first ore deposits in the Chief Mining District were found is unknown, but it probably was shortly after the initial discoveries in 1868 in the Pioche Mining District, 27 km to the north (Callaghan, 1936). The Chief district was organized in 1870 and had an estimated production of $25,000 during the next few years. Production records for the district are incomplete. The first recorded shipment of ore was in 1896, followed by shipments of unknown value in subsequent years (Callaghan, 1936). An estimated 2,000 ounces of gold, 11,000 ounces of silver, 45,000 pounds of lead, and 2,000 pounds of copper, with a total value of about $70,000, were tabulated for the period 1907–1953 (Callaghan, 1936, table 1; Tschanz and Pampeyan, 1970, table 28). There is little information on production from individual

Table 1. Chemical analyses of grab samples of hydrothermally altered and mineralized rocks from the Chief Mining District, Lincoln County, Nevada

[Flame atomic absorption analyses of Te, Tl, and Au by R. Hill, R. O'Leary, and B.H. Roushey; DC-ARC AES analyses of other elements by B.M. Adrian, D. Detra, and R.T. Hopkins. Ca, Fe, Mg, Na, and Ti in percent, all other values in parts per million. Lower limit of determination of each element given in parentheses. N, not detected at limit of detection; H, interference; <, detected, but below limit of detection; >, greater than. P at or below limit of detection except in samples 777 (0.5 percent) and 812 (0.2 percent); Bi not detected except in sample 781 (15 ppm); Ge, Sn, and Th not detected; Nb at or below limit of detection except in sample 812 (20 ppm); W only detected in sample 781 (20 ppm)]

Sample number	378a	469b	751	765	777	778	781	793	794	802	812	866	1121c	1122a
							Chemical analyses of samples							
Te (0.05)	N	N	N	0.4	1.4	3.6	0.9	1.7	0.2	<	N	0.1	N	N
Tl (0.05)	<	0.35	0.15	0.35	0.95	0.2	0.3	0.2	2.2	3.1	0.5	2.8	0.55	0.45
Au (0.05)	N	N	N	N	N	N	1.1	N	1.1	N	N	0.05	N	N
Ca (0.05)	0.2	>20	0.2	0.15	0.5	0.05	<	15	10	7	0.2	1	1.5	5
Fe (0.05)	2	1	0.7	2	3	20	7	7	2	7	0.3	7	5	7
Mg (0.02)	0.3	1.5	0.1	0.7	0.1	0.03	0.1	0.3	2	2	0.3	0.3	1	3
Na (0.2)	N	<	<	2	N	<	0.2	N	<	<	0.2	0.5	>5	5
Ti (0.002)	0.3	0.07	0.02	0.5	0.07	0.02	0.2	0.03	0.007	0.1	1	0.02	0.5	0.7
Ag (0.5)	N	N	N	<	1	5	20	1	10	<	<	100	N	N
As (200)	N	N	N	N	500	10,000	10,000	300	500	200	N	300	N	N
B (0.10)	N	10	10	70	50	10	2,000	15	15	50	150	70	<	<
Ba (20)	70	30	70	300	1,000	700	100	200	5,000	2,000	150	500	1,000	1,000
Be (1)	2	<	2	<	5	<	2	<1	<1	<	2	1.5	<1	1
Cd (20)	N	N	N	N	70	N	N	N	N	N	N	70	N	N
Co (10)	10	N	<	<	15	N	15	10	<	N	N	10	15	20
Cr (10)	100	10	10	<	<	10	150	<	<	15	70	20	50	50
Cu (5)	20	5	5	5	500	50	100	15	30	7	5	150	30	30
Ga (5)	5	15	N	70	N	H	20	N	7	15	50	7	50	50
La (50)	<	N	N	70	100	N	50	N	N	N	100	N	100	100
Mn (10)	150	700	200	100	>5,000	50	2,000	5,000	5,000	5,000	200	5,000	300	1,000
Mo (5)	N	N	N	N	15	10	50	<	10	15	N	N	N	N
Ni (5)	20	5	5	<	70	<	7	10	7	5	<	5	15	20
Pb (10)	20	10	N	30	20	10,000	20,000	500	10,000	100	50	15,000	50	50
Sb (100)	N	N	N	N	<	200	700	<	<	N	N	150	N	N
Sc (5)	7	10	<	10	N	N	10	7	<	5	10	5	7	15

Table 1. Chemical analyses of grab samples of hydrothermally altered and mineralized rocks from the Chief mining district, Lincoln County, Nevada—Continued

Sample number	378a	469b	751	765	777	778	781	793	794	802	812	866	1121c	1122a
Sr (100)	<	200	<	200	500	150	1,000	100	1,000	200	N	100	300	700
V (10)	100	<	20	100	100	100	100	20	15	50	150	500	100	150
Y (10)	15	15	<	20	30	N	10	20	15	15	20	15	20	30
Zn (200)	N	N	N	N	700	300	15,000	500	3,000	500	N	10,000	N	N
Zr (10)	150	50	10	150	100	10	200	10	<	50	300	70	200	200

Lithology and location of samples

378a	Fault zone between Zabriskie Quartzite and Cobalt Canyon stock, lat 37°40'09" N., long 114°31'31" W.
469b	Metamorphosed limestone at contact with Cobalt Canyon stock, lat 37°39'33" N., long 114°30'51" W.
751	Hydrothermally altered and quartz veined Cobalt Canyon stock, lat 37°40'36" N., long 114°30'14" W.
765	Hydrothermally altered local lava flows and tuffs near contact with Cobalt Canyon stock, lat 37°41'11" N., long 114°30'58" W.
777	Quartz veins, mineralized rocks in Zabriskie Quartzite from prospect pit 250 m east of Gold Stake vein, lat 37°41'19" N., long 114°31'38" W.
778	Quartz veins and mineralized rocks in Wood Canyon Formation from a shaft on Gold Stake vein, lat 37°41'16" N., long 114°31'46" W.
781	Mineralized quartz veins on north side of a shaft of Republic Mine, lat 37°41'17" N., long 114°32'03" W.
793	Mineralized rocks in Highland Peak Formation brecciated by Stampede Detachment, from dump of SOA Mine, lat 37°41'56" N., long 114°31'17" W.
794	Mineralized vein in Highland Peak Formation at entrance to Gold Chief Mine, lat 37°41'50" N., long 114°31'20" W.
802	Mineralized vein in fault zone in Highland Peak Formation at Lucky Chief No. 3 Pit, lat 37°41'51" N., long 114°32'01" W.
812	Hydrothermally altered Cobalt Canyon stock, lat 37°42'17" N., long 114°32'05" W.
866	Mineralized rocks in fault zone of Lucky Hobo Mine, lat 37°41'42" N., long 114°31'51" W.
1121c	Hydrothermally altered Cobalt Canyon stock, lat 37°40'29" N., long 114°30'04" W.
1122a	Sulfide minerals in hydrothermally altered chilled contact of Cobalt Canyon stock, lat 37°40'34" N., long 114°30'16" W.

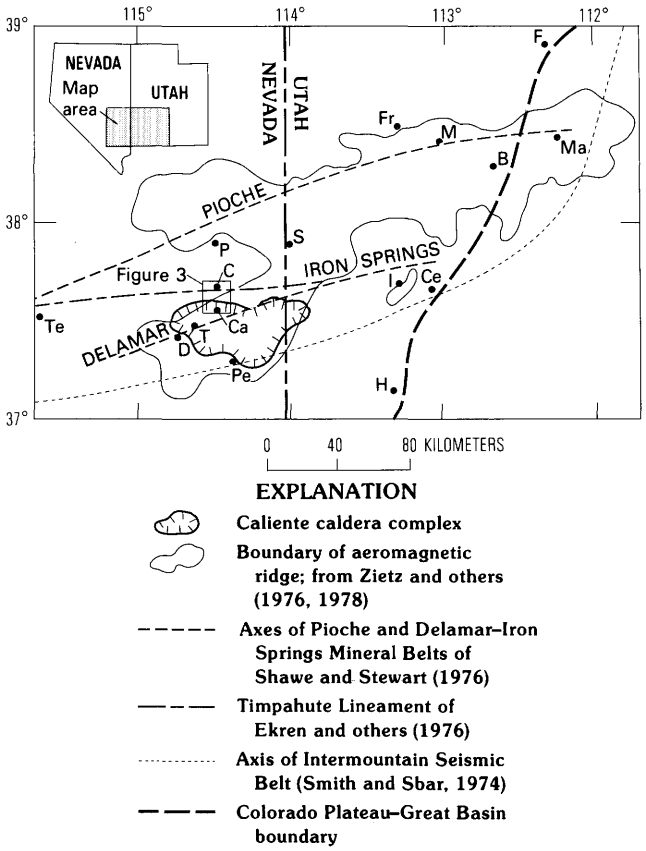

Figure 2. Tectonic setting of Chief Mining District, Lincoln County, Nevada. B, Beaver; C, Chief Mining District; Ca, Caliente; Ce, Cedar City; D, Delamar; F, Fillmore; Fr, Frisco; H, Hurricane; M, Milford; Ma, Marysvale; P, Pioche; Pe, Pennsylvania Mining District; S, Stateline Mining District; T, Taylor (Easter) Mine; Te, Tempiute Mining District.

mines other than some records that show that the Gold Chief Mine was by far the principal producer and the largest mine in the district. By 1911, the Gold Chief had an inclined shaft about 130 m long and drifts totalling about 300 m in length (Callaghan, 1936). Production was insignificant after 1941, and mining probably ceased in the 1960's. As a result of renewed interest in heap-leach processing of disseminated gold ore, claims recently were staked throughout the district as well as in the area adjacent to the main mass of the Cobalt Canyon stock (described below), which is centered about 1.5 km south of the district. An area north of the Lucky Hobo Mine was apparently drilled by Texas Gulf International in 1982 (Tingley, 1984). Homestake Mining Company did a geologic and geochemical study, authored by S.D. Olmore, of the district in 1985, including 12 reverse-circulation drill holes.

Prospects on the northern town limits of Caliente are considered to be part of the Chief Mining District (Tingley, 1984), but, because no production records are known for the area near these prospects and no orebodies are exposed there, they are not discussed in this report.

GEOLOGY

Stratigraphy

Most rocks in the Chief Mining District (fig. 3) consist of resistant, reddish-brown, pink, gray, and white, mostly thin-bedded, planar and crossbedded, dense, vitreous orthoquartzite correlated by Callaghan (1936) with the Prospect Mountain Quartzite of Late Proterozoic and Early Cambrian age (details on regional stratigraphy of this and other Paleozoic units in the area are in Merriam, 1964, and Tschanz and Pampeyan, 1970). Stewart (1974, 1984) measured a stratigraphic section through this continental and near-shore marine quartzite sequence in Antelope Canyon, 6 km south of the district, and correlated it with Stirling Quartzite of Late Proterozoic age, Wood Canyon Formation of Late Proterozoic and Early Cambrian age, and Zabriskie Quartzite of Early Cambrian age. We followed Stewart's stratigraphy in our mapping. The Stirling Quartzite is composed of light-colored, unfossiliferous, generally pure quartzite that is typically coarser grained than the two younger formations and is at least 600 m thick (base not exposed); a prominent basalt lava flow is in its upper part. The Wood Canyon Formation is a dark-colored sequence of interbedded quartzite, siltstone, and shale that is about 320 m thick and that contains animal tracks, burrows, and a thin basalt flow in its upper part. The Zabriskie Quartzite is mostly white, pure quartzite that is as thick as 140 m and that contains local animal tracks and burrows.

The Lower and Middle Cambrian Pioche Shale conformably overlies the Zabriskie Quartzite and is well exposed in an incomplete section in and north of Antelope Canyon. It consists of a soft, green, locally fossiliferous, micaceous marine shale and subordinate siltstone, sandstone, and limestone and is as thick as 250 m in the Pioche area. Conformably overlying the Pioche in the Antelope Canyon area are two thin Middle Cambrian marine units, the Lyndon Limestone, a resistant medium- and dark-gray limestone about 20 m thick, and the Chisholm Shale, a soft brown nonmicaceous shale about 30 m thick.

Lower parts of Middle and Upper Cambrian Highland Peak Formation are exposed in the Antelope Canyon area. This formation consists of resistant, light- to dark-gray, black, and white, marine limestone and dolomite that has a maximum thickness of about 1,500 m in the Pioche area (Merriam, 1964). Numerous members have been mapped north and west of the Chief Range, where they are well

Figure 3 (facing page). Generalized geology of Chief Mining District and vicinity, Lincoln County, Nevada. A, Advance Mine; C, Contact Mine; G, Gold Chief Mine; H, Lucky Hobo Mine; L, Lucky Chief Mine; O, Old Democrat Mine; R, Republic Mine; S, Gold Stake Mine; So, SOA Mine.

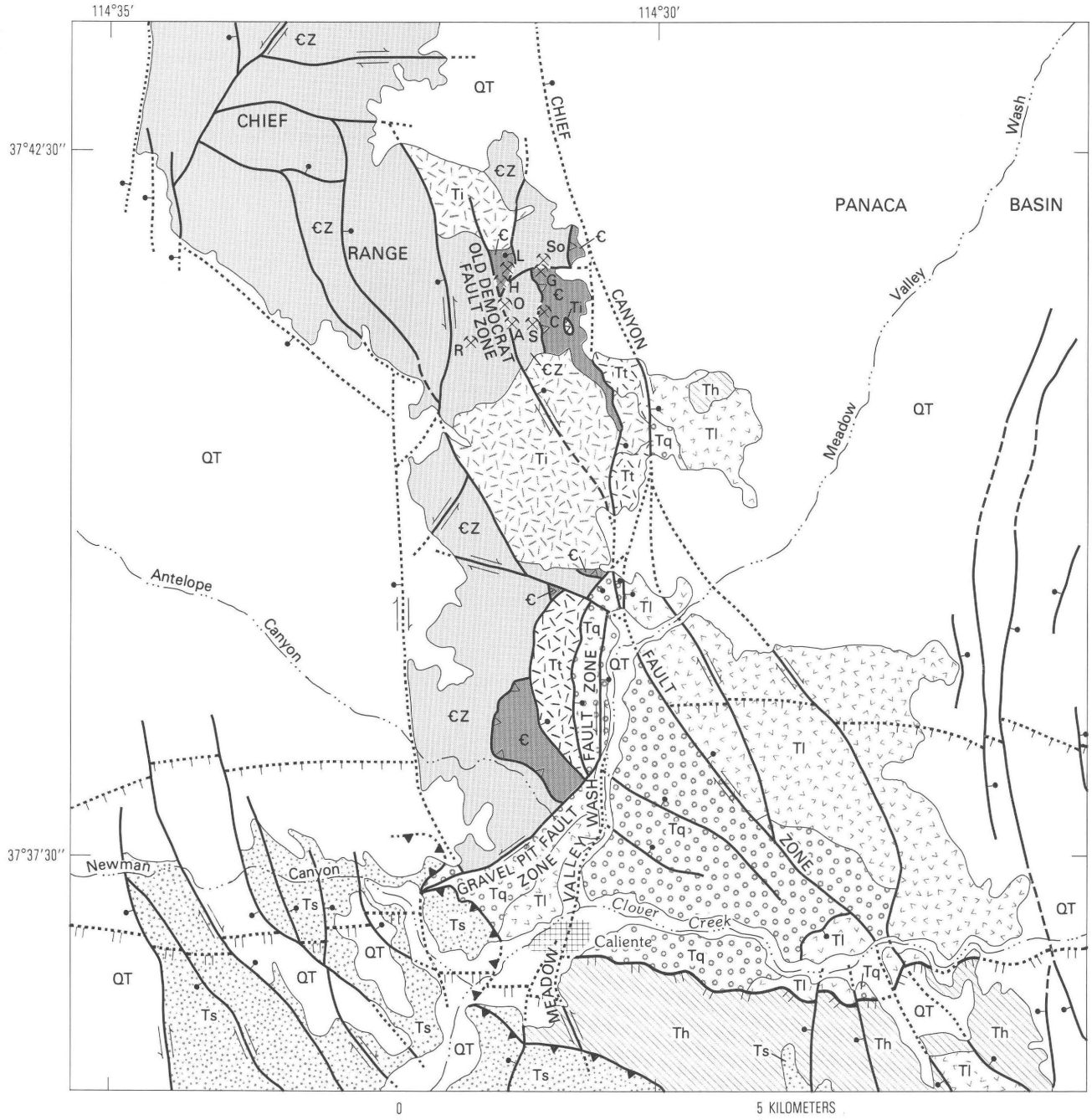

EXPLANATION

Cenozoic

- QT — Surficial and basin-fill sediments
- Ts — Tuffs and sedimentary rocks of 14–12 Ma
- Th — Hiko Tuff
- Tl — Lava flows of Indian Cove
- Tq — Quichapa Group
- Ti — Cobalt Canyon stock
- Tt — Oligocene tuffs and lava flows
- € — Cambrian limestone and shale
- €Z — Cambrian and Proterozoic quartzite
- **High-angle fault**—Dashed where approximately located, dotted where concealed
- **Newman Canyon Detachment**—Teeth on upper plate
- **Stampede Detachment**—Teeth on upper plate
- **Delamar caldera**—Dotted where concealed
- **Clover Creek caldera**—Concealed

exposed (Axen, 1986; Lewis, 1987; Axen and others, 1988; Sleeper, 1989; Burke, 1991), but in the Antelope Canyon area only the basal Peasley Member and overlying Burrows Member (Merriam, 1964) are exposed. In the mining district, light-gray limestone only about 50 m thick is exposed; it is contact metamorphosed by the underlying Cobalt Canyon stock (see below) and can only be assigned tentatively to the Highland Peak Formation.

Tertiary volcanic rocks unconformably overlie Proterozoic and Cambrian units in an area north of Antelope Canyon that is within 3 km of the southern margin of the mining district. Most of the volcanic rocks here are complexly faulted by a series of oblique-, normal-, and strike-slip faults; these same rocks are better exposed west of the Chief Range. The lowest volcanic unit (Oligocene) in the faulted area north of Antelope Canyon consists of hydrothermally altered local lava flows and tuffs intertongued and overlain by the Isom Formation, which consists of a series of mostly brown, crystal-poor, trachytic, regional ash-flow tuffs with a probable caldera source on the northern side of Escalante Valley north of Modena, Utah, and has a $^{40}Ar/^{39}Ar$ date of about 27 Ma (Best, Christiansen, and Blank, 1989).

The overlying Quichapa Group contains, in ascending order, regional ash-flow sheets of the Leach Canyon Formation, Swett and Bauers Tuff Members of the Condor Canyon Formation, and Harmony Hills Tuff (Anderson and Rowley, 1975). The Leach Canyon Formation is a soft, pink, poorly to moderately welded, crystal-poor, rhyolite ash-flow tuff; it has an average age of 24.0 Ma based on three K-Ar dates on biotite, sanidine, and plagioclase by Armstrong (1970) and two fission-track dates on zircon by Kowallis and Best (1990), but there is significant variation in these dates (26.7–21.6 Ma). The Swett and Bauers Tuff Members are resistant, reddish-brown and light-purple, densely welded, crystal-poor, rhyolitic ash-flow tuff; the Bauers has two $^{40}Ar/^{39}Ar$ dates averaging 22.8 Ma (Best, Christiansen, and others, 1989, table R3). The Harmony Hills Tuff is a resistant, greenish-gray, moderately welded, crystal-rich, andesitic ash-flow tuff that has a probable age of about 22.5–22 Ma based on isotopic dates on overlying (Rowley and others, 1989) and underlying rocks.

A sequence of resistant, fresh, mostly gray, red, and brown lava flow rocks and subordinate flow breccia and volcanic mudflow breccia and minor fluvial sandstone rests unconformably on the Harmony Hills or older rocks 2.5 km southeast of the mining district. This sequence was named the lava flows of Indian Cove (Rowley and Shroba, 1991) for the area where it attains its greatest thickness (about 500 m) 5 km southeast of the mining district. It probably formed as isolated or coalesced volcanic domes composed of high-alkali andesite and trachyandesite and subordinate high-alkali dacite and trachydacite. A lava flow from the unit yielded a Miocene plateau $^{40}Ar/^{39}Ar$ date on sanidine of 21.9±0.1 Ma (L.W. Snee, preliminary unpub. data, 1990; Snee and others, 1990). Pinching out against this dome complex, but locally exposed on its northern flank about 2.5 km southeast of the mining district (Rowley and Shroba, 1991), is resistant, tan, poorly to moderately welded, crystal-poor, rhyolite ash-flow tuff of the Hiko Tuff (Dolgoff, 1963), which has an average $^{40}Ar/^{39}Ar$ date of 18.6 Ma (Taylor and others, 1989). Locally derived sedimentary rocks and interbedded ash-flow tuff of the Kane Wash Tuff (14 Ma; Novak, 1984) overlie the Hiko Tuff south and west of Caliente and are in turn overlain by the tuff of Etna (which we earlier miscorrelated with the Ox Valley Tuff of Cook, 1960); these units are included in unit Ts of figure 3.

The youngest rocks in the area (unit QT of fig. 3) are fluvial and lacustrine sedimentary rocks exposed in areas surrounding the Chief Range. Most of these sedimentary rocks are basin-fill deposits associated with the youngest (basin-range) episode of extensional faulting, but sandstone, conglomerate, and air-fall tuff at least 200 m thick (sedimentary rocks of Newman Canyon of Rowley and others, 1991) that predate basin-fill sedimentary rocks south of the Chief Range and overlie the tuff of Etna have yielded a K-Ar date on sanidine of 13.8±0.9 Ma (H.H. Mehnert, preliminary unpub. data, 1990; Snee and others, 1990). Among the basin-fill deposits, the most extensive unit fills the Panaca Basin east of the mining district. This unit consists of soft, tan, salmon, and light-green sandstone, limestone, siltstone, mudstone, and claystone of the upper Miocene and Pliocene Panaca Formation. Only the upper part, about 400 m thick, of the formation is exposed (Rowley and Shroba, 1991) and based on vertebrate fossils it is as young as the Blancan III mammalian age of 3.7–3.2 Ma (Repenning, 1987). Overlying the Panaca Formation are mostly coarse grained surficial deposits ranging in age from Pliocene to Holocene. Chief among these deposits is a series of alluvial-fan deposits of different ages that underlie five or more well-expressed geomorphic surfaces. In contrast to the fine-grained sediments of the Panaca Formation that were deposited in a closed basin, these coarse sands, gravels, and fanglomerates, as well as rounded fluvial gravels, are interpreted to represent deposition following the development of through-flowing drainage in the Panaca Basin via Meadow Valley Wash to the Colorado River, which is about 170 km south of the mining district.

Intrusive Rocks

A large, irregular, discordant intrusive mass of quartz monzonite porphyry, herein called the Cobalt Canyon stock, underlies most of the Chief Mining District at shallow depth and is exposed as plutons, plugs, dikes, sills, and faulted slivers within and near the district. Hydrothermal solutions from the stock and (or) circulating meteoric groundwater heated by the stock are believed to be the source of most metals in the district. Callaghan (1936) was the first to map parts of the stock and to recognize its association with the orebodies.

Ekren and others (1977) mapped the main mass of the stock, which is centered about 1.5 km south of the district. Our mapping reveals separate plutons, plugs, dikes, and sills (fig. 3) and interprets these bodies to be apophyses of one stock at depth. In addition to the plutonic rocks shown in figure 3, dikes, small plugs, and faulted slivers of the same lithology have been noted in several mines and prospects. From north to south, these bodies include (1) a plug 250 m northeast of the entrance to the Gold Chief Mine (Callaghan, 1936, fig. 2) and drill-hole cuttings (Homestake Mining Company) of quartz monzonite porphyry on the road (from a drill hole sited on the road) 100 m southeast of that mine, which indicate the presence of plutonic rock at depth; (2) a silicified dike in "the fault west of the Gold Chief Mine" (presumably the Stampede Detachment, which is exposed here) and a sill in limestone just south of the mine (Callaghan, 1936, p. 10); (3) drill-hole cuttings of pyrite-bearing porphyry on the road 450 m southeast of the entrance to the Gold Chief Mine; (4) several plugs near the Lucky Hobo Mine (Callaghan, 1936, fig. 2, p. 29) and an altered dike along the Stampede Detachment exposed in a prospect trench about 200 m west of the mine; (5) a "lens" exposed in the main shaft and samples from the dump of the Old Democrat Mine (Callaghan, 1936, p. 24); (6) chips of porphyry next to a vertical shaft along the road in the bottom of Cobalt Canyon less than 100 m east down the canyon from the Old Democrat Mine and drill-hole cuttings of fresh porphyry along the same road another 100 m down the canyon; (7) several plugs and dikes between the Advance and Contact Mines (Callaghan, 1936, fig. 2); (8) a plug on the ridge just south of the Contact Mine and an altered dike in the mine itself (Callaghan, 1936, p. 10, 21–23); and (9) a 1-m-wide dike in the Stampede Detachment exposed in a trench on top of the ridge just south of the Contact Mine.

Rock of the Cobalt Canyon stock is gray, tan, green, and khaki, locally grusy, quartz monzonite porphyry that consists of 35–55 percent phenocrysts of plagioclase, subordinate clinopyroxene, and minor biotite and iron-titanium oxide minerals in a fine-grained, holocrystalline groundmass of sanidine, subordinate to minor quartz, and minor clinopyroxene, iron-titanium oxide minerals, and biotite. The intrusive mass has fine-grained holocrystalline chilled margins and, in northwestern exposures, includes a large body of black, coarse-grained pyroxenite. Locally the intrusion is deuterically and hydrothermally altered at and near intrusive and fault contacts. The Cobalt Canyon stock is of Oligocene age, based on a 24.8-Ma average of two $^{40}Ar/^{39}Ar$ plateau dates on mineral separates, 24.9±0.1 Ma on sanidine and 24.7±0.1 Ma on biotite (L.W. Snee, preliminary unpub. data, 1990; Snee and others, 1990), from a sample collected from the chilled margin of the main mass about 1 km east-southeast of the district (Rowley and others, 1991).

A second variety of intrusive rock is named the porphyry of Meadow Valley Wash (Rowley and Shroba, 1990, 1991). The unit consists of widely scattered dikes and plugs, too small to be shown in figure 3, of high-alkali dacite that was intruded along major oblique-slip and strike-slip faults in the area. The light-gray and pink, locally grusy rock is characterized by large (as long as 2 cm) feldspar phenocrysts. The rock consists of about 35 percent phenocrysts of plagioclase, subordinate biotite, subordinate to minor sanidine, quartz, and hornblende, minor iron-titanium-oxide minerals, and traces of clinopyroxene, all in a glassy groundmass. It is named for exposures in the canyon of Meadow Valley Wash about 5 km south-southeast of the mining district, but the same rock has been mapped along a fault about 3 km south-southwest of the district, where it crops out along the Meadow Valley Wash and Chief Canyon Fault Zones. It also is present along the Gravel Pit Fault Zone and at several other locations in the northern Caliente caldera complex. Plugs of similar lithology were noted along a northwest-striking fault zone just east of Panaca Summit, about 30 km northeast of the mining district (unit Tp of Best and others, 1991), and in a major north-northwest-striking fault zone (Swadley and Rowley, 1992) on the northern side of the Delamar Mining District, about 30 km southwest of the Chief Mining District (P.D. Rowley, unpub. mapping, 1990). A sample from a dike of the porphyry of Meadow Valley Wash intruded along the Chief Canyon Fault Zone in the canyon of Meadow Valley Wash is Miocene in age, based on a 19.4-Ma average of two $^{40}Ar/^{39}Ar$ plateau dates on mineral separates, 19.3±0.1 Ma for a well-defined spectrum on sanidine and 19.5±0.1 Ma for a slightly less defined spectrum on hornblende; 22.5 Ma for a disturbed spectrum on biotite from the same sample was discounted (L.W. Snee, preliminary unpub. data, 1990; Snee and others, 1990).

Caliente Caldera Complex

The Caliente caldera complex contains two small epithermal gold districts and may control the large nearby Delamar epithermal gold district (see later discussion). The caldera complex is also the source of several ash-flow tuffs exposed near the Chief Mining District. Williams (1967) was the first to suggest, on the basis of regional stratigraphy and isopach data, that the Leach Canyon and Condor Canyon Formations were derived from centers in the Caliente-Panaca area. Noble and others (1968) and Noble and McKee (1972) did the first geologic reconnaissance study in this area and proposed that the Caliente depression, which they defined as a circular volcano-tectonic basin at least 32 km in diameter that extends from about 7 km east of Caliente eastward almost to the Utah State line, was the source of regional ash-flow sheets of the Harmony Hills, Racer Canyon, Hiko, and Ox Valley Tuffs. Reconnaissance mapping by Ekren and others (1977), combined with Bouguer gravity data, much refined the extent and location of the feature, which they called the Caliente caldron complex. Instead of being circular, they determined that it is elongated east-west (64 km by

29 km), extending from 25 km west of Caliente to almost the Utah State line, and that it is centered farther south than previously inferred; they recognized that the Hiko Tuff was derived from the western part of the complex.

Our detailed mapping in the north-central and northwestern parts of the complex and our reconnaissance studies in the northeastern part, combined with aeromagnetic and Bouguer gravity data (Blank and Kucks, 1989), indicate that the Caliente caldera complex extends into Utah and thus is somewhat larger (at least 80 km east-west by 35 km north-south) than was previously thought. The complex consists of several inset calderas of widely different ages, four of which we have named (Rowley and Siders, 1988). The oldest is the Clover Creek caldera, the source of the Bauers Tuff Member (22.8 Ma; Best, Christiansen, and others, 1989) and perhaps the source of the petrologically similar Swett Tuff Member, both of the Condor Canyon Formation. The Clover Creek caldera, although complexly faulted and mostly covered, is 4 km south-southeast of the mining district and underlies the north-central part of the Caliente caldera complex. The Delamar caldera, the source of the Hiko Tuff (18.6 Ma; Taylor and others, 1989), is 8 km south of the mining district and makes up the western part of the caldera complex. The other two named calderas produced unnamed ash-flow tuffs that are not known to crop out outside the caldera complex; these tuffs are as young as about 15 Ma (Mehnert and others, 1989). The tuff of Etna and at least one other ash-flow sequence probably also were derived from the Caliente caldera complex. The Delamar and younger calderas clearly formed during an episode of major faulting (described later) and thus are characterized by a complex combination of faults and structural and topographic caldera walls (Rowley, Anderson, and others, 1990). The Clover Creek caldera may have formed during the same episode of faulting.

Although the southern exposed margin of the Cobalt Canyon stock (24.8 Ma) is almost adjacent to the Clover Creek caldera (22.8 Ma), the difference between the two ages of these bodies argues against a genetic tie. Nonetheless, the stock may have been synchronous with an early, as yet undocumented, phase of magmatism in this long-lived caldera complex. In fact, isopach data led Williams (1967) to suggest that the source of the Leach Canyon Formation (24.0? Ma) was the northern part of the Caliente caldera complex, but this hypothesis has not been verified because this part of the complex is only partly mapped and is mostly buried by much younger rocks.

STRUCTURE

Mineral Belts

Mineralization in the Chief Mining District probably was controlled by both regional tectonic features and local structures. Numerous mineral belts have been proposed for many years to describe alignments of mining districts in the Great Basin. Bagby (1989) summarized some of this literature and showed two major provinces of mineral belts, one in central and western Nevada in which precious metals are the most significant products and in which districts are aligned along northwest-trending zones and one in eastern Nevada and western Utah in which base metals are the most significant products and in which districts are aligned along generally east-trending zones.

The Chief Mining District is within the Delamar–Iron Springs mineral belt of Shawe and Stewart (1976), which also includes the Tempiute, Delamar, and Iron Springs mining districts and is south of the Pioche mineral belt (fig. 2). It might be more appropriate to call these alignments igneous belts because they contain most of the volcanic and intrusive rocks in southwestern Utah and southeastern Nevada and are well delineated by aeromagnetic anomalies (fig. 2) (Zietz and others, 1976, 1978). Cenozoic and perhaps older east-trending alignments of structures and igneous centers also are well known in this part of the Great Basin (Ekren and others, 1976; Rowley and others, 1978). One of these, the Timpahute Lineament (fig. 2) of Ekren and others (1976), intersects the Chief district; Ekren and others (1976, 1977) suggested that it controlled emplacement of the Cobalt Canyon stock, the northern side of the Caliente caldera complex, and numerous other features. Stewart and others (1977) also called attention to the east-trending grain of the geology of the Great Basin, especially patterns of Tertiary igneous activity. Other, mostly older (Oligocene to early Miocene), east-trending topographic alignments, dikes, and other features were noted by Best (1988) in southeastern Nevada and southwestern Utah. Also noteworthy is the fact that most faults strike east in the Bull Valley Mountains of Utah (Hintze, 1980) and Clover Mountains of Nevada, which are east and southeast of the Chief district, and that the Intermountain Seismic Belt (Smith and Sbar, 1974) swings west-southwest through southern Utah and Nevada (fig. 2), centered at about the latitude of the Caliente caldera complex. The probable control of the belts, lineaments, and other aligned features is the same, namely old, deep-seated, east-striking faults or basement flaws, some of which have been reactivated during the Tertiary (Rowley and others, 1978). In stark contrast, almost all major younger (post–middle Miocene) faults strike north, northeast, and northwest.

Pre–Upper Oligocene Detachment Faults

Recent geologic mapping demonstrates at least three episodes of Tertiary extensional faulting in the Chief district. These episodes were recognized also by Bartley and others (1988), Taylor and others (1989), and Taylor (1990) in an east-west transect north of the district. The oldest episode involves a north-striking, east-dipping, low-angle fault, first recognized by Callaghan (1936), that separates Zabriskie

Quartzite on the west from Highland Peak Formation on the east; Callaghan also recognized that the fault is a major structure because the entire thickness of the Pioche Shale is faulted out. He called it a "probable" thrust fault and noted that it is better exposed in Antelope Canyon than in the mining district and that many orebodies are in the wide breccia zones developed along the structure. Tschanz and Pampeyan (1970, plate 3) traced this structure northward along the eastern side of the Chief Range and correlated it with a west-dipping low-angle fault on the western side of the Highland Range, which is north of the Chief Range; they named the structure the "Highland thrust fault" and considered it to be of "Laramide" age. In a brief discussion of thrust faults in Lincoln County, however, Tschanz and Pampeyan (1970, p. 82–83) cited field relations, especially in the northern Bristol Range about 50 km north of the Chief district, that suggest that this fault may be Tertiary in age and may not be a thrust. The name "Stampede detachment" was proposed by Axen and others (1988) for outcrops near Stampede Gap in the northwestern Highland Range that Tschanz and Pampeyan correlated with their Highland thrust; Axen and colleagues mapped the east-dipping Stampede Detachment along the eastern Chief Range and southwestern Highland and Bristol Ranges and in the Pioche area (Bartley and others, 1988, fig. 2). Axen and others (1988) recognized that the low-angle normal fault is related to extension that predates the oldest (late Oligocene) volcanism in the area; movement of the upper plate of the Stampede Detachment was to the east. The detachment is primarily a bedding-parallel fault in the Pioche Shale or, less commonly, in the Chisholm Shale or lower Highland Peak Formation, and the rocks in this part of the section are generally attenuated and locally cut out. The age of the Stampede Detachment is poorly constrained, but Axen and others (1988) and we consider it to be Tertiary; the geometry of the detachment resembles faults mapped by Nutt and Thorman (this volume) in the Drum Mountains of western Utah that they consider to be of Sevier(?) age. Throw on the Stampede Detachment decreases southward, and the fault has not been recognized at the latitude of the Caliente caldera complex. The fault is well exposed in the Chief District despite having been contact metamorphosed. Gouge and fault breccia as thick as 20 m along the fault are favorable sites for mineralized rocks.

Miocene Faults

The major episode of faulting in and near the Chief Mining District is Miocene in age (at least as old as 19–12 Ma). Faults of this episode consist of low-angle normal (detachment) faults and high-angle strike-slip, oblique-slip, and normal faults (fig. 3). Those faults that strike east or northwest tend to have right slip or oblique (right) slip, whereas those that strike north or northeast tend to have left slip or oblique (left) slip. An example of a major high-angle oblique-slip-fault zone is the Chief Canyon Fault Zone (fig. 3). Where exposed about 2 km southeast of the district, the fault zone strikes north and is almost vertical; we consider it to be an oblique-slip fault based both on strike-slip and dip-slip slickensides and on reidel shears (see Angelier and others, 1985; Petit, 1987) that indicate its eastern side was offset down and to the right. Farther south, it veers south-southeast and requires the same sense of oblique slip to explain slickensides and geologic relations. The amount of movement on this part of the fault is constrained by outflow Bauers Member to the north and intracaldera Bauers Member to the south; on the basis of this poorly constrained margin of the Clover Creek caldera, we estimate right slip of 1 km or more. Where the Chief Canyon Fault Zone cuts the Delamar caldera, west of lower Barnes Canyon about 10 km south-southeast of the district, the zone is expressed as a narrow, complex horst of propylitically and argillically altered rocks in which the predominant offset is normal (R.E. Anderson, unpub. data, 1989). The northern part of the Chief Canyon Fault Zone, east and northeast of the district, is not exposed but was inferred on the basis of a steep Bouguer gravity gradient (Blank and Kucks, 1989); considering that the fault here strikes north and separates the 700-m-high Chief Range from the Panaca Basin, it is likely that this segment of the fault zone is younger than the southern part of the fault zone and that it is a basin-range fault (see next section).

Other faults west of the Chief Canyon Fault Zone and 4–6 km south of the mining district confirm that major deformation occurred during this Miocene episode (fig. 3). The Meadow Valley Wash Fault Zone strikes north along the western side of the canyon of Meadow Valley Wash; a 2-km-long wedge of the Clover Creek caldera on the east against Bauers outflow tuff and Oligocene volcanic rocks on the west indicates at least 2 km of left slip and probable displacement down to the east. The fault zone is joined on the east, just north of Antelope Canyon, by the north-northeast-striking Gravel Pit Fault Zone that separates another 2-km-long wedge of the Clover Creek caldera on the east from Stirling Quartzite, Wood Canyon Formation, and Zabriskie Quartzite on the west. Field evidence argues against the Clover Creek caldera having been west of the fault, so we interpret the Gravel Pit Fault Zone as an oblique-slip fault of at least 2 km of left slip and probable downthrow to the east; limited slickenside data, including reidel shears, support this interpretation. Dikes and plugs of the porphyry of Meadow Valley Wash, as much as 300 m across, have been intruded along the Meadow Valley Wash, Gravel Pit, and Chief Canyon fault zones. Preliminary $^{40}Ar/^{39}Ar$ dates on the porphyry indicate that most deformation on these faults had taken place by 19 Ma. Other nearby faults having the same attitude and throw and interpreted to belong to the same Miocene episode are younger, whereas still others may be older.

High-angle faults are abundant in the Chief Range, but, because most rocks are Proterozoic and Cambrian quartzite, the age of faulting and amounts of slip are not well

constrained. Abundant slickensides in the brittle quartzite indicate mostly oblique, normal, right, and left slips on these faults. Probably most date to the Miocene episode of faulting, but we cannot rule out the possibility that some faults in the Chief Range predate the Miocene episode and thus may be of the same age as the Stampede Detachment or perhaps older; because of their unusual strike, a series of east-striking faults, some shown on figure 3, are particularly suspect as older features. In addition, some faults in the interior of the Chief Range, like those that bound it, must be younger basin-range faults (see next section). The age of faults is somewhat better constrained in the mining district because most faults there offset Tertiary volcanic rocks and the Cobalt Canyon stock. Unfortunately, few shears were found in the grus of the stock, but mapping indicates that the southwestern and northern sides of the stock are bounded by faults. The Old Democrat Fault Zone (fig. 3) is typical of the deformation along faults in the Chief Range. It is a significant fault zone that has several splays, local fault-breccia zones as wide as a few meters, and opposing dips to strata on opposite sides of the zone. The fault plane locally dips steeply east and in other places dips steeply west; quartzite east of the fault zone is younger than quartzite to the west. Slickensides on several splays at the Old Democrat Mine indicate oblique slip on east-dipping fault planes and right slip and reverse slip on west-dipping fault planes. The Old Democrat, Advance, and perhaps Lucky Hobo mines, as well as several unnamed prospects, are along the Old Democrat Fault Zone and its splays; apparently these mines were developed in old (24.8 Ma) orebodies offset by the fault zone, although metals are present along some faults and may indicate remobilization of metals by groundwater during or after deformation. The earliest phase of high-angle faulting of the Miocene episode probably is in fact Oligocene in age and synchronous with emplacement of the Cobalt Canyon stock and epithermal mineralization, as in the Walker lane of western Nevada (see, for example, John and others, 1989; Hardyman and Oldow, 1991).

A major low-angle normal fault, the Highland Detachment of Axen (1986), is exposed at the northwestern end of the Chief Range (Burke and Axen; 1990; Burke, 1991). From here it can be traced northward as a fairly continuous feature along the western sides of the Highland and northern Bristol Ranges. Parts of it were mapped as the "Laramide" Highland Thrust Fault and other parts were mapped as the "post-Laramide" Bristol Thrust Fault (Tschanz and Pampeyan, 1970). Axen (1986), Lewis (1987), Axen and others (1988), Bartley and others (1988), Sleeper (1989), and Burke and Axen (1990) interpreted exposures of the Highland Detachment along the Chief, Highland, and Bristol Ranges to be the breakaway of the detachment. In contrast to the much older Stampede Detachment, the Highland Detachment dips west and movement of its upper plate was to the west. These geologists have not identified the Highland Detachment to the east, and they interpreted that it continues in the subsurface under ranges to the west.

The hanging wall of the Highland Detachment, on the western sides of the Chief and Highland Ranges, contains a complex sequence of intertongued, mostly soft, coarse-grained landslide deposits and mudflow breccia, minor alluvial deposits, and rhyolitic air-fall and possibly ash-flow tuff that comprise the McCullough Formation of Axen and others (1988). These rocks are syntectonic, having been deposited contemporaneously with movement on the detachment (Axen and others, 1988; Sleeper, 1989; Burke and Axen, 1990; Burke, 1991). One of the air-fall tuff beds in the McCullough Formation, perhaps from a source in the Caliente caldera complex, has a $^{40}Ar/^{39}Ar$ date of 15.3 Ma (Axen and others, 1988; Taylor and others, 1989), thereby giving a minimum age for detachment faulting. Andesitic volcanic mudflow breccia, andesitic flow breccia, and small andesitic lava flows, called the volcanic rocks of Klondike Spring (Rowley and others, 1991), that underlie the McCullough Formation may also be syntectonic with the Highland Detachment.

In the Caliente caldera complex south of the mining district, north-northwest-striking high-angle right-slip, oblique-slip, and normal faults are abundant and one low-angle detachment fault (Newman Canyon Detachment) is exposed (Bowman, 1985; R.E. Anderson and P.D. Rowley, unpub. mapping, 1986–1990; Angelier and others, 1987; Mehnert and others, 1989; Michel-Noël and others, 1990; Rowley and others, 1990). In places caldera margins are a complex combination of faults and topographic and structural margins, arguing that these faults were active during formation of the Delamar caldera (18.6 Ma; Taylor and others, 1989) and younger calderas (as young as 15 Ma; Mehnert and others, 1989). Fault offsets that decrease upward in the stratigraphic section ("growth faults" of Bowman, 1985) indicate that the faults were also active during deposition of postcaldera tuffs of the Kane Wash Tuff (14 Ma; Novak, 1984) and the overlying tuff of Etna (also 14 Ma). These tuffs are unconformably overlain by the conglomerate of Ash Canyon (Rowley and Shroba, 1990, 1991) and intertongued basalt lava flows that have K-Ar dates of about 12 Ma (Mehnert and others, 1989) in exposures about 12 km south-southeast of the Chief Mining District. Although our early mapping indicated that the conglomerate and basalt also unconformably overlie faults of the Miocene episode (Mehnert and others, 1989), later mapping indicates that some of these faults cut rocks at least as young as the conglomerate and basalt (Snee and others, 1990). The similar ages of many of the faults, whether detachment or high angle, in the Caliente caldera complex, Chief Range, and Chief district indicate that the faults formed in a major Miocene eposide, from at least 19 to 12 Ma, the main extensional episode in this part of Nevada.

Upper Miocene and Pliocene Basin-Range Faults

Displacements on Neogene faults have strongly influenced development of much of the present-day large-scale

topography in the eastern Great Basin, especially imprinting this topography with a prominent north-south grain. These Neogene faults are known as basin-range faults and are generally younger than about 10 Ma (Anderson and others, 1983). They may have formed under an extension direction (with least principal stress oriented west-northwest) that had been rotated clockwise about 60° from the Miocene extension direction (with least principal stress oriented west-southwest) (Anderson and Ekren, 1977; Zoback and others, 1981; Anderson and others, 1983; Anderson, 1989). Near the Chief Mining District, most basin-range faults strike north, such as those in the Panaca Basin (fig. 3). The oldest exposed basin-fill deposits, the conglomerate of Ash Canyon and intertongued 12-million-year-old basalts, are cut by mostly north-striking basin-range faults. Younger Tertiary basin-fill sedimentary rocks, including the Panaca Formation, are also cut by such faults. Some basin-range faults in the area are Quaternary in age, such as north-striking faults in Delamar Valley about 20 km west of the Chief Mining District (Tschanz and Pampeyan, 1970; Ekren and others, 1977). Similar faults control the position of some north-trending streams about 15 km south-southeast of the mining district (R.E. Anderson, unpub. mapping, 1989).

Old basin-range faults are not as easy to identify as younger ones, but many old faults have greater displacement than younger ones. The north-trending Chief Range is probably a basin range, bounded by basin-range faults whose displacements must be at least that of the 700-m height of the range above the adjacent Panaca Basin. Faults on the western and southern sides of the range (upper left part of fig. 3) are locally well exposed and consist of high-angle faults containing slickensides that indicate normal slip. The buried northern part of the Chief Canyon Fault Zone, extending north from just east of the mining district, is interpreted to be the range-bounding fault that separates the Chief Range from the Panaca Basin. If so, it is much younger than the southern part and perhaps is a reactivated part of the Miocene oblique-slip fault zone that is farther to the south.

ORE DEPOSITS

Epithermal fissure-vein precious-metal deposits are common in and adjacent to calderas (see, for example, Hayba and others, 1986; Heald and others, 1987; Lipman, this volume). Most such deposits are related to the plumbing systems of calderas, in which late-forming intrusions produce convection cells of meteoric water. Orebodies form in the upper parts of these plumbing systems, and thus younger, less eroded calderas are generally better sites for exploration than are older buried ones. The Caliente caldera complex is poorly known geologically and has not been adequately explored for epithermal gold; however, it contains relatively young calderas, suggestive of good exploration potential. The Chief Mining District, near the northern edge of the complex, and the major Delamar Mining District (Callaghan, 1937; Tchanz and Pampeyan, 1970; Tingley, 1984), near the southwestern edge of the complex (fig. 2), are both deeply eroded epithermal gold systems. In both districts, most orebodies are in brittle quartzite of the Stirling Quartzite, Wood Canyon Formation, and Zabriskie Quartzite, which must have shattered like glass during faulting, preparing the rocks for mineralization, which took place during intrusive activity that apparently was synchronous with faulting. Both districts probably are of the adularia-sericite type (Heald and others, 1987) of epithermal deposits. Analyses of grab samples (Tingley, 1984, appendix B, samples 1740–1755) from the Delamar district show gold values of as much as 22 ppm, silver values of as much as 300 ppm, and anomalous values of copper, lead, and zinc. East-striking structures, including rhyolite dikes associated with some orebodies, are common in the district (Callaghan, 1937). The Delamar district has recently (1990–91) been explored and studied by Alma American Mining Company and Fischer-Watt Gold Company (S.P. Bingham and G.B. Allen, written commun., 1990).

Another known adularia-sericite type of epithermal system underlies the Taylor (or Easter) Mine, located within the caldera complex 13 km east-northeast of Delamar and 15 km southwest of Caliente (fig. 2). Tingley (1984, appendix B, sample 579) reported values of gold of 18 ppm and of silver of 70 ppm from a grab sample from the mine. Sparse slickenside data suggest that the structure is simple, namely a normal fault zone in Hiko intracaldera tuff (Delamar caldera) that strikes N. 80° E. and dips 50° to the north; this fault may be a dilational response to right slip along a nearby concealed east-striking fault (R.R. Kern, oral commun., 1990). Banded quartz veins that contain comb structure and follow the fault have low base-metal contents but relatively high gold contents, and locally the tuff is intensely hydrothermally altered within a zone that is at least 100 m wide on either side of the fault. The orebodies are in a high-level epithermal system (G.B. Allen and S.P. Bingham, oral commun., 1990) that has been previously drilled and explored by Homestake Mining Company and other firms (Charley Martin, oral commun., 1990) and in 1990–91 by FMC Gold Company (J.L. Askey and J.B. Harlan, oral common., 1990).

In addition, the small, poorly known Pennsylvania mining district on the southern margin of the caldera complex (fig. 2) is probably an epithermal gold system (Tchanz and Pampeyan, 1970; Tingley, 1984); values of gold of as much as 180 ppm and of silver of as much as 1,500 ppm, as well as anomalous values of copper, lead and zinc, were reported from grab samples (Tingley, 1984, appendix B, samples 1701–1707).

Orebodies in the Chief Mining District are deeply eroded epithermal fissure-vein deposits that occupy breccia and low-angle faults of the Stampede Detachment Fault and high-angle faults and joints within quartzite. Most of the

following descriptions of the ore deposits are those of Callaghan (1936). Callaghan noted evidence for replacement of some country rocks by ore minerals—for example, quartzite in the Old Democrat Mine (fig. 3) and limestone or dolomite in the Lucky Chief Mine. He found that all ore is oxidized, except for some sulfide minerals (galena) in the Republic and Gold Chief mines. He recognized three types of vein deposits. The first, which has the highest amounts of gold and silver in the district, is the arsenian type, which is found in the Advance, Old Democrat, Republic, and Lucky Hobo mines. Typically, the ore in these veins is a green to brown, vuggy aggregate of supergene scorodite that replaced arsenopyrite and is locally replaced in turn by a brown micaceous mineral (arsenosiderite?) and by iron-oxide minerals; quartz, jarosite, cerussite, descloizite, mimetite, beudantite, and manganese-oxide minerals also are present. The second type of vein deposit, which is the most economically productive in the district although it contains relatively low proportions of gold and silver, is characterized by a network of tabular barite crystals and scattered grains of galena; chalcedonic quartz is present as veins in barite, and cavities between barite crystals locally contain quartz, calamine, mimetite, and manganese- and iron-oxide minerals. This type of deposit is present along the Stampede Detachment in the Gold Chief and Lucky Chief mines. The third type of vein deposit, from which most of the lead was produced, includes irregular and pipelike masses of cerussite in the Republic and Lucky Chief mines; in addition to cerussite, ores contain fine-grained quartz, opal, plumbojarosite, and manganese- and iron-oxide minerals. A fourth type of vein, which is barren or contains low amounts of gold and silver but is exposed in many prospect pits, consists of lenses and small bodies of red iron oxide in quartzite resulting from fault breccia cemented by iron oxide and comb quartz. In addition, Tingley (1984) noted fine-grained disseminated sulfide minerals and silicified quartzite wallrock in the Advance Mine. Furthermore, in 1985, Homestake Mining Company discovered, by reverse-circulation drilling, a large body of disseminated pyrite (2–10 percent by volume) and phyllically altered rock of the Cobalt Canyon stock at about 110 m depth below, east, and south of the Gold Chief Mine. Although chemical analyses reveal anomalous amounts of arsenic and several other elements, the body does not contain appreciable amounts of gold or silver, but it is suggestive of a porphyry copper deposit (data from a 1986 report by S.D. Olmore of Homestake Mining Company that was made available for publication courtesy of Homestake Mining Company in 1990).

The only published chemical analyses of orebodies in the Chief District are by the USGS and include atomic absorption analyses of As, Au, Sb, and Zn and semiquantitative spectrographic analyses of other elements for 12 grab samples (Tingley, 1984, appendix B) and flame atomic absorption analyses of Te, Tl, and Au and direct-current arc and alternating-current spark emission spectrographic field analyses of other elements for 14 grab samples that we collected (table 1). The analyses suggest that the various veins are not much different geochemically from each other except for those in mines in the Stampede Detachment, which contain somewhat less arsenic. There is no evidence from these meager geochemical data that the veins are of more than one age. The different vein types of Callaghan (1936) cannot be discerned using the geochemical data, although those veins that are high in arsenic (arsenian type) are in the Advance, Republic, Lucky Hobo, and Gold Stake mines, as he noted; these veins, however, contain some of the highest values of lead and other base metals, in contrast to his descriptions of the minerals in these veins. Overall, the analyses show that veins contain gold and silver as well as relatively high values of other indicator elements (As, B, Sb, Te, Tl; samples were not analyzed for Hg or U) typical of epithermal precious-metal deposits (Silberman and Berger, 1986). Anomalous values of gold and silver are in veins in the Gold Chief (highest overall gold value, at 3.9 ppm; sample 120 of Tingley, 1984), Lucky Hobo (highest overall silver value, at 2,000 ppm; sample 123 of Tingley, 1984), Republic, Advance, Lucky Chief, SOA, and Gold Stake mines and in a prospect (sample 126 of Tingley) southwest of the Contact Mine. Even more anomalous values are those of lead and zinc and, to a much lesser extent, of copper; high values of iron, magnesium, and manganese also are characteristic. These higher values of base metals and silver, in fact, provide evidence of vertical geochemical zoning in the Chief district (Silberman and Berger, 1986) and indicate, along with the field evidence, that the district has been deeply eroded. It is likely that the veins containing the highest amounts of gold and silver were removed by erosion long ago.

CONCLUSIONS

The Chief Mining District is a minor mining district, but the lessons it provides may help in finding ore deposits elsewhere in and near the Caliente caldera complex. The district contains deposits of a deeply eroded epithermal fissure-vein system. The heat source that led to the transportation of most metals was provided by the Cobalt Canyon stock (24.8 Ma), which underlies the district. Metals most likely were leached from country rocks, then precipitated during convective overturn of groundwater heated by the stock; some metals, however, may have been derived from hydrothermal solutions from the intrusion itself. The stock may represent an early magmatic event in the adjacent Caliente caldera complex, although it predates the known main episode of magmatism (23–14 Ma) in the complex, which has controlled mineralization of three other epithermal gold districts. The tectonic control on the location of the stock and the caldera complex is not well constrained but may result partly from an east-trending grain in underlying rocks, perhaps the result of pre–middle Tertiary east-striking faults, some of which

were reactivated, and partly from the Miocene episode of faulting.

Most orebodies in the district are in brecciated fault zones of the Tertiary Stampede Detachment system, an east-dipping bedding-parallel normal fault that separates quartzite below the detachment from limestone and dolomite above it; the detachment was active prior to late Oligocene volcanism, well before mineralization. As in the major Delamar Mining District to the southwest, brittle quartzite was extremely shattered in and near faults, providing sites for mineralization. At some of these sites, ore was localized along high-angle faults and joints in quartzite. Some of these structures probably formed during emplacement of the Cobalt Canyon stock, which may also have localized a porphyry copper ore deposit. Structures of the Miocene episode of high-angle oblique-slip faulting that began before 19 Ma may have localized some metals. Early phases of the Miocene episode of faulting in fact may have been synchronous with, and provided control on, emplacement of the Cobalt Canyon stock. Some ore could have resulted from younger igneous activity such as the porphyry of Meadow Valley Wash or from remobilization of existing orebodies by groundwater heated during deformation. The history and structure of the Chief District have many similarities to those of epithermal gold districts in the Walker lane of western Nevada (John and others, 1989; Hardyman and Oldow, 1991). Evidence for geochemical zoning in which amounts of gold decrease with depth and evidence for deep erosion that removed most of the roof over the Cobalt Canyon stock indicate that the likelihood is low for discovering new gold orebodies in the district. The possibility of finding other gold deposits in and near the Caliente caldera complex, however, is probably much better.

REFERENCES CITED

Anderson, J.J., and Rowley, P.D., 1975, Cenozoic stratigraphy of the southwestern High Plateaus of Utah, *in* Anderson, J.J., Rowley, P.D., Fleck, R.J., and Nairn, A.E.M., eds., Cenozoic geology of southwestern High Plateaus of Utah: Geological Society of America Special Paper 160, p. 1–52.

Anderson, R.E., 1989, Tectonic evolution of the Intermontane System; Basin and Range, Colorado Plateau, and High Lava Plains, *in* Pakiser, L.C., and Mooney, W.D., eds., Geophysical framework of the continental United States: Geological Society of America Memoir 172, p. 163–176.

Anderson, R.E., and Ekren, E.B., 1977, Late Cenozoic fault patterns and stress fields in the Great Basin and westward displacement of the Sierra Nevada block—Comment and reply: Geology, v. 5, no. 7, p. 388–392.

Anderson, R.E., Zoback, M.L., and Thompson, G.A., 1983, Implications of selected subsurface data on the structural form and evolution of some basins in the northern Basin and Range province, Nevada and Utah: Geological Society of America Bulletin, v. 94, p. 1055–1072.

Angelier, Jacques, Colletta, Bernard, and Anderson, R.E., 1985, Neogene paleostress changes in the Basin and Range—A case study at Hoover Dam, Nevada-Arizona: Geological Society of America Bulletin, v. 96, p. 347–361.

Angelier, Jacques, Faugére, Émeric, Michel-Noël, Gérard, and Anderson, R.E., 1987, Bassins en extension et tectonique synsedimentaire—Examples dans les "Basin and Range" (U.S.A.), *in* Genése et évolution des bassins sédimentaires: Total Compagnie Francaise des Pétroles, Notes et Mémoires no. 21, p. 51–72.

Armstrong, R.L., 1970, Geochronology of Tertiary igneous rocks, eastern Basin and Range Province, western Utah, eastern Nevada, and vicinity, U.S.A.: Geochimica et Cosmochimica Acta, v. 34, p. 203–232.

Axen, G.J., 1986, Superposed normal faults in the Ely Springs Range, Nevada—Estimates of extension: Journal of Structural Geology, v. 8, no. 6, p. 711–713.

Axen, G.J., Lewis, P.R., Burke, K.J., Sleeper, K.G., and Fletcher, J.M., 1988, Tertiary extension in the Pioche area, Lincoln County, Nevada, *in* Bartley, J.M., Axen, G.J., Taylor, W.J., and Fryxell, J.E., Cenozoic tectonics of a transect through eastern Nevada near 38° N latitude, *in* Weide, D.L., and Faber, M.L., eds., This extended land—Geological journeys in the southern Basin and Range: Geological Society of America, Cordilleran Section, Field Trip Guidebook, p. 3–5.

Bagby, W.C., 1989, Patterns of gold mineralization in Nevada and Utah, *in* Shawe, D.R., and Ashley, R.P., eds., United States gold terranes—Part I: U.S. Geological Survey Bulletin 1857-B, p. 11–21.

Bartley, J.M., Axen, G.J., Taylor, W.J., and Fryxell, J.E., 1988, Cenozoic tectonics of a transect through eastern Nevada near 38° N latitude, *in* Weide, D.L., and Faber, M.L., eds., This extended land—Geological journeys in the southern Basin and Range: Geological Society of America, Cordilleran Section, Field Trip Guidebook, p. 1–20.

Best, M.G., 1988, Easterly trending Oligocene to early Miocene (30–20 Ma) paleotopography and other geologic features, southeastern Great Basin: Geological Society of America Abstracts with Programs 1988, v. 20, no. 3, p. 143.

Best, M.G., Christiansen, E.H., and Blank, R.H., Jr., 1989, Oligocene caldera complex and calc-alkaline tuffs and lavas of the Indian Peak volcanic field, Nevada and Utah: Geological Society of America Bulletin, v. 101, p. 1076–1090.

Best, M.G., Christiansen, E.H., Deino, A.L., Gromm, C.S., McKee, E.H., and Noble, D.C., 1989, Excursion 3A—Eocene through Miocene volcanism in the Great Basin of the western United States: New Mexico Bureau of Mines and Mineral Resources Memoir 47, p. 91–133.

Best, M.G., Miller, D.S., Radke, L.E., and Kowallis, B.J., 1991, Preliminary geologic map of the Panaca Summit and Prohibition Flat quadrangles, Lincoln County, Nevada, and Iron County, Utah: U.S. Geological Survey Open-File Report 91–124, 22 p.

Blank, H.R., and Kucks, R.P., 1989, Preliminary aeromagnetic, gravity, and generalized geologic maps of the USGS Basin and Range–Colorado Plateau transition zone study area in southwestern Utah, southeastern Nevada, and northwestern Arizona (the "BARCO" project): U.S. Geological Survey Open-File Report 89–432, 16 p., scale 1:250,000.

Bowman, S.A., 1985, Miocene extension and volcanism in the Caliente caldera complex, Lincoln County, Nevada: Golden, Colorado School of Mines, M.S. thesis, 143 p.

Burke, K.J., 1991, Tertiary extensional tectonism in the northern Chief and southernmost Highland Ranges, Lincoln County, Nevada: Flagstaff, Northern Arizona University, M.S. thesis, 91 p.

Burke, K.J., and Axen, G.J., 1990, Structural geometry and timing of deformation in the northern Chief and southernmost Highland Ranges near Pioche, Nevada: Geological Society of America Abstracts with Programs, v. 22, no. 3, p. 11.

Callaghan, Eugene, 1936, Geology of the Chief district, Lincoln County, Nevada: University of Nevada Bulletin, v. 30, no. 2 (Nevada Bureau of Mines Bulletin 26), 29 p.

_____ 1937, Geology of the Delamar district, Lincoln County, Nevada: University of Nevada Bulletin, v. 31, no. 5 (Nevada Bureau of Mines Bulletin 30A), 69 p.

Cook, E.F., 1960, Geologic atlas of Utah—Washington County: Utah Geological and Mineralogical Survey Bulletin 70, 119 p.

Dolgoff, Abraham, 1963, Volcanic stratigraphy of the Pahranagat area, Lincoln County, southeastern Nevada: Geological Society of America Bulletin, v. 74, p. 875–900.

Ekren, E.B., Bucknam, R.C., Carr, W.J., Dixon, G.L., and Quinlivan, W.D., 1976, East-trending structural lineaments in central Nevada: U.S. Geological Survey Professional Paper 986, 16 p.

Ekren, E.B., Orkild, P.P., Sargent, K.A., and Dixon, G.L., 1977, Geologic map of Tertiary rocks, Lincoln County, Nevada: U.S. Geological Survey Miscellaneous Investigations Series Map I–1041, scale 1:250,000.

Hardyman, R.F., and Oldow, J.S., 1991, Tertiary tectonic framework and Cenozoic history of the central Walker lane, Nevada, *in* Raines, G.L., Lisle, R.E., Schafer, R.W., and Wilkinson, W.H., eds., Geology and ore deposits of the Great Basin: Geological Society of Nevada Symposium Proceedings, v. 1, p. 279–301.

Hayba, D.O., Bethke, P.M., Heald, Pamela, and Foley, N.K., 1986, Geologic, mineralogic, and geochemical characteristics of volcanic-hosted epithermal precious-metal deposits, *in* Berger, B.R., and Bethke, P.M., eds., Geology and geochemistry of epithermal systems: Reviews in Economic Geology, v. 2, p. 29–167.

Heald, Pamela, Foley, N.K., and Hayba, D.O., 1987, Comparative anatomy of volcanic-hosted epithermal deposits—Acid-sulfate and adularia-sericite types: Economic Geology, v. 82, no. 1, p. 1–26.

Hintze, L.F., 1980, Geologic map of Utah: Salt Lake City, Utah Geological and Mineral Survey, scale 1:500,000.

John, D.A., Thomason, R.E., and McKee, E.H., 1989, Geology and K-Ar geochronology of the Paradise Peak mine and the relationship of pre-basin and range extension to early Miocene precious metal mineralization in west-central Nevada: Economic Geology, v. 84, p. 631–649.

Kowallis, B.J., and Best, M.G., 1990, Fission track ages from volcanic rocks in southwestern Utah and southeastern Nevada: Isochron/West, no. 55, p. 24–27.

Le Bas, M.J., Le Maitre, R.W., Streckeisen, A., and Zanettin, B., 1986, A chemical classification of volcanic rocks based on the total alkali-silica diagram: Journal of Petrology, v. 27, pt. 3, p. 745–750.

Lewis, P.R., 1987, Structural geology of the northern Burnt Springs Range and Robber Roost Hills, Lincoln County, Nevada: Flagstaff, Northern Arizona University, M.S. thesis, 90 p.

Mehnert, H.H., Anderson, R.E., and Rowley, P.D., 1989, Constraints on age of faulting and youngest volcanism, western Caliente caldera complex and vicinity, Lincoln County, Nevada [abs.]: Eos, v. 70, no. 43, p. 1414.

Merriam, C.W., 1964, Cambrian rocks of the Pioche mining district, Nevada: U.S. Geological Survey Professional Paper 469, 55 p.

Michel-Noël, G., Anderson, R.E., and Angelier, Jacques, 1990, Fault kinematics and estimates of strain partitioning of a Neogene extensional fault system in southeastern Nevada, chapter 7, *in* Werncke, B.P., ed., Basin and Range extensional tectonics near the latitude of Las Vegas, Nevada: Geological Society of America Memoir 176, p. 155–180.

Noble, D.C., and McKee, E.H., 1972, Description and K-Ar ages of volcanic units of the Caliente volcanic field, Lincoln County, Nevada, and Washington County, Utah: Isochron/West, no. 5, p. 17–24.

Noble, D.C., McKee, E.H., Hedge, C.E., and Blank, H.R., Jr., 1968, Reconnaissance of the Caliente depression, Lincoln County, Nevada [abs.]: Geological Society of America Special Paper 115, p. 435–436.

Novak, S.W., 1984, Eruptive history of the rhyolitic Kane Springs Wash volcanic center, Nevada: Journal of Geophysical Research, v. 89, no. B10, p. 8603–8615.

Petit, J.P., 1987, Criteria for the sense of movement on fault surfaces in brittle rocks: Journal of Structural Geology, v. 9, no. 516, p. 597–608.

Repenning, C.A., 1987, Biochronology of the microtine rodents of the United States, *in* Woodburne, M.O., ed., Cenozoic mammals of North America: University of California Press, chap. 8, p. 236–268.

Rowley, P.D., Anderson, R.E., Snee, L.W., and Mehnert, H.H., 1990, Geology and structural setting of the western Caliente caldera complex, Lincoln County, Nevada: Geological Society of America Abstracts with Programs, v. 22, no. 3, p. 79–80.

Rowley, P.D., Lipman, P.W., Mehnert, H.H., Lindsey, D.A., and Anderson, J.J., 1978, Blue Ribbon lineament, an east-trending structural zone within the Pioche mineral belt of southwestern Utah and eastern Nevada: U.S. Geological Survey Journal of Research, v. 6, no. 2, p. 175–192.

Rowley, P.D., McKee, E.H., and Blank, H.R., Jr., 1989, Miocene gravity slides resulting from emplacement of the Iron Mountain pluton, southern Iron Springs mining district, Iron County, Utah [abs.]: Eos, v. 70, no. 43, p. 1309.

Rowley, P.D., and Shroba, R.R., 1990, Geologic map of the Indian Cove quadrangle, Lincoln County, Nevada: U.S. Geological Survey Open-File Report 90–224, 15 p.

_____1991, Geologic map of the Indian Cove quadrangle, Lincoln County, Nevada: U.S. Geological Survey Geologic Quadrangle Map GQ–1701, scale 1:24,000.

Rowley, P.D., Shroba, R.R., Simonds, F.W., Burke, K.J., Axen, G.J., and Olmore, S.D., 1991, Geologic map of the Chief Mountain quadrangle, Lincoln County, Nevada: U.S. Geological Survey Open-File Report 91–135, 33 p.

Rowley, P.D., and Siders, M.A., 1988, Miocene calderas of the Caliente caldera complex, Nevada-Utah [abs.]: Eos, v. 69, no. 44, p. 1508.

Rowley, P.D., Snee, L.W., Mehnert, H.H., Anderson, R.E., Axen, G.J., Burke, K.J., Simonds, F.W., and Shroba, R.R., 1990, Structural setting of the Chief mining district, eastern Chief Range, Lincoln County, Nevada [abs.], *in* Thorman, C.H., ed., Workshop on application of structural geology to mineral and energy resources of the central region: U.S. Geological Survey Open-File Report 90–508, p. 12–13.

Samson, S.D., and Alexander, E.C., Jr., 1987, Calibration of the interlaboratory $^{40}Ar/^{39}Ar$ dating standard, MMhb–1: Chemical Geology, v. 66, p. 27–34.

Shawe, D.R., and Stewart, J.H., 1976, Ore deposits as related to tectonics and magmatism, Nevada and Utah: Transactions of American Institute of Mining, Metallic, and Petroleum Engineers, v. 260, p. 225–232.

Silberman, M.L., and Berger, B.R., 1986, Relationship of trace-element patterns to alteration and morphology in epithermal precious-metal deposits, *in* Berger, B.R., and Bethke, P.M., eds., Geology and geochemistry of epithermal systems: Reviews in Economic Geology, v. 2, p. 203–232.

Sleeper, K.G., 1989, Structural geology of the Black Canyon Range, The Bluffs, and southwestern Highland Range, Lincoln County, Nevada: Flagstaff, Northern Arizona University, M.S. thesis, 113 p.

Smith, R.B., and Sbar, M.L., 1974, Contemporary tectonics and seismicity of the western United States with emphasis on the Intermountain Seismic Belt: Geological Society of America Bulletin, v. 85, p. 1205–1218.

Snee, L.W., Mehnert, H.H., Rowley, P.D., Anderson, R.E., and Scott, R.B., 1990, New isotopic ages demonstrate extensional faulting of 19–12 Ma in the western Caliente caldera complex and vicinity, Lincoln County, Nevada [abs.]: Eos, v. 71, no. 43, p. 1612.

Steiger, R.H., and Jäger, E., 1977, Subcommission on geochronology—Convention on the use of decay constants in geo- and cosmochronology: Earth and Planetary Science Letters, v. 36, p. 359–362.

Stewart, J.H., 1974, Correlation of uppermost Precambrian and lower Cambrian strata from southern to east-central Nevada: U.S. Geological Survey Journal of Research, v. 2, no. 5, p. 609–618.

_____1984, Stratigraphic sections of Lower Cambrian and Upper Proterozoic rocks in Nye, Lander, and Lincoln Counties, Nevada, and Sonora, Mexico: U.S. Geological Survey Open-File Report 84–691, 53 p.

Stewart, J.H., Moore, W.J., and Zietz, Isidore, 1977, East-west patterns of Cenozoic igneous rocks, aeromagnetic anomalies, and mineral deposits, Nevada and Utah: Geological Society of America Bulletin, v. 88, p. 67–77.

Streckeisen, A., 1976, To each plutonic rock its proper name: Earth Science Reviews, v. 12, p. 1–33.

Swadley, WC, and Rowley, P.D., 1992, Geologic map of the Pahroc Spring SE quadrangle, Lincoln County, Nevada: U.S. Geological Survey Open-File Report 92–7, 22 p.

Taylor, W.J., 1990, Spatial and temporal relations of Cenozoic volcanism and extension in the North Pahroc and Seaman Ranges, eastern Nevada, *in* Wernicke, B.P., ed., Basin and Range extensional tectonics near the latitude of Las Vegas, Nevada: Geological Society of America Memoir 176, p. 181–193.

Taylor, W.J., Bartley, J.M., Lux, D.R., and Axen, G.J., 1989, Timing of Tertiary extension in the Railroad Valley–Pioche transect, Nevada—Constraints from $^{40}Ar/^{39}$ Ar ages of volcanic rocks: Journal of Geophysical Research, v. 94, no. B6, p. 7757–7774.

Tingley, J.V., 1984, A mineral inventory of the Caliente resource area, Caliente district, Lincoln County, Nevada: Nevada Bureau of Mines and Geology Open-File Report 84–1, 56 p., appendixes.

Tschanz, C.M., and Pampeyan, E.H., 1970, Geology and mineral deposits of Lincoln County, Nevada: Nevada Bureau of Mines and Geology Bulletin 73, 188 p.

Williams, P.L., 1967, Stratigraphy and petrography of the Quichapa Group, southwestern Utah and southeastern Nevada: Seattle, University of Washington, Ph.D. thesis, 182 p.

Zietz, Isidore, Gilbert, F.P., and Kirby, J.R., 1978, Aeromagnetic map of Nevada—Color coded intensities: U.S. Geological Survey Geophysical Investigations Map GP–922, scale 1:1,000,000.

Zietz, Isidore, Shuey, Ralph, and Kirby, J.R., Jr., 1976, Aeromagnetic map of Utah: U.S. Geological Survey Geophysical Investigations Map GP–907, scale 1:1,000,000.

Zoback, M.L., Anderson, R.E., and Thompson, G.A., 1981, Cainozoic evolution of the state of stress and style of tectonism of the Basin and Range province of the western United States: Philosophical Transactions of Royal Society of London, v. A300, p. 407–434.

Chapter I

Extensional Geometry in the Northern Grant Range, East-Central Nevada—Implications for Oil Deposits in Railroad Valley

By KAREN LUND and L. SUE BEARD

U.S. GEOLOGICAL SURVEY BULLETIN 2012

APPLICATION OF STRUCTURAL GEOLOGY TO MINERAL AND
ENERGY RESOURCES OF THE CENTRAL AND WESTERN UNITED STATES

CONTENTS

FIGURES

Extensional Geometry in the Northern Grant Range, East-Central Nevada—Implications for Oil Deposits in Railroad Valley

By Karen Lund[1] *and* L. Sue Beard[2]

Abstract

Heterogeneous extension in the northern Grant Range is manifested by a stacked set of curviplanar low-angle attenuation faults that formed concurrent with arching of the range about a north-northwest axis. The style and amount of attenuation was controlled by the lithologic character and structural depth of the units and, locally, by the geometry of the arch. On the east side of the range, a stacked array of low-angle attenuation faults are subparallel with bedding, attenuation is distributed across the many stacked fault zones, and except at highest crustal levels these faults do not cut to the surface. On the west side of the range (steeper side of the arch), the curviplanar low-angle attenuation faults converge into a single west-dipping fault zone along which the total amount of extension is probably greater than in other parts of the range. Here, the stratigraphic separation (or juxtaposition) of Mississippian units over Middle Cambrian units results in an extensional culmination. Windows into the culmination expose a distinct geometry in the curviplanar low-angle fault array which indicates that low-angle attenuation faulting was synchronous with arching of the range.

Cross sections incorporating seismic and drill-hole data suggest that the low-angle attenuation faults in the range extend into Railroad Valley to the west of the Grant Range with no significant offset by high-angle normal faults. Therefore, the topographic expression of the Grant Range and Railroad Valley may be due to synchronous arching and low-angle faulting. These new data and interpretations provide insight into the enigmatic structures buried in Railroad Valley. Thus, both petroleum source and reservoir rocks in Railroad Valley oil fields are in relatively immature but extensively fractured rocks of the upper plate of the extensional culmination.

[1]U.S. Geological Survey, Box 25046, MS905, Denver, Colorado 80225.

[2]U.S. Geological Survey, Flagstaff, Arizona 86001.

INTRODUCTION

The northern Grant Range and adjoining Railroad Valley are in the middle of the northern Basin and Range province in east-central Nevada (fig. 1). The rocks in the Grant Range show effects of complex deformation but are nonetheless dominantly in proper stratigraphic order and upright. Railroad Valley, to the west, is one of the widest and deepest valleys in Nevada and contains the first oil well and most productive oil fields in the State.

Previous mapping in the Grant, Horse, and White Pine Ranges (fig. 1) shows that the Paleozoic rocks are cut by many low-angle faults, but two different conclusions have been made about the age and origin of the faulting. Mesozoic to early Tertiary compressional tectonism was thought to have caused the younger-on-older low-angle faults observed in Paleozoic rocks of the northern Grant Range (Kirkpatrick, 1960; Huttrer, 1963; Hyde, 1963; Hyde and Huttrer, 1970), as well as both the younger-on-older and older-on-younger low-angle faults in the southern Grant Range (Cebull, 1967, 1970). Alternatively, mapping of both Paleozoic and Tertiary rocks in the northern Grant, Horse, and White Pine Ranges by Moores and others (1968) resulted in the conclusion that, because the structural geometry of Tertiary rocks is essentially the same as that of underlying Paleozoic rocks, folding and low-angle younger-on-older faults were formed by late Tertiary block uplift, basement extension, and compression.

Recent work demonstrates that both of these deformational events and structural processes (late Mesozoic compression and late Tertiary extension) occurred in the Grant Range. In the central Grant Range, a pre–Late Cretaceous macroscopic east-vergent overturned fold in metamorphosed Cambrian rocks (Cebull, 1967), which probably formed in the Mesozoic (Fryxell, 1988), was cut by two sets of Tertiary low-angle attenuation faults—early east-dipping faults cut by later west-dipping faults (Fryxell, 1984, 1988). In the northern Grant Range, Cambrian and Lower Ordovician

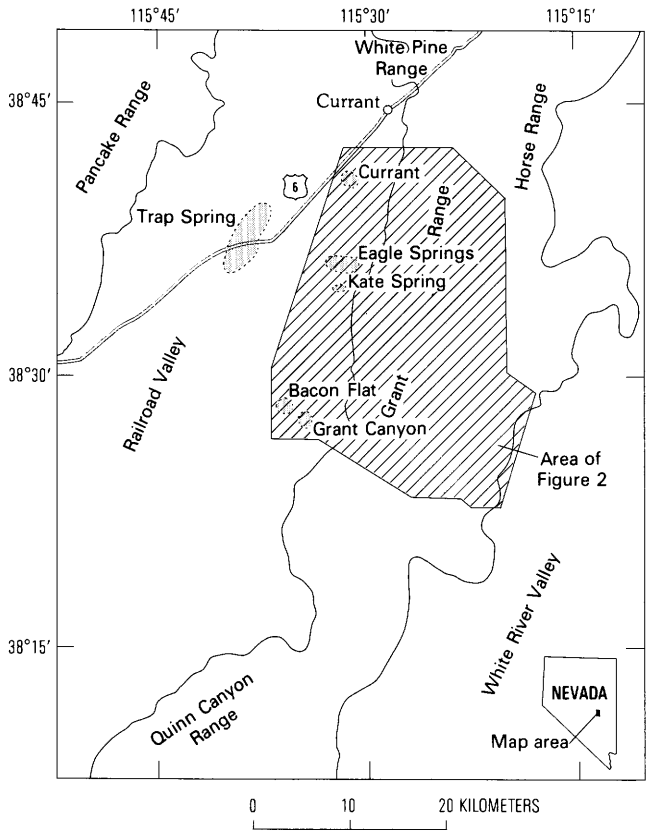

Figure 1. Index map showing location of study area and nearby oil fields (enclosed by dotted lines), east-central Nevada.

rocks were also metamorphosed and ductilely deformed at moderate to deep structural levels before being sliced and attenuated by a series of younger-on-older faults that deform rocks of all ages exposed in the range. These younger-on-older faults are part of a system of low-angle attenuation faults (faults that thin the section) (Lund and Beard, 1986, 1987; Camilleri and others, 1987; Lund and others, 1987, 1988; Camilleri, 1989).

The most recent structural event has traditionally been thought to be formation of the Grant Range and Railroad Valley by a down-to-the-west, steep normal fault(s) along the west flank of the range, a model that is in accordance with classic Basin and Range styles (Stewart, 1978). A steep range-front fault and related minor faults are commonly depicted on maps and subsurface structural and seismic interpretations (Moores and others, 1968; Bortz and Murray, 1979; Guion and Pearson, 1979; Vreeland and Berrong, 1979; Effimoff and Pinezich, 1981; Anderson and others, 1983; Poole and Claypool, 1984; Kleinhampl and Ziony, 1985; Flanigan, 1988; Read and Zogg, 1988; Veal and others, 1988). Minor offset of Holocene alluvial fans and lake terraces, as well as the presence of a prominent line of springs and a sharp gravity gradient (Lund and others, 1987, 1988; Blank, 1991), indicates that some faulting has occurred along the range front. However, a sign-bit Vibroseis seismic line across the Grant Canyon oil field (Potter and others, 1991, fig. 1) also published by Veal and others (1988), indicates that there is no significant offset of the low-angle fault system by a major range-front fault at that latitude.

The recently mapped structural geometry of the northern Grant Range and the interest in the geology of Railroad Valley because of oil exploration have provided reasons to try to integrate the new field data from the range with published drill-hole and seismic data from the valley. Our purpose is to provide a preliminary model for understanding the geometry and timing of formation of the valley relative to structures exposed in the range and for evaluating the structural setting of the oil occurrences in Railroad Valley.

Acknowledgments.—Geologic mapping was accomplished during evaluation of the Blue Eagle and Riordans Well wilderness study areas by the U.S. Geological Survey. We are indebted to the numerous project members whose mapping contributed to our understanding of the geology of the northern Grant Range: B. Nevins, R. Demetrion, A.R. Pyke, D. Schneidereit, J.L. Snee, M. Elrick, J.E. Fryxell, and P.A. Camilleri. Discussions and (or) field trips with F.G. Poole, F.J. Kleinhampl, P.M. Sheehan (University of Wisconsin at Madison), R.J. Ross, Jr., J.G. Johnson (Oregon State University), and M.E. Taylor helped us with stratigraphic problems. We thank R.B. Scott, D.M. Miller, C.H. Thorman, H.R. Blank, Jr., W.J. Perry, Jr., C.J. Potter, J.A. Grow, and S.E. Boyer (University of Washington) for helpful discussions about aspects of the structure. Reviews by W.J. Perry, Jr., and A.R. Wallace improved the manuscript.

GEOLOGIC SETTING

During the Paleozoic, this area was on the continental shelf of western North America and was the site of deposition of more than 6,000 m (Kellogg, 1963; Moores and others, 1968) of predominantly carbonate rocks. In the northern Grant Range, Upper Cambrian to Middle Ordovician carbonate rocks are variably metamorphosed to greenschist facies; they include phyllite, phyllitic marble, and calcareous and dolomitic marble (Lund and others, 1987, 1988; Camilleri, 1989). Rocks higher in the stratigraphic section show no visible effects of metamorphism. Upper Ordovician to Middle Devonian units form a thick dolostone section (Ely Springs, Laketown, Sevy, and Simonson Dolostones); the Middle and Upper Devonian Guilmette Formation is a thick unit of interbedded limestone and dolostone. The Upper Devonian and Lower Mississippian Pilot Shale is absent because of nondeposition (Poole and others, 1977). The Lower Mississippian Joana Limestone contains both massive encrinitic limestone and dark limestone with argillaceous partings. The Mississippian Chainman Shale is the

older of two oil source beds in the section (Poole and Claypool, 1984). The thick Upper Mississippian to Pennsylvanian Ely Limestone is the youngest Paleozoic unit. Rocks of the northern Grant Range were not deformed during the Paleozoic orogenies; the area is east of the regions most affected by deformation associated with the Antler (Devonian and Mississippian) and Sonoma (Permian and Triassic) orogenies (fig. 1).

Mesozoic terrigenous deposits are absent because of either nondeposition or erosion. Lacustrine deposits of the Sheep Pass Formation are Paleocene and Eocene in age in the northern Grant Range (Fouch, 1979); the Sheep Pass Formation is the second principle oil source rock (Poole and Claypool, 1984). Beds of the Sheep Pass Formation disconformably overlie Paleozoic strata (Moores and others, 1968). These beds accumulated in local basins (Fouch, 1979) that may have been formed by upper crustal structural extension (Vandervoort and Schmitt, 1990) in the hinterland during Sevier (late Mesozoic to early Tertiary) thrust faulting.

As much as 1,700 m of Oligocene to Miocene rhyolitic welded and nonwelded tuffs were deposited disconformably on the older rocks (Moores and others, 1968). They have an uneven distribution and both local and distant sources (Cook, 1960; Scott, 1965; Moores and others, 1968; Best and others, 1989). The tuffs were deposited prior to or during the early phases of crustal extension. Syntectonic sedimentary rocks of the Miocene and Pliocene Horse Camp Formation both gradationally and unconformably overlie the volcanic rocks (Moores, 1968). As much as 3,300 m of the Horse Camp Formation were deposited in the northern Grant Range and in Railroad Valley; this thickness is a composite figure and less than this can be expected in the Horse Camp sedimentary basins. In actual thickness, Oligocene to Holocene deposits probably do not exceed 3,500 m in Railroad Valley or the Horse Camp Basin in the northern Grant Range (Moores, 1968; Bortz and Murray, 1979; Flanigan, 1988; Read and Zogg, 1988; Veal and others, 1988).

ATTENUATION STRUCTURES

The structural geometry of the northern Grant Range is dominated by a stacked set of younger-on-older low-angle attenuation faults that omit strata; most of these faults are at low angles to bedding and separate the stratigraphic units into structural plates. Both the strata and low-angle attenuation faults are asymmetrically arched about a north-northwest-trending axis. Along the range crest, beds are almost horizontal, whereas those on the east side dip east and those on the west flank dip west (fig. 2); the west limb of the arch is steeper than the east. The style and amount of attenuation on the low-angle faults and in the intervening plates was controlled by lithologic character and structural position (depth) and is also related to location on the arch.

Styles of Attenuation

On the east side of the range at highest structural levels, attenuation was accomplished by large-scale block rotation above low-angle attenuation faults. Large blocks of Mississippian to Tertiary rocks, which generally amount to a kilometer or more of stratigraphic section, form east-dipping ridges on the east side of the range crest. Bedding attitudes in these blocks are from about 20° to 80° to the east. The blocks were tilted during attenuation, mostly along low-angle attenuation faults in the Chainman Shale and Sheep Pass Formation but also in the Joana Limestone, at various levels in the volcanic section, and in the syntectonic Horse Camp Formation. These faults acted as sole faults or decollement zones. Thus, Mississippian to Pennsylvanian and younger rocks are structurally decoupled from older rocks. At the decoupling zones, stratigraphic section is attenuated or eliminated; silicification (jasperoid formation) is particularly common along faults in the Chainman Shale and Joana Limestone. The rotated blocks are remarkably intact, and there is little internal brecciation.

Rocks of the middle and lower structural levels are separated into multiple structural plates by a prominent series of stacked low-angle attenuation faults and are not involved in the large-scale rotated blocks that characterize structures of the higher level. Faults from middle and lower levels do not cut to the surface in the northern Grant Range.

At middle structural levels, the massive dolostones that dominate the Ordovician to Devonian rocks are separated into several structural plates or domains by bounding low-angle attenuation faults that are subparallel with bedding. Thus, individual structural plates are commonly lithologic packages, and, conversely, stratigraphic units are generally attenuated and bounded by low-angle attenuation faults. Important faults of this type are present at the top and bottom of the Guilmette Formation, near the base of the Simonson Dolostone, near the Silurian-Devonian boundary, and at the top of the Eureka Quartzite. The low-angle attenuation faults are, in part, products of (and result from) many high- to moderate-angle, small- to medium-scale faults that coalesced into the specific stratigraphic horizons. Thus, the low-angle attenuation faults at these stratigraphic horizons acted as zones of decoupling between separately extending structural plates.

Attenuation internal to structural plates at middle levels occurred by many different types of extensional structures. Minor low- to moderate-angle attenuation faults, which are difficult to map, caused bedding discordance throughout the section. On the west side of the range, major sets of down-to-the-east, medium-scale attenuation faults are isolated within several different structural plates. These minor fault sets are antithetic to movement on the main system and caused bedding to rotate to the west, thereby steepening the dip of rocks westward into Railroad Valley. Elsewhere, 10-m-scale domino-style attenuation faults are also present. Paleozoic carbonate rocks at middle structural levels are

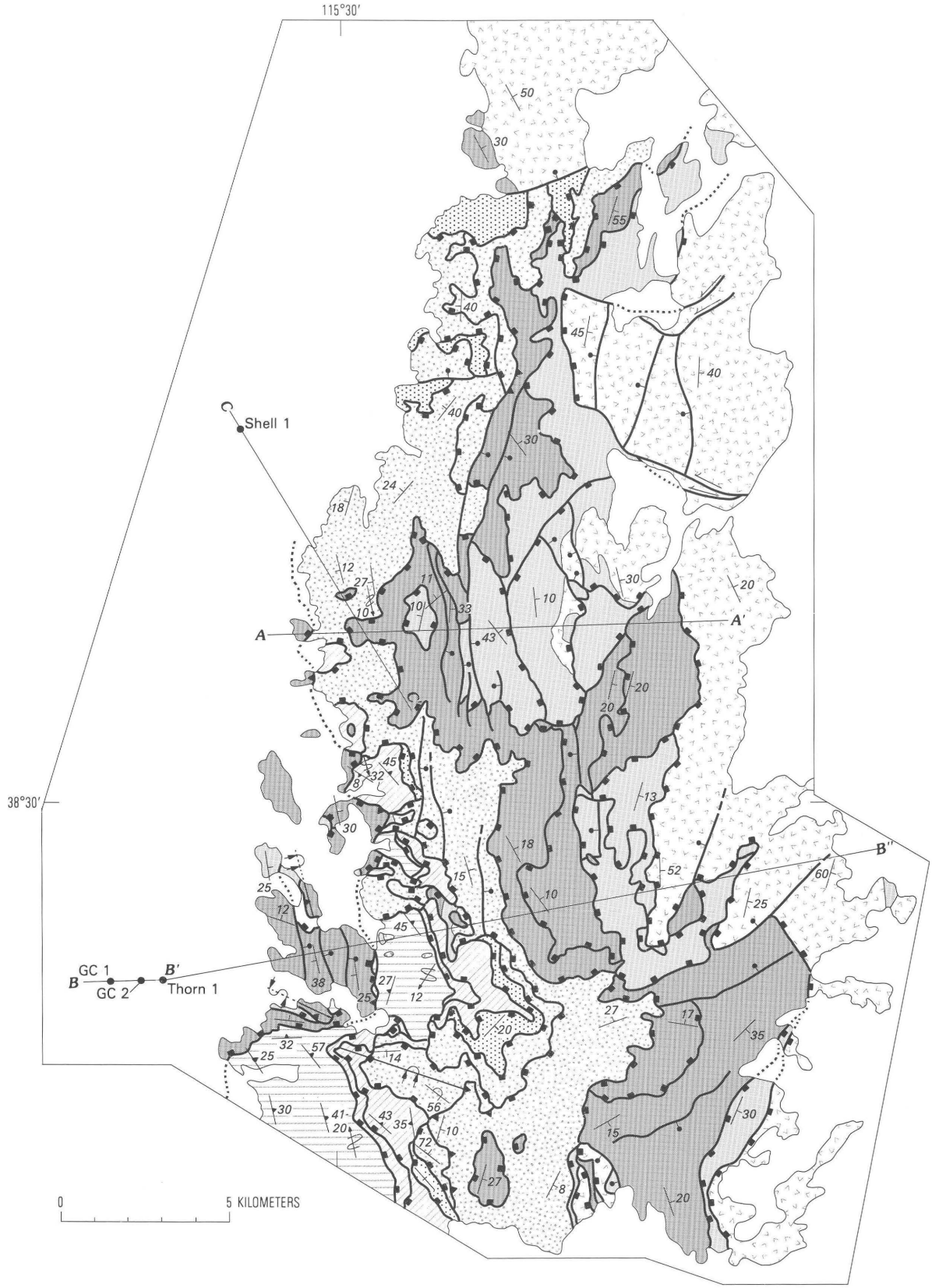
115°30′
38°30′
Shell 1
A
A′
B
B′
B″
GC 1
GC 2
Thorn 1
0
5 KILOMETERS

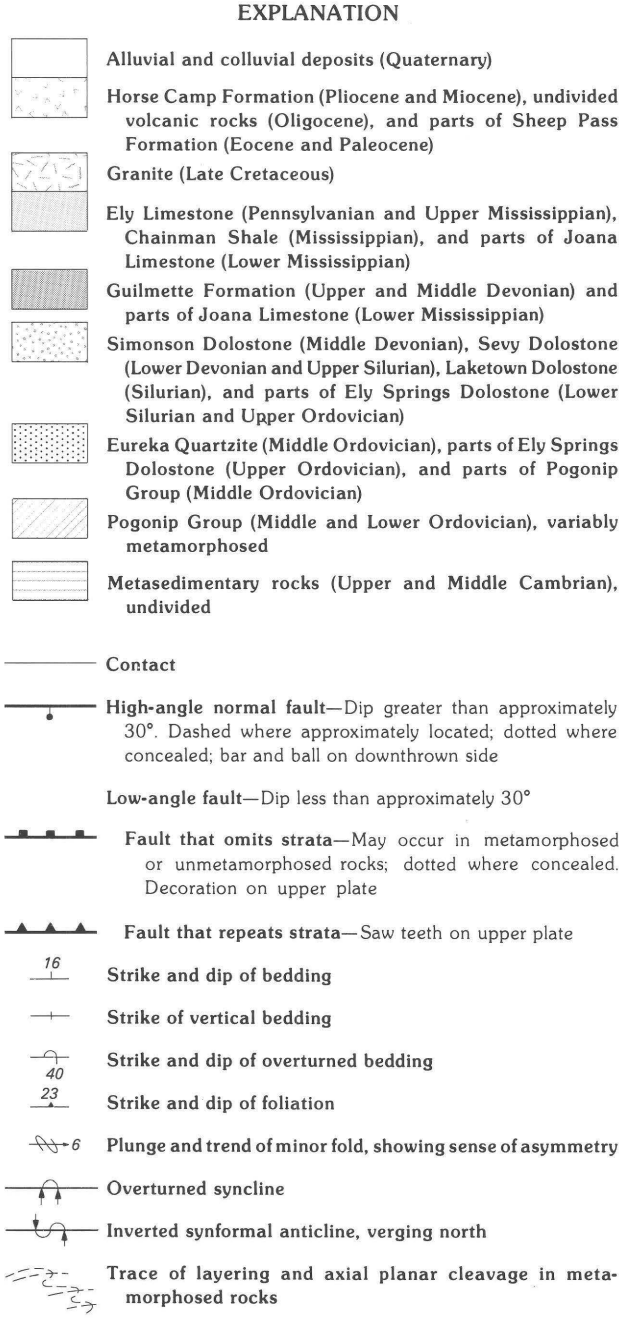

Figure 2 (above and facing page). Tectonic map of northern Grant Range, east-central Nevada. Lines of sections *A–A'*, *B–B'–B"*, and *C–C'* (fig. 3) are also shown. Location of subsurface data used in cross sections indicated by names of drill holes: Shell 1, GC1 (Grant Canyon 1), GC2 (Grant Canyon 2), and Thorn 1. Geology mapped by K. Lund and L.S. Beard, 1984–1987; B. Nevins, 1984; R. Demetrion, A.R. Pyke, and D. Schneidereit, 1985; P.A. Camilleri, M. Elrick, and J.E. Fryxell, 1986; J.L. Snee, 1987; geology of Tertiary volcanic rocks simplified from Scott (1965).

commonly brittlely attenuated and form spectacular breccias; millimeter-scale fragments dominate the dolostone breccias, whereas centimeter- to meter-scale fragments characterize breccias in the limestone beds.

Below the Eureka Quartzite at lower structural levels, Middle Ordovician and older rocks are metamorphosed and ductilely deformed (presumably during Mesozoic shortening). Brittle attenuation structures are superimposed on earlier ductile structures (Lund and others, 1987, 1988; Camilleri, 1989). Macroscopically, the styles of attenuation at this lowest level are similar to those of the middle level except that brittle deformation is less pervasive. Low-angle attenuation faults that are subparallel with bedding and with cleavage also attenuate strata at this level, although associated minor attenuation faults are less common. Breccia zones generally only a few meters thick perhaps reflect the deeper structural level or the pre-existing metamorphic fabric.

Geometry of Attenuation Structures

The stacked low-angle attenuation faults display a peculiar geometry. On the east side of the range, the low-angle attenuation faults are subparallel with bedding and with each other. On the west limb of the arch, the stacked array of low-angle attenuation faults from all structural levels converges into a single 18°–30° west-dipping low-angle attenuation fault zone that extends westward toward Railroad Valley (fig. 3). Where the stacked array of low-angle attenuation faults converges, an extensional culmination is formed. This culmination is well exposed in extensional eyelid windows (Boyer and Elliot, 1982) in several canyons (or valleys) on the west side of the range. In the windows, a stack of at least five major low-angle attenuation faults, which are seen on the east side of the windows, converges to form a single west-dipping fault on the west side of the windows. The convergence forms a consistent geometric pattern: deeper low-angle attenuation faults are more arched than the higher level faults and appear to be truncated where they merge with the higher level faults (Lund and Beard, unpublished mapping, 1984–1987; Lund and Beard, 1987; Camilleri, 1989, 1990; Lund and others, 1991). This pattern in a stacked fault system, where older faults are more tightly folded than younger, indicates that folding and faulting were contemporaneous (Gilluly, 1960).

The single west-dipping fault zone cuts down section in the footwall to the west and includes lenses and slivers (as thick as 200 m) of the intervening cut-out plates; these slivers are similar to features described elsewhere as chaos structures (Wright and Troxel, 1969), nappes (Wernicke, 1981; Lister and Davis, 1989), and extensional duplexes (Gibbs, 1984; Root, 1990) and have been noted in and east of the White Pine Range to the north (Walker and others, 1986).

Additionally, several examples of macroscopic to mesoscopic overturned folds and older-on-younger faults (faults that omit section, fig. 2) are present at specific locations with respect to the low-angle attenuation fault system (Lund and others, 1991). These enigmatic structures are in the upper

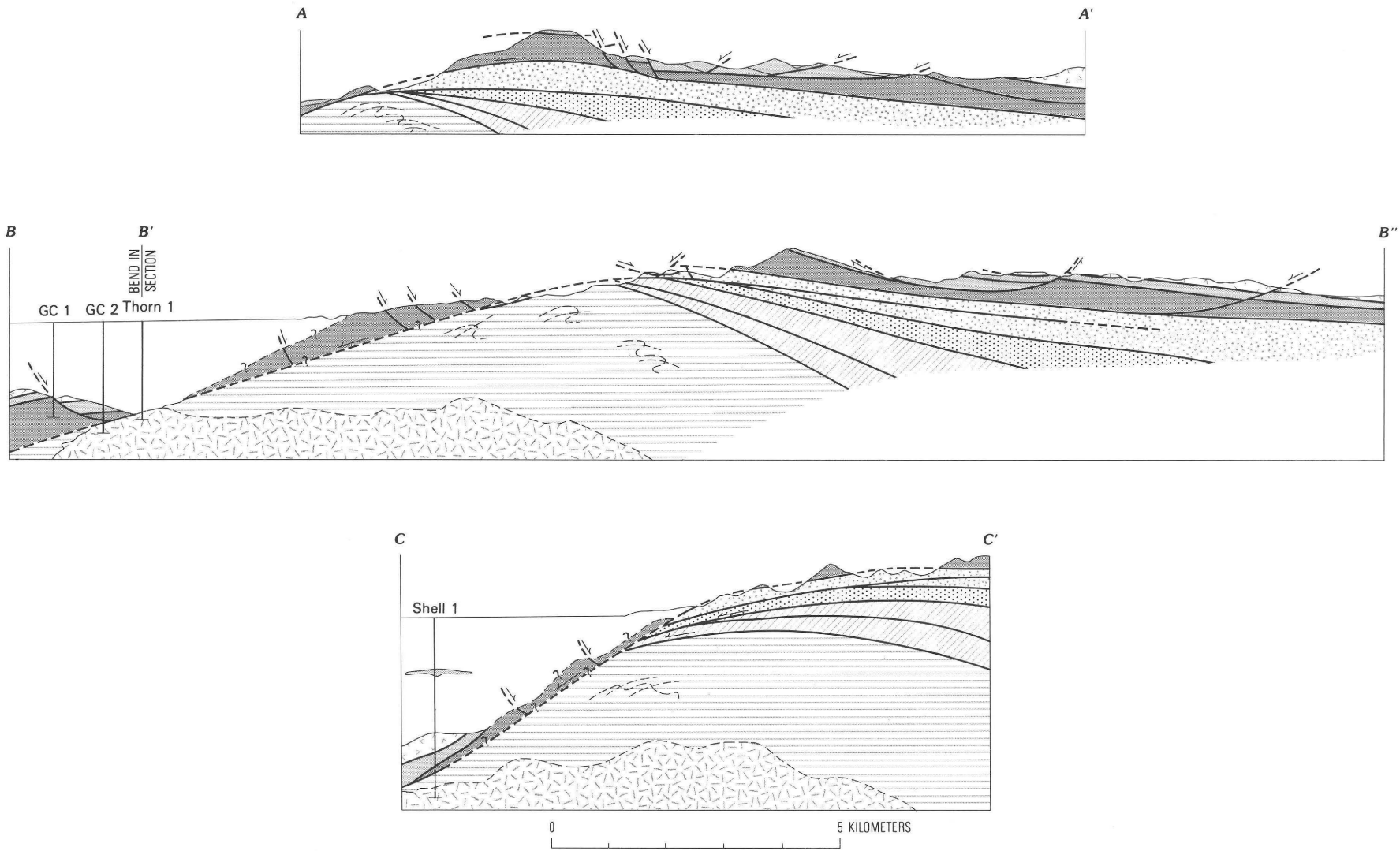

Figure 3. Cross sections showing tectonic relations in northern Grant Range, east-central Nevada. Lines of sections shown in figure 2; units same as in figure 2; no vertical exaggeration. Subsurface information generalized from drill hole data: Shell 1 (Bortz and Murray, 1979); GC1 (Grant Canyon 1), GC2 (Grant Canyon 2), and Thorn 1 (Veal and others, 1988). Surface data from Lund and others (1987, 1988).

plate to the west-dipping fault, and in areas where the stacked low-angle attenuation faults converge. They are also in or near east-trending down-to-the-north fault zones that are transverse to the main north-northwest-trending arch of the range (fig. 2). Where asymmetric, structures near the major down-to-the-west fault are west vergent. Those on the down-to-the-north zones show north vergence. These structures are local, isolated from each other by extensional faults, and cannot be reconstructed as continuous pre-extensional features. The local shortening structures, although possibly the result of Mesozoic compression, were alternatively possibly caused by complex extensional duplexing and (or) by local shortening associated with the overall extension.

The sense of motion along the low-angle attenuation faults is inferred from the geometry of the fault system. No asymmetric ductile fabrics or striated surfaces were found associated with the fault zones (Lund and Beard, unpublished mapping, 1984–1987; Camilleri, 1989), and, probably because the fault zones are subparallel with bedding along most of their length, no offset elements were identified along the low-angle faults. Observation of the faults in the fanned array indicates that relatively more stratigraphic section is omitted and apparent displacement increases westward along each fault. The increase in apparent displacement may be accounted for in part by mesoscopic extensional deformation within the structural plates between each of the attenuation faults; this internal strain may accumulate westward as increased slip on individual attenuation faults. In addition, the entire fault system cuts down section to the west and fanning in the fault system converges westward (Lund and Beard, unpublished mapping, 1984–1987; Camilleri, 1989; Lund and others, 1991). This geometry suggests that the extensional motion was to the west; this is opposite to the sense that would be inferred from an imbricate fan in a thrust setting in which the thrust faults branch in the direction of motion (Gilluly, 1960; Boyer and Elliot, 1982). In summary, the major west-dipping low-angle attenuation fault has the geometry of a west-dipping, west-directed ramp that defines a discrete zone of localized extension to the west, compared with the more diffuse extension in the east part of the range where the fan of attenuation faults is found.

Age of Extension

Deposition of the Oligocene volcanic sequence probably mostly predates extension in the northern Grant Range because there is little angular discordance at the base of or within the volcanic sequence (Scott, 1965; Moores and others, 1968); however, deposition of the Miocene and Pliocene Horse Camp Formation (which remains poorly dated) probably spanned a period of major extension because units display the geometry of growth-faulted sedimentary deposits and include syntectonic deposits (Moores, 1968; Moores and others, 1968). Lower strata of the Horse Camp Formation are tilted as much as 80°, and tilting decreases upward such that younger strata exhibit only minor tilting (Moores and others, 1968). In the central Grant Range, extensional faults cut a tuff dated at 27.8 Ma (Fryxell, 1988). Taylor and others (1989) show that, in the Quinn Canyon Range at the south end of the Grant Range, early extension occurred between 32 and 27 Ma and that peak extension occurred about 14 Ma.

IMPLICATIONS FOR OIL EXPLORATION

Oil from source rocks in the Mississippian Chainman Shale and Paleocene and Eocene Sheep Pass Formation has been produced from reservoirs in Oligocene volcanic rocks, Sheep Pass Formation, Upper Mississippian to Pennsylvanian Ely Limestone, Middle and Upper Devonian Guilmette Formation, Upper Silurian and Lower Devonian Sevy and Middle Devonian Simonson Dolostones, and even from Middle Ordovician Eureka Quartzite (Poole and Claypool, 1984; Flanigan, 1988; Read and Zogg, 1988). The oil traps have long been recognized as structural (Bortz and Murray, 1979; Foster, 1979), but the low-angle attenuation faults in the northern Grant Range have only recently been modelled in cross sections of Railroad Valley (Flanigan, 1988; Read and Zogg, 1988). Although these new models incorporate low-angle attenuation faults into the cross sections, neither the overall structural geometry nor individual faults have been previously linked or integrated from the Grant Range to Railroad Valley.

Published seismic lines for the east side of Railroad Valley show prominent low-angle reflectors, but these reflectors are unexplained on interpretive cross sections (Bortz and Murray, 1979; Anderson and others, 1983; Veal and others, 1988). Many drill holes in the Eagle Springs, Kate Spring, and Grant Canyon fields have been drilled through upper Paleozoic (or younger) rocks directly into early Paleozoic metamorphic rocks or into plutonic rocks (Bortz and Murray, 1979; Flanigan, 1988; Veal and others, 1988); the plutonic rocks are thought to be equivalent to the Late Cretaceous Troy granite (Fryxell, 1988). These metamorphic and plutonic rocks form the lower plate culmination. Thus, the low-angle fault system that dominates the structural geometry of the range can also be extended beneath the valley. For the Grant Canyon oil fields (fig. 3), the depth information from drill holes and the attitudes of reflectors on seismic reflection profiles show that the major west-dipping low-angle fault on the west side of the northern Grant Range continues into Railroad Valley at the same attitude as in the range and with no significant offset (Potter and others, 1991). For Kate Spring and Eagle Springs oil fields to the north, modification of the controlling low-angle attenuation fault system by minor steeper normal faults is more plausible. Significantly, the Railroad Valley oil reservoirs are all in complexly faulted and brecciated rocks (Bortz and Murray, 1979; Poole and Claypool, 1984; Flanigan, 1988; Read and

Zogg, 1988; Veal and others, 1988) that are in the upper plate to this major west-dipping fault.

Previously published petroleum exploration models indicate that oil was found in areas where seismic studies show topographic highs buried beneath valley fill (Bortz and Murray, 1979; Foster, 1979; Flanigan, 1988). These highs were interpreted to be horst blocks formed by minor high-angle normal faults that were part of a high-angle range-front fault system. Alternatively, our study indicates that these buried highs may reflect the irregular topography of the pre-Quaternary (pre-burial) erosional surface that developed on the complexly faulted upper plate of the low-angle attenuation fault system.

CONCLUSIONS

The major structural event preserved in the northern Grant Range is middle to late Tertiary extension that was manifested by synchronous low-angle attenuation faulting and arching. Cross sections incorporating seismic and drillhole data show that the low-angle attenuation fault system in the range extends into Railroad Valley. Although high-angle faults do occur along the range front based on surface geologic and geophysical data, the low-angle attenuation fault system in the area of Grant Canyon oil field is probably not offset (fig. 3); more modification of the low-angle fault system could be expected to the north. Thus, the relief between the range and valley may have been largely caused by arching synchronous with formation of the low-angle attenuation fault system, which dips only 18°–30° west, rather than by a high-angle range-front fault.

This structural geometry suggests the need for a new model for petroleum exploration in the region. In Railroad Valley, both petroleum source and reservoir rocks are in the upper plate to the structural culmination that was formed by the low-angle attenuation fault system; rocks in the upper plate are relatively immature and extensively fractured. The intense fracturing of upper plate rocks and the juxtapositioning of immature source rocks over less fractured, metamorphosed rocks were instrumental in localizing petroleum reservoirs in Railroad Valley.

REFERENCES CITED

Anderson, R.E., Zoback, M.L., and Thompson, G.A., 1983, Implications of selected subsurface data on the structural form and evolution of some basins in the northern Basin and Range province, Nevada and Utah: Geological Society of America Bulletin, v. 94, p. 1055–1072.

Blank, H.R., 1991, Aeromagnetic and gravity data for the Lund 1°×2° Quadrangle, Nevada and Utah—An overview, *in* Flanigan, D.M.H., Hansen, Mike, and Flanigan, T.E., eds., Geology of White River Valley, the Grant Range, eastern Railroad Valley and western Egan Range, Nevada Petroleum Society 1991 Fieldtrip Guidebook: Nevada Petoleum Society, 1991 Fieldtrip Guidebook, p. 55–58.

Bortz, L.C., and Murray, D.K., 1979, Eagle Springs oil field, Nye County, Nevada, *in* Newman, G.E., and others, eds., Basin and Range symposium and Great Basin field conference: Denver, Rocky Mountain Association of Geologists, p. 441–435.

Boyer, S.E., and Elliot, David, 1982, Thrust systems: American Association of Petroleum Geologists Bulletin, v. 66, p. 1196–1230.

Camilleri, P.A., 1989, Superposed compressional and extensional strain in Lower Paleozoic rocks of the northwestern Grant Range, Nevada: Corvallis, Oregon State University, M.S. thesis, 84 p.

Camilleri, P.A., Lund, Karen, and Beard, L.S., 1987, Superposed compressional and extensional strain in metamorphosed Lower Paleozoic rocks of the northern Grant Range, east-central Nevada: Geological Society of America Abstracts with Programs, v. 19, p. 609.

Cebull, S.E., 1967, Bedrock geology of the southern Grant Range, Nye County, Nevada: Seattle, University of Washington, Ph.D. thesis, 130 p.

_____1970, Bedrock geology and orogenic succession in southern Grant Range, Nye County, Nevada: American Association of Petroleum Geologists Bulletin, v. 54, p. 1828–1842.

Cook, E.F., 1960, Great Basin ignimbrites, *in* Boettcher, J.W., and Sloan, W.W., Jr., eds., Geology of east-central Nevada: Intermountain Association of Petroleum Geologists and Eastern Nevada Geological Society, 11th Annual Field Conference Guidebook, p. 134–141.

Effimoff, Igor, and Pinezich, A.R., 1981, Tertiary structural development of selected valleys based on seismic data, Basin and Range province, northeastern Nevada, *in* Extensional tectonics associated with convergent plate boundaries: Royal Society of London Philosophical Transactions, ser. A, v. 300, no. 1454, p. 435–442.

Flanigan, D.M.H., 1988, Kate Spring field discovery, Nevada Basin and Range: The Mountain Geologist, v. 25, p. 159–169.

Foster, N.H., 1979, Geomorphic exploration used in the discovery of Trap Spring oil field, Nye County, Nevada, *in* Newman, G.W., and others, eds., Basin and Range symposium and Great Basin field conference: Denver, Rocky Mountain Association of Geologists, p. 441–453.

Fouch, T.D., 1979, Character and paleogeographic distribution of Upper Cretaceous(?) and Paleogene nonmarine sedimentary rocks in east-central Nevada, *in* Armentrout, J.M., Cole, M.R., and TerBest, H., Jr., eds., Cenozoic paleogeography of the western United States: Society of Economic Paleontologists and Mineralogists, Pacific Coast Paleogeography Symposium 3, p. 97–112.

Fryxell, J.E., 1984, Structural development of the west-central Grant Range, Nye County, Nevada: Chapel Hill, University of North Carolina, Ph.D. thesis, 139 p.

_____1988, Geologic map and descriptions of stratigraphy and structure of the west-central Grant Range, Nye County, Nevada: Geological Society of America Map and Chart Series MCH064, 15 p., scale 1:24,000.

Gibbs, A.D., 1984, Structural evolution of extensional basin margins: Geological Society of London Journal, v. 141, p. 609–620.

Gilluly, James, 1960, A folded thrust in Nevada—Inferences as to time relations between folding and faulting: American Journal of Science, Bradley Volume, v. 258–A, p. 68–79.

Guion, D.J., and Pearson, W.C., 1979, Gravity exploration for petroleum in Railroad Valley, Nevada, *in* Newman, G.W., and others, eds., Basin and Range symposium and Great Basin field conference: Denver, Rocky Mountain Association of Geologists, p. 549–556.

Huttrer, G.W., 1963, Structure and stratigraphy of the central Grant Range, Nevada: Seattle, University of Washington, M.S. thesis, 59 p.

Hyde, J.H., 1963, Structure and stratigraphy of the north central Grant Range, Nevada: Seattle, University of Washington, M.S. thesis, 63 p.

Hyde, J.H., and Huttrer, G.W., 1970, Geology of central Grant Range, Nevada: American Association of Petroleum Geologists Bulletin, v. 54, p. 503–521.

Kellogg, H.E., 1963, Paleozoic stratigraphy of the southern Egan Range, Nevada: Geological Society of America Bulletin, v. 74, p. 685–708.

Kirkpatrick, D.H., 1960, Structure and stratigraphy of the northern portion of the Grant Range, east-central Nevada: Seattle, University of Washington, M.S. thesis, 79 p.

Kleinhampl, F.J., and Ziony, J.I., 1984, Geology of northern Nye County, Nevada: Nevada Bureau of Mines and Geology Bulletin 99A, 172 p.

Lister, G.S., and Davis, G.A., 1989, The origin of metamorphic core complexes and detachment faults formed during Tertiary continental extension in the northern Colorado River region, U.S.A.: Journal of Structural Geology, v. 11, p. 65–94.

Lund, Karen, and Beard, L.S., 1986, Structural history of the northern Grant Range, east-central Nevada—Overprinting of structural styles: Geological Society of America Abstracts with Programs, v. 18, p. 392.

_____1987, Heterogeneous extensional geometries in the northern Grant Range, east-central Nevada: Geological Society of America Abstracts with Programs, v. 19, p. 751.

Lund, Karen, Beard, L.S., Blank, H.R., Jr., Hofstra, A.H., and Hamilton, M.M., 1988, Mineral resources of the Riordans Well Wilderness Study Area, Nye County, Nevada: U.S. Geological Survey Bulletin 1731–H, 16 p.

Lund, Karen, Beard, L.S., and Perry, W.J., Jr., 1991, Structures of the northern Granty Range and Railroad Valley, Nye county, Nevada: Implications for oil occurrences, *in* Flanigan, D.M.H., Hansen, Mike, and Flanigan, T.E., eds., Geology of White River Valley, the Grant Range, eastern Railroad Valley and western Egan Range, Nevada: Nevada Petroleum Society, 1991 Fieldtrip Guidebook, p. 1–6.

Lund, Karen, Nash, J.T., Beard, L.S., Blank, H.R., Jr., and Tuftin, S.E., 1987, Mineral resources of the Blue Eagle Wilderness Study Area, Nye County, Nevada: U.S. Geological Survey Bulletin 1731–D, 19 p.

Moores, E.M., 1968, Mio-Pliocene sediments, gravity slides, and their tectonic significance, east-central Nevada: Journal of Geology, v. 76, p. 88–98.

Moores, E.M., Scott, R.B., and Lumsden, W.W., 1968, Tertiary tectonics of the White Pine–Grant Range region, east-central Nevada, and some regional implications: Geological Society of America Bulletin, v. 79, p. 1703–1726.

Poole, F.G., and Claypool, G.E., 1984, Petroleum source-rock potential and crude-oil correlation in the Great Basin, *in* Woodward, Jane, Meissner, F.F., and Clayton, J.L., eds., Hydrocarbon source rocks of the greater Rocky Mountain region: Denver, Rocky Mountain Association of Geologists, p. 179–229.

Poole, F.G., Sandberg, C.A., and Boucot, A.J., 1977, Silurian and Devonian paleogeography of the western United States, *in* Stewart, J.H., Stevens, C.H., and Fritsche, A.E., eds., Paleozoic paleogeography of the western United States: Society of Economic Paleontologists and Mineralogists, Pacific Coast Paleogeography Symposium 1, p. 39–65.

Potter, C.J., Grow, J.A., Lund, K., Perry, W.J., Jr., Miller, J.J., and Lee, M.W., 1991, Comparison of basin geometry and faulting styles along a regional seismic-reflection profile from Railroad Valley to Lake Valley, Nevada: American Association of Petroleum Geologists Bulletin, v. 75, p. 1137.

Read, D.L., and Zogg, W.D., 1988, Description and origin of the Devonian dolomite oil reservoir, Grant Canyon field, Nye County, Nevada, *in* Goolsby, S.M., and Longman, M.W., eds., Occurrence and petrophysical properties of carbonate reservoirs in the Rocky Mountain region: Denver, Rocky Mountain Association of Geologists, p. 229–240.

Root, K.G., 1990, Extensional duplex in the Purcell Mountains of southeastern British Columbia: Geology, v. 18, p. 419–421.

Scott, R.B., 1965, The Tertiary geology and ignimbrite petrology of the Grant Range, east-central Nevada: Houston, Rice University, Ph.D. thesis, 116 p.

Stewart, J.H., 1978, Basin-range structure in western North America—A review, *in* Smith, R.B., and Eaton, G.P., eds., Cenozoic tectonics and regional geophysics of the western Cordillera: Geological Society of America Memoir 152, p. 1–31.

Vandervoort, D.S., and Schmitt, J.G., 1990, Cretaceous to early Tertiary paleogeography in the hinterland of the Sevier thrust belt, east-central Nevada: Geology, v. 18, p. 567–570.

Veal, H.K., Duey, H.D., Bortz, L.C., and Foster, N.H., 1988, Grant Canyon and Bacon Flat Oil Fields, Railroad Valley, Nye County, Nevada: The Mountain Geologist, v. 25, p. 193–209.

Vreeland, J.H., and Berrong, B.H., 1979, Seismic exploration in Railroad Valley, Nevada, *in* Newman, G.W., and others, eds., Basin and Range symposium and Great Basin field conference: Denver, Rocky Mountain Association of Geologists, p. 557–569.

Walker, C.T., Dennis, J.G., and Lumsden, W.W., 1986, Lenticular stretch structures in eastern Nevada—Possible trapping mechanism in supposed graben: American Association of Petroleum Geologists Bulletin, v. 70, p. 481–482.

Wernicke, Brian, 1981, Low-angle normal faults in the Basin and Range Province—Nappe tectonics in an extending orogen: Nature, v. 291, p. 645–648.

Wright, L.A., and Troxel, B.W., 1969, Chaos structure and Basin and Range normal faults—Evidence for a genetic relationship: Geological Society of America Special Paper 121, p. 580–581.

Chapter J

Late Paleozoic Structure of the Southern Part of the Uinta Basin, Utah, from Seismic Reflection Data

By CHRISTOPHER J. POTTER, REX TANG, and TIMOTHY J. HAINSWORTH

U.S. GEOLOGICAL SURVEY BULLETIN 2012

APPLICATION OF STRUCTURAL GEOLOGY TO MINERAL AND ENERGY RESOURCES OF THE CENTRAL AND WESTERN UNITED STATES

CONTENTS

PLATE

FIGURES

Late Paleozoic Structure of the Southern Part of the Uinta Basin, Utah, from Seismic Reflection Data

By Christopher J. Potter[1], Rex Tang[2], *and* Timothy J. Hainsworth[3]

Abstract

Seismic reflection data from the southern part of the Uinta Basin near Price, Utah, reveal a network of late Paleozoic faults that produced abrupt variations in stratigraphic thicknesses in a structurally complex 30-mi (48 km)-wide northwest-southeast-trending trough. This zone is west of the ancestral Uncompahgre Uplift, north of the Emery Uplift, and east of the Oquirrh Basin. In this zone, Pennsylvanian and Permian clastic rocks locally are several thousand feet thicker than in directly adjacent areas to the north and south.

Faults that displaced strata below the Kaibab Limestone but did not displace the Kaibab were active between Chesterian (top of Doughnut Formation) and Leonardian (Kaibab Limestone) time. High-angle reverse and normal faults occur in a block-faulting pattern similar to that observed in upper Paleozoic rocks in the Piceance basin in northwestern Colorado; thrust faults occur in a local north-south trending belt. In localized zones of strong Mesozoic and (or) Cenozoic reactivation of the late Paleozoic faults, original fault styles are not clear.

West of Price, along the northern edge of the Emery Uplift, the principal Paleozoic faults are northwest-striking, northeast-directed reverse faults that have as much as 5,000 ft (1,525 m) of throw. This fault set is almost colinear with the Uncompahgre Fault (which also underwent late Paleozoic reverse movement) but dips in the opposite direction. Pennsylvanian rocks are locally absent on reverse-fault-bounded structural highs. Steep northwest-striking normal faults are also present.

East and northeast of Price, west-directed thrust faults (and several east-directed backthrusts) controlled late Paleozoic deformation. High-angle reverse and normal faults are also present.

The major northwest-striking reverse faults and the west-directed thrusts accommodated displacements that are compatible with late Paleozoic oblique sinistral-reverse slip on the Uncompahgre Fault. The major reverse faults record a shortening direction parallel to that associated with the Uncompahgre Fault. The west-directed thrust faults probably formed in response to the strike-slip component of movement of the Uncompahgre block as it moved west against the late Paleozoic basin. The probable genetic tie between the Uncompahgre fault and faults in the study area implies that the latter faults were most active during Desmoinesian time. Northwest-trending normal faults may record a relaxation of regional compressive stresses following Ancestral Rockies orogenesis. This interpretation relates all of these late Paleozoic faults to Ancestral Rockies tectonism. Most of the late Paleozoic faults in the study area have undergone only minor post-Paleozoic reactivation or deformation, although major Mesozoic and Cenozoic reactivation locally has occurred.

INTRODUCTION

Regional unconformities and thick sedimentary basins in the central Rocky Mountains, Colorado Plateau, and northeastern part of the Great Basin preserve an impressive record of late Paleozoic ("Ancestral Rockies") orogenesis, but many regional structures of this age have been obscured by younger tectonism, basin development, and volcanism. With few exceptions, major late Paleozoic faults at the margins of Precambrian exposures have been reactivated or overprinted by Laramide-age (Late Cretaceous to Eocene) or younger faults. In order to understand late Paleozoic faulting, it is necessary to separate younger movement from Paleozoic movement or to identify unreactivated Paleozoic structures. Identification of late Paleozoic faults that have not been reactivated (or have undergone only minor reactivation) is best accomplished using subsurface (well and seismic) data (for example, Frahme and Vaughn, 1983). In this study, seismic reflection data from the southern part of the Uinta Basin, near Price, Utah, are used to illustrate the style of late Paleozoic deformation northwest of the ancestral Uncompahgre Uplift.

Acknowledgment.—We thank Grant Norpac, Inc., for permission to publish seismic reflection sections EU–1–85, EU–5, EU–6, and EU–9.

[1]U.S. Geological Survey, Box 25046, MS939, Denver, Colorado 80225.

[2]The Louisiana Land and Exploration Company, 2950 North Loop West, Suite 1200, Houston, Texas 77092.

[3]P.O. Box 461841, Aurora, Colorado 80046.

REGIONAL SETTING

The study area (fig. 1) is on the south flank of the Laramide-age Uinta Basin, directly north of the San Rafael Swell. Tertiary faults (for example, the Clear Creek and Fish Creek Grabens; Osmond, 1965), as well as numerous late Paleozoic fault blocks and small basins that can be defined on seismic reflection data (this report), are present in the area. The Paleozoic basins and faults accommodated displacements in a zone bounded by four major late Paleozoic geologic features: the ancestral Uncompahgre Uplift, the Emery Uplift, the Paradox Basin, and the Oquirrh Basin (fig. 2). Buried late Paleozoic faults have also been identified in seismic data from the Piceance Basin of northwestern Colorado, northeast of the Uncompahgre Uplift (Waechter and Johnson, 1985), and the San Juan Basin of northwestern New Mexico (Huffman and Taylor, 1989). The style and regional significance of buried late Paleozoic structures in the study area are examined in this report.

The late Paleozoic faults that bound the ancestral Uncompahgre Uplift (fig. 2) can be traced into the study area in the subsurface (Stone, 1977). The Uncompahgre Fault, on the southwest side of the uplift, underwent southwest-directed reverse motion in late Paleozoic time (Frahme and Vaughn, 1983; White and Jacobsen, 1983). Stone (1977) inferred that there was also a significant left-lateral component to late Paleozoic displacement on the Uncompahgre Fault, whereas Stevenson and Baars (1986) argued for right-lateral motion. The Garmesa Fault forms the northeast boundary of the uplift. It underwent much less displacement than the Uncompahgre Fault; movement was oblique, dominated by left-lateral slip (Stone, 1977). Late Paleozoic displacements on these faults diminished to zero within, or just east of, the study area, where displacements were accommodated along a system of intersecting shorter faults. Laramide reactivation occurred along the Garmesa Fault, east of the study area (Osmond, 1965), but apparently did not occur along the northwestern part of the Uncompahgre Fault (Heyman, 1983).

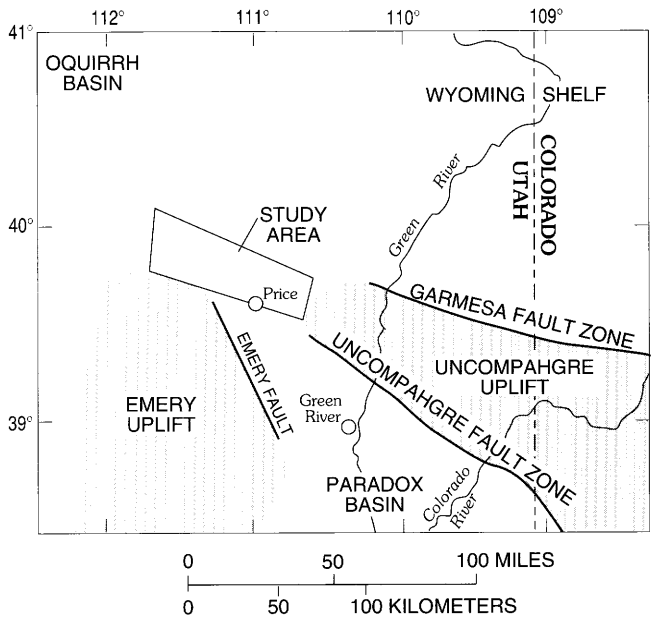

Figure 2. Late Paleozoic geologic setting of study area in southern part of Uinta Basin, Utah.

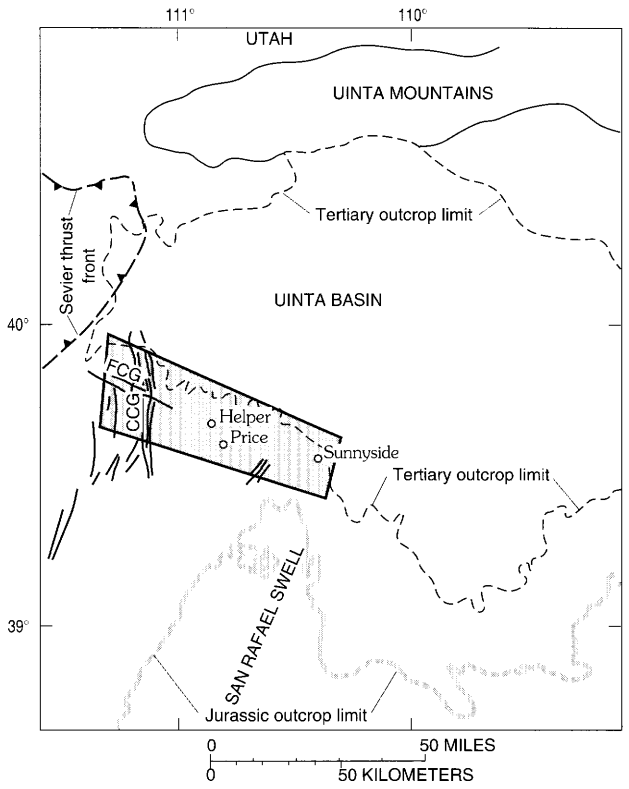

Figure 1. Regional geologic setting of study area (screened pattern), northeastern Utah. CCG, Clear Creek Graben; FCG, Fish Creek Graben.

Szabo and Wengerd (1975) documented a subsurface late Paleozoic fold and fault belt striking N. 60° W. beneath the Paradox Basin adjacent to the south flank of Uncompahgre Uplift. The northwestern end of this belt merges into the "Price graben" of Szabo and Wengerd (1975) between Green River and Price. The "Price graben" formed in late Paleozoic time and is bounded on the northeast by the Uncompahgre Fault and on the southwest by the Emery Fault (fig. 2) (Szabo and Wengerd, 1975); part of it occupies the southeastern part of the study area. The present study indicates that it is not a true graben and that the late Paleozoic structure of the Price area is more complex than that portrayed by Szabo and Wengerd (1975).

Hite (1975) documented a northeast-striking fault set in the Paradox Basin and presented evidence for left-lateral

displacement along these faults. Some of this displacement is clearly Jurassic or younger, but the earlier history of this fault set is poorly understood (Hite, 1975).

Southwest of Price, the Emery Fault, oriented approximately N. 30° W., forms the northeastern boundary of the late Paleozoic Emery Uplift (Szabo and Wengerd, 1975) (fig. 2). Several N. 60° W.-trending faults developed within the Emery Uplift, oblique to the Emery Fault (Szabo and Wengerd, 1975).

The San Rafael Swell (fig. 1) developed during the Laramide across the grain of the Emery Uplift. Laramide deformation is responsible for the present northerly regional dip in the study area, which is at the north-plunging end of the San Rafael Swell and on the north-dipping south flank of the Uinta Basin. Younger fault zones are prominent in the western part of the study area on the Wasatch Plateau. These include the north-trending Clear Creek Graben and the northwest-trending Fish Creek Graben (Osmond, 1965) (fig. 1). The seismic data examined in this study demonstrate that the Fish Creek Graben reactivated late Paleozoic faults.

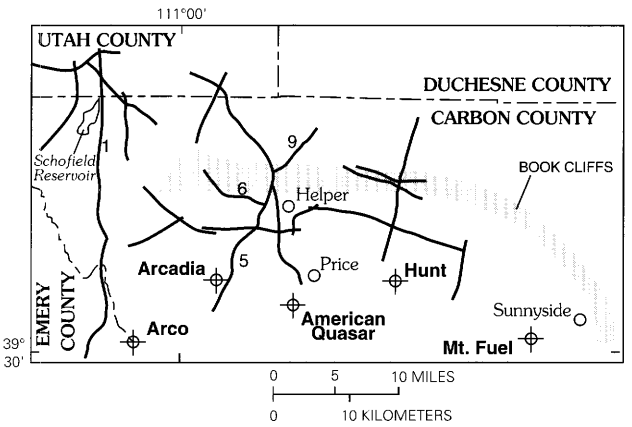

Figure 4. Location of seismic reflection lines examined in this study (heavy lines) and deep wells that penetrate upper Paleozoic section. Numbered lines (1, 5, 6, 9) refer to Grant-Norpac seismic lines EU–1–85, EU–5, EU–6, and EU–9, which are shown on plate 1. Wells: Arco, Arco Hiawatha 1; Arcadia, Arcadia Telonis 1; American Quasar, American Quasar 311 Drunkards Wash; Hunt, Hunt 116 State; Mt. Fuel, Mountain Fuel 1 Sunnyside.

Regional Late Paleozoic Stratigraphy—Correlation With Reflection Data

A stratigraphic column for the upper Paleozoic rocks of the study area is shown in figure 3. These strata are penetrated by deep wells at several locations, and key reflections from this interval can be traced on seismic reflection lines that can be tied to these wells (fig. 4). Identifications of key stratigraphic horizons were calibrated using sonic logs and velocity surveys in the wells.

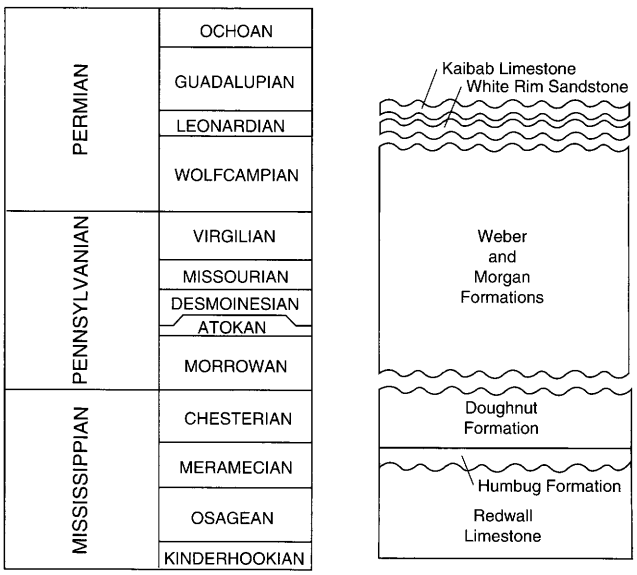

Figure 3. Upper Paleozoic stratigraphy of study area in southern part of Uinta Basin, Utah.

The deepest Paleozoic reflector generally recognized in the area is the top of the Mississippian carbonate rocks correlative with the Redwall and Leadville Limestones. Franczyk (1991) uses the term Madison Limestone in the area north of the Emery Uplift, and the name Deseret Limestone is commonly used in industry logs of well and seismic data in the vicinity of Price. These rocks will be called Redwall in this report, following Hintze (1988). On the seismic lines examined in this study, the Redwall reflection (lines EU–5 and EU–9, plate 1) is a doublet that cannot be traced entirely across any of the seismic lines, probably because of signal penetration problems. The relatively unreflective interval above the Redwall represents the Humbug Formation and the Doughnut Formation (commonly referred to as the Manning Canyon Shale on well logs in the study area). A well-defined doublet at the base of an overlying set of banded reflections (lines EU–5 and EU–9, plate 1) marks the top of the Doughnut. The banded reflection sequence corresponds to mixed clastic and carbonate rocks of the Pennsylvanian and Permian "undifferentiated Weber and Morgan Formations" (Franczyk, 1991). A prominent reflection from the Kaibab Limestone (of Leonardian and locally Guadalupian age; Hintze, 1988) lies above the Weber and Morgan reflections.

In this study, local thickness variations are documented in the interval between the Doughnut and Kaibab reflections (fig. 5). This interval is occupied mainly by the Weber and Morgan Formations. In many cases, the thickness of the Weber and Morgan abruptly changes across Pennsylvanian or Permian faults. On seismic sections, these faults displace Mississippian reflections but do not displace the Kaibab reflection (lines EU–5 and EU–9, plate 1, fig. 6). They are

the primary evidence used to interpret the late Paleozoic structural evolution of the region and are mapped in the subsurface in this study (fig. 5). On some seismic sections, a "Pl" (for lower Permian) reflection is identified within the Pennsylvanian and Permian section (fig. 6). This reflection is tentatively correlated with the top of an interbedded marine limestone, sandstone, and shale unit of Virgilian and Wolfcampian age (lower Cutler beds of Loope and others, 1990; includes rocks assigned to Elephant Canyon Formation by Baars, 1962). Similar to the Kaibab, the Pl reflection is not typically cut by late Paleozoic faults.

DATA

An extensive network of intersecting seismic lines was examined in this study; locations of selected seismic lines are shown in figure 4. Sonic logs and velocity surveys in wells along the seismic lines were used to verify the correlation between reflections and the stratigraphic section. Two-way travel times for the Doughnut to Kaibab interval were measured along these lines, and these travel times were converted to the thicknesses shown on figure 5. This conversion was calibrated using several deep wells (Hunt 1–16 State, American Quasar 31–1 Drunkards Wash, Arcadia Telonis 1) that penetrate upper Paleozoic rocks near the reflection lines (fig. 4). Because the average seismic velocity for this stratigraphic interval differs in each of these wells and would certainly vary throughout the study area, thickness values are approximate.

Fault geometry and sense of offset along late Paleozoic faults were determined based on identification of hanging-wall and footwall cutoffs of Mississippian reflections. Faults illustrated on figure 5 were identified on more than one seismic line in almost every case. Identification of several of the faults on three or more seismic lines permitted

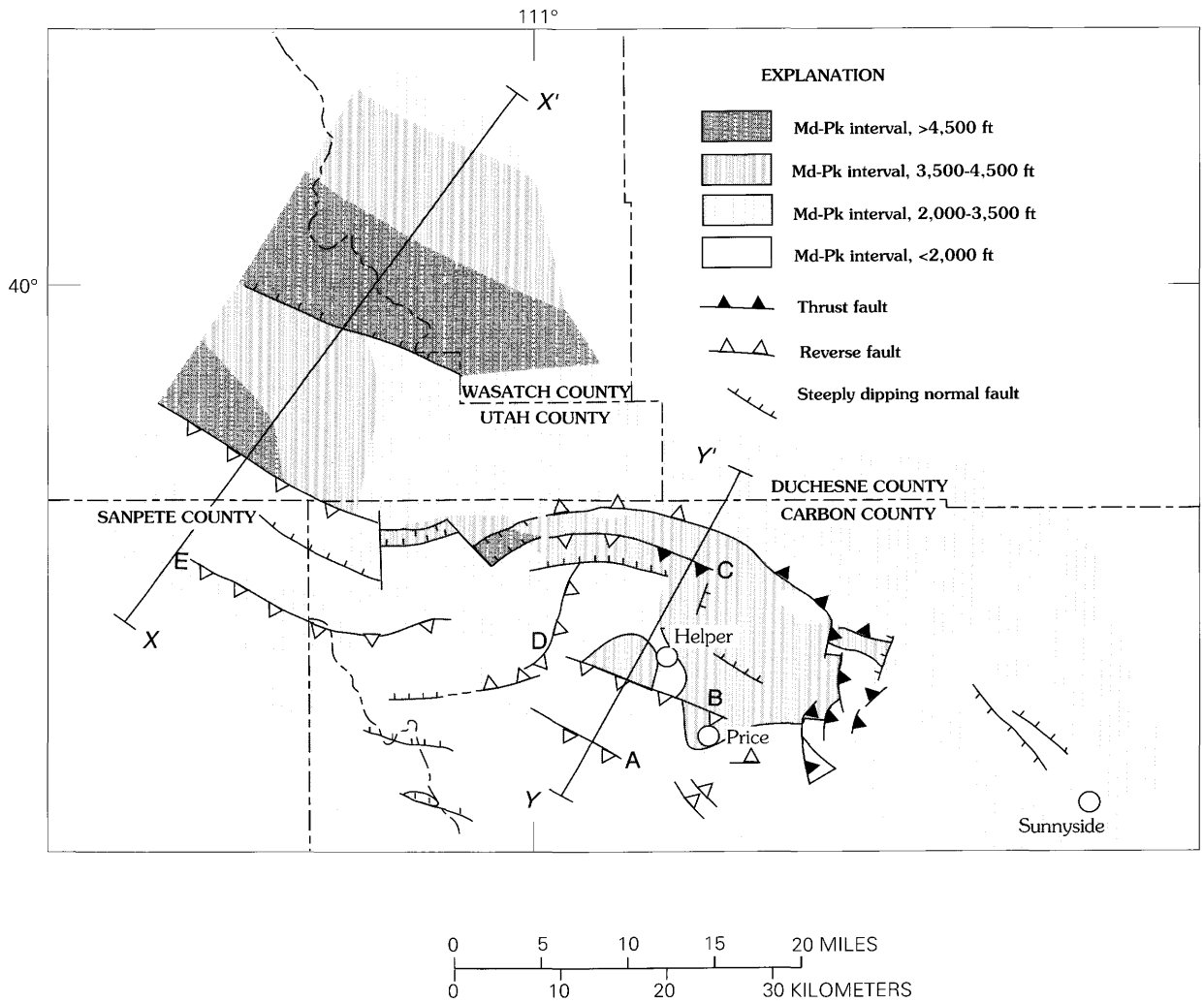

Figure 5. Thickness variations for Doughnut Formation (Md) to Kaibab Limestone (Pk) interval; faults identified or inferred based on reflection data are shown. Lines of sections *X–X'* and *Y–Y'* (fig. 7) are also shown. **A**, **B**, **C**, **D**, and **E** are faults shown on plate 1 and discussed in text.

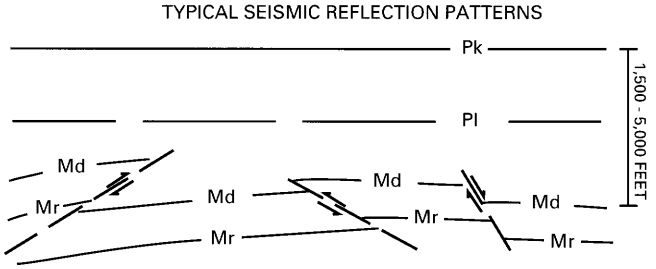

Figure 6. Seismic reflection patterns observed for late Paleozoic faulting in study area. Subhorizontal solid and dashed lines are schematic representations of reflections. In this idealized diagram, Mississippian reflectors are offset by faults and Permian reflectors are not. Examples of actual data (plate 1) demonstrate that in some cases Permian and Mesozoic reflectors have been gently folded above Paleozoic faults by minor Laramide reactivation of faults. Pk, Kaibab Limestone; Pl, top of Upper Pennsylvanian–Lower Permian interbedded limestone, shale, and sandstone sequence; Md, Doughnut Formation; Mr, Redwall Limestone.

detailed observation of along-strike variations in offset and fault geometry.

Seismic data that illustrate the structural styles are shown on plate 1. These Vibroseis data (lines EU–1–85, EU–5, EU–6, and EU–9) were recorded by Grant Norpac, Inc., in July 1983 (EU–5), June 1984 (EU–6, EU–9), and June 1985 (EU–1). Lines EU–5, EU–6, and EU–9 were acquired using a 16-second, 14–80-Hz source sweep, a shot point interval of 440 ft (134 m), 96 geophone groups with 220-ft (67 m) spacing, and a nominal stacking fold of 24. Line EU–1 was acquired using a 16-second, 10–56-Hz source sweep, a shot point interval of 330 ft (101 m), 120 geophone groups with 165-ft (50 m) spacing, and a nominal stacking fold of 30.

Seismic lines EU–5 and EU–9 form a 17-mi (27 km)-long northeast-southwest transect in the vicinity of Helper (plate 1). Along these seismic lines, the Doughnut to Kaibab interval gradually thickens from southwest to northeast from approximately 1,500 to 3,600 ft (457–1,097 m), and three northeast-directed reverse and thrust faults (**A**, **B**, **C**) intersect the lines. The geometry of each of these faults is constrained by hanging-wall and footwall cutoffs of Mississippian reflectors (Redwall and Doughnut). Based on these relationships, faults **A**, **B**, and **C** dip approximately 30°, 50° , and 10° SE., respectively. Updip from fault **A**, a local increase in dip in the Mesozoic reflectors indicates minor Laramide (?) reactivation of this fault.

Local discordances (truncation or onlap) within the Pennsylvanian and Permian banded zone attest to uplift of individual fault blocks. Near the Arcadia Telonis 1 well (line EU–5, plate 1), inclined reflections in the banded Pennsylvanian and Permian sequence in the hanging wall of fault **A** are locally truncated. The Pl reflection appears to be folded above, and perhaps offset by, fault **A**. A dipping reflection in the interval between the Pl and Pk reflections (fig. 5) is truncated and overlain by subhorizontal reflections. To the north, the Pl reflection continues undeformed above faults **B** and **C**. Just south of fault **C**, there is a southward-onlapping pattern at a lower stratigraphic level within the banded Pennsylvanian and Permian reflections. Thus, within these two seismic lines, several local unconformities provide evidence for localized erosion and (or) nondeposition at slightly different stratigraphic positions.

Line EU–6 (plate 1), which extends to the northwest from the intersection of lines EU–5 and EU–9 near Helper (fig. 4), illustrates gradual northwesterly thinning of the Doughnut to Kaibab interval on the upthrown (southeast) side of a minor steeply dipping fault (**D**). The fault geometry is not well constrained by the seismic data here, and the dip of Doughnut reflections away from the fault in both directions suggests that an arch is locally developed. Southeast of the fault, a local angular unconformity is defined by the onlapping of Pennsylvanian and Permian strata above the gently southeast dipping Doughnut reflector. It is possible that fault-induced arching produced a submarine, or barely emergent, topographic high across which younger layers onlapped. Arching of reflectors above fault **D** in the Kaibab through Dakota section demonstrates that post-Paleozoic deformation persisted in this zone and probably included Laramide reactivation of the fault.

Line EU–1 (plate 1) is a 26-mi (42 km)-long, north-south seismic line in the western part of the study area. Data quality on line EU–1 is inferior to that of the other seismic lines discussed here, especially in an 8-mi (13 km) interval (denoted by shading along the top of the line drawing in plate 1) near Schofield Reservoir (fig. 4). The poorer data quality may be related to raypath complexities produced by young structures; line EU–1 follows the Clear Creek Graben, and the Fish Creek Graben crosses the seismic line near Schofield Reservoir (Osmond, 1965). The data quality deteriorates significantly in the Fish Creek Graben, and the graben itself is not well imaged. The Mesozoic or younger faults that are apparent on plate 1 may be related to the Clear Creek Graben; the seismic line is highly oblique to the strike of this north-trending fault zone.

Although the Paleozoic section is not well imaged on line EU–1, some significant trends are apparent. The southern part of the line is on the north flank of the Emery Uplift, as evidenced by the absence of the Doughnut Formation along the southern one-third of this line and in the nearby Arco Hiawatha 1 well. North of fault **E**, the Redwall to Kaibab interval abruptly thickens and discontinuous Doughnut reflections may be present (plate 1). In the northern part of the line EU–1, there are obvious Doughnut reflections. The abrupt variation in thickness of the late Paleozoic section across fault **E** indicates that the fault was active during late Paleozoic time. Other faults on this seismic line may have undergone Paleozoic movement, but all of these faults also underwent younger movement, as shown by the offset of the Kaibab and younger reflectors. Thus, it is difficult to obtain a clear picture of late Paleozoic movement for these faults.

STRUCTURAL PATTERNS AND THICKNESS VARIATIONS

The overall pattern of faults and thickness variations is shown on figure 5. In most of the study area, the thickness of the Doughnut to Kaibab interval varies from about 1,500 to about 4,500 ft (457–1,372 m); the variation is principally controlled by local syndepositional faulting. The interval is thinnest (1) west and southwest of Helper, corresponding to the north flank of the Emery Uplift, and (2) around Sunnyside, at the northwest end of the ancestral Uncompahgre Uplift (fig. 5).

West of Price, the principal Paleozoic faults are northwest-striking, northeast-directed reverse faults that step off of the northern and northeastern margins of the Emery Uplift and have as much as 5,000 ft (1,525 m) of throw (figs. 5, 7). Across one of these faults, the preserved thickness of the Doughnut to Kaibab interval varies from zero (where the entire interval has been locally eroded) to more than 5,000 ft (1,525 m). Steep northwest-striking normal faults are also present.

North of Helper, a thickened late Paleozoic section in an east-west striking subbasin occupies a footwall position with respect to two bounding reverse faults that have opposing displacement directions (figs. 5, 7). The more northerly of the two reverse faults merges to the southeast with a northerly striking, west-directed thrust system that controlled late Paleozoic deformation east and northeast of Price.

The structural style in this thrust system resembles that of a foreland thrust belt, in contrast to the block-faulting style that is evident to the west. Figure 8 illustrates imbricate thrust structure observed on a seismic line about 6 mi (10 km) east of Price. A few backthrusts, as well as high-angle reverse and normal faults, are also present (fig. 5).

The reflection patterns indicate that many of the late Paleozoic faults in this region are essentially growth faults, regardless of geometry (normal, thrust, or reverse). Although local truncation and onlapping relationships within the Morgan and Weber Formations are indicative of

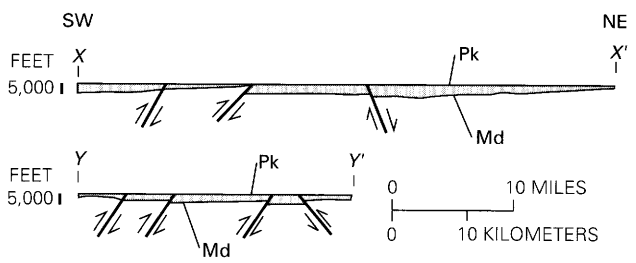

Figure 7. Cross sections *X–X'* and *Y–Y'* showing variations in thickness in Doughnut Formation (Md) to Kaibab Limestone (Pk) interval, and traces of major faults. Datum is top of Kaibab Limestone; no vertical exaggeration. Shaded area is Md–Pk interval. Lines of sections are shown in figure 5.

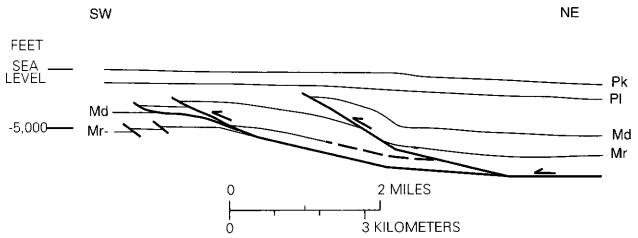

Figure 8. Cross section interpreted from migrated seismic section about 6 mi (10 km) east of Price, illustrating imbricate thrust structure that is part of small north-south-striking thrust system. Thrust faults shown here have produced about 1.2 mi (2.0 km) of shortening. Solid lines are traced from reflections, dashed lines are interpreted continuations of stratigraphic horizons, and stippled lines are inferred faults. Vertical exaggeration approximately 0.85. Stratigraphic symbols denote top of unit as inferred from seismic data. Pk, Kaibab Limestone; Pl, top of Upper Pennsylvanian–Lower Permian interbedded limestone, shale, and sandstone sequence; Md, Doughnut Formation; Mr, Redwall Limestone.

local emergence of fault blocks, most of the faulting probably occurred in a relatively shallow submarine setting during Pennsylvanian and Permian deposition and did not result in widespread subaerial exposures.

Mesozoic and Tertiary reactivation and overprinting are most apparent near the Clear Creek and Fish Creek Grabens and near Sunnyside (fig. 1). Young faulting occurred in other parts of the study area, but in most cases the late Paleozoic structures have not been greatly modified by younger faulting.

DISCUSSION

Fault patterns in the study area present a complex picture dominated by high-angle (block) faulting in the western part of the study area and by thrust faulting in the eastern part. Reverse and thrust faulting are predominant, but normal faults are locally important.

A distinctive style of faulting is associated with each of the two Ancestral Rockies uplifts that bound the study area. Northwest-striking, steeply southwest dipping reverse faults bound the Emery Uplift on its northern and northeastern sides, whereas a north-striking, west-directed local thrust system bounds the ancestral Uncompahgre Uplift at its northwest end. The other faults may comprise an interference pattern between these two principal zones, as will be discussed later in this section.

The northwesterly strike of reverse faults that step off the north end of the Emery Uplift is almost parallel to the strike of the Uncompahgre Fault, known to be a major late Paleozoic reverse fault (fig. 9). The faults are also parallel to the N. 60° W.-striking faults documented by Szabo and Wengerd (1975) within the Emery Uplift. Although the

Uncompahgre Fault dips northeast and the faults north of the Emery Uplift dip southwest, the orientation of all of these faults is compatible with regional northeast-southwest shortening.

West-directed thrusting at the northwest end of the Uncompahgre Uplift requires that the Uncompahgre block moved west with respect to the late Paleozoic sedimentary basin in the study area. Such movement agrees with Stone's (1977) conclusion that the Uncompahgre Fault experienced significant strike-slip motion in addition to its well-documented reverse slip (Frahme and Vaughn, 1983). Several miles of left-lateral motion on the Uncompahgre Fault could have been transferred to the west-directed thrust system, in which shortening occurred in front of the west-driven Uncompahgre Uplift.

The curved fault pattern north and northwest of Helper is part of a complex zone of accommodation between the Uncompahgre and Emery Uplifts. The two uplifts are bounded by en echelon reverse fault zones (fig. 9) that require either a strike-slip zone or a complex curved fault zone between the two uplifts. Northwest-southeast motion of the Uncompahgre or Emery blocks would further complicate the structure in the intervening region. Along the curved faults north and northwest of Helper, high-angle reverse displacement (and local low-angle thrusting) occurred on east to northwesterly striking segments. Individual reverse faults pass into low-angle thrusts at their southeast ends; to the south, this fault geometry is replaced by the north-south thrust system described above. The curved faults in this accommodation zone appear to have been flattened and rotated toward the orientation of the north-south thrust system; such rotation is a further expression of shortening associated with northwesterly movement of the ancestral Uncompahgre Uplift.

The fault pattern in and near the study area is consistent with a general northeast-southwest orientation for regional compression. Slight variations in the regional stress field during Pennsylvanian and Permian time could have produced alternating reverse and strike-slip motion on major pre-existing zones of weakness that trend about N. 60° W. (For example, regional compression oriented between N. 45° E. and N. 15° E. could produce reverse displacement on the Uncompahgre Fault and the northwesterly trending faults north of the Emery Uplift; easterly excursions of regional compression direction would produce sinistral strike slip on the same faults.) The reflection data provide information only on dip-slip motion; there may have been a considerable strike-slip component of motion on some of the northwesterly striking subsurface faults in the study area.

Normal faults are also present, both parallel and orthogonal to the dominantly northwest trends of the reverse faults. Northeasterly striking normal faults are compatible with the northeast-southwest regional compression direction proposed above. The northwesterly striking normal faults may have developed in response to "post-Ancestral Rockies"

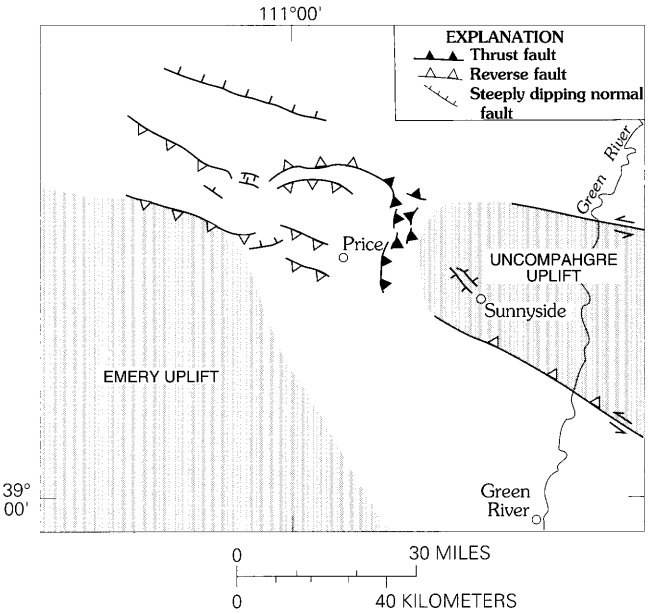

Figure 9. Paleozoic geologic setting of study area including major faults identified in this study.

(and pre-Kaibab) relaxation of the northeast-southwest compression. It is also possible that movement on some of these faults included a strike-slip component.

It is difficult to closely constrain the timing of movement on the late Paleozoic faults discussed here. The faults displace reflectors correlated with the Meramecian and Chesterian Doughnut Formation and do not offset reflectors correlated with the Leonardian Kaibab Limestone. In examples cited above, local unconformities (surfaces of truncation and onlap) were identified within the banded reflection zone in the Weber and Morgan Formations; these are surfaces of erosion and (or) nondeposition above fault blocks and are overlain by reflectors that are not affected by the late Paleozoic faulting. The Pl reflection is stratigraphically higher than almost all of these local unconformities and postdates most of the faults. If the Pl reflector marks the top of the Virgilian and Wolfcampian interbedded carbonate and clastic sequence, as suggested above, almost all of the late Paleozoic faulting would have to be pre-Wolfcampian. Relationships near fault A on line EU–5, illustrated in plate 1, are the only examples of slightly younger Permian deformation cited here. Thus, the late Paleozoic faulting in the study area was certainly post-Chesterian and pre-Leonardian and probably pre-Wolfcampian in most cases. If, as suggested above, the faults are genetically tied to the displacement on the Uncompahgre Fault, they were most active in Desmoinesian time because Desmoinesian sedimentation patterns strongly suggest that the Uncompahgre Uplift was rising most rapidly at this time (Szabo and Wengerd, 1975; Johnson and others, in press).

Kluth and Coney (1981) interpreted Ancestral Rockies orogenesis as the remote foreland expression of the Ouachita-Marathon orogeny, which was produced by collision between South America–Africa and a peninsular projection of the North American craton. Budnick (1986) proposed that the Ancestral Rockies were formed along the Wichita megashear in response to the collision of eastern North America with Africa (Alleghanian orogeny). These two models have different kinematic implications for the structures in and near the study area (Budnick, 1986). A right-lateral component of displacement on northwesterly striking faults would be consistent with the Kluth and Coney model, whereas a left-lateral component of displacement would be consistent with the Budnick model. Because the study area is small, the buried fault patterns cannot rule out either model; however, the fault patterns are most compatible with the model of Budnick (1986), which requires left-lateral shear along northwesterly trending faults and east- to northeast-directed compression. The relevant observations in the study area include the reverse component of movement on northwesterly striking faults and the local north-south thrust belt that provides evidence for westward motion of the Uncompahgre block relative to the Paleozoic sedimentary rocks in the Price area. This study produced no evidence, however, that the Uncompahgre Fault and the study area are part of a megashear along which 72–93 mi (120–150 km) of left-lateral displacement occurred, as suggested by Budnick (1986). Instead, our analysis implies that strike-slip displacement on the Uncompahgre Fault was probably less than 6 mi (10 km).

REFERENCES CITED

Baars, D.L., 1962, Permian system of the Colorado Plateau: American Association of Petroleum Geologists Bulletin, v. 46, p. 149–218.

Budnick, R.T., 1986, Left-lateral intraplate deformation along the Ancestral Rocky Mountains; implications for late Paleozoic plate motions: Tectonophysics, v. 132, p. 195–214.

Frahme, C.W., and Vaughn, E.B., 1983, Paleozoic geology and seismic stratigraphy of the northern Uncompahgre front, Grand County, Utah, *in* Lowell, J.D., ed., Rocky Mountain foreland basins and uplifts: Rocky Mountain Association of Geologists Guidebook, p. 201–211.

Franczyk, K.J., 1991, Phanerozoic stratigraphic and time-stratigraphic cross sections along line *C–C′*, Uinta and Piceance basin area, southern Uinta Mountains to northern Henry Mountains: U.S. Geological Survey Miscellaneous Investigations Series Map I–2184–C.

Heyman, O.G., 1983, Distribution and structural geometry of faults and folds along the northwestern Uncompahgre uplift, western Colorado and eastern Utah, *in* Averett, W.R., ed., Northern Paradox Basin–Uncompahgre uplift: Grand Junction Geological Society Guidebook, p. 45–57.

Hintze, L.F., 1988, Geologic history of Utah: Brigham Young University Geology Studies Special Publication 7, 202 p.

Hite, R.J., 1975, An unusual northeast-trending fracture zone and its relations to basement wrench faulting in northern Paradox Basin, Utah and Colorado: Four Corners Geological Society Field Conference, 8th, Canyonlands Guidebook, p. 217–223.

Huffman, A.C., Jr., and Taylor, D.J., 1989, San Juan Basin faulting—More than meets the eye [abs.]: American Association of Petroleum Geologists Bulletin, v. 73, p. 1161.

Johnson, S.Y., Chan, M.A., and Konopka, E.H., in press, Pennsylvanian and Early Permian paleogeography of the Uinta-Piceance basin region, northwest Colorado and northeast Utah: U.S. Geological Survey Bulletin 1787–CC.

Loope, D.B., Sanderson, G.A., and Verville, G.J., 1990, Abandonment of the name "Elephant Canyon Formation" in southeastern Utah; physical and temporal implications: The Mountain Geologist, v. 27, p. 119–130.

Kluth, C.F. and Coney, P.J., 1981, Plate tectonics of the Ancestral Rocky Mountains: Geology, v. 9, p. 10–15.

Osmond, J.C., 1965, Geologic history of site of Uinta Basin, Utah: American Association of Petroleum Geologists Bulletin, v. 49, p. 1957–1973.

Stevenson, G.M., and Baars, D.L., 1986, The Paradox—A pull-apart basin of Pennsylvanian age, *in* Peterson, J.A., ed., Paleotectonics and sedimentation in the Rocky Mountain region, U.S.: American Association of Petroleum Geologists Memoir 41, p. 513–539.

Stone, D.S., 1977, Tectonic history of the Uncompahgre uplift, *in* Veal, H.K., ed., Exploration frontiers of the central and southern Rockies: Rocky Mountain Association of Geologists Field Conference, 1977, Guidebook, p. 23–30.

Szabo, E., and Wengerd, S.A., 1975, Stratigraphy and tectogenesis of the Paradox Basin: Four Corners Geological Society Field Conference, 8th, Canyonlands Guidebook, p. 193–211.

Waechter, N.B., and Johnson, W.B., 1985, Seismic interpretation in the Piceance Basin, northwest Colorado, *in* Gries, R.R., and Dyer, R.C., eds., Seismic exploration of the Rocky Mountain region: Rocky Mountain Association of Geologists and Denver Geophysical Society, p. 247–258.

White, M.A., and Jacobson, M.I., 1983, Structures associated with the southwest margin of the ancestral Uncompahgre uplift, *in* Averett, W.R., ed., Northern Paradox Basin–Uncompahgre uplift: Grand Junction Geological Society Guidebook, p. 33–39.

Chapter K

Audio-Magneto-Telluric Investigation at Turkey Creek Caldera, Chiricahua Mountains, Southeastern Arizona

By ROBERT M. SENTERFIT and DOUGLAS P. KLEIN

U.S. GEOLOGICAL SURVEY BULLETIN 2012

APPLICATION OF STRUCTURAL GEOLOGY TO MINERAL AND
ENERGY RESOURCES OF THE CENTRAL AND WESTERN UNITED STATES

CONTENTS

FIGURES

Audio-Magneto-Telluric Investigation at Turkey Creek Caldera, Chiricahua Mountains, Southeastern Arizona

By Robert M. Senterfit[1] *and* Douglas P. Klein[1]

Abstract

Electromagnetic induction data obtained using distant field sources, mostly of natural origins in the audio-magneto-telluric frequency range of 4.5–27,000 Hz, were analyzed to depict the geoelectric structure of the Turkey Creek volcanic center, an inferred mid-Tertiary rhyolitic caldera about 20 km in diameter and located about 10 km south of the Chiricahua National Monument in the Chiricahua Mountains of southeastern Arizona. The data for each station consist of scalar electromagnetic measurements at discrete frequencies for two orthogonal magnetic and electric field pairs. Thirty-two stations were occupied, spaced about 0.5 km apart. Observations made along profiles across the caldera ring structure and on either side of the structure indicate that a unit having a resistivity of about 2,500 ohm-m probably represents the monzonite within the mapped caldera ring structure. At a depth of about 2,000 m a unit of similar resistivity in the Cretaceous-Precambrian sedimentary rocks surrounding the caldera is inferred to be overlain by a unit of lower resistivity that probably represents Cretaceous sedimentary rocks and weathered near-surface material.

High resistivity values are noted for the deeper core intrusive rocks in contrast with the lower resistivity values for the tuffs and flow rocks. High resistivity units associated with inferred ring structures are present on the east side of the structure and absent on the north and west flanks of the volcanic center.

INTRODUCTION

Data from 32 audio-magneto-telluric (AMT) soundings (4.5–27,000 Hz) were collected in the summer of 1989 in the area of the Turkey Creek caldera in the Chiricahua Mountains of southeastern Arizona (fig. 1). The objective of this work was to aid in the geologic mapping of the structural and lithologic relationships in the area by providing information on the electrical structure of the subsurface. It seemed likely that there would be distinguishable resistivity contrasts between Tertiary tuff units, pre-Tertiary sedimentary units, and Tertiary intrusive rocks of this area. The sounding data were collected along six profiles (fig. 1) located to provide a reconnaissance picture of the geoelectrical structure to interpretative depths of about 2–5 km. Soundings were placed across the west and east edges of an inferred caldera structure (du Bray and Pallister, 1991) at locations mostly dictated by available access.

The AMT method consists of recording natural electromagnetic field variations and their corresponding induced electric fields in the Earth at discrete frequencies. The principles of the AMT method correspond to those of the magneto-telluric (MT) method (Cagniard, 1953; Vozoff and others, 1963; Vozoff, 1972), except that the signals measured are at higher frequencies and originate mainly from atmospheric electrical disturbances (spherics) rather than from ionospheric or magnetospheric phenomena. Strangway and others (1973) discussed the potential and limitations of the AMT method in mineral exploration. Case histories of the AMT method in mineral and geothermal environments have been described by Strangway and Kozier (1979), Hoover and others (1976), and Hoover and Long (1976). Previous AMT or MT studies investigating the structural and lithologic relations in volcanic areas include those by Hoover and others (1976) and Hermance and others (1984) (Long Valley, California); Leary and Phinney (1974), Stanley and others (1977), and Stanley (1982) (Yellowstone, Wyoming and Idaho); Long (1985) (Questa, New Mexico); and Fitterman and others (1988) (Newberry volcano, Oregon).

Much of the geology of the Turkey Creek caldera is exposed in cross section as a result of extensional Basin and Range faulting and associated erosion (Marjaniemi, 1969; Latta, 1983). The caldera formed about 25 Ma, during the Oligocene, in response to eruption of silicic ash-flow tuff of the Rhyolite Canyon Tuff (fig. 1). Precaldera volcanic rocks of the area include rhyolitic tuffs to intermediate-composition flow rocks. A large central monzonite porphyry unit is

[1]U.S. Geological Survey, Box 25046, MS960, Denver, Colorado 80225.

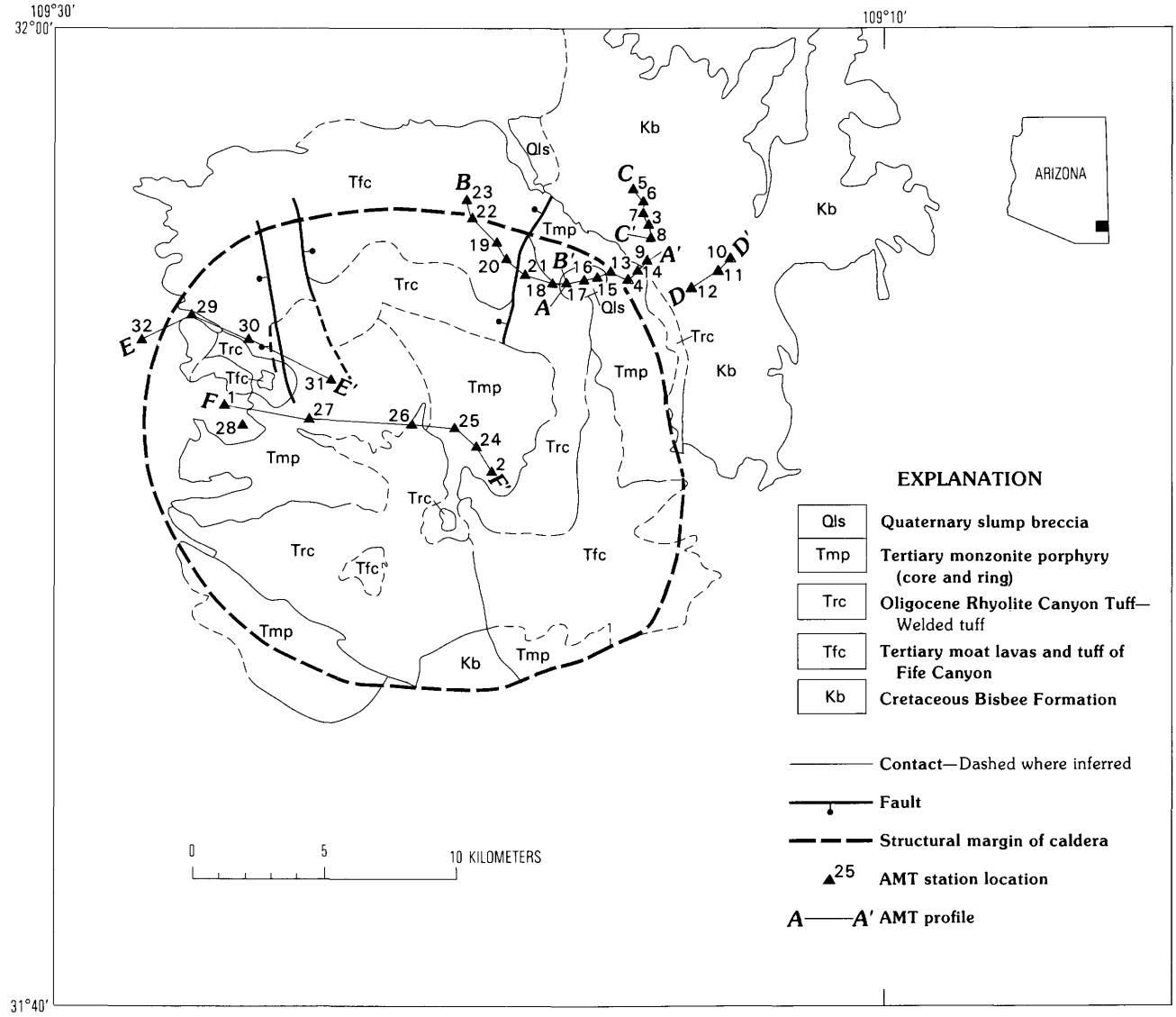

Figure 1. Location of audio-magneto-telluric soundings in Turkey Creek caldera area, Chiricahua Mountains, southeastern Arizona. Profiles *A–A'* through *F–F'* are presented as contoured, composite one-dimensional cross sections in figures 2–7. Generalized geology from du Bray and Pallister (1991).

intrusive into the domed intracaldera tuff (Lipman, 1984). The caldera is bordered by Cretaceous sedimentary rocks of the Bisbee Formation to the east where the ring structure is best exposed. The caldera borders are less certain to the north where they disappear under rhyolite flow rocks and tuff, to the west where the caldera is bordered by alluvium, and to the south where adjacent calderas may be present.

DATA ACQUISITION AND PROCESSING

The scalar AMT system used by the U.S. Geological Survey (Hoover and others, 1976, 1978; Hoover and Long, 1976) records in analog form two sets of orthogonal magnetic (H) and electric (E) field amplitudes for each of several frequency bands. The system has the capability for 16 narrow-band frequencies distributed logarithmically in the range of 4.5–27,000 Hz. Typically, measurements at all bands are attempted, but atmospheric signal conditions can preclude acquisition of reliable data for some frequencies. The 32 stations in this report were observed in May 1989. The signals sought were all natural in origin except for the 14,000-Hz and the 27,000-Hz bands, which partly utilize navigation and communication signals.

Simultaneous peaks from each pair of orthogonal E-H records were scaled and combined to compute apparent resistivity (in ohm-meters, proportional to [E/H]) for the two observed E and H field orientations. Typically, 8–16

samples from each analog record form the basis for computing estimates of resistivity/north-south (Rns) and resistivity/east-west (Rew). The reduced data were edited to reject data considered inconsistent with the trend of the sounding curve (the bilogarithmic plot of apparent resistivity versus frequency). Selection of data for rejection was performed independently on the Rns and Rew curve for each station. A smooth approximation to the data is required by the electromagnetic response of the Earth (Weidelt, 1972). Furthermore, shifts between the two curves can have interpretable geologic significance with regard to heterogeneity or anisotropy in the Earth (Vozoff, 1972; Strangway and others, 1973).

The observation sites were to some extent limited by accessibility by road; however, most stations were sited at the most optimum locations for determination of structures and lithologic contrasts within, across, and outside the ring structure. At sites where the ring structure was assumed to be near, the E-lines were oriented parallel with and perpendicular to the inferred structure such that the apparent resistivity for both E-parallel and E-perpendicular polarizations was directly measured. Apparent resistivity values thus obtained can be compared with those from theoretical two-dimensional type-curves corresponding to the appropriate polarization (Strangway and others, 1973). At sites where the location of the ring structure was not known or could not be inferred, the E-lines were oriented north-south and east-west, respectively.

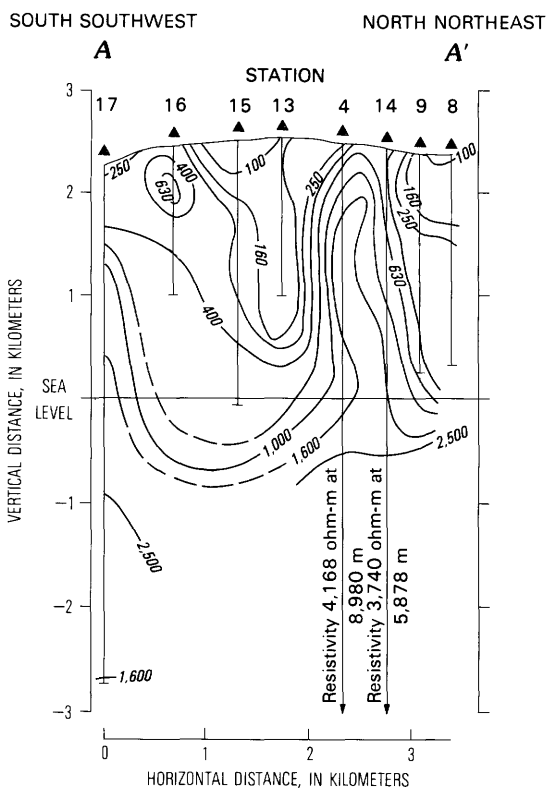

Figure 2. Contoured resistivity-depth section for profile *A–A'* across eastern ring structure of Turkey Creek caldera. Resistivity contours are based on one-dimensional modeling (Bostick, 1977) at each AMT station. The modeling fits an approximation to the geometric mean of observed Rxy and Ryx curves at each station. Contours are in units of ohm-meters at roughly equal log intervals (multiples of 10, 16, 25, 40, 63, and 100).

An estimate of the resistivity distribution with depth was obtained by transforming the smoothed data to a resistivity-depth function using Bostick's method (Bostick, 1977; Bostick and others, 1977, Goldberg and Rotstein, 1982). The results of this transformation provide a one-dimensional approximation of the depth-resistivity distribution at each station. The response of the resulting layered model for each station was computed using the forward-modeling algorithm described by Schmucker (1971) and is presented along with the observed data for each profile. The resulting one-dimensional interpretations based on the above computations are presented as contoured composite sections for each of the profiles.

Limitations of one-dimensional models are that inaccuracies and poor resolution may result because of scatter and bias in the measurements and because of the limited range and number of frequencies observed (Oldenburg, 1979). More important in regard to the data in our study, however, is the fact that almost all the data show a response to lateral resistivity variations as indicated by a shift between the Rns and Rew parts of the sounding curve. This shift is referred to as apparent anisotropy. In our one-dimensional analysis, the curve transformed using Bostick's method (1977) was a hand-smoothed average of the Rns and Rew data. The data points were subjectively weighted based on their quality. If the data are considered equally, the resulting curve is equivalent to using the geometric mean sounding curve, which for two-dimensional structures is an invariant curve even for tensor (phase-amplitude measurements) data (Berdichevsky and Dimitriev, 1976; Eggers, 1982; Park and Livelybrooks, 1989). Nevertheless, direct information about the dimensionality of structures is lost in this approach.

RESISTIVITY PATTERNS INTERPRETED FROM ONE-DIMENSIONAL MODELING

To illustrate the resistivity structure, six profiles were constructed. Each profile illustrates the distribution of resistivity with depth as interpreted by contouring the results of one-dimensional Bostick transformations for the soundings along the profile. Because the Bostick method initially provides a smoothly varying depth-resistivity curve, the depths for a logarithmic sequence of resistivity values (multiples of 10, 16, 25, 40, 63, and 100 ohm-m) were selected directly from the transformation for each station. The sounding curves and the calculated response of the one-dimensional layered model for the Bostick transformation are shown for each station on the profile.

Profile *A–A′*—The Eastern Ring Structure

Profile *A–A′* (fig. 2) extends from south-southeast (station 17) to north-northeast (station 8) across a part of the eastern ring structure of Turkey Creek caldera. The ring structure proper, or the combined zone of ring dikes and breakaway faults of the caldera collapse, is believed to be roughly centered in a zone marked by a quartz monzonite intrusive body (fig. 1). The quartz monzonite body is bordered on the southwest by welded tuff of the Rhyolite Canyon Tuff, partly covered by slump breccia, and bordered on the northeast by sedimentary rocks of the Cretaceous Bisbee Formation.

Station 13 is at or near the inferred contact of the porphyry of the core structure with the ring. Station 14 is at an exposed contact between the annular ring of quartz monzonite and monzonite porphyry (both combined into the Tmp unit of fig. 1) and the Bisbee Formation composed of arkose, graywacke, thin limestone, basalt, and diabase.

The resistivity of the near-surface rocks along profile *A–A′* ranges from 63 to about 160 ohm-m or more. These resistivity values are typical for fractured and weathered surface rocks or alluvium of this survey, although lower values commonly are measured in basin environments. The thickness of the surface layer (not explicit in the contours of fig. 2 because of the scale and contour interval) varies from 20–40 m within the ring structure to 400 m in the outlying rocks.

The 160 to 400 or 630 ohm-m resistivity zone is similar in configuration to the deeper and higher resistivity zone (>630 ohm-m). The contact between the lower resistivity tuffs or sedimentary rocks (<630 ohm-m) and the higher resistivity (>630 ohm-m) core or ring intrusive rocks is believed to be roughly marked by the transition resistivity contours of 630–1,000 ohm-m. Note particularly the zone between stations 13 and 9, where a sharp lateral change in resistivity and the high resistivity of the near-surface material correspond in part to the mapped quartz monzonite and other intrusive rocks (unit Tmp) near the ring structure. The high resistivity values (greater than 630 or 1,000 ohm-m) extend from a depth of about 50 m to about 2–2.5 km, where the contours flatten to form a ubiquitous high-resistivity, semihorizontal layer that is indicated in the lower frequencies of the data at all stations. In the vicinity of the ring structure at stations 4 and 14, the high resistivity values are inferred to represent unaltered parts of the intrusive rock unit. At depth, both below the ring structure and elsewhere, the high resistivity values may be the result of either the intrusive rocks of the monzonite porphyry unit and related intrusive rocks or other basement rocks.

Although station 13 is also in the area of mapped intrusive rocks, resistivity values here are significantly lower than those measured between stations 4 and 14. These lower values, less than 250 ohm-m, suggest either local alteration or a higher fault and fracture density with included pore fluids. The distinct separation of the two apparent resistivities (Rns and Rew) at stations 4, 13, and 14 is indicative of major lateral contrasts in resistivity.

The high resistivity values of the ring structure are clearly bounded by lower resistivity values of less than 250 ohm-m, typically less than 160 ohm-m. In the area to the east, below stations 9 and 8, the lower resistivity values are associated with sedimentary rocks of the Bisbee Formation. To the west, the similar low resistivity values probably are associated with slump breccia at stations 15, 16, and 17. The transition to higher resistivity values is rather sharp at a depth of about 2.2 km below stations 9 and 8, whereas below stations 15, 16, and 17 the transition from 400 to 1,000 ohm-m is more gradual and of considerable thickness. These data most likely indicate units consisting of altered intercaldera tuff or altered and fractured intrusive or basement rocks above the higher resistive basement. This zone of intermediate resistivity (400–1,000 ohm-m) is at a depth of about 1.8 km below station 15 and at decreasing depths and is thicker toward station 16.

Profile *B–B′*—The Northern Moat and Caldera Interior

Profile *B–B′*(fig. 3) begins at station 23, above the Tertiary moat lavas of Fife Canyon and trends south-southeast across the contact with the welded tuffs of the Rhyolite Canyon Tuff at station 21. The profile crosses the contact with the ring monzonite porphyry at stations 18 and 17, where profile *B–B′* intersects profile *A–A′*. For the most part, profile *B–B′* is parallel with and inside of the inferred ring structure; station 22 is on the inferred ring structure and station 23 is outside of the inferred caldera boundary. The inferred caldera boundary at station 22 is uncertain because this area is covered by rhyolite flow rocks and tuffs.

The contoured section for profile *B–B′* (fig. 3) shows a low-resistivity surface layer of 40–160 ohm-m between stations 23 and 21. The low-resistivity layer is about 700 m thick at station 23; it thins southward to station 22, then thins rapidly to 30 m at stations 19 and 21, and pinches out by station 20. This layer is interpreted to represent the configuration of the rhyolite tuffs along profile. These tuffs are not significantly altered at the surface but must be sufficiently porous and have sustained sufficient pore fluid ionic activity to cause this relatively low resistivity. We have no petrophysical data to verify this, but the near-surface data are quite conclusive of the low resistivity values. The base of the zone is, however, rather uncertain because there are no sharp gradients in the contour intervals to at least the 1,000-ohm-m contour. Although we assume that resistivity values greater than 1,000 ohm-m are representative of basement rocks (probably core intrusive rocks of unit Tmp), it would be highly arbitrary to assign interfaces without further one- and two-dimensional modeling trials.

Bearing in mind the above, we propose that the generalized zones of 40–160 ohm-m, 250–400 ohm-m, and 1,000

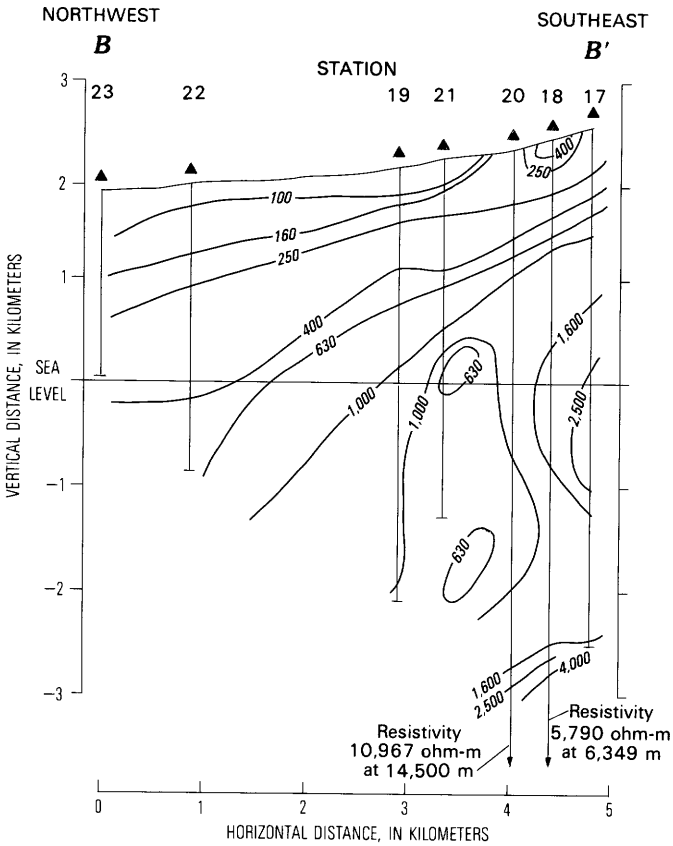

Figure 3. Contoured resistivity-depth section for profile *B–B'* in northern moat area and interior of Turkey Creek caldera. Resistivity contours are based on one-dimensional modeling (Bostick,1977) at each AMT station. The modeling fits an approximation to the geometric mean of observed Rxy and Ryx curves at each station. Contours are in units of ohm-meters at roughly equal log intervals (multiples of 10, 16, 25, 40, 63, and 100).

ohm-m and greater represent, respectively, shallow and "wet" tuffs, intermediate-depth tuffs of probably lower porosity ("drier"), and intrusive basement rocks. The upper tuffaceous rocks thin to the southeast, and the high-resistivity basement rocks significantly shallow to the southeast. The correspondence between variations in the thickness of the 250–400-ohm-m zone, as based on steps in the 400-ohm-m contour, and the location of mapped faults near stations 19 and 22 (du Bray and Pallister, 1991) suggests that zone thickness is in part fault controlled.

Station 22 is at the inferred ring structure boundary. We consider the lack of an anomaly below stations 22 and 23 comparable to that on profile *A–A'* at stations 4 and 14 to be significant. The data show that near station 22 unaltered intrusive rocks are no shallower than about 1.5 km. It is possible that intrusive rocks or faults associated with a ring structure may have been altered to the extent that there is little resistivity contrast with the tuffs; however, based on comparison with profile *A–A'*, it is more probable either that the caldera boundary is north of station 23 or south of station 22 or that faults and intrusive rocks associated with a ring structure are buried beneath tuffs more than 1–1.5 km deep.

Profiles *C–C'* and *D–D'*—Cretaceous Rocks Northeast of the Caldera

Profile *C–C'* (fig. 4) is entirely along the Cretaceous Bisbee Formation in an area of high relief. The short (1.6 km) north-south profile begins at station 5 and merges to the south with profile *A–A'* at station 8. Station 3 is at the top of Onion Gap Pass, a topographic saddle along profile. Most observations were taken along a relatively narrow ridge, and the largest topographic variations are lateral to the profile.

The data along profile show the lack of a significant layer of low resistivity (not explicit on figure 4 because of scale and contour interval). The relatively high resistivity values (greater than 1,000 ohm-m) near the surface indicate the absence of surface alluvium and weathered and conductive pore-water rocks near the surface and are considered typical

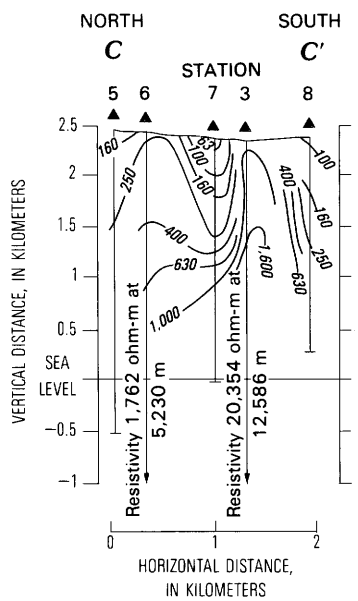

Figure 4. Contoured resistivity-depth section for profile *C–C'* in area of Cretaceous rocks northeast of Turkey Creek caldera and merging with profile *A–A'* across the caldera boundary. Resistivity contours are based on one-dimensional modeling (Bostick,1977) at each AMT station. The modeling fits an approximation to the geometric mean of observed Rxy and Ryx curves at each station. Contours are in units of ohm-meters at roughly equal log intervals (multiples of 10, 16, 25, 63, 40, and 100).

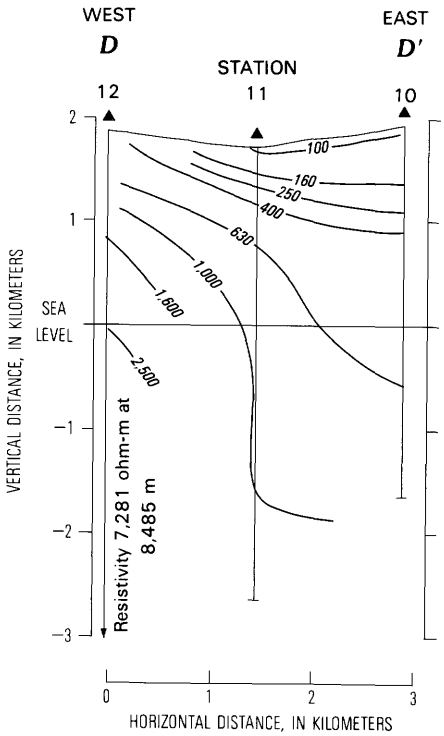

Figure 5. Contoured resistivity-depth section for profile *D–D'* in area of Cretaceous rocks east of Turkey Creek caldera, along East Turkey Creek drainage. Resistivity contours are based on one-dimensional modeling (Bostick,1977) at each AMT station. The modeling fits an approximation to the geometric mean of observed Rxy and Ryx curves at each station. Contours are in units of ohm-meters at roughly equal log intervals (multiples of 10, 16, 25, 40, 63, and 100).

of topographically high, well-drained terrane. The lowest resistivity values are at depths where fluids probably have become stabilized.

Considerable variation in the one-dimensional modeled resistivity values for the upper 1–1.5 km may suggest significant heterogeneity in the Bisbee Formation; however, some of the variation may be an artifact of severe topographic effects that are unaccounted for in one-dimensional modeling. A small isolated low (less than 100 ohm-m) is at a depth of 0.1–0.5 km at station 7 and, with smaller dimension, at station 5. Resistivity values greater than 250 ohm-m are between these lows. The wedge of 1,600-ohm-m material between stations 3 and 8 is poorly constrained; it results from the high resistivity in the one-dimensional model for station 3. The resistivity structure below station 8 is best seen in profile *A–A'*(fig. 2).

Combined contour models for the east end of profile *A–A'*and the south end of profile *C–C'* suggest that the configuration of basement beneath the Bisbee Formation is probably represented roughly by the 630-ohm-m contour at a depth of 1–5 km. Because of the uncertainty associated with the combined effects of resistivity variations in the Bisbee Formation, topography, and limitations of one-dimensional modeling, it is not considered proper to assess the detailed configuration of the slope or structure on the basement rock.

Profile *D–D'* (fig. 5) consists of three stations, 10, 11, and 12, along the East Turkey Creek drainage in the Cretaceous Bisbee Formation. These data were acquired in an area of much more favorable topography for AMT soundings than that for profile *C–C'*, and the apparent heterogeneity in the resistivity of the Bisbee as contoured for profile *C–C'* is not reflected in profile *D–D'*. The data taken along profile *D–D'* show significant shifts (anisotropy) between the Rns and Rew curves; however, the one-dimensional modeling produces relatively smoothly varying resistivity variations that are believed to reflect the major aspects of the subsurface basement structure.

The large shifts in the lower frequencies at stations 12 and 11 may well be related to the sharply thickening Bisbee Formation east of station 11, as inferred from the 250–630-ohm-m contours. Part of the higher resistivity west of station 11 is inferred to reflect the edge of the quartz monzonite intrusive rocks of the Turkey Creek caldera ring structure. East of station 11, the 1,000-ohm-m contour, or perhaps the 630–1,000-ohm-m zone, is inferred to reflect the general configuration of igneous-metamorphic basement rocks.

Profiles *E–E'* and *F–F'*—West Flank of Turkey Creek Caldera

The location of the west flank of the Turkey Creek caldera is problematic and highly inferential from the standpoint of geologic mapping because the caldera boundary area is not as well exposed as it is on the east flank. Two roughly parallel AMT profiles were established across the inferred boundary to explore the geoelectric structure in an attempt to provide some subsurface information on this questionable boundary.

Profile *E–E'*(fig. 6) extends from west to east up Rock Creek Canyon, from station 32 on the west to station 31 on the east. Stations 32 and 29, which have resistivity values of 100 ohm-m or less from the surface to a depth of about 1,000 m, indicate the presence of a significant thickness of alluvium or perhaps alluvium overlaying relatively low resistivity moat lavas of Fife Canyon (compare with profile *B–B'*). Higher resistivity values of 400 ohm-m are encountered at about 2,000 m depth, but resistivity values typical of intrusive or basement rocks (as on profile *A–A'*) were not measured along the eastern part of this profile.

At station 29, at the entrance of Rock Creek Canyon, the welded tuffs and rhyolite lavas of the Rhyolite Canyon Tuff are shown in the AMT data as the shift between the Rns and

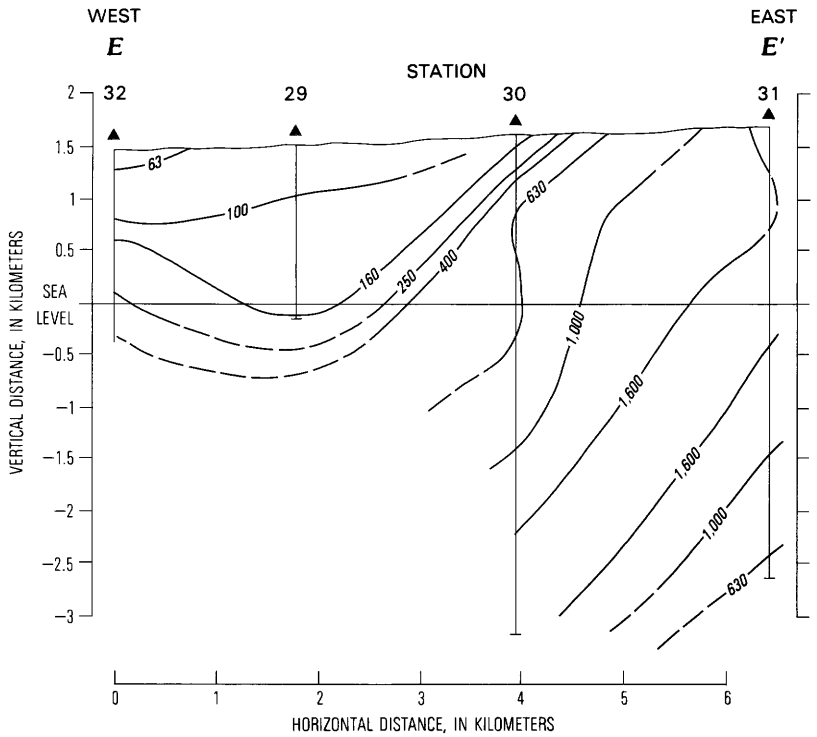

Figure 6. Contoured resistivity-depth section for profile *E–E′* on west flank of Turkey Creek caldera, along Rock Creek Canyon. Resistivity contours are based on one-dimensional modeling (Bostick,1977) at each AMT station. The modeling fits an approximation to the geometric mean of observed Rxy and Ryx curves at each station. Contours are in units of ohm-meters at roughly equal log intervals (multiples of 10, 16, 25, 40, 63, and 100).

Rew curves (fig. 6). Farther east at station 30, the low-resistivity layer thins to less than 100 m and disappears between stations 30 and 31. At the east end of the profile, station 31 on the monzonite porphyry of the core intrusion shows resistivity values greater than 1,600 ohm-m from the surface downward to the maximum depth sensed.

Profile *F–F′* (fig. 7) extends from west (station 1) to east (station 2) along Turkey Creek Canyon road. In comparison with profile *E–E′*, the low-resistivity layer, less than 400 ohm-m, is limited to the upper 200 m at station 1, thins to the east toward station 27, and disappears east of station 27. Because profiles *E–E′* and *F–F′* are essentially parallel with each other, the higher resistivity rocks (> 630 ohm-m) may be assumed to be the same unit beneath both profiles. These high-resistivity rocks, assumed to represent the intrusive unit, apparently are at depths of less than 1–1.5 km along the western section of profile *F–F′*. This suggests a north-trending deepening of the intrusive unit in the area of the west ends of profiles *F–F′* and *E–E′*.

High resistivity values of 1,000 ohm-m or greater are within 30 m of the surface in the area of stations 26, 25, and 14. In this area, anomalous lower resistivity values (less than 1,000 ohm-m at 0.5 km) are beneath stations 26 and 24. To a lesser magnitude, the buried low-resistivity anomaly is also sensed at station 25. Outcrops of intracaldera welded tuff of the Rhyolite Canyon Tuff between stations 26 and 25 may be responsible for this anomaly. The Rhyolite Canyon outcrop widens south of station 26 (fig. 1) and is also present within about 1 km of stations 25, 24, and 2. It is likely that the contoured anomaly on profile *F–F′* (fig. 7) results from lateral sensing of this unit, which we assume has lower resistivity than the intrusive unit. Thus, the contours are not believed to represent a low-resistivity anomaly at depth. Similarly, we do not place great significance on the low resistivity values (160–630 ohm-m) in the surface layer at station 2. The data may be sensing alteration or weathering in the intrusive unit at station 2, but one-dimensional modeling here is inadequate for confident inferences.

The main conclusion we draw from profiles *E–E′* and *F–F′* is that, within a depth of about 2 km, there is no intrusive structure on the west ends of these lines that corresponds to that of the ring boundary to the east (profile *A–A′*, fig. 2). If such a ring structure exists in this area, it is buried beneath a combination of alluvium and relatively low resistivity moat lavas at a depth of at least 2 km, probably 3 km. The data are otherwise in accord with geologic mapping.

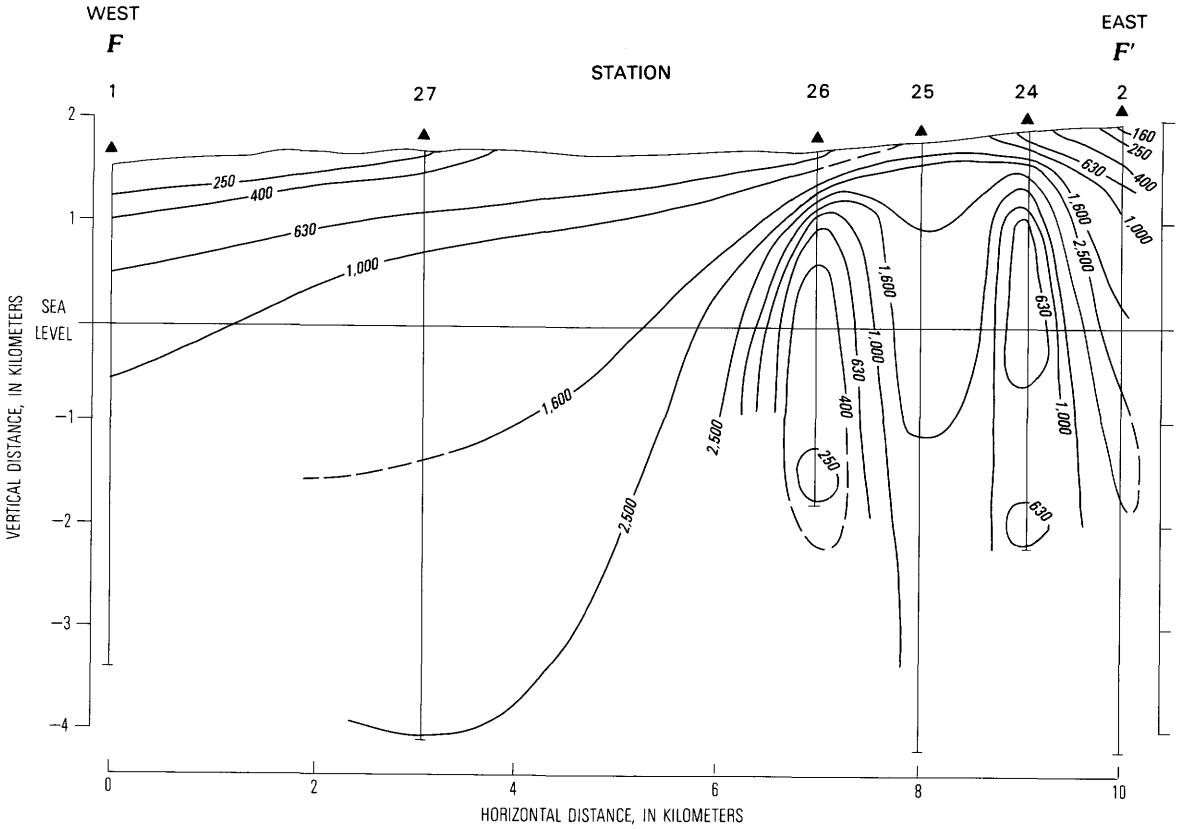

Figure 7. Contoured resistivity-depth section for profile *F–F'* on west flank of Turkey Creek caldera, along Turkey Creek Canyon road. Resistivity contours are based on one-dimensional modeling (Bostick,1977) at each AMT station. The modeling fits an approximation to the geometric mean of observed Rxy and Ryx curves at each station. Contours are in units of ohm-meters at roughly equal log intervals (multiples of 10, 16, 25, 40, 63, and 100).

CONCLUSIONS

The AMT experiment reported here provides (1) a test of the electrical signature of an exposed and well-mapped area of volcanic intrusive rocks, inferred from geological evidence (Marjanieme, 1969; Latta, 1983; Lipman, 1984; du Bray and Pallister, 1991) to be a ring structure of the Turkey Creek caldera, and (2) several applied exploratory references that may be of value in mapping the volcanic structure at depth. Because the interpretations are based on one-dimensional modeling, there may be some distortion in the resistivity sections of the profiles (figs. 2–7), but some of the major features shown in the profiles provide a first-order indication of subsurface conditions.

Profiles *A–A'*, *B–B'*, *C–C'*, and *D–D'* (figs. 2–5) are mostly within the area of mapped border structures of the rhyolitic volcanic center (fig. 1) (du Bray and Pallister, 1991). The intrusive rocks here are generally of high resistivity (1,000 ohm-m or more), in contrast to lower resistivity (typically 160–400 ohm-m) exterior (east)-bordering Cretaceous sedimentary rocks (Bisbee Formation), interior (west) bordering slump units, and moat lavas and tuffs (Rhyolite Canyon Tuff). The moat tuffs and lavas show particularly low resistivity values (63–100 ohm-m) in the upper 1 km (profile *B–B'*, fig. 3). These resistivity contrasts make it quite straightforward to identify intrusive rocks associated with the edge of the volcanic center and locally to identify the core intrusive or high-resistivity basement rocks at depth. The AMT data provide information to depths of about 1.5–3.5 km, depending on the resistivity of the nearer surface material (resolution at depth decreases when shallower material is less resistive).

At least one area mapped as intrusive rocks (near station 13, profile *A–A'*, fig. 2) shows anomalously low resistivity values (about 250 ohm-m) that may suggest local alteration or intense fracture density. Such an area may be a candidate for exploration for possible mineralization if geologic evidence for alteration is found. Profile *B–B'* (stations 23 and 22, fig. 3), below the inferred northern border of the volcanic center, indicates no high-resistivity structures above a depth of about 2.5 km. In this area, deeper moat lavas are of higher resistivity (greater than 160 ohm-m to as much as 630 or 1,000 ohm-m) and may thicken toward the north at least partly in response to structural (fault) control. The latter conclusion is based on correspondence of the thickening with mapped faults (du Bray and Pallister, 1991).

Profiles *E–E′* and *F–F′* (figs. 6, 7) were established to map the western border of the Turkey Creek volcanic center. In this area there are no surface manifestations of border intrusive rocks similar to those mapped on the east. The AMT data identify the interior (core) intrusion as a high resistivity unit (> 1,000 ohm-m) and a possible unit of alluvium and (or) moat lavas and tuffs having resistivity values of 60–400 ohm-m. These results are in agreement with geologic mapping except that no evidence of high-resistivity intrusive rocks has been found in the area of the inferred border of the volcanic center. The depth of penetration here (at the western ends of profiles *E–E′* and *F–F′*) is about 4 km.

REFERENCES CITED

Berdichevsky, M.N., and Dimitriev, V.I., 1976, Basic principles of interpretation of magnetotelluric sounding curves, *in* Adam, A., ed., Geoelectric and geothermal studies (east-central Europe, Soviet Asia): Budapest, Akademiai Kiado, KAPG Geophysical Monograph, p. 1650221.

Bostick, F.X., Jr., 1977, A simple almost exact method of MT analysis: Workshop on Evaluation of Electrical Methods in the Geothermal Environment, Snowbird, Utah, November 1976, University of Utah Report, p. 175–177.

Bostick, F.X., Jr., Smith, H.W., and Boehl, J.E., 1977, A simplified one-dimensional magnetotelluric inversion method, *in* Magnetotelluric and DC dipole-dipole soundings on northern Wisconsin: Austin, University of Texas, Final technical report prepared under contract N00014–76–C, 0484, Office of Naval Research, and Grant GA–38827, National Science Foundation, appendix I.

Cagniard, L., 1953, Basic theory of the magnetotelluric method: Geophysics, v. 18, no. 3, p. 605–635.

du Bray, E.W., and Pallister, J.S., 1991, An ash-flow caldera in cross section—Ongoing field and geochemical studies of the Turkey Creek caldera, Chiricahua Mountains, SE Arizona: Journal of Geophysical Research, v. 96, p. 13435–13457.

Eggers, D.E., 1982, An eigenstate formulation of the magnetotelluric impedance tensor: Geophysics, v 47, p. 1204–1214.

Fitterman, D.V., Stanley, W.D., and Bisdorf, R.J., 1988, Electric structure of Newberry volcano, Oregon: Journal of Geophysical Research, v. 93, no. B9, p. 10119–10134.

Goldberg, S., and Rotstein, Y., 1982, A simple form of presentation of magnetotelluric data using the Bostick transform: Geophysical Prospecting, v. 30, p. 211–216.

Hermance, J.F., Slocum, W.M., and Neumann, G.A., 1984, The Long Valley/Mono Basin volcanic complex—A preliminary magnetotelluric and magnetic variation interpretation: Journal of Geophysical Research, v. 89, p. 8325–8337.

Hoover, D.B., Frischknecht, F.C., and Tippens, C.L., 1976, Audiomagnetotelluric sounding as a reconnaissance exploration technique in Long Valley, California: Journal of Geophysical Research, v. 81, no. 5, p. 801–809.

Hoover, D.B., and Long, C.L., 1976, Audiomagnetotelluric methods in reconnaissance geothermal exploration: Second United Nations Symposium Development and Utilization Geothermal Resources, Proceedings, v. 2, p. 1059–1064.

Hoover, D.B., Long, C.L., and Senterfit, R.M., 1978, Some results from audiomagnetotelluric investigations in geothermal areas: Geophysics, v. 43, no. 7, p. 1501–1514.

Latta, J., 1983, Geochemistry and petrology of the ash flows of Chiricahua National Monument, Arizona, and their relation to the Turkey Creek Caldera: Tucson, University of Arizona, M.S. thesis, 194 p.

Leary, P., and Phinney, R.A., 1974, A magnetotelluric traverse across the Yellowstone region: Geophysical Research Letters, v. 1, no. 6, p. 265–268.

Lipman, P.W., 1984, The roots of ash-flow calderas in western North America—Windows into the tops of granitic batholiths: Journal of Geophysical Research, v. 89, no. B10, p. 8801–8841.

Long, C.L., 1985, Regional audio-magnetotelluric study of the Questa caldera, New Mexico: Journal of Geophysical Research., v. 90, p. 11270–11274.

Marjaniemi, D.K., 1969, Geologic history of an ash-flow sequence and its source area in the Basin and Range province of southeastern Arizona: Tucson, University of Arizona, Ph.D. thesis, 176 p.

Oldenburg, D.W., 1979, One-dimensional inversion of natural source magnetotelluric observations: Geophysics, v. 44, no. 7, p. 1218–1244.

Park, S.K., and Livelybrooks, D.W., 1989, Quantitative interpretation of rotationally invariant parameters in magnetotellurics: Geophysics, v. 54, p. 1483–1490.

Schmucker, Ulrich, 1971, Interpretation of induction anomalies above non-uniform surface layers: Geophysics, v. 36, no. 1.

Stanley, W.D., 1982, Magnetotelluric soundings on the Idaho National Engineering Facility, Idaho: Journal of Geophysical Research, v. 87, no. B4, p. 2683–2691.

Stanley, W.D., Boehl, J.E., Bostick, F.X., Jr., and Smith, H.W., 1977, Geothermal significance of magnetotelluric sounding in the eastern Snake River Plain–Yellowstone region: Journal of Geophysical Research, v. 82, p. 2501–2514.

Strangway, D.W., and Kozier, A., 1979, Audio-frequency magnetotelluric sounding—A case history at the Cavendish geophysical test range: Geophysics, v. 44, no. 8, p. 1429–1446.

Strangway, D.W., Swift, C.M., Jr., and Holmer, R.C., 1973, The application of audio-frequency magnetotellurics (AMT) to mineral exploration: Geophysics, v. 38, no. 6, p. 1159–1175.

Vozoff, K., 1972, The magnetotelluric method in the exploration of sedimentary basins: Geophysics, v. 37, no. 1, p. 98–141.

Vozoff, K., Hasegawa, H., and Ellis, R.M., 1963, Results and limitations of magnetotelluric surveys in simple geologic situations: Geophysics, v. 28, no. 5, part 1, p. 778–792.

Weidelt, P., 1972, The inverse problem of geomagnetic induction: Journal of Geophysics, v. 38, p. 257–289.

Chapter L

Ash-Flow Calderas as Structural Controls of Ore Deposits—Recent Work and Future Problems

By PETER W. LIPMAN

U.S. GEOLOGICAL SURVEY BULLETIN 2012

APPLICATION OF STRUCTURAL GEOLOGY TO MINERAL AND ENERGY RESOURCES OF THE CENTRAL AND WESTERN UNITED STATES

CONTENTS

FIGURES

Ash-Flow Calderas as Structural Controls of Ore Deposits—Recent Work and Future Problems

By Peter W. Lipman[1]

Abstract

Field, petrologic, geochronologic, and geophysical studies of Oligocene ash-flow calderas and associated igneous rocks in the southern Rocky Mountains and Mesozoic volcanic systems in southeastern Arizona illustrate the applications of volcanic structural geology to problems of localization of ore deposits and associated hydrothermal systems. Examples include (1) molybdenum deposits along the most deeply subsided and recurrently intruded southern margin of the 26-Ma Questa caldera; (2) 25-Ma mineralization along the recurrently faulted Creede Graben in the central San Juan Mountains; (3) little studied hydrothermal alteration south of Creede that defines a coherent pattern related to ring intrusions along the southern margin of the newly recognized 27.1-Ma South River caldera; and (4) localization of porphyry copper mineralization along intrusions related to several Late Cretaceous–early Tertiary calderas in southern Arizona. Caldera structures are common loci for mineralization because they are the near-surface structural expression of crustal magmatic processes involving major petrologic modification of crustal compositions. Misinterpretation of caldera features in complex mineralized terranes commonly has led to inappropriate exploration strategies.

INTRODUCTION

Caldera structures, ranging in scale from ring faults and graben systems to smaller scale faults and joints, can develop in response to the rise, differentiation, and solidification of upper crustal magmatic systems, commonly of batholithic scale (Lipman, 1984, 1988). Hydrothermal systems and associated ore deposits form where volcanic structures intersect upper parts of the magma bodies. Ash-flow calderas provide important structural control for subsequent mineralizing events (Steven and others, 1974; McKee, 1979; Rytuba, 1981), but the depths, transport rates, and source of metals in caldera-related deposits remain poorly understood. The stratigraphically complex sequences that record volcanic evolution are typically imperfectly preserved due to subsequent tectonism and erosion, as well as commonly being enveloped in a haze of hydrothermal alteration. Both magma bodies and volcanic structures evolve rapidly relative to geochronologic resolution, and timing of volcanic structural evolution, magmatism, and mineralization is difficult to constrain with adequate precision. A major challenge, both for mineral explorationists and volcanologists studying the altered and incompletely preserved volcanic rocks associated with ore deposits, is to apply and utilize volcanologic concepts and processes identified through study of younger and simpler volcanic systems. Recent studies on caldera systems of varying ages and structural levels by myself and others in the U.S. Geological Survey, academia, and industry are reviewed to provide insights on interactions between caldera-related processes and mineralization.

GENERAL CALDERA MODEL: RELATION TO MINERALIZATION

Recent general models for structural and volcanic evolution of ash-flow calderas (fig. 1), briefly summarized here, relate major structural features to sequential stages of premonitory volcanism, eruption and associated caldera collapse, resurgent magmatism and accompanying uplift of the caldera floor, and late hydrothermal activity and mineralization (Smith and Bailey, 1968; Lipman, 1984).

Most ash flows have erupted from sites of closely preceding volcanism that records initial shallow accumulation of caldera-related magma; some radial and circumferential structures may be initiated at this stage. Most large calderas collapse during ash-flow eruptions as indicated by thick ponding of late eruptive products within the concurrently subsiding depression. Structural boundaries of calderas are single ring faults or composite ring-fault zones that mostly dip vertically to steeply inward. Some relatively small

[1]U.S. Geological Survey, MS910, 345 Middlefield Road, Menlo Park, California 94025.

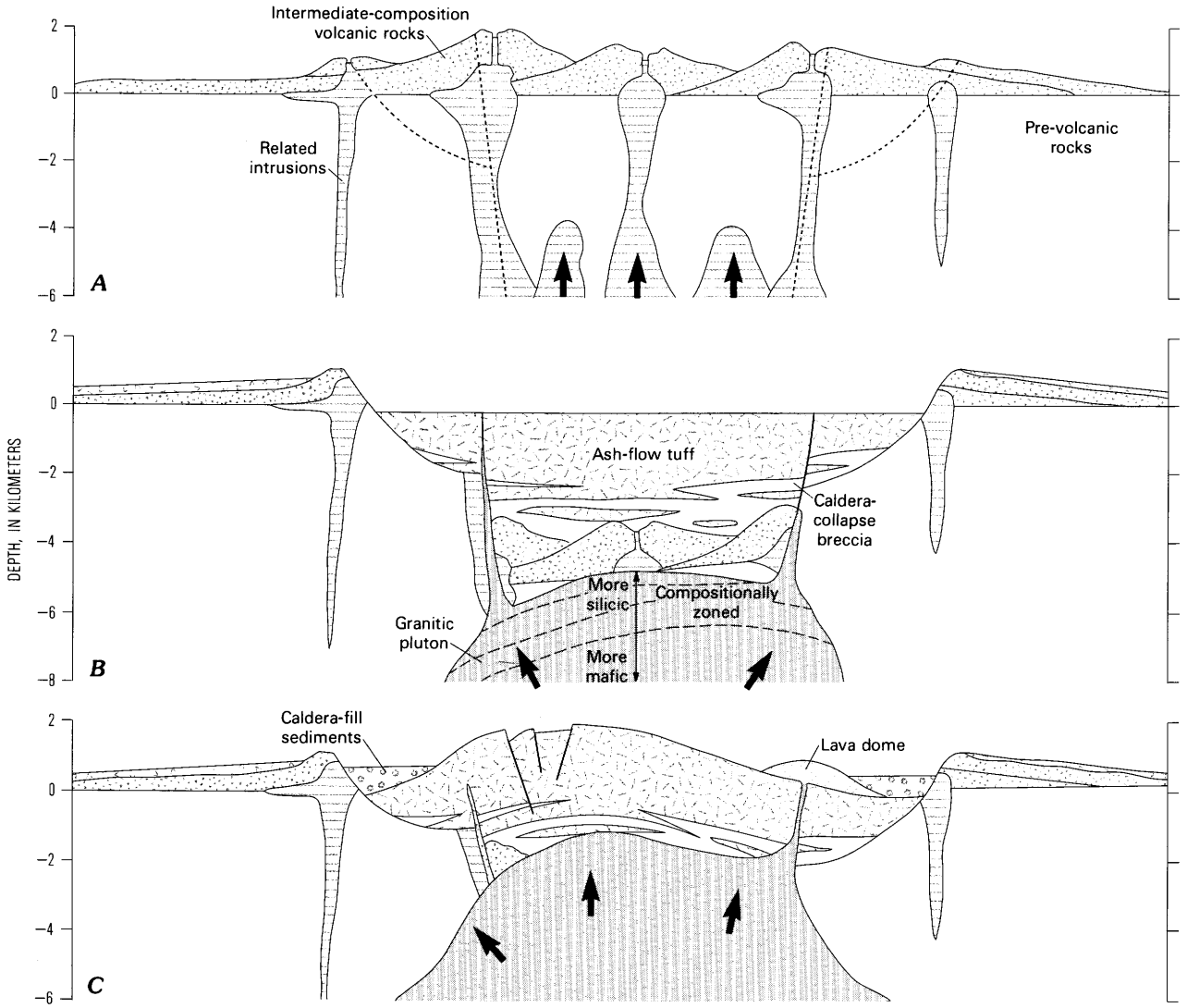

Figure 1. Generalized caldera model. Modified from Lipman (1984). *A*, Precollapse volcanism. Clustered intermediate-composition stratovolcanoes grow over isolated small high-level plutons that mark beginning of accumulation of batholithic-size silicic magma body that will feed ash-flow eruptions. Uplift related to emplacement of plutons may lead to development of arcuate ring fractures. Site of subsequent caldera collapse indicated by dotted lines; heavy arrows indicate upward movement of magma. *B*, Caldera geometry just after ash-flow eruptions and concurrent caldera collapse. Central area of clustered earlier volcanoes caves into collapsed area. Intracaldera tuff ponds during subsidence and is an order of magnitude thicker than cogenetic outflow ash-flow sheet. Initial collapse along ring faults is followed by slumping of oversteepened caldera walls and accumulation of voluminous collapse breccias that interfinger with ash-flow tuff in the caldera fill. Caldera floor subsides asymmetrically and is tilted to left side of diagram. Main magma body underlies entire caldera area and is compositionally zoned (or was prior to eruptions), becoming more mafic downward. *C*, Resurgence and postcaldera deposition. Resurgence here is asymmetrical with greatest uplift in area of greatest prior collapse. Extensional graben faults form over crest of dome. Some resurgent uplift is accommodated by movement along ring faults in sense opposite that during caldera subsidence. Magma body has risen into volcanic pile and intruded cogenetic intracaldera welded tuff. Original caldera floor has been almost entirely obliterated by rise of magma chamber to near level of prevolcanic land surface. Caldera moat is partly filled by lava domes and volcaniclastic sediments. Hydrothermal activity and mineralization are dominant late in cycle.

volume pyroclastic eruptions are associated with incomplete hinged caldera subsidences or structural sags; larger systems are completely bounded by ring faults. Scalloped topographic walls beyond the structural boundaries of most calderas are due to secondary gravitational slumping during subsidence, and associated caldera-collapse slide breccias interleaved with thick tuff are a signature of intracaldera accumulations. Most exposed caldera floors are a structurally coherent plate or cylinder bounded by a ring fault or dike, indicating pistonlike caldera collapse. Deviations from circular shape commonly reflect the influence of regional structures.

Postcollapse volcanism may occur from varied vent geometries within ash-flow calderas; ring-vent eruptions are common in resurgent calderas and reflect renewed magmatic supply. Large intrusions related to resurgence are exposed centrally within some calderas; ring dikes and other intrusions along bounding ring fractures are common in regional extensional environments. Resurgence within calderas may yield a symmetrical dome, accompanied by keystone-graben faulting, or more geometrically complex uplift structures; resurgence is most common in large calderas (greater than 10 km diameter) in cratonic crust and is associated with large silicic intrusions. In addition to resurgence within single calderas, broader magmatic uplift within many silicic volcanic fields reflects isostatic adjustments following the emplacement of associated subvolcanic batholiths.

Hydrothermal activity and mineralization accompany all stages of ash-flow magmatism and become dominant late during caldera evolution. Some mineralization is closely tied to late stages of the caldera magmatic cycle, but much rich mineralization is millions of years younger than caldera collapse, where the caldera served primarily as a structural control for genetically unrelated intrusions and their associated hydrothermal systems.

Examples of the diverse relations between caldera evolution and associated mineralization for several representative regions in the western United States are summarized below.

QUESTA MAGMATIC SYSTEM, NEW MEXICO

The 26–18-Ma Questa magmatic system (fig. 2), expressed at the surface as the Latir volcanic field, contains a relatively simple example of an intracontinental caldera related to major mineralization. The volcanic field, caldera, and associated intrusions are remarkably exposed in cross section due to structural and topographic relief along the eastern margin of the Rio Grande Rift in northern New Mexico (Lipman, 1988; Lipman and Reed, 1989). Diverse geologic, petrologic, geochronologic, geophysical, and mineral resource studies provide a framework for evaluating interactions between magmatic processes, caldera evolution, and mineralization in a extensional cratonic environment.

Exposed levels increase in depth from the mid-Tertiary depositional surface in northern parts of the igneous complex to plutonic rocks originally at depths of 3–5 km in the south. Erosional remnants of an ash-flow sheet of weakly peralkaline rhyolite (Amalia Tuff) and andesitic to dacitic precursor lavas, disrupted by rift-related faults, are preserved as far as 45 km beyond their sources at the Questa caldera. Broadly comagmatic batholithic granitic rocks, exposed over an area of 20 by 35 km, range from mesozonal granodiorite to epizonal porphyritic granite and aplite (Lipman and Reed, 1989). Shallower silicic phases are exposed primarily within the caldera. Compositionally and texturally distinct granites form resurgent intrusions within the caldera and discontinuous mineralized ring intrusions along its margins; a batholithic mass of granodiorite extends for 20 km south of the caldera and locally grades upward to granite below its flat-lying roof. A negative Bouguer gravity anomaly (15–20 mGal; Cordell and others, 1986), which encloses exposed granitic rocks and coincides with boundaries of the Questa caldera, defines boundaries of the shallow batholith that was emplaced into lower parts of the volcanic sequence and in underlying Precambrian rocks. Paleomagnetic pole positions indicate that successively crystallized granitic plutons cooled through Curie temperatures during the interval of caldera formation, initial regional extension, and rotational tilting of the volcanic rocks (Hagstrum and Lipman, 1986). Isotopic ages for the intrusions range from 26 Ma within the caldera, indistinguishable from the ash-flow sheet, to as young as 18 Ma in the southern deeper parts of the composite batholith (Lipman and others, 1986; K. Foland and G. Czamanske, unpub. $^{40/39}$Ar ages); younger radiometric ages to the south probably reflect both continued magmatism and slower cooling in deeper parts of the magmatic system. These relations indicate that the batholithic complex broadly represents the source magma for the volcanic rocks, into which the Questa caldera collapsed, and that the magma was mostly liquid during regional tectonic disruption.

Petrologic and isotopic studies indicate that the volcanic rocks constitute intermittently quenched samples of upper parts of the Questa magma bodies at early stages of crystallization; in contrast, comagmatic granitic rocks preserve an integrated record of protracted crystallization of the magmatic residue as volcanism waned (Johnson and others, 1989). Multiple differentiation processes were active during evolution of the Questa magmatic system: crystal fractionation, replenishment by mantle and lower crustal melts of varying chemical and isotopic character, mixing of evolved and primitive magmas, upper crustal assimilation, and perhaps volatile transfer (Johnson and others, 1990). As a result, an evolving cluster of coalesced magma chambers generated diverse assemblages of broadly cogenetic rocks within a few million years. Modelling of the fractionation processes indicates that large volumes of mantle-derived basalt interacted with the lower crust; return of ultramafic residua to the mantle (fig. 2) is required to have kept crustal thickness and surface elevations from having reached impossibly high values.

Major molybdenum stockwork deposits are associated with the most fractionated granitic and aplitic intrusions along the southern caldera margin (Leonardson and others, 1983); similar but lower grade deposits also are present near the roof of a late intrusion south of the caldera. Molybdenum is concentrated along the roofs of intrusive cupolas that are localized within fault-controlled horsts related to regional extensional faulting. The highest ore grades are also associated with low-angle fractures influenced by the southern

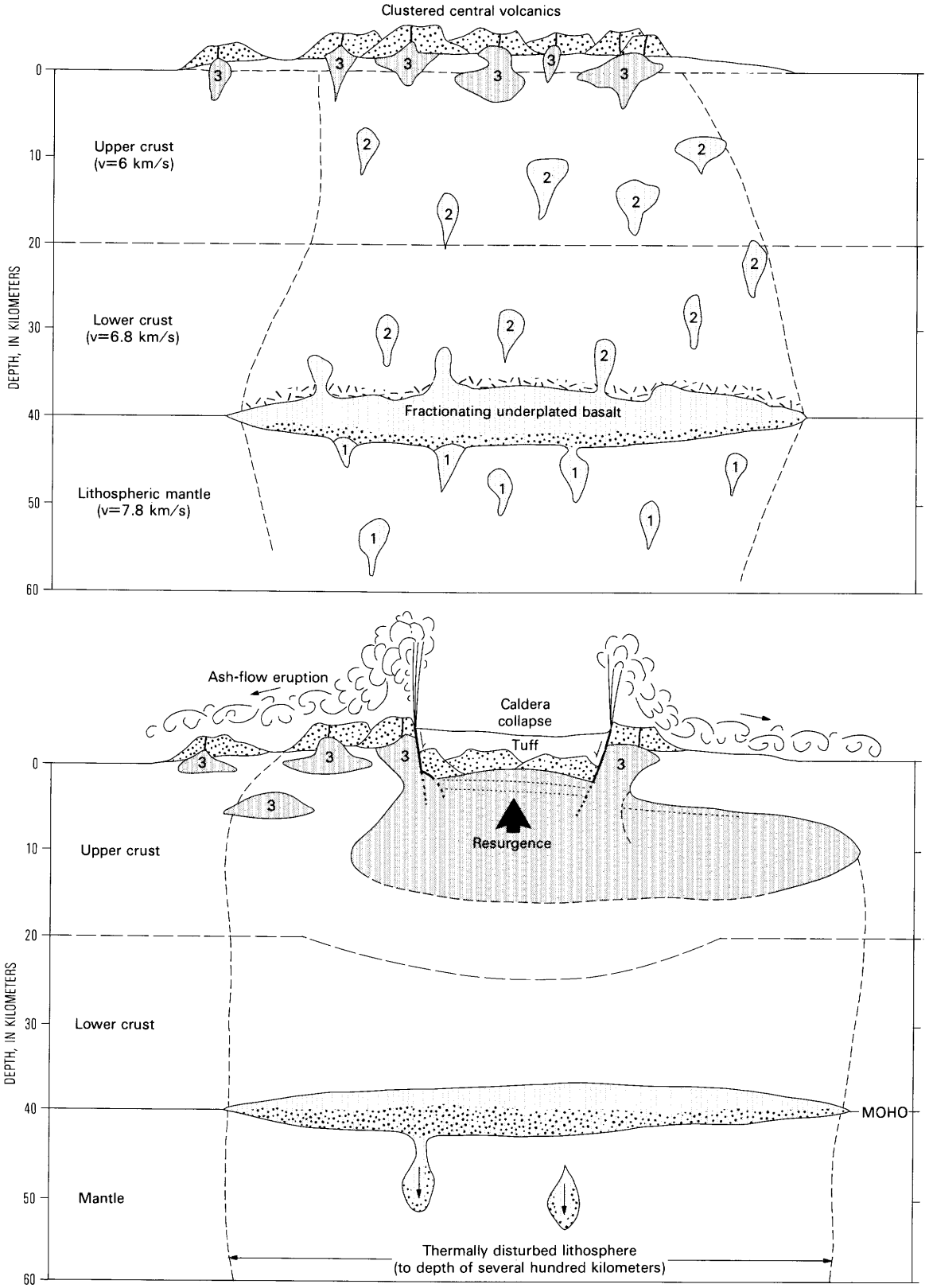
Clustered central volcanics
Upper crust
(v=6 km/s)
Lower crust
(v=6.8 km/s)
Lithospheric mantle
(v=7.8 km/s)
Fractionating underplated basalt
DEPTH, IN KILOMETERS
0
10
20
30
40
50
60
Ash-flow eruption
Caldera
collapse
Tuff
Resurgence
Upper crust
Lower crust
Mantle
MOHO
Thermally disturbed lithosphere
(to depth of several hundred kilometers)

Figure 2 (facing page). Crustal model illustrating generalized evolution of Latir volcanic field and cogenetic intrusions. Schematic sections are oriented north-south to minimize complicating effects of developing Rio Grande Rift. Details of magmatic features not to scale. Seismic *P*-wave velocities are regional present-day values for southern Rocky Mountains. Modified from Lipman (1988). *A*, Growth of central volcanoes during early (waxing) magmatism and initial accumulation of magmas in upper crust, before caldera formation (28–26.5 Ma). Primitive basaltic magma (phase 1 diapirs) rises from below lithosphere (subducted slab interacting with asthenosphere?), partly equilibrates with lithospheric mantle as it rises, ponds near base of crust, causes partial melting in lower crust (xxx), and crystallizes (heavy stipple) and fractionates as heat is transferred. Magmas segregating and rising within crust (phase 2 diapirs) are mixtures of fractionated mantle basalt and crustal melts. These magmas feed central volcanoes (stippled) and small subvolcanic plutons (phase 3 bodies). Uplift of igneous area (from horizontal short-dashed line; not to scale) is due to buoyant ponding of basalt at base of crust, to rise of lower crustal melts into upper crust, and to thermal expansion of lithosphere associated with magmatism. *B*, Later (waning) magmatism, during ash-flow eruption, caldera subsidence and resurgence, and consolidation of shallow crustal batholith (26.5 Ma). Compositionally varied cupolas develop in upper crust, along top of broadly laccolithic batholith. Southern roof of batholith solidified at crustal level several kilometers deeper than subcaldera northern part, perhaps because of more mafic mean composition. Compositional gradients near roof, becoming more mafic downward, are indicated by dotted lines. Crystallized and fractionated basaltic magma underplates and mixes with lower crustal material, replacing more evolved melts that have migrated upward; basal underplated material (heavy stipple) consists of ultramafic cumulates that merge in physical and chemical properties with lithospheric mantle, or may be sufficiently dense to sink deeper into mantle. Thermally weakened crust will accommodate extension along magmatic loci where plate stresses are conducive, permitting later mantle basalt to reach surface with less residence time and chemical interaction with lower crust (inception of Rio Grande Rift). Slow cooling of crustal section, during waning of magmatism and later, will cause subsidence over core of batholith, but broader regional uplift related to lower density of crust, and perhaps thinning of lithospheric mantle, will remain.

wall of the caldera (Leonardson and others, 1983). The worldwide association of molybdenum deposits with highly evolved granites indicates that molybdenum is concentrated by processes of igneous differentiation rather than mobilized from upper crustal country rocks by magma-related hydrothermal circulation. Such magmatic concentration processes may be favored by the open-system behavior between the lower crust and upper mantle indicated for the Questa magmatic system, in which mantle-derived heat fuels protracted crystal fractionation of silicic differentiates. Thus, formation of the Questa deposits probably required an especially favorable structural setting that involved concurrently intersecting caldera-related and regional rift faults in association with an evolved magmatic system driven by open-system interactions between mantle and lower crust.

CENTRAL SAN JUAN CALDERA CLUSTER, COLORADO

The San Juan volcanic field consists mainly of intermediate composition lavas and breccias, erupted at about 35–30 Ma from scattered central volcanoes, overlain by at least 15 widespread voluminous ash-flow sheets erupted at 30–26 Ma from caldera sources. It thus represents a slightly earlier (pre–Rio Grande Rift), larger, and more volcanologically complex analogue of the Latir-Questa system.

The much studied central caldera cluster, active at 28–26 Ma, contains six calderas (fig. 3), which host the major epithermal base- and precious-metal veins of the Creede District (Steven and Ratte, 1965; Steven and Lipman, 1976; Lipman and Sawyer, 1988; Lipman and others, 1989). The caldera-related ash-flow sheets of the central cluster represent some of the largest volume pyroclastic eruptions known in Earth history (at least 3,000 km^3 for the 27.8-Ma Fish Canyon Tuff) and vary in composition from dacite to low-silica rhyolite, in contrast to the high-silica rhyolite tuff erupted from the Questa caldera. Erosion has been insufficient to expose any granitic rocks associated with the central caldera cluster, but the calderas lie axially within a large negative gravity anomaly interpreted to reflect the presence of a composite batholith at shallow depth (Plouff and Pakiser, 1972). Detailed resolution of the rapid sequence of volcanic and structural events within the central cluster is possible because of high-resolution $^{40/39}Ar$ dates for all major ash-flow sheets (Lanphere, 1988).

Exposed levels of the central calderas are dominated by topographic walls, resurgent domes containing keystone graben faults, and intervening moat depressions that localized thick postcollapse volcanic and sedimentary deposits (fig. 3). All caldera structural boundaries (inferred to be ring faults) are covered, but combined geologic and geophysical data suggest that the aligned north-trending keystone graben faults of three western calderas (27.3-Ma Bachelor, 26.6-Ma Creede, and 26.1-Ma San Luis) were localized along the western segment of the concealed ring fault bounding the large earlier (27.8 Ma) La Garita caldera (Bethke and Lipman, 1987). Creede vein mineralization (25.1 Ma) is associated with late movement along these graben faults. The faults thus have had complex movement histories, first as a segment of the early La Garita ring fault, then as three separate keystone grabens related to resurgent doming of discrete calderas at 0.5–0.6-m.y intervals, and again about 1 m.y. later during vein mineralization. Additional periods of fault movement are possible, and an important lesson from the central cluster is the complex history of mineralized structures that could only be resolved under exceptionally favorable circumstances, provided at Creede by the recurrent datable volcanic events within a relatively brief time span. Restudy of the key junction area for three of the calderas in the northern part of the mining district (Lipman and Sawyer,

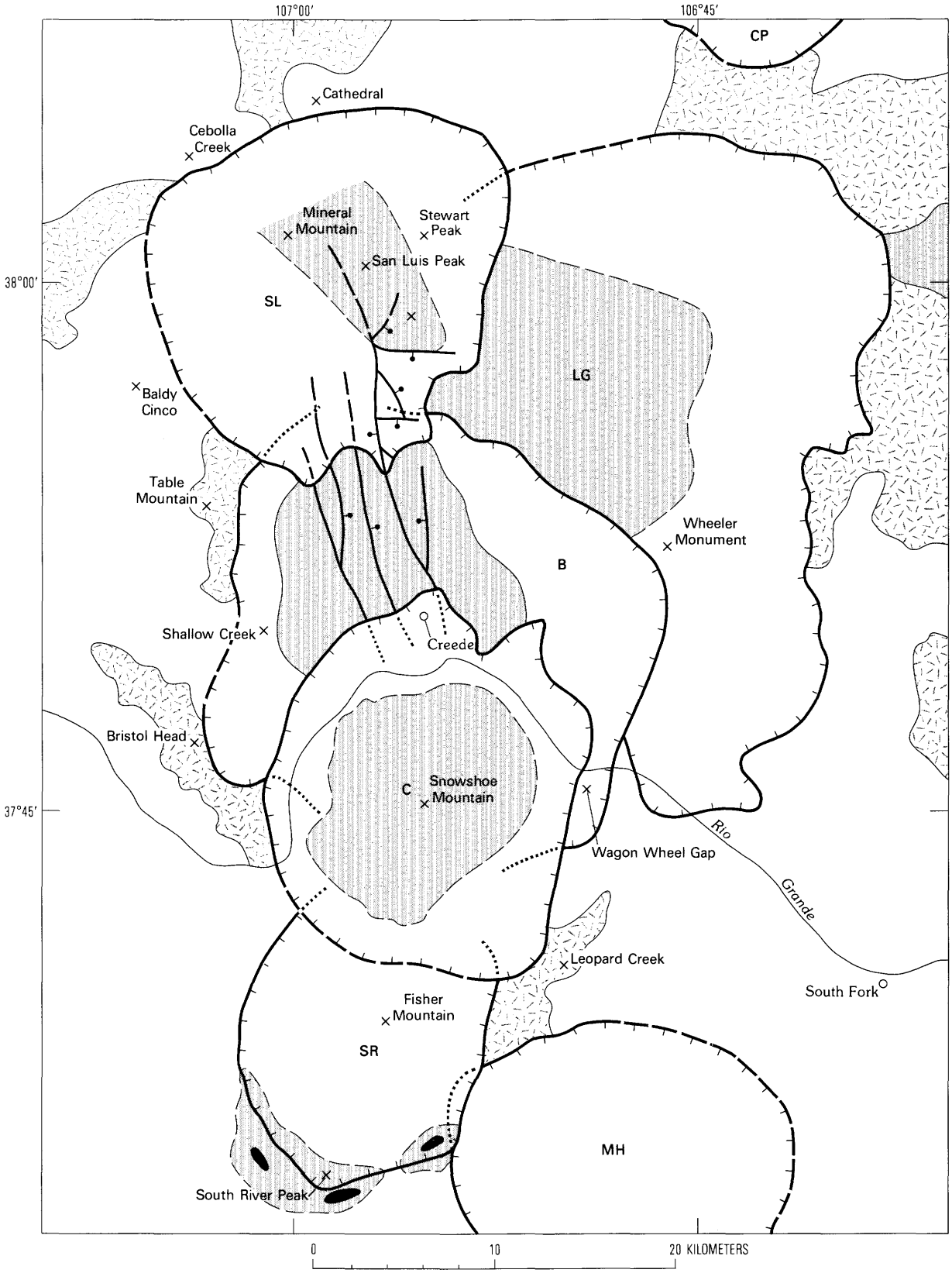
107°00′
106°45′
38°00′
37°45′
CP
Cathedral
Cebolla Creek
Mineral Mountain
Stewart Peak
San Luis Peak
SL
LG
Baldy Cinco
Table Mountain
Wheeler Monument
B
Shallow Creek
Creede
Bristol Head
C
Snowshoe Mountain
Wagon Wheel Gap
Rio Grande
Leopard Creek
South Fork
Fisher Mountain
SR
MH
South River Peak
0
10
20 KILOMETERS

Figure 3 (facing page). Generalized geology of central San Juan caldera cluster. Caldera margins are indicated by hachured lines (dashed where approximate, dotted where concealed); heavy stipple pattern indicates intracaldera resurgent uplifts. Key to calderas: B, Bachelor; C, Creede; CP, Cochetopa Park; LG, La Garita; MH, Mount Hope; SL, San Luis; SR, South River. Random hatch pattern indicates early intermediate-composition volcanic rocks (precaldera); unpatterned areas are caldera-related ash-flow tuffs and lavas; solid black areas are andesite-monzodiorite intrusions along south margin of South River caldera; screened pattern indicates approximate area of pyritic and argillic hydrothermal alteration. Generalized faults (bar and ball on downthrown side) shown only for the Creede Graben area. Modified from Lipman and Sawyer (1988).

1988) shows how misinterpretation of some caldera-wall unconformities as faults and some caldera-fill landslide deposits as brecciated intrusions has been confusing for mineral exploration strategies.

The Creede vein mineralization and associated hydrothermal system cut across the three western calderas, apparently driven by a heat source in the northern part of the district (fig. 4). Fluid flow was asymmetrically down the paleo- (and present-day) topographic gradient (Bethke and Lipman, 1987). Geologic, isotopic, and fluid-inclusion data suggest that ore deposition was controlled by special circumstances involving mixing of deep-circulating brines from playa sediments of the Creede caldera moat with dilute meteoric fluids. Mining production is dominated by silver and base-metal sulfides, and lead isotopic compositions of galena indicate that the bulk of the lead, and presumably most other metals, in the Creede ores has been leached from Precambrian rocks at depths of 3–5 km or more (Doe and others, 1979). The ore lead is notably more radiogenic than the associated Tertiary volcanic rocks. Thus, special circumstances of volcanic structural control, compositions of ore fluids, and sources of metals are all involved in genesis of the Creede deposits; apparent lack of ore deposits at some other San Juan calderas may reflect absence of such overlapping favorable conditions.

Essentially all ores produced from the San Juan region are now known to have been localized by caldera structures, except for local minor production from the cores of precaldera central volcanoes. Even some previously seemingly isolated loci for intense pyritic mineralization and supergene alteration along the southern margin of the central cluster have recently been found to occur in proximity to ring intrusions along the southern margin of the recently recognized South River caldera (fig. 3) (Lipman and others, 1989). The presence of this 27.1-Ma caldera was missed during earlier studies because, unlike previously recognized calderas of the central cluster, the South River caldera did not resurge after ash-flow eruption ceased but rather was filled to overflowing with postcollapse lavas. The presently recognized population of calderas in the western United States is probably heavily biased toward such more readily identifiable resurgent calderas. Accordingly, additional unrecognized mineralized areas may be associated with obscure nonresurgent calderas.

MINERALIZED MESOZOIC CALDERAS OF SOUTHEASTERN ARIZONA

Southeastern Arizona and adjacent areas constitute one of the largest porphyry copper provinces in the world (Titley, 1982). Most of the deposits are associated with Late Cretaceous–early Tertiary (Laramide-age) intrusions; related volcanic rocks, ranging in composition from andesite to silicic rhyolite record the development of a continental-margin volcanic arc. Porphyry copper mineralization has commonly been regarded as associated with the roots of andesitic volcanoes (Sillitoe, 1973; Branch, 1976), or with intrusions that did not vent, and with antithetic to caldera structures (Sillitoe, 1980). Although silicic volcanism has commonly been considered unrelated to such copper mineralization—in contrast to its generally recognized association with porphyry molybdenum systems such as Questa—reevaluation of the magmatic setting of the Arizona province suggests a widespread association of silicic caldera-related volcanism and porphyry copper mineralization (Lipman and Sawyer, 1985, 1986).

Recognition of large-scale volcanic features in the mineralized Arizona rocks is complicated by hypogene alteration and multiple structural complexities including Laramide compressive deformation, mid-Tertiary low-angle extensional faulting, and late Cenozoic block faulting. More than half of the pre-Cenozoic bedrock is covered, and only fragments of calderas are exposed. The igneous rocks in southeastern Arizona also contain striking structural and stratigraphic features for which unusual hypotheses have been proposed: widespread intrusive pyroclastic phenomena" (Watson, 1968), regional "exotic-block" breccias (Simons and others, 1966), and the concept of "volcanic orogeny" (Mayo, 1971). Reinterpretation of these features, using recent models of caldera formation and silicic volcanism gained through study of active or little eroded terranes, suggests the presence of 10–15 large Mesozoic caldera fragments (Lipman and Sawyer, 1985). Definitive characteristics of the caldera fragments include (1) ash-flow deposits more than 1 km thick, having features of intracaldera ponding; (2) interleaved "exotic block" breccias in tuffaceous matrix, interpreted as megabreccias resulting from caldera-wall landsliding; and (3) local granitic bodies, interpreted as caldera ring intrusions, along arcuate structural boundaries of the thick volcanic sequences. Three caldera fragments that host porphyry copper mineralization associated with the late granitic intrusions have been restudied in detail: Silver Bell, Sierrita, and Tucson.

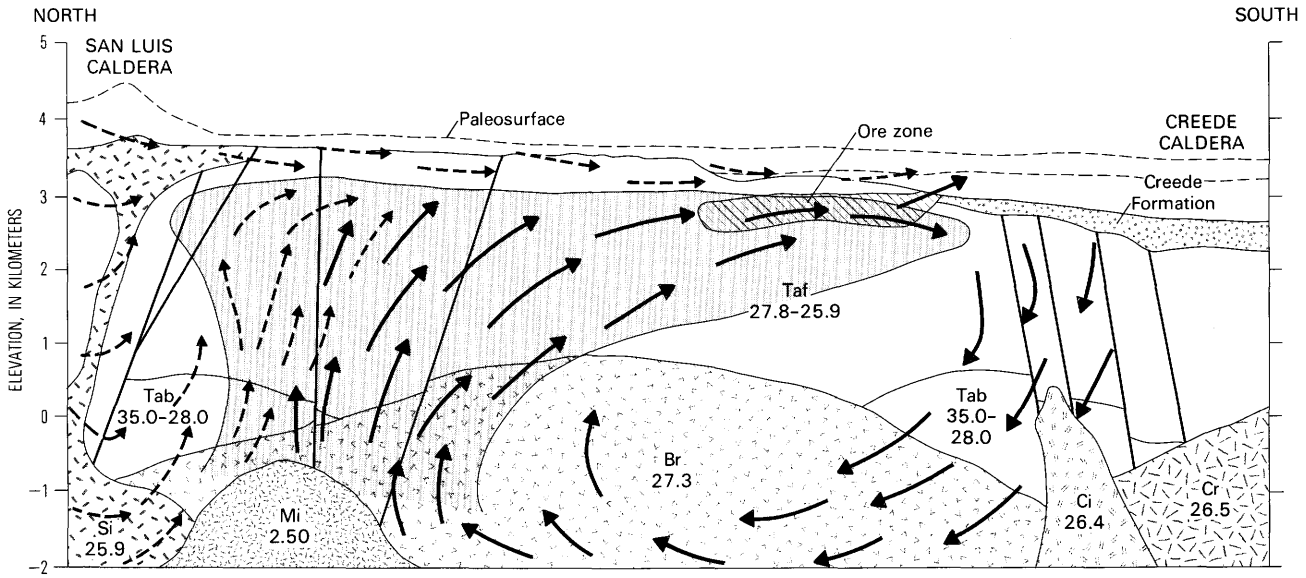

Figure 4. Diagrammatic north-south section longitudinally along Creede Graben along crest of resurgent dome within Bachelor caldera (fig. 3) showing inferred geometry of fossil hydrothermal system in relation to mineralization. Graben faults and mineralization extend across three calderas. Volcanic units (ages in Ma): Tab, precaldera andesite flows and breccias; Taf, intracaldera ash-flow tuffs. Inferred caldera-related intrusions: Br, resurgent intrusion of Bachelor caldera; Cr, resurgent intrusion of Creede caldera; Ci, ring intrusion of Creede caldera; Si, ring intrusion of San Luis caldera: Mi, mineralization-related intrusion. Solid arrows show inferred circulation of saline fluids derived from Creede Formation; dashed arrows show inferred circulation of dilute meteoric fluids derived from high northern area. No vertical exaggeration. Modified from Bethke and Lipman (1987).

Upper Cretaceous volcanic rocks (73–69 Ma) are closely associated with porphyry copper deposits in the Silver Bell Mountains (fig. 5*A*), where caldera subsidence is indicated by thick intracaldera tuff, interlayered collapse breccia, arcuate bounding faults, and ring intrusions (Sawyer, 1989). In the Sierrita Mountains (Lipman and Fridrich, 1990) (fig. 5*B*), Tertiary tilting is inferred to provide an oblique section through an upper crustal magmatic system, including a Laramide-age caldera containing thick welded tuffs and slide breccias, subcaldera batholith (Ruby Star Granodiorite), and major associated copper deposits (Sierrita-Esperanza, Twin Buttes, Mission-Pima, and San Xavier). Detailed mapping and petrologic studies in the Tucson Mountains, between the Silver Bell and Sierrita areas, indicate that thick ash-flow tuffs and multiple associated lenses of megabreccia (Cat Mountain Tuff, Tucson Mountain Chaos) accumulated within a Late Cretaceous trap-door caldera that was resurgently deformed by a large intrusion (Amole pluton); porphyry-type alteration and subeconomic copper mineralization occurred locally adjacent to the intrusion (Lipman and Fridrich, 1990). Broadly similar mineralization-related Mesozoic calderas have also been interpreted for the Santa Rita and Tombstone areas (fig. 5), based on field reconnaissance and reinterpretation of published data.

In the northern Dos Cabezas Mountains, thick varicolored pyroclastic breccias, exposed in oblique cross section due to Tertiary rotational faulting, were interpreted as intrusive by Erickson (1986); recent mineral resource studies by the U.S. Geological Survey report discrete breccia lithologies and intrusive breccia pipes considered to be potentially significant structural controls of mineralization (Drewes, 1985; Drewes and others, 1988). Alternatively, the entire breccia sequence, including under- and over-lying welded tuffs, has been interpreted as a single thick depositional ash-flow cooling unit, of variable lithic content, that filled a Laramide-age caldera (Lipman and Sawyer, 1985, 1986). The "breccia pipes" mapped by Drewes, rather than being intrusive bodies, are marked by unmappable irregular gradations within variably altered massive lithic tuff of the caldera fill; some areas of dark rock are propylitically altered, others are reddish due to oxidation or bleached by supergene leaching of pyritic rock. Such variable alteration, which is common in caldera-fill sequences, has different (and more limited) significance for mineral exploration than breccia-pipe structures.

Other mineralized areas associated with Mesozoic intrusions could represent the roots of calderas that are so deeply eroded that only precaldera rocks are preserved. For example, as suggested to me by David Sawyer of the U.S. Geological Survey, the major San Manuel–Kalamazoo porphyry copper deposit may be a western structurally dismembered part, perhaps representing a deeper structural level, of the mineralized caldera system that is fragmentarily preserved 15 km to the east at Copper Canyon (Lipman and Sawyer, 1985). Both mineralized areas are associated with ~69-Ma monzogranite porphyry that intrudes upper crustal rocks

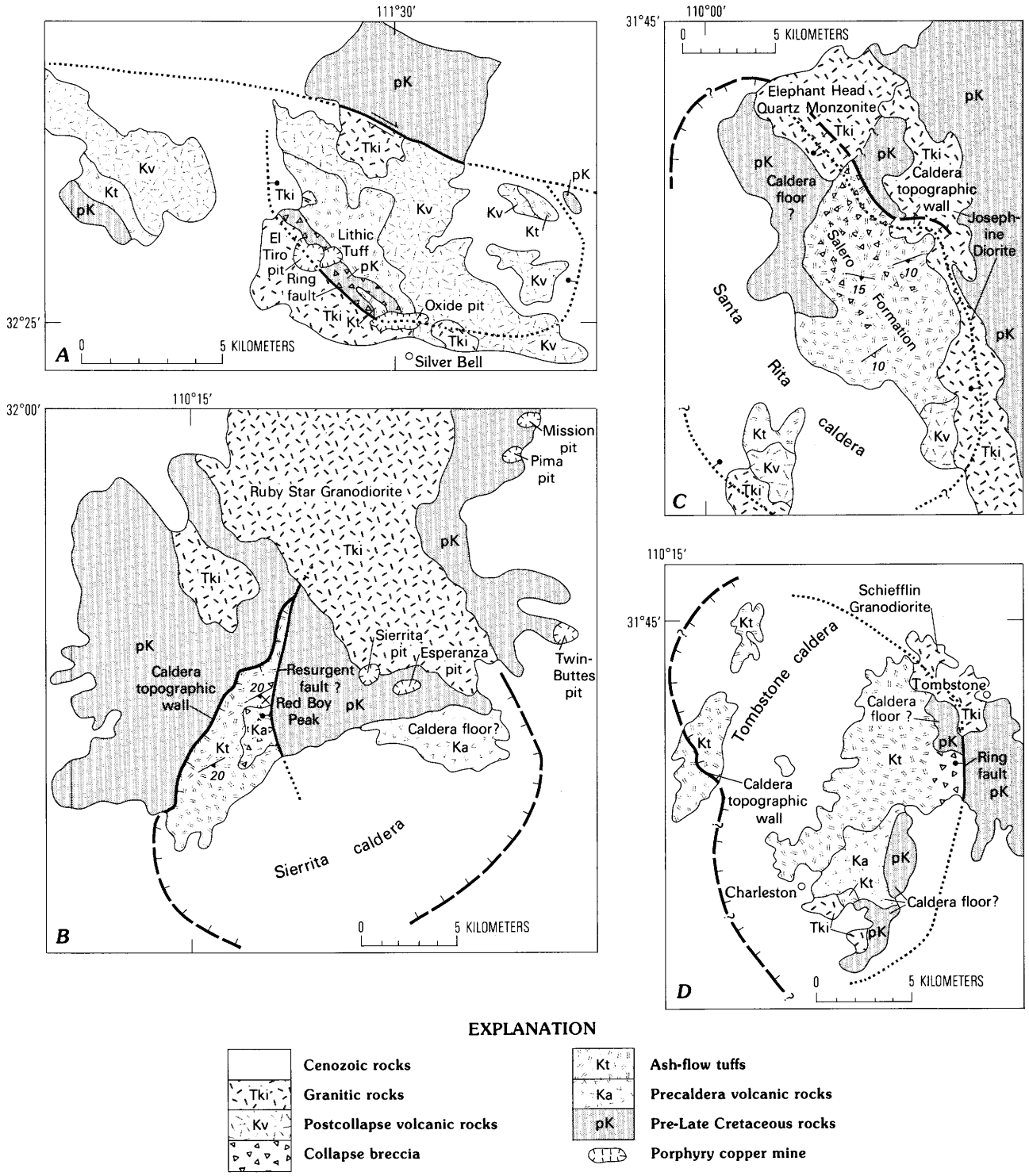

Figure 5. Generalized geology of four mineralized areas in southeastern Arizona interpreted as containing fragments of Late Cretaceous calderas. Caldera margins shown by hachured lines, dashed where approximately located. See text for discussion of individual areas. Modified from Lipman and Sawyer (1985).

northeast of the Santa Catalina core complex, and they may have been disrupted by extensional faults in a manner similar to that demonstrated on smaller scale for the San Manuel–Kalamazoo deposit (Lowell, 1968). Possibly analogous offsets of Laramide-age porphyry deposits by detachment faulting have been documented on the east flank of the Sierrita Mountains (summarized in Titley, 1982).

Relations between mineralization and older Mesozoic volcanism in southeastern Arizona, apparently mainly Jurassic in age, are even less understood than those for Laramide-age deposits. Fragments of several calderas and associated outflow tuffs are preserved in the Canelo Hills–Huachuca Mountains, Patagonia Mountains, and Pajarito Mountains (Lipman and Sawyer, 1985; Riggs and others, 1990). Local mineralization of these volcanic rocks, and association of the porphyry copper deposit at Bisbee with a Jurassic intrusion, suggests additional mineral potential associated with the Jurassic caldera-related rocks.

An instructive association of probable Jurassic caldera volcanism and copper porphyry mineralization is the Courtland-Gleeson District. There, lithologically intermixed Paleozoic rocks, previously mapped in detail as a complex Mesozoic thrust fault zone (Gilluly, 1956; Drewes, 1981), consist of megablocks depositionally enclosed in rhyolitic welded tuff that is spatially associated with a large Jurassic granitic intrusion. Less altered Cretaceous welded tuff (Sugarloaf Quartz Latite) unconformably overlies (rather than in thrust contact as mapped by Gilluly and Drewes) both the tuffaceous megabreccia and Jurassic intrusive rocks, suggesting that these rocks are parts of a caldera complex that was mineralized in the Jurassic. My reinterpretation of these lithologic complexities as due to primary volcanic depositional processes, rather than to Mesozoic thrust tectonics, provides a new structural framework for mineral exploration in the district.

The clustering of Mesozoic porphyry copper deposits in Arizona may be partly due to level of erosion, intermediate between that of the base- and precious-metal veins of a San Juan volcanic field and deeper plutonic mineralization such as the tungsten skarns in the Sierra Nevada. Widespread preservation of Mesozoic caldera fragments in southern Arizona, in contrast to limited preservation of outflow volcanic sequences, probably reflects both the lower structural levels represented by the subsided caldera fills and the greater resistance to erosion characteristic of the thick well-indurated caldera-fill material. The spacing of identified caldera fragments in southeastern Arizona is comparable to that in well-preserved Tertiary volcanic fields such as the San Juan region, and the original caldera density may have been even greater in Arizona, especially if effects of Tertiary extension and cover by basin alluvium are considered. Recognition that many of the most important Arizona ore deposits are structurally localized along caldera margins and related subvolcanic structures and intrusions provides a new conceptual framework for further exploration for concealed deposits.

DISCUSSION

The structural association between caldera magmatism and varied ore-deposit types, including epithermal base- and precious-metal veins, both copper and molybdenum porphyries, and deeper level replacement ores, is now well established (Steven and others, 1976; McKee, 1979; Rytuba, 1981). Important topics in need of further study include the life span of caldera-related hydrothermal systems and associated mineralizing processes. The time constraint depends on the longevity of the magmatic heat source, which in turn involves interplay between convective-conductive cooling and replenishment by addition of new magma to the upper crustal system. Especially valuable will be multidisciplinary studies of exceptionally young mineralized systems exposed by rapid tectonic uplift; most such systems are outside the United States. For example, at a recently recognized 2.5-Ma ash-flow caldera in the north-central Caucasus Mountains (Russia), associated Pleistocene granites and major molybdenum-tungsten deposits (broadly analogous to Questa, New Mexico) have been exposed by 3–5 km of Quaternary uplift (present rates as much as 12 mm/yr) due to the impingement of Africa and Arabia against the Eurasian craton (Lipman and others, 1990). In this system, apparent cooling ages indicated by available K-Ar determinations on the granites vary from essentially contemporaneous with the caldera-related tuff to as much as 1 m.y. younger; ongoing detailed chronologic studies utilizing isotopic and fission-track methods should provide a high-resolution record of magmatic cooling, fluid flow, and temporal evolution in the roots of this major mineralized geothermal system.

Another long-standing question concerns the sources of the metals in caldera-hosted and other igneous-related mineral deposits. The relative roles of metal transport from great depths by magmas versus concentration of ores from upper crustal country rocks has been controversial since the 19th century. Oxygen isotope studies show that most igneous-related ores were deposited from hydrothermal fluids in which deeply circulating meteoric water was a major or dominant component (Taylor, 1974) and that associated igneous bodies served mainly as the thermal engines to drive a convecting hydrothermal system (Norton, 1982). Calderas, as the surface expressions of large shallow silicic magmatic systems, are particularly favorable sites for such processes. For example, lead in epithermal veins in the San Juan volcanic field is more radiogenic than in associated igneous rocks and mainly must have been leached by hydrothermal fluids from Precambrian rocks that underlie the volcanic field (Doe

and others, 1979). Some would argue that most Phanerozoic ore deposits represent recycling of metals originally concentrated in the Precambrian, especially as massive sulfide deposits generated during processes of crustal formation (Hutchinson, 1980). Other metals, such as in molybdenum, uranium, and beryllium deposits, are consistently associated with distinctively evolved silicic magmas commonly emplaced during regional extension; these metals probably were concentrated as incompatible components during magmatic differentiation (Christiansen and others, 1983; Stein and Hannah, 1985). Even these metals, along with their host magmas, probably were mostly recycled from lower cratonic crust that has been variably melted and mobilized by mantle-generated mafic magmas.

Other priority targets for more detailed studies include young or even presently forming caldera-related mineralization encountered in geothermal exploration drilling, as in New Zealand and at the Valles caldera in New Mexico (Ewers and Keays, 1977; Hulin and others, 1987). Such situations permit direct observation of the deep geometry and physical conditions in mineralizing geothermal systems.

Another attractive target for future research involves research drilling through well-documented caldera-related ore deposits into deep parts of the fossil geothermal environment and possibly into the intrusive heat source, as proposed for Creede, Colorado (Bethke and Lipman, 1987). Crustal sections providing natural exposures from the near-surface environment down to the fossil magma chamber, as represented by a solidified batholith, occur naturally only due to complex structures, as at Questa, New Mexico, and Sierrita, Arizona, that leave significant ambiguities concerning the original geometry. Research drilling into structurally straightforward systems provides the only available method to overcome such ambiguities in the third dimension.

Acknowledgments.—The areal studies and concepts discussed here mainly represent a decade of products from my U.S. Geological Survey Roots of Ash-Flow Calderas Project, which has been supported mainly by the Geothermal Research and National Geologic Mapping Programs. Significant parts of this work were carried out in close collaboration with Philip Bethke, Jon Hagstrum, Clark Johnson, David Sawyer, John C. Reed, Jr., and others in the Survey, academia, and industry too numerous to acknowledge individually.

REFERENCES CITED

Bethke, P.M., and Lipman, P.W., 1987, Deep environment of volcanogenic epithermal mineralization—Proposed research drilling at Creede, Colorado: EOS, v. 68, p. 187–189.

Branch, C.D., 1976, Development of porphyry copper and stratiform volcanogenic ore bodies during the life cycle of andesitic strato-volcanoes, *in* Johnson, R.W., ed., Volcanism in Australasia: Amsterdam, Elsevier, p. 337–342.

Christiansen, E.H., Burt, D.M., Sheridan, M.F., and Wilson, R.T., 1983, The petrogenesis of topaz rhyolites from the western United States: Contributions to Mineralogy and Petrology, v. 85, p. 16–32.

Cordell, L., Long, C.L., and Jones, D.W., 1986, Geophysical expression of the batholith beneath Questa caldera: Journal of Geophysical Research, v. 90, p. 11263–11274.

Doe, B.R., Steven, T.A., Delevaux, M.H., Stacey, J.S., Lipman, P.W., and Fisher, F.S., 1979, Genesis of ore deposits in the San Juan volcanic field, southwestern Colorado—Lead isotopic evidence: Economic Geology, v. 74, p. 1–26.

Drewes, H., 1981, Tectonics of southern Arizona: U.S. Geological Survey Professional Paper 1114, 96 p.

_____1985, Geologic map and structure sections of the Dos Cabezas Quadrangle, Cochise County, Arizona: U.S. Geological Survey Miscellaneous Investigations Map I–1570.

Drewes, H., Klein, D.P., and Birmingham, S.D., 1988, Volcanic and structural controls of mineralization in the Dos Cabezas Mountains of southeastern Arizona: U.S. Geological Survey Bulletin 1676, 45 p.

Erickson, R.C., 1986, Comment on "Mesozoic ash-flow caldera fragments in southeastern Arizona and their relation to porphyry copper deposits": Geology, v. 14, p. 539–540.

Ewers, G.R., and Keays, R.R., 1977, Volatile and precious-metal zoning in the Broadlands geothermal field, New Zealand: Economic Geology, v. 72, p. 1337–1354.

Gilluly, J., 1956, General geology of central Cochise County, Arizona: U.S. Geological Survey Professional Paper 281, 169 p.

Hagstrum, J.T., and Lipman, P.W., 1986, Paleomagnetism of the structurally deformed Latir volcanic field, northern New Mexico—Relations to formation of the Questa caldera and development of the Rio Grande rift: Journal of Geophysical Research, v. 91, p. p. 7383–7402.

Hulin, J.B., Nielson, D., Goff, F., and Charles, R., 1987, Molybdenum mineralization in an active geothermal system, Valles caldera, New Mexico: Geology, v. 15, p. 748–752.

Hutchinson, R.W., 1980, Massive base metal sulfide deposits as guides to tectonic evolution: Geological Society of Canada Special Paper 20, p. 659–684.

Johnson, C.M., Czamanske, G.K., and Lipman, P.W., 1989, Geochemistry of intrusive rocks associated with the Latir volcanic field, New Mexico, and contrasts between evolution of plutonic and volcanic rocks: Contributions to Mineralogy and Petrology, v. 103, p. 90–109.

Johnson, C.M., Lipman, P.W., and Czamanske, G.K., 1990, H, O, Sr, Nd, and Pb isotope geochemistry of the Latir volcanic field and cogenetic intrusions, New Mexico, and relations between evolution of a continental magmatic center and modifications of the lithosphere: Contributions to Mineralogy and Petrology, v. 104, p. 99–124.

Lanphere, M.A., 1988, High-resolution $^{40}Ar/^{39}Ar$ chronology of Oligocene volcanic rocks, San Juan Mountains, Colorado: Geochemica et Cosmochimica Acta, v. 52, p. 1425–1434.

Leonardson, R.W., Dunlap, G., Starquist, V.L., Bratton, G.P., Meyer, J.W., Osborn, L.W., Atkin, S.A., Molling, P.A., Moore, R.F., and Olmore, S.D., 1983, Preliminary geology and molybdenum deposits at Questa, New Mexico, *in* The genesis of Rocky Mountain ore deposits—Changes with

time and tectonics: Denver Regional Exploration Geologists Symposium Proceedings, p. 151–155.

Lipman, P.W., 1984, The roots of ash-flow calderas: Windows into granitic batholiths: Journal of Geophysical Research, v. 89, p. 8801–8841.

_____1988, Evolution of silicic magma in the upper crust: The mid-Tertiary Latir volcanic field and its cogenetic granitic batholith, northern New Mexico, USA: Transactions of the Royal Society of Edinburgh, v. 79, p. 265–288.

Lipman, P.W., and Fridrich, C.J., 1990, Cretaceous caldera systems: Tucson and Sierrita Mountains: Arizona Geological Survey Special Paper 7, p. 51–65.

Lipman, P.W., Mehnert, H.H., and Naeser, C.W., 1986, Evolution of the Latir volcanic field, northern New Mexico, and its relation to the Rio Grande rift, as indicated by K-Ar and fission-track dating: Journal of Geophysical Research, v. 91, p. 6329–6346.

Lipman, P.W., and Reed, J.C., Jr., 1989, Geologic map of the Latir volcanic field and adjacent areas: U.S. Geological Survey Miscellaneous Investigations Map I–1907.

Lipman, P.W., and Sawyer, D.A., 1985, Mesozoic ash-flow caldera fragments in southeastern Arizona and their relation to porphyry copper deposits: Geology, v. 13, p. 652–656.

_____1986, Reply on "Mesozoic ash-flow caldera fragments in southeastern Arizona and their relation to porphyry copper deposits": Geology, v. 14, p. 540–541.

_____1988, Preliminary geology of the San Luis Peak Quadrangle and adjacent areas, San Juan volcanic field, southwestern Colorado: U.S. Geological Survey Open-File Report 88–359, 35 p.

Lipman, P.W., Sawyer, D.A., and Hon, K., 1989, Central San Juan caldera cluster, *in* Chapin, C.E., and Zidak, J., eds., Field excursions to volcanic terranes in the western United States, v. 1—Southern Rocky Mountain region: New Mexico Bureau of Mines and Mineral Resources Memoir 46, p. 330–350.

Lipman, P.W., Tsvetkov, A.A., Gurbenov, A.G., and Kovalenko, V.I., 1990, Newly recognized Pleistocene ash-flow caldera at Chegem River in the northern Caucasus Mountains (USSR), contemporaneous granitic intrusions, and associated Mo-Wo ore deposits: International Volcanologic Congress, Mainz, Federal Republic of Germany, Abstract Volume, (unpaginated).

Lowell, J.D., 1968, Geology of the Kalamazoo ore body, San Manuel district, Arizona: Economic Geology, v. 63, p. 645–654.

Mayo, E.B., 1971, Defense of "volcanic orogeny": Arizona Geological Society Digest, v. 9, p. 39–60.

McKee, E.H., 1979, Ash-flow sheets and calderas—Their genetic relation to ore deposits in Nevada: Geological Society of America Special Paper 180, p. 205–211.

Nielson, D.L., and Hulin, J.B., 1984, Internal geology and evolution of the Redondo Dome, Valles caldera, New Mexico: Journal of Geophysical Research, v. 89, p. 8695–8711.

Norton, D.L., 1982, Fluid and heat transport phenomena typical of copper-bearing pluton environments, *in* Titley, S.R., ed., Advances in geology of the porphyry copper deposits: Tucson, University of Arizona Press, p. 59–72.

Plouff, D., and Pakiser, L.C., 1972, Gravity study of the San Juan Mountains, Colorado: U.S. Geological Survey Professional Paper 800–B, p. 183–190.

Riggs, N., Haxel, G., and Busby-Spera, C., 1990, The early Jurassic Cordilleran magmatic arc in southern Arizona—Plutons to sand dunes: Arizona Geological Survey Special Paper 7, p. 90–103.

Rytuba, J.J., 1981, Relation of calderas to ore deposits in the western United States: Arizona Geological Society Digest, v. 14, p. 227–236.

Sawyer, D.A., 1989, Field guide to the Late Cretaceous Silver Bell caldera and porphyry copper mineralization in the Silver Bell Mountains, *in* Field excursions to volcanic terranes in the western United States, v. 1—Southern Rocky Mountain region: New Mexico Bureau of Mines and Mineral Resources Memoir 46, p. 127–132.

Sillitoe, R.H., 1973, The tops and bottoms of porphyry copper deposits: Economic Geology, v. 68, p. 799–815.

_____1980, Cauldron subsidence as a possible inhibitor of porphyry copper formation: Japan Mining Geology Special Issue, v. 8, p. 85–93.

Simons, F.S., Raup, R.B., Hayes, P.T., and Drewes, H., 1966, Exotic blocks and coarse breccias in Mesozoic volcanic rocks of southeastern Arizona: U.S. Geological Survey Professional Paper 550–D, p. D12–22.

Smith, R.L., and Bailey, R.A., 1968, Resurgent cauldrons: Geological Society of America Memoir 116, p. 613–662.

Stein, H.J., and Hannah, J.L., 1985, Movement and origin of ore fluids in Climax-type systems: Geology, v. 13, p. 469–474.

Steven, T.A., and Lipman, P.W., 1976, Calderas of the San Juan volcanic field, southwestern Colorado: U.S. Geological Survey Professional Paper 958, 35 p.

Steven, T.A., Luedke, R.G., and Lipman, P.W., 1974, Relation of mineralization to calderas in the San Juan volcanic field, southwestern Colorado: U.S. Geological Survey Journal of Research, v. 2, p. 405–409.

Steven, T.A., and Ratte, J.C., 1965, Geology and structural control of ore depositions in the Creede district, San Juan Mountains, Colorado: U.S. Geological Survey Professional Paper 487, 90 p.

Taylor, H.P, Jr., 1974, The application of oxygen and hydrogen isotope studies to problems of hydrothermal alteration and ore deposition: Economic Geology, v. 69, p. 843–883.

Titley, S.R., 1982, Some features of tectonic history and ore genesis in the Pima mining district, *in* Titley, S.R., ed., Advances in geology of the porphyry copper deposits: Tucson, University of Arizona Press, p. 387–406.

Watson, B.N., 1968, Intrusive volcanic phenomena in southern and central Arizona: Arizona Geological Society Guidebook 3, p. 147–153.

☆ U.S. GOVERNMENT PRINTING OFFICE: 1992—774-049/66,015 REGION NO. 8